

University of Alberta

**The Role of Multivalent Metal Cations and Organic
Complexing Agents in Bitumen-Mineral Interactions in
Aqueous Solutions**

By

Weibing Gan



A thesis submitted to the Faculty of Graduate Studies and Research
in partial fulfillment of the requirements for the degree of
Doctor of Philosophy

in

Materials Engineering

Department of Chemical and Materials Engineering

Edmonton, Alberta

Fall 2008



Library and
Archives Canada

Published Heritage
Branch

395 Wellington Street
Ottawa ON K1A 0N4
Canada

Bibliothèque et
Archives Canada

Direction du
Patrimoine de l'édition

395, rue Wellington
Ottawa ON K1A 0N4
Canada

Your file *Votre référence*
ISBN: 978-0-494-46320-8
Our file *Notre référence*
ISBN: 978-0-494-46320-8

NOTICE:

The author has granted a non-exclusive license allowing Library and Archives Canada to reproduce, publish, archive, preserve, conserve, communicate to the public by telecommunication or on the Internet, loan, distribute and sell theses worldwide, for commercial or non-commercial purposes, in microform, paper, electronic and/or any other formats.

The author retains copyright ownership and moral rights in this thesis. Neither the thesis nor substantial extracts from it may be printed or otherwise reproduced without the author's permission.

AVIS:

L'auteur a accordé une licence non exclusive permettant à la Bibliothèque et Archives Canada de reproduire, publier, archiver, sauvegarder, conserver, transmettre au public par télécommunication ou par l'Internet, prêter, distribuer et vendre des thèses partout dans le monde, à des fins commerciales ou autres, sur support microforme, papier, électronique et/ou autres formats.

L'auteur conserve la propriété du droit d'auteur et des droits moraux qui protègent cette thèse. Ni la thèse ni des extraits substantiels de celle-ci ne doivent être imprimés ou autrement reproduits sans son autorisation.

In compliance with the Canadian Privacy Act some supporting forms may have been removed from this thesis.

Conformément à la loi canadienne sur la protection de la vie privée, quelques formulaires secondaires ont été enlevés de cette thèse.

While these forms may be included in the document page count, their removal does not represent any loss of content from the thesis.

Bien que ces formulaires aient inclus dans la pagination, il n'y aura aucun contenu manquant.

■+■
Canada

ABSTRACT

A systematic investigation was carried out to study the interactions between bitumen (or hexadecane) and minerals (quartz, kaolinite and illite) in aqueous solutions containing multivalent metal cations Ca^{2+} , Mg^{2+} and $\text{Fe}^{2+}/\text{Fe}^{3+}$, in the absence and presence of organic complexing agents (oxalic acid, EDTA and citric acid). A range of experimental techniques, including coagulation measurement, visualization of bitumen-mineral attachment, metal ion adsorption measurement, zeta potential measurement, Fourier-transform infrared spectroscopy and X-ray photoelectron spectroscopic analyses, were employed in the investigation. Free energy changes of adsorption of metal cations on the minerals and bitumen were evaluated using the James & Healy thermodynamic model. Total interaction energies between the minerals and bitumen were calculated using classical DLVO theory.

It was observed that while the tested minerals showed varying degrees of mutual-coagulation with bitumen (or hexadecane), the presence of the multivalent metal cations could prominently increase the mutual coagulation. It was also found that such enhancement of the mutual coagulation was only significant when the metal cations formed first-order hydroxyl complexes (such as CaOH^+ , MgOH^+ , etc.) or metal hydroxides (such as $\text{Fe}(\text{OH})_3$, $\text{Mg}(\text{OH})_2$, etc.). Therefore, the increase of the bitumen-mineral mutual coagulation by the metal cations was strongly pH dependent.

Organic complexing agents (oxalic acid, citric acid and EDTA) used in this study, citric acid in particular, significantly reduced or virtually eliminated the mutual coagulation between bitumen (or hexadecane) and minerals caused by metal cations Ca^{2+} , Mg^{2+} , Fe^{2+} and Fe^{3+} . Due to its ability to substantially lower the mutual coagulation between bitumen and mineral particles, citric acid was found the most effective in improving bitumen-mineral liberation in solutions containing the multivalent metal cations at pH 8–10. In small scale flotation experiments to recover the residual bitumen from Syncrude Froth Treatment Tailings, the addition of up to 2×10^{-3} mol/L citric acid improved the separation efficiency by 24 percentage points. The sequential additions of 1.5×10^{-3} mol/L

citric acid and 30 mg/L polyacrylamide further increased the flotation separation efficiency, which was attributed to the improved liberation of bitumen from the minerals by the citric acid, and the flocculation of the liberated mineral fines by the polyacrylamide. The latter was expected to reduce the mechanical entrainment of the liberated mineral fines. Pretreatment of the Froth Treatment Tailings in an ultrasonic bath was also effective for bitumen liberation and recovery from the Froth Treatment Tailings.

Through measurements of zeta potentials of the minerals and adsorption densities of the metal cations on mineral surfaces, coupled with speciation diagrams, it was shown that the multivalent metal cations functioned in the studied systems through three distinctly different mechanisms. These included electrical double layer compression by the metal cations; adsorption of the first-order metal hydroxyl species; and adsorption of the metal hydroxides on the mineral particles. Reversibility of adsorption and analyses by X-ray photoelectron spectroscopy (XPS) and attenuated total reflectance Fourier-transform infrared spectroscopy (ATR-FTIR) indicated that the adsorption of the first-order metal hydroxyl species on quartz and kaolinite was through electrostatic attraction, while that of metal hydroxides was possibly through chemisorption.

It was also shown that classical DLVO theory could be used to describe and predict bitumen-mineral interactions with and without the presence of citric acid. The energy barriers for the interaction between bitumen and the minerals were greatly raised in the presence of citric acid, as a contribution to the repulsive electrical double layers interaction between bitumen droplets and mineral particles.

ACKNOWLEDGEMENTS

Many people have helped me and contributed to my research. First and foremost, I would like to express my deepest gratitude to Professor Q. Liu, my supervisor, for his guidance in the planning and execution of this research. Without his encouragement and support, this research would not have been completed. Indeed, I have learned a lot from the invaluable guidance and challenging discussions with him. It has been my honor and a privilege to be his Ph.D. student.

The financial support from Natural Sciences and Engineering Research Council of Canada (NSERC) and Syncrude Canada Ltd, the courtesy for providing oil sands tailings and bitumen froth samples by Syncrude Canada Ltd., are also acknowledged.

I am very indebted to Professor P.Y.K. Choi and Dr. Chunli Li for helping with molecular dynamics simulation to obtain ionic radii of some metal ionic species, and for their valuable discussion and inputs for this research.

I would like to thank Professors T.H. Etsell and P.Y.K. Choi who have served on my supervisory committee and have taken the time to read my draft dissertation and given me an opportunity to discuss its weakness so that my scientific knowledge is increased.

I appreciate the help from Dr. Mingli Cao and Mr. Brendon Crozier in carrying out some experiments. My thanks are also extended to Drs. Xiaodong Ma, Yongkai Zhu and my fellow Ph.D. students Jihua Gong and Patrick Kerr, for creating a pleasant working environment, for their friendship and support.

Finally, I want to thank my wife Bo and my son Shan for their love and unwavering support in the past several years, without which this work would not have been possible.

TABLE OF CONTENTS

1	INTRODUCTION.....	1
1.1	Bitumen Extraction from Oil Sands.....	1
1.2	Issues in Bitumen-Mineral Liberation	2
1.3	Objectives	5
1.4	Research Methodologies.....	6
1.5	Organization of the Thesis.....	7
2	LITERATURE REVIEW.....	9
2.1	Bitumen Recovery from Oil Sands Tailings.....	9
2.1.1	Column Flotation and Mechanical Flotation Processes.....	10
2.1.2	Sorption (Agglomeration)-Flotation Process.....	10
2.1.3	“Oleophilic Sieve” Process.....	11
2.2	Characteristics of Bitumen and Minerals in the Oil Sands.....	12
2.2.1	Bitumen.....	12
2.2.2	Quartz	13
2.2.3	Kaolinite	14
2.2.4	Illite.....	15
2.3	Interactions between Bitumen and Minerals.....	15
2.3.1	Effect of Temperature.....	16
2.3.2	Effect of NaOH.....	16
2.3.3	Effect of Clays and Mineral Slimes.....	17
2.3.4	Effect of Electrolytes	19
2.3.5	Effect of Organic Complexing Agents	20
2.4	Colloidal Particle Interactions.....	23
2.4.1	Classical DLVO Theory	23
2.4.2	Extended DLVO Theory: Incorporating non-DLVO interactions.....	26
2.4.3	Adsorption of Multivalent Metal Cations on Minerals.....	30
2.4.4	Ionic Equilibrium: Speciation Diagrams	33
3	EFFECT OF MULTIVALENT METAL CATIONS ON BITUMEN-MINERAL COAGULATION	34
3.1	Introduction.....	34

3.2	Experimental	34
3.2.1	Materials and Chemicals.....	34
3.2.2	Experimental Methods.....	36
3.3	Coagulation between Hexadecane and Mineral Solids.....	38
3.3.1	Quartz	38
3.3.2	Kaolinite	41
3.3.3	Illite.....	43
3.4	Coagulation between Model Oil and Mineral Solids.....	43
3.4.1	Effect of Agitation Speed	44
3.4.2	Quartz	44
3.4.3	Kaolinite	46
3.4.4	Illite.....	47
3.4.5	Mineral Mixtures	48
3.4.6	Effect of Montmorillonite.....	49
3.5	Coagulation between Solvent-Diluted-Bitumen and Mineral Solids	50
3.5.1	Quartz	50
3.5.2	Kaolinite	52
3.5.3	Illite.....	53
3.6	Summary.....	54
4	EFFECT OF COMPLEXING AGENTS ON BITUMEN-MINERAL COAGULATION IN THE PRESENCE OF METAL IONS	57
4.1	Introduction.....	57
4.2	Experimental	57
4.2.1	Materials and Chemicals.....	57
4.2.2	Experimental Methods.....	58
4.3	Coagulation between Model Oil and Minerals	58
4.3.1	Quartz	58
4.3.2	Kaolinite	63
4.3.3	Illite.....	64
4.4	Coagulation between Solvent-Diluted-Bitumen and Minerals	65
4.4.1	Quartz	65

4.4.2	Kaolinite	71
4.4.3	Illite.....	72
4.5	Summary.....	73
5	BITUMEN LIBERATION AND SEPARATION FROM OIL SANDS FROTH TREATMENT	
	TAILINGS	75
5.1	Introduction.....	75
5.2	Experimental.....	75
5.2.1	Materials and Chemicals.....	75
5.2.2	Experimental Techniques	76
5.3	Effect of Complexing Agents	78
5.4	Effect of Sequential Additions of Citric Acid and Polyacrylamide.....	80
5.5	Combined Effect of Citric Acid and an External Magnetic Field	81
5.6	Combined Effect of Citric Acid and Ultrasonic Treatment.....	82
5.7	Summary.....	84
6	MECHANISMS OF ACTION OF THE METAL IONS – ELECTROKINETIC STUDIES.....	85
6.1	Introduction.....	85
6.2	Experimental.....	85
6.2.1	Materials	85
6.2.2	Experimental Methods.....	86
6.3	Zeta Potentials of Minerals	87
6.3.1	Quartz	87
6.3.2	Kaolinite	89
6.3.3	Illite.....	91
6.4	Zeta Potentials of Model Oil and Bitumen	93
6.4.1	Model Oil.....	93
6.4.2	Bitumen.....	95
6.5	Interaction Energy between Bitumen and Minerals.....	98
6.5.1	Quartz-Bitumen Interaction Energies	99
6.5.2	Kaolinite-Bitumen Interaction Energies	100
6.5.3	Illite-Bitumen Interaction Energies	101
6.6	Summary.....	102

7	MECHANISMS OF ACTION OF THE METAL IONS – ADSORPTION STUDIES.....	104
7.1	Introduction.....	104
7.2	Experimental.....	104
7.2.1	Materials	104
7.2.2	Experimental Methods.....	105
7.3	Adsorption of Ca^{2+} , Mg^{2+} and Fe^{3+} on Minerals and Bitumen	106
7.3.1	On Quartz.....	106
7.3.2	On Kaolinite.....	110
7.3.3	On Illite.....	111
7.3.4	On Bitumen.....	113
7.3.5	Quantification of the Adsorbed Metal Ions by XPS	114
7.3.6	Characterization of the Adsorbed Metal Ions by ATR-FTIR.....	117
7.4	Thermodynamics of the Adsorption of Metal Ionic Species	120
7.4.1	James and Healy’s Thermodynamic Model	121
7.4.2	Ionic Radii of Metal Hydroxyl Species	122
7.5	Speciation of Ca^{2+} , Mg^{2+} and Fe^{3+} in Aqueous Solutions.....	126
7.5.1	Without Any Complexing Agent.....	126
7.5.2	Oxalic Acid.....	127
7.5.3	Citric Acid	129
7.5.4	EDTA.....	132
7.6	Mechanisms of Bitumen (Oil)-Mineral Interaction	134
7.6.1	Effect of Ca^{2+} , Mg^{2+} and Fe^{3+}	134
7.6.2	Effect of Complexing Agents	136
7.7	Summary.....	139
8	CONCLUSIONS AND RECOMMENDATIONS.....	140
8.1	General Findings.....	140
8.1.1	Effect of Multivalent Metal Cations on Bitumen(oil)-Mineral Coagulation	140
8.1.2	Effect of Complexing Agents on Bitumen(oil)-Mineral Coagulation.....	141
8.1.3	Effect of Citric Acid on Bitumen Liberation.....	142
8.2	Claims of Original Research.....	143

8.3 Recommendations for Further Research.....	144
REFERENCES.....	145
APPENDIX I CALCULATION OF TOTAL INTERACTION ENERGY	155
APPENDIX II QUANTIFICATION OF ADSORBED METAL CATIONS BY XPS ANALYSIS	160
APPENDIX III ADSORPTION THERMODYNAMICS	163
APPENDIX IV SPECIATION DIAGRAMS	166

LIST OF TABLES

Table 3-1	Chemical reagents used in the experiments.....	36
Table 4-1	Chemical reagents used in the experiments.....	58
Table 5-1	Separation efficiency of bitumen at various concentrations of complexing agents (see Figure 5-2).....	79
Table 7-1	Quantification of metal cations adsorbed on glass slide and $-63+25$ μm quartz by XPS.....	115
Table 7-2	Quantification of adsorbed metal cations on bitumen by XPS.....	117
Table 7-3	Van der Waals radii of metal ionic species obtained by molecular dynamics simulation.....	124
Table 7-4	Calculated free energy of adsorption for metal ionic species on minerals and bitumen at 25°C	125
Table 7-5	Stability constant ($\log K_1$) of metal-organic complexes (see Appendix IV).....	137
Table A-1	Parameters used for the calculation of total interaction energies between bitumen and minerals with classical DLVO theory.....	156
Table A-2	Total interaction energy (kT) of bitumen with quartz in solution containing 10^{-3} mol/L metal ions with or without the presence of 10^{-3} mol/L citric acid, calculated by classical DLVO theory. For a plot of the calculation results see Figure 6-11.....	157
Table A-3	Total interaction energy (kT) of bitumen with kaolinite in solution containing 10^{-3} mol/L metal ions with or without the presence of 10^{-3} mol/L citric acid, calculated by classical DLVO theory. For a plot of the calculation results see Figure 6-12.....	158
Table A-4	Total interaction energy (kT) of bitumen with illite in solution containing 10^{-3} mol/L metal ions with or without the presence of 10^{-3} mol/L citric acid, calculated by classical DLVO theory. For a plot of the calculation results see Figure 6-13.....	159
Table A-5	XPS analysis of adsorbed Ca^{2+} , Mg^{2+} and Fe^{3+} on quartz surface.....	160

Table A-6	XPS analysis of adsorbed Ca^{2+} , Mg^{2+} and Fe^{3+} on glass slide.....	161
Table A-7	Element quantification of bitumen film without any treatment by XPS.	162
Table A-8	XPS analysis of adsorbed Ca^{2+} , Mg^{2+} and Fe^{3+} on bitumen film.	162
Table A-9	Selected parameters used in the calculation of free energy change of adsorption of metal species.....	164
Table A-9	The change in free energy of adsorption of metal ionic species on minerals and bitumen at different pH at 25°C, kJ/mol	165
Table A-10	Selected formation constants of metal hydroxyl products and organic acids at 25°C (I = 0.001M).....	168
Table A-11	Selected formation constants of metal-complexes at 25°C (I = 0.001M).....	169
Table A-12	Speciation of 10^{-3} mol/L of Ca^{2+} , Mg^{2+} and Fe^{3+} (see Figure 7-10).....	170
Table A-13	Speciation of 10^{-3} mol/L Ca^{2+} in 10^{-3} mol/L oxalic acid at 25°C (see Figure 7-11).	171
Table A-14	Speciation of 10^{-3} mol/L Mg^{2+} in 10^{-3} mol/L oxalic acid at 25°C (see Figure 7-12).	172
Table A-15	Speciation of 10^{-3} mol/L Fe^{3+} in 10^{-3} mol/L oxalic acid at 25°C (see Figure 7-13).	173
Table A-16	Speciation of 10^{-3} mol/L Ca^{2+} in 10^{-3} mol/L citric acid at 25°C (see Figure 7-14).	174
Table A-17	Speciation of 10^{-3} mol/L Mg^{2+} in 10^{-3} mol/L citric acid at 25°C (see Figure 7-15).	175
Table A-18	Speciation of 10^{-3} mol/L Fe^{3+} in 10^{-3} mol/L citric acid at 25°C (see Figure 7-16).	176
Table A-19	Speciation of 10^{-3} mol/L Ca^{2+} in 10^{-3} mol/L EDTA at 25°C (see Figure 7-17).	177
Table A-20	Speciation of 10^{-3} mol/L Mg^{2+} in 10^{-3} mol/L EDTA at 25°C (see Figure 7-18).	178
Table A-21	Speciation of 10^{-3} mol/L Fe^{3+} in 10^{-3} mol/L EDTA at 25°C (see Figure 7-19).....	179

LIST OF FIGURES

Figure 1-1	Schematic of the Clark hot water extraction (CHWE) process (Houlihan, 1982).....	2
Figure 2-1	Molecular structure of oxalic acid, citric acid, and ethylenediaminetetraacetic acid (EDTA).....	22
Figure 3-1	Experimental setup for bitumen (oil)-minerals coagulation.	37
Figure 3-2	Experimental setup for visualization of bitumen (oil)-mineral adhesion.	37
Figure 3-3	Coagulation of hexadecane with quartz at different pH with and without Ca^{2+}	39
Figure 3-4	Microphotographs of hexadecane droplets and $-63+25 \mu\text{m}$ quartz at pH ~ 11 (a) in the absence and (b) in the presence of $10^{-3} \text{ mol/L Ca}^{2+}$	40
Figure 3-5	Coagulation of hexadecane with quartz at different pH with and without 10^{-3} mol/L metal cations.....	42
Figure 3-6	Coagulation of hexadecane with kaolinite at different pH with and without $10^{-3} \text{ mol/L Ca}^{2+}$	42
Figure 3-7	Coagulation of hexadecane with illite at different pH with and without $10^{-3} \text{ mol/L Ca}^{2+}$	43
Figure 3-8	Effect of agitation speed on the coagulation of model oil with quartz.	44
Figure 3-9	Coagulation of model oil with quartz at different pH with and without 10^{-3} mol/L metal ions.....	45
Figure 3-10	Coagulation of model oil with kaolinite at different pH with and without 10^{-3} mol/L metal ions.	46
Figure 3-11	Coagulation of model oil with illite at different pH with and without 10^{-3} mol/L metal ions.....	47
Figure 3-12	Coagulation of model oil with mineral mixtures (quartz:kaolinite:illite = 80:14:6) at different pH with and without $10^{-3} \text{ mol/L Ca}^{2+}$ addition.	48
Figure 3-13	Effect of added montmorillonite on the coagulation of model oil with mineral mixtures (quartz:kaolinite:illite = 80:14:6), pH 7–8.....	49

Figure 3-14 Coagulation between bitumen and quartz at different concentrations of Ca^{2+} and Fe^{3+}	51
Figure 3-15 Coagulation of bitumen with quartz at different pH with and without 10^{-3} mol/L metal ions.....	51
Figure 3-16 Coagulation of bitumen with kaolinite at different pH with and without 10^{-3} mol/L metal ions.	52
Figure 3-17 Coagulation of bitumen with illite at different pH with and without 10^{-3} mol/L metal ions.....	54
Figure 4-1 Coagulation of model oil with quartz at different concentrations of complexing agents in solutions containing 10^{-3} mol/L Ca^{2+} , pH 9.8–10.2.....	59
Figure 4-2 Microphotographs of model oil droplets with $-63+25$ μm quartz with 10^{-3} mol/L Ca^{2+} at pH ~ 10 (a) in the absence and (b) in the presence of 2×10^{-3} mol/L citric acid.....	60
Figure 4-3 Coagulation of model oil with quartz at different concentrations of complexing agents in solutions containing 10^{-3} mol/L Mg^{2+} , pH 9.8–10.2.....	61
Figure 4-4 Coagulation of model oil with quartz at different concentrations of complexing agents in solutions containing 10^{-3} mol/L Fe^{2+} , pH 7.7–8.3.....	62
Figure 4-5 Coagulation of model oil with quartz at different concentrations of complexing agents in solutions containing 10^{-3} mol/L Fe^{3+} , pH 7.7–8.3.....	63
Figure 4-6 Coagulation of model oil with kaolinite at different concentrations of citric acid in the presence of 10^{-3} mol/L metal ions.	64
Figure 4-7 Coagulation of model oil with illite at different concentrations of citric acid in the presence of 10^{-3} mol/L metal ions.....	65
Figure 4-8 Coagulation of bitumen with quartz at different concentrations of complexing agent in the presence of 10^{-3} mol/L Ca^{2+} , pH 9.8–10.2.	66
Figure 4-9 Coagulation of bitumen with quartz at different concentrations of complexing agent in the presence of 10^{-3} mol/L Mg^{2+} , pH 9.8–10.2.....	66

Figure 4-10 Coagulation of bitumen with quartz at different concentrations of complexing agent in the presence of 10^{-3} mol/L Fe^{2+} , pH 7.7–8.3.	67
Figure 4-11 Coagulation of bitumen with quartz at different concentrations of complexing agent in the presence of 10^{-3} mol/L Fe^{3+} , pH 7.7–8.3.	68
Figure 4-12 Microphotographs of bitumen droplets and $-63+25 \mu\text{m}$ quartz at pH ~ 10 with the addition of 10^{-3} mol/L Ca^{2+} in (a) absence and (b) presence of 10^{-3} mol/L citric acid.....	69
Figure 4-13 Microphotographs of bitumen droplets and $-63+25 \mu\text{m}$ quartz at pH ~ 7.8 with the addition of 10^{-3} mol/L Fe^{3+} in (a) absence and (b) presence of 10^{-3} mol/L citric acid.....	70
Figure 4-14 Coagulation of bitumen with kaolinite at different concentrations of citric acid in the presence of 10^{-3} mol/L metal ions.	72
Figure 4-15 Coagulation of bitumen with illite at different concentrations of citric acid in the presence of 10^{-3} mol/L metal ions.....	73
Figure 5-1 Experimental setup for flotation in an external magnetic field.....	78
Figure 5-2 Separation efficiency of bitumen from oil sands froth treatment tailings at different concentrations of complexing agent, pH ~ 8.3	79
Figure 5-3 Separation efficiency of bitumen from oil sands froth treatment tailings at different concentration of polyacrylamide (PAM) at a pulp temperature of 40°C , pH ~ 8.3	81
Figure 5-4 Separation efficiency of bitumen from oil sands froth treatment tailings at different intensities of external magnetic field, pH ~ 8.3	82
Figure 5-5 Separation efficiency of bitumen from oil sands froth treatment tailings at different sonication pretreatment with or without citric acid addition, pH ~ 8.3	83
Figure 6-1 Zeta potential of quartz at different pH in the absence and presence of 10^{-3} mol/L metal ions.....	88
Figure 6-2 Zeta potential of quartz at different pH in the presence of 10^{-3} mol/L metal ions and 10^{-3} mol/L citric acid.....	88
Figure 6-3 Zeta potential of kaolinite at different pH in the presence of 10^{-3} mol/L metal ions.	90

Figure 6-4	Zeta potential of kaolinite at different pH in the presence of 10^{-3} mol/L metal ions and 10^{-3} mol/L citric acid.	90
Figure 6-5	Zeta potential of illite at different pH in the presence of 10^{-3} mol/L metal ions.	92
Figure 6-6	Zeta potential of illite at different pH in the presence of 10^{-3} mol/L metal ions and 10^{-3} mol/L citric acid.	92
Figure 6-7	Zeta potential of model oil droplet at different pH in the presence and absence of 10^{-3} mol/L metal ions.	93
Figure 6-8	Zeta potential of model oil droplet at different pH in the presence of 10^{-3} mol/L metal ions and 10^{-3} mol/L citric acid.	94
Figure 6-9	Zeta potential of bitumen droplet at different pH in the presence and absence of 10^{-3} mol/L metal ions.	95
Figure 6-10	Zeta potential of bitumen droplet at different pH in the presence of 10^{-3} mol/L metal ions and 10^{-3} mol/L citric acid.	96
Figure 6-11	Total interaction energy of bitumen with quartz in aqueous solution containing 10^{-3} mol/L metal ions with and without the presence of 10^{-3} mol/L citric acid.	99
Figure 6-12	Total interaction energy of bitumen with kaolinite in aqueous solution containing 10^{-3} mol/L metal ions with and without the presence of 10^{-3} mol/L citric acid.	101
Figure 6-13	Total interaction energy of bitumen with illite in aqueous solution containing 10^{-3} mol/L metal ions with and without the presence of 10^{-3} mol/L citric acid.	102
Figure 7-1	Adsorption density of metal ions on quartz with initial concentration of 10^{-3} mol/L at different pH.	108
Figure 7-2	Adsorption density of Ca^{2+} on quartz at different concentration of citric acid, pH ~10.	110
Figure 7-3	Adsorption density of Ca^{2+} and Mg^{2+} on kaolinite with initial concentration of 10^{-3} mol/L at different pH.	111
Figure 7-4	Adsorption of Ca^{2+} and Mg^{2+} on kaolinite at different concentrations of citric acid. pH ~10.	112

Figure 7-5 Adsorption density of Ca^{2+} and Mg^{2+} on illite with initial concentration of 10^{-3} mol/L at different pH.....	112
Figure 7-6 Adsorption of Ca^{2+} and Mg^{2+} on bitumen with initial concentration of 10^{-3} mol/L at different pH.....	114
Figure 7-7 ATR-FTIR spectra of $-20 \mu\text{m}$ quartz with and without treatment by $0.1 \text{ mol/L Ca}^{2+}$ solution.....	118
Figure 7-8 ATR-FTIR spectra of $-20 \mu\text{m}$ quartz with and without treatment by $0.01 \text{ mol/L Fe}^{3+}$ solution.....	119
Figure 7-9 ATR-FTIR spectra of $-20 \mu\text{m}$ quartz with and without treatment by citric acid in the presence of Ca^{2+} and Fe^{3+}	120
Figure 7-10 Speciation diagram of 10^{-3} mol/L of Ca^{2+} , Mg^{2+} and Fe^{3+} in aqueous solution. Constructed using data from Furia (1972), Butler and Cogley (1998), Weistin and Rasmuson (2005) and Dean (1999).....	126
Figure 7-11 Speciation diagram of 10^{-3} mol/L of Ca^{2+} in aqueous solution containing 10^{-3} mol/L oxalic acid. Constructed using data from Furia (1972), Butler and Cogley (1998), Weistin and Rasmuson (2005) and Dean (1999).	128
Figure 7-12 Speciation diagram of 10^{-3} mol/L of Mg^{2+} in aqueous solution containing 10^{-3} mol/L oxalic acid. Constructed using data from Furia (1972), Butler and Cogley (1998), Weistin and Rasmuson (2005) and Dean (1999).	128
Figure 7-13 Speciation diagram of 10^{-3} mol/L of Fe^{3+} in aqueous solution containing 10^{-3} mol/L oxalic acid. Constructed using data from Furia (1972), Butler and Cogley (1998), Weistin and Rasmuson (2005) and Dean (1999).	129
Figure 7-14 Speciation diagram of 10^{-3} mol/L of Ca^{2+} in aqueous solution containing 10^{-3} mol/L citric acid. Constructed using data from Furia (1972), Butler and Cogley (1998), Weistin and Rasmuson (2005) and Dean (1999).	130
Figure 7-15 Speciation diagram of 10^{-3} mol/L of Mg^{2+} in aqueous solution containing 10^{-3} mol/L citric acid. Constructed using data from Furia	

(1972), Butler and Cogley (1998), Weistin and Rasmuson (2005) and Dean (1999).	131
Figure 7-16 Speciation diagram of 10^{-3} mol/L of Fe^{3+} in aqueous solution containing 10^{-3} mol/L citric acid. Constructed using data from Furia (1972), Butler and Cogley (1998), Weistin and Rasmuson (2005) and Dean (1999).	131
Figure 7-17 Speciation diagram of 10^{-3} mol/L of Ca^{2+} in aqueous solution containing 10^{-3} mol/L EDTA. Constructed using data from Furia (1972), Butler and Cogley (1998), Weistin and Rasmuson (2005) and Dean (1999).	132
Figure 7-18 Speciation diagram of 10^{-3} mol/L of Mg^{2+} in aqueous solution containing 10^{-3} mol/L EDTA. Constructed using data from Furia (1972), Butler and Cogley (1998), Weistin and Rasmuson (2005) and Dean (1999).	133
Figure 7-19 Speciation diagram of 10^{-3} mol/L of Fe^{3+} in aqueous solution containing 10^{-3} mol/L EDTA. Constructed using data from Furia (1972), Butler and Cogley (1998), Weistin and Rasmuson (2005) and Dean (1999).	133
Figure 7-20 Zeta potential of $\text{Fe}(\text{OH})_3$ precipitates at different pH with and without the addition of organic complexing agents.	138

LIST OF NOMENCLATURE

A	Hamaker constant (J)
A_{132}	Hamaker constant of phase 1 and phase 2 through a medium 3 (J)
c	speed of light in vacuum (2.998×10^8 m/s)
C	electrolyte concentration (mol/L)
e	elementary electron charge (1.602×10^{-19} C)
F	Faraday's constant (96485 C·mol ⁻¹)
G	Gibbs free energy (J)
H	distance between two surfaces (m)
I	ionic strength
k	Boltzmann constant (1.381×10^{-23} J·K ⁻¹)
K_1	formation constant
N	Avogadro constant (6.022×10^{23} mol ⁻¹)
R_1	radius of spherical particle 1 (m)
R_2	radius of spherical particle 2 (m)
T	absolute temperature (K)
V_E	electrostatic double layer interaction energy (J)
V_{HB}	hydrophobic interaction energy (J)
V_{Total}	total interaction energy (kT)
V_V	van der Waals interaction energy (J)
z_i	valency of ion i
Δ	change or difference in
ϵ	permittivity of a substance (F·m ⁻¹)
ϵ_0	permittivity of vacuum (8.854×10^{-12} F·m ⁻¹)
$\epsilon_{r,i}$	relative dielectric constant of a substance i
ζ	zeta potential at shear plane in an electric double layer (V)
κ	inverse Debye length (m ⁻¹)
κ^{-1}	Debye length (m)
Ψ	electrostatic potential (V)
Ψ_0	electrostatic surface potential (V)

1 INTRODUCTION

1.1 Bitumen Extraction from Oil Sands

Alberta oil sands, the largest known non-conventional oil resource in the world, have a proven reserve equivalent to about 174 billion barrels of oil (Canada Energy Board, 2006). They normally consist of 10 wt% of bitumen and 85 wt% of mineral solids dominated by quartz, kaolinite, and illite (Bayliss and Levinson, 1976; Kessick, 1979; Ignasiak et al., 1983). Currently, among the total output of over one million barrels of oil per day, up to 50% of the crude bitumen is produced by using Clark Hot Water Extraction (CHWE) process (Canada Energy Board, 2006).

The CHWE process, as shown in Figure 1-1, is composed of conditioning, primary separation, air flotation and dilution centrifuging. The conditioning process is accomplished in a hydro-transport pipeline in which bitumen was liberated from oil sands with the aids of steam, caustic soda and other additives. The conditioned pulp is introduced to a Primary Separation Vessel (PSV) for bitumen flotation and removal of sand tailings. The middling discharged from PSV is fed to scavenging process performed by conventional froth flotation cell to recover the residual bitumen, which is combined with PSV froth to form the “Froth” product for froth treatment. The tailings of PSV and scavenging are combined and rejected to tailings pond as “Primary Tailings”.

The “Froth” product is sent to “Froth Treatment Plant” to remove entrained fine solids and water. This is accomplished by dilution with organic solvent (naphthenic or paraffinic hydrocarbons), followed by settling and centrifuging. The Froth Treatment Plant generates a solvent-diluted bitumen (dilbit) stream and centrifuge tailings (“Froth Treatment Tailings”). The dilbit is transported to an upgrader to recover the solvent and to produce synthetic crude, while the froth treatment tailings are discharged to tailings pond.

The froth treatment tailings produced from the above bitumen extraction process contain residual bitumen that accounts for about 2% of the overall oil production. At the current production rate, this is equivalent to an annual loss of more than 3 million barrels of oil. There is, therefore, an economic incentive in recovering the lost bitumen from the froth treatment tailings. Recovery of the residual bitumen would also alleviate some of the environmental impacts of the tailings on the region, and allow the recovery of the heavy minerals (titanium and zirconium minerals) which are enriched in the tailings.

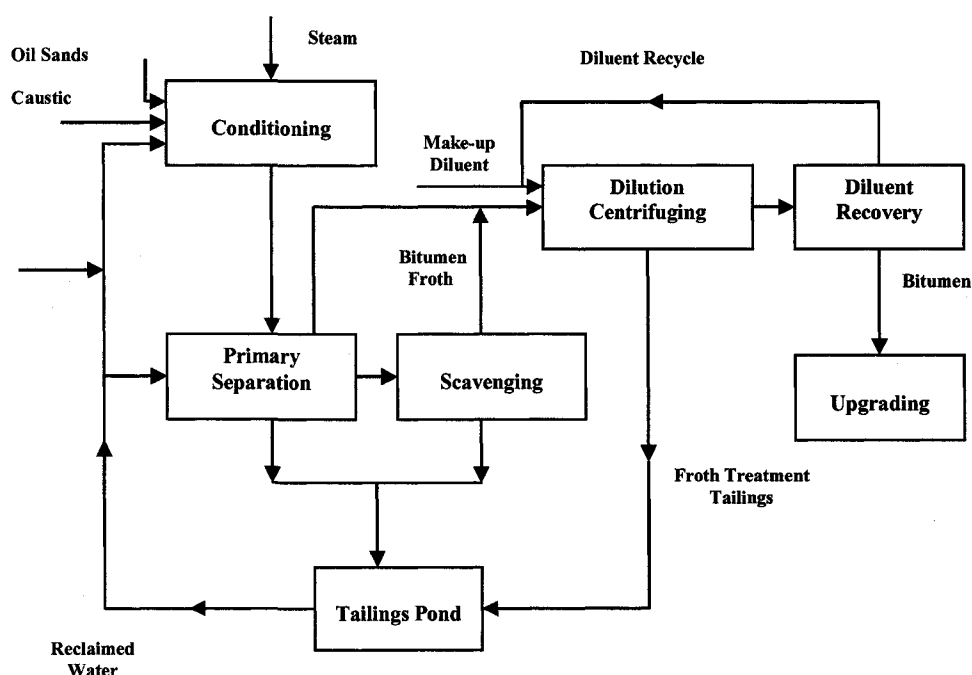


Figure 1-1 Schematic of the Clark hot water extraction (CHWE) process (Houlihan, 1982)

1.2 Issues in Bitumen-Mineral Liberation

Poor bitumen-mineral liberation in CHWE process results in degraded froth quality and reduced bitumen recovery, by floating the unliberated minerals and/or discharging the bitumen-bearing minerals to tailings pond. Therefore, high degree of bitumen liberation from mineral solids is a prerequisite for effective recovery by flotation. The degree of

liberation depends on pulp physicochemical conditions such as pulp temperature, pH and pulp chemical composition (i.e., the presence of various ionic species), etc. To recover the residual bitumen, it is necessary to establish the right chemical conditions in the pulp to achieve a high degree of bitumen liberation from mineral solids.

Metal cations undermine bitumen-mineral liberation since they alter the pulp chemical conditions and the interfacial properties, through reactions with various anions or adsorption on the surfaces of bitumen and mineral matters. These metal cations, primarily sodium, calcium, magnesium and ferrous, are originated from soluble metal salts which are carried into the oil sand deposits from the overburden by ground water (Clark and Pasternack, 1932). They are released into process water during the extraction process. A number of studies have shown that the multivalent hydrolysable metal cations such as Ca^{2+} , Mg^{2+} and Fe^{3+} cause lower bitumen recovery and deteriorated froth quality. In pilot plant flotation tests using three different oil sands feeds, Clark and Pasternack (1932) found that the progressive addition of the chloride salts of Ca^{2+} , Mg^{2+} and Fe^{3+} led to a dramatic reduction in bitumen recovery from about 95% to about 35%. Similar observations were reported later by Zhou et al. (1999), Kasongo et al. (2000) and Basu et al. (2004). The detrimental effect of the metal cations could be traced to inadequate bitumen liberation and/or poor bitumen flotation.

In contrast, better bitumen liberation and recovery from oil sands is anticipated if multivalent metal cations are eliminated from the pulp. Precipitation, complexation and ionic exchange are three approaches often used to remove these metal cations. In the first approach, an inorganic chemical, e.g., carbonate, phosphate or hydroxide, is added to the pulp to form insoluble compounds with the metal cations, and the precipitates formed should not interact with bitumen droplets under process conditions. With complexation approach, suitable complexing ligands are used to mask metal cations by forming metal-organic complexes. Ionic exchange is usually applied to the systems in the absence of solid phase.

Organic acids are complexation agents commonly used to eliminate metal cations in aqueous solutions, and find widespread applications in wastewater treatment and other industries. Oxalic acid and citric acid could effectively remove ferric ions from iron stained kaolinite (Ambikadevi and Lalithambika, 2000). Ethylenediaminetetraacetate (EDTA) was used to extract heavy metals from contaminated soil (Tandy et al., 2004). Liu and Zhang (2000) found that citric acid could remove calcium ions from chalcopyrite surfaces to increase flotation selectivity between chalcopyrite and galena using dextrin. Bichard and Edward (1967) proposed that organic acids could be used to remove multivalent metal cations in bitumen froth treatment.

Although the detrimental effect of multivalent metal cations such as Ca^{2+} and Mg^{2+} on bitumen recovery is well recognized, there is no consensus regarding how the metal ions affect the interactions between bitumen and minerals. Some researchers (Liu et al., 2002; Long et al., 2006) believed that Ca^{2+} “bridged” the bitumen and minerals. While the others (Zhou et al., 1999) considered that the adsorption of CaOH^+ on the bitumen/quartz interfaces was responsible. In addition, whether or not the metal cations are adsorbed on bitumen remains unknown, since no report is available. Thus, there is a need to systematically examine how multivalent metal cations affect bitumen (oil)-mineral interaction.

Multivalent metal cations have to be adsorbed on (or desorbed from) the bitumen/water or mineral/water interfaces to significantly affect the interaction between bitumen and mineral matters. Adsorption of metal ionic species at the oxide mineral/water interfaces has been extensively studied. A number of theoretical models, including ionic exchange, formation of surface complexes, solvation and specific adsorption, have been proposed. Among these, the surface complexation model proposed by James and Healy (1972c) is widely accepted.

In the surface complexation model, James and Healy (1972c) considered that metal ions were adsorbed on hydrous oxides through surface complex formation (e.g., metal hydroxyl complexes). In the adsorption of metal cations on negatively charged oxide

surface from aqueous solutions, the free energy of adsorption was composed of three distinct terms contributed by the attractive coulombic force, the repulsive secondary solvation force, and the specific “chemical” interaction. The secondary solvation energy was inversely related to the hydrated metal ionic radii which were equal to the sum of the metal crystal radii and the diameter of one water molecule. Although the calculated solvation energy predicted reasonably well the adsorption behaviors of Co^{2+} , Cr^{3+} and Fe^{3+} on SiO_2 (James and Healy 1972c), the assumption that metal cations and their first-order hydroxyl complexes have the same effective radii was not well founded. The effective radii of the first-order metal hydroxyl species have to be established in order to correctly quantify their free energy of adsorption. However, these data are not available in the literature. Therefore, obtaining correct ionic radii of hydrolyzed metal ions will allow a better evaluation of thermodynamic data to predict their adsorption on oxide/hydroxide surfaces.

In addition, the effect of multivalent metal cations and organic complexing agents on bitumen-mineral interaction can be assessed by total interaction energy proposed by Derjaguin-Landau-Verwey-Overbeek (DLVO). Classical DLVO theory includes the contribution of electrical double layer force and universal attractive van der Waals forces. The former is determined by many variables including solution pH, types and concentration of electrolyte. Thus, investigating the effect of multivalent metal ions and complexing agents on surface electrical properties (e.g., zeta potential) is necessary to understand the interaction between bitumen and minerals.

1.3 Objectives

From the foregoing description, the objectives of this study are:

- 1) To systematically examine the effects of multivalent metal cations such as Ca^{2+} , Mg^{2+} , Fe^{2+} and Fe^{3+} on oil (bitumen) – mineral interactions in aqueous solutions, at different solution pH and in the presence and absence of organic complexing agents.

2) To develop a theoretical understanding of the observed phenomena from the perspectives of thermodynamics, solution chemistry, and surface and colloid science.

This research will result in a better understanding of the roles of multivalent metal cations and other additives on the interactions between an inorganic phase (minerals) and an organic phase (oil or bitumen). The primary drive for the current research is to recover the residual bitumen from the oil sands froth treatment tailings. However, the research results may find applications in bitumen extraction, liquid-liquid separation, froth flotation, waste treatment and soil de-contamination.

1.4 Research Methodologies

Both experimental and theoretical studies are carried out to accomplish these objectives. The following experimental and analytical work has been conducted:

1) Coagulation tests: To monitor and quantify the aggregation or dispersion between mineral particles and oil (bitumen) droplets under various solution conditions. These tests are supplemented by visualization of the adhesion between mineral particles and oil (bitumen) droplets through micro-imaging under a stereomicroscope.

2) Froth flotation: Flotation separation of the residual bitumen from froth treatment tailings under various solution chemistry conditions, such as different concentrations of added organic acids, flocculants, sonication treatment, and absence/presence of an external magnetic field.

3) Adsorption studies: The adsorption densities of metal cations on mineral surfaces and bitumen droplets are studied under various solution conditions. The nature of the adsorbed species on minerals and on oil (bitumen) surfaces is characterized by X-ray photoelectron spectroscopy (XPS) and attenuated total reflectance Fourier-transform infrared spectroscopy (ATR-FTIR).

4) Zeta potential measurements: Zeta potentials of bitumen (oil) and minerals at different solution conditions are measured.

5) Speciation of the metal cations and organic acids in aqueous solutions: Thermodynamic formation constants are used to calculate the predominant species at different pH, and the results are plotted as speciation diagrams.

6) Theoretical analysis: This mainly involves calculation of secondary solvation energies of various metal ionic species using the James-Healy model, and calculation of the total interaction energies between bitumen and minerals using classical DLVO theory.

1.5 Organization of the Thesis

This thesis begins with Chapter One which contains an introduction to the background, objectives and methodologies of the study. This is followed by:

Chapter Two which reviews the literature on the interactions between bitumen and minerals, with a focus on the effect of multivalent metal cations and organic complexing agents, as well as the fundamental theories that govern the interaction between colloidal particles in aqueous solutions.

Chapter Three which presents the experimental results on the mutual coagulation between oil (hexadecane, or hexadecane doped with sodium oleate) or bitumen and minerals (quartz, kaolinite and illite) in aqueous solution containing multivalent metal cations.

Chapter Four which presents the experimental findings with regard to the effect of organic complexing agents on bitumen (or model oil)-mineral coagulation in the presence of Ca^{2+} , Mg^{2+} , Fe^{2+} and Fe^{3+} ions.

Chapter Five which demonstrates that organic complexing agents can markedly improve bitumen liberation and recovery from oil sands froth treatment tailings. Results on residual bitumen flotation with the use of citric acid combined with other additives or force fields (such as selective flocculants, external magnetic field, and sonication energy) are also presented.

Chapters Six and Seven constitute a study on the mechanistic aspects of the observed phenomena. Chapter Six presents results on the electrokinetic potentials (zeta potentials) of droplets of the bitumen or model oil, of the mineral particles including quartz, kaolinite and illite, in the absence and presence of metal cations or organic complexing agents. The measured zeta potential values are used to calculate the total potential energy of interaction between bitumen droplets and particles of various minerals using DLVO theory to evaluate the effect of electrostatic interactions on bitumen-mineral coagulation. Chapter Seven focuses on the speciation and adsorption of metal cations on minerals and bitumen at different pH, which identifies the metal ionic species that are responsible for the mutual coagulation between bitumen and minerals, and the role of the organic complexing agents in eliminating the detrimental effects of the metal ions.

Finally, Chapter Eight presents a summary of the general findings as a result of this study and provides recommendations for future study.

2 LITERATURE REVIEW

Bitumen extraction from oil sands has been practiced in northern Alberta for over 50 years during which a wealth of relevant literature has been generated. A comprehensive literature review is conducted and presented in this chapter. The review concerns three topics pertinent to this study: bitumen recovery from oil sands tailings, interaction between bitumen and minerals, and fundamentals of interaction between colloidal particles in aqueous solution.

2.1 Bitumen Recovery from Oil Sands Tailings

The Clark Hot Water Extraction (CHWE) process as described in the previous chapter has been greatly improved since its first piloting in the 1930s and first commercial operation in the 1960s. The progress in technology has resulted in a significant increase in processing capacity and decrease in energy consumption. To a large extent, this is attributed to the adaptation of a hydro-transport pipeline in the conditioning operation (Hindle et al., 1992) and Low Energy Extraction Process (LEEP) which lowered the slurry temperature from 80°C to about 35°C (Surry, 1990). In addition, some efforts have also been made to prevent the loss of bitumen to oil sands tailings. For example, in 1985, Syncrude Canada Ltd installed a Tailings Oil Recovery (TOR) system which increased bitumen recovery by 2 to 20 percentage points depending on the feed ore grade (Cymerman and Kwong, 1995). Nevertheless, appreciable amount of residual bitumen is discarded to tailings ponds. For instance, bitumen loss in froth treatment tailings alone accounts for approximately 2% of the total oil production from Alberta oil sands, equivalent to a loss of 3 million barrels of oil per year at the current production rate (Canada Energy Board, 2006).

During the past two decades, extensive studies have been carried out to recover the residual bitumen from tailings. A number of methods such as air sparging (Hall and Tollefson, 1979; 1980; 1984), froth flotation (St. Denis and Kessick, 1982; Hamshar et al., 1993; Cheng et al., 1999), oleophilic separation (Kruyer, 1982), agglomeration-screening

(Majid et al., 1983; Kumar et al., 1986), and agglomeration-flotation (Hall and Tollefson, 1987; Coleman et al., 1995) have been proposed and tested.

2.1.1 *Column Flotation and Mechanical Flotation Processes*

From 1979 to 1984, Hall and Tollefson reported that the residual bitumen in the final extraction tailings could be recovered by column flotation with air sparging. Up to 80% recovery of bitumen from the final extraction tailings was achieved. Temperature, agitation, air sparging rate & dispersion, and the presence of CO₂ affected recovery (Hall and Tollefson, 1979; 1980; 1984). However, no information on the froth quality of their work was available. St. Denis and Kessick (1982) achieved ~100% bitumen recovery from the sludge of Suncor tailings pond as the sludge was diluted with water at a ratio of sludge:water = 1:2 and floated for 60 minutes. The effect of feed concentration, chemical addition (NaOH or Ca(OH)₂), and flotation time was investigated. However, the requirement of large amount of dilution water was a potential problem. Hamshar et al. (1993) recovered the residual bitumen from various sources of tailings, including Suncor Pond 1, Pond 2 and Syncrude fine tailings, by flotation. The effect of temperature, aeration rate, flotation time, feed dilution and water-soluble polymer was explored. The recovery of bitumen ranged from 40 to 80% with low froth quality. Cheng et al. (1999) used froth flotation and stationery separation to recover bitumen from Suncor plant tailings. The influence of flotation time, agitation, aeration rate and dispersion was studied.

2.1.2 *Sorption (Agglomeration)-Flotation Process*

Majid et al. (1983) disclosed that carbonaceous hydrophobic solids (collectors) from a variety of sources could be used to agglomerate the organics in oil sands tailings. The organics were then washed off by solvent and the collectors were recycled. Up to 90% of the residual bitumen could be recovered. Similarly, Kumar et al. (1986) used Suncor coke to recover the residual bitumen from the tailings sludge, by blending the coke with the sludge containing 20–40 wt% of solids to form agglomerates, then recovering the

agglomerates by screening. They investigated the effects of coke particle size, BET surface area, and chemical additives on the recovery of the residual bitumen. However, they did not mention how the bitumen was separated from the coke. Hall and Tollefson (1987) applied sorption(coke)-scavenging scheme for bitumen recovery. Suncor coke was used as a sorbent for residual bitumen in both the primary and centrifuge tailings. The bitumen-loaded coke was then floated and “coked” again to recover the bitumen and the coke sorbent recycled after steam stripping. More than 90% of the residual bitumen in the tailings samples was recovered. Coleman et al. (1995) obtained 93% bitumen recovery at a froth product grade of 17.8% using agglomeration(coal)-flotation, in which Suncor mature fine tailings (MFT) were agglomerated with ground and oil-conditioned coal ($70\% < 74 \mu\text{m}$), then floated.

2.1.3 “Oleophilic Sieve” Process

Kruyer (1982) used an “oleophilic sieve” to recover bitumen from both oil sands feed and tailings. Bitumen recovery was reported to be close to 100% even with low-grade ores. However, the problem with this process was that the small bitumen droplets tend to be carried away by the streams.

The foregoing review indicates that the processes of residual bitumen recovery fall into two broad categories: sorbent aggregation and froth flotation. In the former, hydrophobic solids (coke, coal, etc.) are used as sorbents to recover the residual bitumen, and the sorbent-residual bitumen aggregates are then removed by flotation. The recovered bitumen is usually associated with the sorbent. In the latter, froth flotation is used for bitumen recovery, which cannot achieve both high recovery and high froth quality simultaneously. The most noteworthy problem for both processes is the entrainment of fine clay particles and mineral slimes into the froth products. For instance, Hamshar et al. (1993) obtained reasonable bitumen recovery from tailings but their bitumen froth had a bitumen:solid ratio of 1:1 even after froth wash, much higher than the typical 6:1 in froth generated from the CHWE process. The causes for the entrainment problem have generally not been determined. Little effort has been made to minimize such entrainment.

2.2 Characteristics of Bitumen and Minerals in the Oil Sands

Bitumen in the Alberta oil sands is a complex mixture of light and heavy hydrocarbons containing polar carboxylic and phenolic groups. The bitumen present in oil sands is associated with minerals predominated by quartz, kaolinite and illite, plus minor amounts of heavy minerals and other clay minerals such as montmorillonite. The nature of bitumen and related minerals can affect bitumen-minerals interactions in aqueous solutions through different mechanisms. Thus, the characteristics of bitumen, quartz, kaolinite and illite are briefly reviewed in the following.

2.2.1 *Bitumen*

As a mixture of hydrocarbons different in molecular weight, composition and bonding characteristics, bitumen possesses different properties, depending on the composition of saturates, aromatics, resins and asphaltene (SARA) (Strausz, 1977). Asphaltene has the most significant impact on bitumen extraction and upgrading process since it contains the various polar moieties mainly carboxylic and phenolic groups (Schramm and Smith, 1985, Strausz, 1977, Yan et al., 1995; Sanford, 1983; Masliyah et al., 2004). It can be dissolved by aromatic solvents such as toluene or naphtha. According to Wu et al. (1999; 2005), aromatic solvent-diluted bitumen submerged in aqueous solution is surrounded by asphaltene “floating” on bitumen/water interface with a protrusion on the water side of around 0–20 nm.

Bitumen droplets carry different charges originated from the dissociation of the polar groups on the bitumen/water interface (Takamura and Chow, 1983; Takamura 1985; Takamura and Wallace 1988). They become more negatively charged at higher solution pH (Takamura and Chow, 1983; Liu et al., 2002) and elevated temperature (Dai and Chung, 1995). Bitumen droplets also exhibit a variation in zeta potential at a given pH as they are diluted by different solvents before being emulsified in water (Schramm et al., 1998). This may be attributed to the different solubility of asphaltene in different solvents.

Thus, a bitumen droplet in aqueous solution can be described as a hydrocarbon with surface polar (carboxylic and phenolic) groups which are ionized depending on the pulp pH. However, it is not clear how these functional groups interact with other ionic species in pulp. On the other hand, to what degree these moieties contribute to the total surface charge of bitumen droplets remains unclear, for non-polar hydrocarbons such as octane and hexadecane also carry a negative charge in aqueous solutions probably due to the preferential adsorption of hydroxyl ions at the oil/water interface (Marinova et al., 1996; Franks et al., 2005; Beattie et al., 2004; 2005). The preferential adsorption of the hydroxyl ions may also contribute to the surface charge of bitumen.

2.2.2 *Quartz*

Made up of SiO₂ tetrahedra, quartz is a major constituent mineral present in oil sands (Masliyah et al., 2004; Liu et al., 2006a). It is hydrophilic in nature and normally does not strongly associate with bitumen. As indicated by Dai and Chung (1995), good liberation and separation is not difficult to achieve for coarse sands (>129 µm) at pH > 6. However, a considerable amount of quartz particles are found in bitumen froth. Fine quartz particles can be mechanically entrained/entrapped in aerated bitumen. Quartz particles less than 100 µm in size can become partially hydrophobic and float to froth due to association with polar hydrocarbons (Dai and Chung, 1995; Sparks et al., 2003).

Quartz particle is negatively charged above the iso-electric point, which is typically at pH 2–3 (Fuerstenau and Raghavan, 1976). Zeta potential measurements (Liu et al., 2003) show that the surface charge of quartz particles is negative at the pH where bitumen extraction is carried out (i.e., pH 8–9), and becomes more negative when solution pH increases (Basu et al., 1997). At a given pH, elevated temperature also results in more negatively charged surfaces (Dai and Chung, 1995). With the addition of divalent cations such as Ca²⁺, or Mg²⁺, the zeta potential of quartz and bitumen becomes less negative, probably due to the compression of the electrical double layers by the added metal ions (Liu et al., 2002). The surface charge of quartz is reversed at pH 10.5 with the addition of 1 mM Mg²⁺ (Fuerstenau and Palmer, 1976; Hanna and Somasundaran, 1976).

2.2.3 *Kaolinite*

Kaolinite [$\text{Al}_4\text{Si}_4\text{O}_{10}(\text{OH})_8$] is a two-layer structured aluminosilicate, comprising an octahedral aluminum oxy-hydroxide sheet and a tetrahedral silicate sheet (Carty, 1999). After cleavage, two types of surfaces are created for kaolinite, the basal surfaces and the edges. The basal surfaces carry a constant negative charge which originates from isomorphous substitution of Si^{4+} by Al^{3+} . The magnitude of the negative charge on the basal surfaces is independent of pH (Zhou and Gunter, 1992; Ma and Eggleton, 1999). On the other hand, the edge, occupied by aluminol (AlOH) and silanol (SiOH) groups, can take various charges due to the protonation and deprotonation of the surface hydroxyl groups, depending on slurry pH (McBride, 1976, Williams and Williams, 1978). The iso-electric point of the edges is believed to be between pH 6 and 9 (Schofield and Samson, 1954; Williams and Williams, 1978). Under acidic conditions, the edge is positively charged through protonation of surface hydroxyl groups, and can interact with negatively charged basal surfaces to form “edge-to-face” flocculation (Schofield and Samson, 1954) through electrostatic attraction. With increasing pH, the surface hydroxyl groups successively undergo deprotonation leading to a reduction and eventually reversal of the positive charges on the edge.

Kaolinite has the capacity of adsorbing metal cations, e.g., Ca^{2+} , Mg^{2+} , on its external surfaces through ionic exchange without affecting its structure (Grim, 1968). The functional hydroxyl groups at the edges are considered responsible for the cation uptake by kaolinite depending on the solution pH, cation and electrolyte concentration (Ferris and Jepson, 1975; Sposito, 1984; Schindler and Stumm, 1987).

Characterized by X-ray diffraction and infrared spectroscopy, the kaolinite from Alberta oil sands is found not expandable (Ignasiak et al., 1983). The smaller kaolinite particles have higher affinity to bitumen, leading to the loss of bitumen into fine tailings and the formation of the bitumen-stabilized sludge in tailings ponds (Ignasiak et al., 1983; Petzold et al., 2004).

2.2.4 Illite

Illite $[(K, H_3O)(Al, Mg, Fe)_2(Si, Al)_4O_{10}(OH)_2 \cdot (H_2O)]$ is a three-layer (2:1) aluminosilicate with two silicate sheets and one alumina sheet (Mitchell, 1993). The surface properties of illite are determined by the degree of amorphous substitution and the ionization of surface functional groups under different solution chemistry conditions.

Very little is known with respect to the properties of illite from the oil sands deposits. Ignasiak et al. (1983) found that less illite, compared to kaolinite, was associated with asphaltene from oil sands, indicating that it was more hydrophilic in nature. By measuring the adsorption isotherms of asphaltene and water to illite and kaolinite, Saada et al. (1995) reached the same conclusions as those of Ignasiak et al. (1983). On the other hand, Long et al. (2006) observed that illite particles did not flocculate in the process water of bitumen extraction (pH ~8.2, with 0.6 mM Mg^{2+} and 1.2 mM Ca^{2+}) in sedimentation tests for a period of 35 minutes, unless 7 mM Ca^{2+} and 5 mM Mg^{2+} were added to the suspension or solution pH was decreased to 2.9.

2.3 Interactions between Bitumen and Minerals

As shown in the previous sections, the high recovery of residual bitumen from oil sands tailings is usually achieved at the expense of degrading froth quality. Furthermore, satisfactory bitumen recovery is even harder to accomplish from fine tailings due to the severe mechanical entrainment of small particles ($<38 \mu m$). We suspect that poor liberation between bitumen and mineral matters accounts for these consequences.

Bitumen-minerals liberation is determined by the combination of all factors which influence the interaction of bitumen with minerals in aqueous solution. These factors include not only the intrinsic properties of bitumen and the minerals, e.g., quartz, kaolinite and illite, but also the physicochemical conditions of the pulp, such as temperature, pH, the presence of ionic species and their concentrations.

2.3.1 *Effect of Temperature*

It is generally agreed that a low temperature benefits bitumen liberation while a high temperature benefits bitumen flotation. This is because bitumen tends to engulf particle or bubble surfaces at high temperatures (Wang and Mikula, 2002). Clearly, solution temperature has conflicting roles in bitumen extraction since high degree of bitumen liberation and good bitumen flotation cannot be obtained at any one temperature. In reality, the inefficiency in either bitumen liberation or its flotation at a certain temperature can be compensated by the use of process reagents.

2.3.2 *Effect of NaOH*

It is observed that the addition of NaOH to oil sands slurry promoted the release of surfactants from the oil sands (presumably from the bitumen), which improve bitumen flotation (Sanford and Seyer, 1979). Schramm and Smith (1985) found that carboxylates released from oil sands drove the electrophoretic mobility of the bitumen droplets to a negative maximum, making their detachment from sands easier. However, in this case, one would expect that the attachment of the bitumen droplets to air bubbles become harder as well since the air bubbles are known to be negatively charged. Schramm and Smith (1985) believed that the attachment of bitumen droplets to air bubbles was through dispersion forces. In a subsequent study, Smith and Schramm (1992) claimed that NaOH was mainly consumed in precipitating multivalent metal ions such as Ca^{2+} , Mg^{2+} , Fe^{2+} , etc., that were present in the pulp. Dai and Chung (1995; 1996) and Basu et al. (1997) also showed that an alkaline pH benefited the liberation of bitumen from sands. Dai and Chung (1995) explained this detachment behavior based on DLVO theory, which implied that the principal detachment force was electrostatic repulsion caused by particle surface charges. However, a NaOH overdose cause bitumen emulsification and loss into tailings (Dai and Chung, 1996), leading to the formation of stabilized fine tailings in tailings ponds (Sanford and Seyer, 1979). A significant decrease in bitumen aeration is observed when the concentration of surfactants is over a critical level, corresponding to high pH (>11) (Schramm et al., 1984; 1985; 2003).

2.3.3 *Effect of Clays and Mineral Slimes*

Basu et al. (1998) found that the presence of clays (either hydrophobic or hydrophilic) did not affect the contact angles of bitumen on glass slides; therefore, the clays did not affect bitumen liberation from sands, and their detrimental roles on bitumen extraction were attributed to other factors. Kasongo et al. (2000) studied the effect of three clay minerals, kaolinite, illite and montmorillonite, on bitumen flotation at pH 7.5 to 8. They observed that, at the 1 wt% dosage that was tested, kaolinite and illite did not have any detrimental effects on bitumen flotation. Montmorillonite influenced bitumen flotation, but only when Ca^{2+} (40 mg/L) was also present. It was not clear if the deteriorated bitumen flotation was due to bitumen-mineral liberation or due to bitumen flotation. This finding was supported by Liu et al. (2004) who used atomic force microscopy (AFM) to measure the interactions between a kaolinite probe and a bitumen droplet. Liu et al. (2004) reported that kaolinite was weakly attached to bitumen with or without 10^{-3} mol/L Ca^{2+} , while montmorillonite was strongly adhered to bitumen in the presence of the Ca^{2+} ions.

On the other hand, Dai and Chung (1995) observed that bitumen could be easily liberated from coarse sands ($>129 \mu\text{m}$) when pulp pH was raised to alkaline region. However, for fine particles ($<100 \mu\text{m}$), the liberation was not possible. Clark and Pasternack (1932) also found that the presence of 2–10% of clay in the oil sands deposit caused substantial decrease in bitumen yields for three different oil sands samples. Similarly, Sanford (1983) and Takamura and Wallace (1988) reported that bitumen recovery was inversely correlated to the fines (clays) content in oil sands. Using a micromechanical device, Moran et al. (2000) observed that contact of bitumen on air bubble surfaces was not possible when kaolinite was present in the system. Their observation seems to contradict those of Kasongo et al. (2000). The tests of Moran et al. (2000) were conducted in simulated process water that contained many different electrolytes, including 0.3 mM CaCl_2 and 0.3 mM MgCl_2 . The composition of the water was more complicated than that used by Kasongo et al. (2000). It was possible that the presence of the various ions caused the difference. Tsamantakis et al. (2005) used the same device as Moran et al.

(2000) and showed that the co-presence of 100 ppm Ca^{2+} and montmorillonite prevented the coalescence of bitumen droplets.

The discrepancy regarding the effects of clays and slimes on bitumen liberation can arise from the differences in experimental techniques and conditions. For instance, Kasongo et al. (2000) did not observe any detrimental effect in the presence of kaolinite and Ca^{2+} , as opposed to Clark and Pasternack (1932) and Moran et al. (2000). This is likely due to the low concentration (1 wt%) of kaolinite that was used (compared to the 2–13 wt% used by Clark and Pasternack, 1932), and the simple water composition compared to the more complicated water composition used by Moran et al. (2000). It should also be noted that kaolinite has different properties on the edges and basal surfaces. It is not clear in the AFM studies by Liu et al. (2004) whether the kaolinite probe used represents the edge or basal surface. If smooth basal surface is probed, the interaction of the slightly negatively charged basal surface with the like-charged bitumen would be weak, compared to the fractured edge surface.

The detrimental effect of clays on bitumen liberation is also evidenced by their high affinity to organic matters as shown by numerous studies. Clays were able to adsorb asphaltene (Bantignies et al., 1998; Tu et al., 2006) on their surfaces. Saada et al. (1995) found that kaolinite had higher affinity for asphaltene than illite, and was preferentially wetted by oil. A number of researchers (Farnand et al., 1985; Kotlyar et al., 1988; 1990; 1995; 1998; 1999; Majid and Sparks, 1983; Majid et al., 1993; Bensebaa et al., 2001; Sparks et al., 2003; Darcovich et al., 1989; Jada et al., 2006) demonstrated that clays and mineral slimes in oil sands were partially covered by solvent-insoluble humic substances, and thus became, to some extent, hydrophobic. Consequently, the hydrophobic clays were either floated along with bitumen (degrading the froth quality), or carried away by the streams with associated bitumen (reducing bitumen recovery), depending on the hydrophobicity of the clays and mineral slimes.

In addition, some amorphous minerals, primarily iron and aluminum oxides, are found tightly bonded by organics (Kotlyar et al., 1987; 1990). They are poorly liberated from

bitumen, and often reported to the bitumen froth. They are considered partially responsible for the formation of mature fine tailings (MFT) in tailing ponds (Omotoso and Mikula, 2004).

2.3.4 *Effect of Electrolytes*

Oil sands extraction pulp contains many ionic species which have complicated effects on bitumen liberation and flotation. High concentrations of monovalent metal ions such as Na^+ and K^+ are known to lower bitumen recovery. Takamura and Wallace (1988) observed the coagulation of kaolinite at high Na^+ concentration and concluded that the coagulation of fines (clays) was the main reason for the poor recovery of low-grade oil sands ores (which usually have high clay contents). Basu et al. (1997) observed that although the contact angles of bitumen on glass slides were larger at pH 11 than at pH 8.2 (thus the bitumen would be easier to detach at pH 11), the presence of high concentrations of Na^+ led the contact angles to drop faster at pH 11 than at pH 8.2, and eventually became lower than that at pH 8.2. However, the concentration of Na^+ that caused such effect was much higher than the concentration of Na^+ that deteriorated bitumen flotation in the commercial circuit. Therefore, Basu et al. (1997) believed that the detrimental effect of Na^+ must originate from other causes than bitumen liberation.

Compared to monovalent ions (Na^+ and K^+), multivalent metal cations such as Ca^{2+} , Mg^{2+} , and $\text{Fe}^{2+}/\text{Fe}^{3+}$ have more complicated roles in bitumen extraction. By studying the effect of Ca^{2+} , Mg^{2+} , Fe^{2+} and Fe^{3+} on bitumen recovery from three high grade oil sands samples, Clark and Pasternack (1932) observed a dramatic reduction (from ~95% to ~35%) of bitumen recovery depending on the concentrations of these multivalent metal cations. Fong et al. (2004) and Ding et al. (2006) also found that the bitumen recovery from Alberta oil sands was reduced in the presence of divalent metal ions (Ca^{2+} , Mg^{2+}) and clays (kaolinite, illite). They postulated that the divalent metal cations promoted the aggregation between bitumen and solids and thus lowered the bitumen recovery. Zhou et al. (1999) observed strong coagulation between bitumen and silica in acidic pH range with a maximum at pH 4, and no coagulation in alkaline pH. This confirmed that bitumen

could be readily liberated from sands at alkaline pH. However, in the presence of Ca^{2+} , the observation was reversed: low degree of coagulation (~20%) was observed at acidic to slightly alkaline pH, and complete coagulation was observed above about pH 10. Thus bitumen liberation from sands was impossible above pH 10 when Ca^{2+} was present. The results were explained in terms of the activation of silica by CaOH^+ which promoted the adsorption of anionic surfactants that were released from bitumen. Adsorption of these surfactants rendered silica surfaces hydrophobic, which then aggregated with bitumen (Zhou et al., 1999).

These multivalent metal cations could interact with both silica surfaces and bitumen droplets, for both were highly negatively charged (the iso-electric point was at about 1.5 for silica and about 3 for bitumen) (Zhou et al., 1999). It was well documented that the negatively charged silica surfaces only reacted with CaOH^+ but not with Ca^{2+} so that strong uptake of calcium by silica only occurred above about pH 10.5 (Fuerstenau and Palmer, 1976). However, Ca^{2+} ions could interact with the negatively-charged bitumen droplets since the charge on bitumen surfaces originated from carboxylic and phenolic groups which can bond to Ca^{2+} . In fact, as discussed earlier, montmorillonite only had a detrimental effect at pH 7.5–8 when 40 mg/L Ca^{2+} was present (Kasongo et al., 2000).

From the forgoing review, it can be seen that the effect of pH, clays and metal cations, and their combinations on bitumen-mineral liberation are still poorly understood. Thus, a systematic study of the roles played by multivalent metal cations in bitumen-mineral, bitumen-bitumen, and bitumen-air interactions is needed to better understand and improve the bitumen extraction process from oil sands.

2.3.5 *Effect of Organic Complexing Agents*

Despite the fact that the detrimental effect of multivalent metal cations on bitumen recovery from oil sands is observed from time to time, very few studies have been conducted to reduce or eliminate this effect.

Theoretically, there are three approaches to remove multivalent metal cations from the aqueous solutions: ionic exchange, precipitation and complexation. In ionic exchange process, metal cations are retained by ionic exchange composites (resins) packed in a column. This method is commonly applied in water treatment (purification) and apparently not suitable for bitumen extraction streams. Metal cations can also be removed by precipitation in the form of low-solubility compounds such as carbonates, phosphates, silicates or hydroxides. However, if the precipitates interact strongly with either bitumen or mineral particles under the process conditions, the physicochemical differences between bitumen and minerals, which are essential to liberation and separation, will diminish owing to the precipitates. For instance, Yan and Masliyah (1994) reported that ultrafine particles, including newly formed precipitates, had a high affinity to oil/water interfaces, and sterically prevented oil droplets from coalescence and aeration. The adverse effect can be more severe. A metal precipitate may carry opposite surface charge to bitumen and minerals; the metal precipitate can act as a binder to bridge bitumen with minerals, leading to undesirable bitumen-minerals aggregation. In spite of this concern, a few studies have been conducted using the precipitation scheme. Li et al. (2005) reported that the addition of 2×10^{-2} mol/L acidified sodium silicate eliminated the adverse effect of 10^{-3} mol/L Ca^{2+} and Mg^{2+} contained in process water, leading to an increase in bitumen recovery. They believed that the precipitation of calcium or magnesium silicate was responsible. Clark and Pasternack (1932) considered that sodium carbonate was a better pH regulator than sodium hydroxide, owing to its ability to precipitate Ca^{2+} and Mg^{2+} as insoluble carbonates in the process water of bitumen extraction.

In contrast, the complexation scheme does not actually remove metal cations from aqueous solution. It only eliminates the free metal cations by forming aqueous soluble metal-ligand complexes. Organic acids such as oxalic acid, citric acid and ethylenediaminetetraacetic acid (EDTA) can be used for this purpose. Since they contain carboxylic groups (as shown in Figure 2-1) which are dissociated at a specific pH, dissociated carboxylic anions can react with the multivalent metal cations to form metal-organic complexes.

However, little study has been published concerning the application of organic acids to bitumen extraction. Only two reports were found relevant. Bichard and Edward (1967), and Beetge et al. (2005) claimed that the addition of chemical reagents containing carboxylic groups benefited bitumen extraction from Alberta oil sands. No systematic experimental results and explanations were provided.

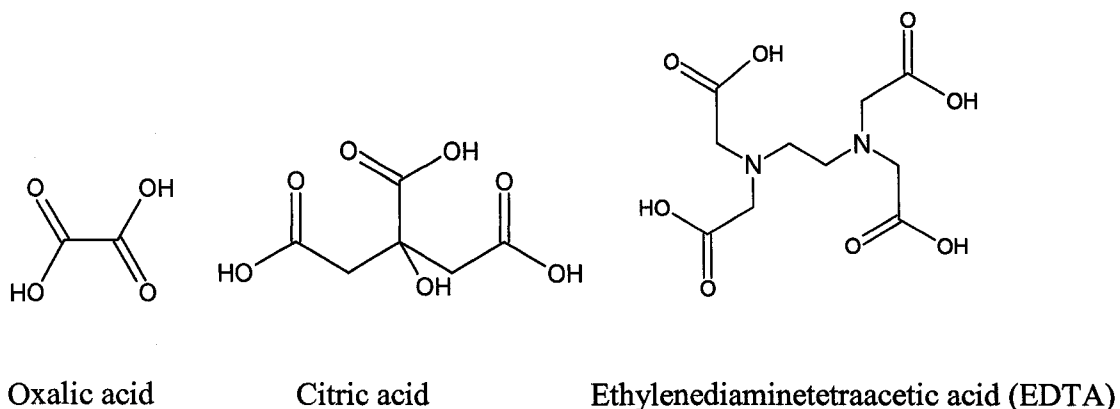


Figure 2-1 Molecular structure of oxalic acid, citric acid, and ethylenediaminetetraacetic acid (EDTA).

Due to the sparse literature in this field, the literature survey was expanded to relevant industries such as mineral processing and environmental engineering.

Many reports indicated that organic acids could remove heavy metal ions from mineral surfaces. Liu and Zhang (2000) found that citric acid could effectively remove calcium ions from chalcopyrite surfaces, thus increasing the selectivity of flotation separation between chalcopyrite and galena using dextrin. Citric acid and EDTA could inhibit the nucleation and crystal growth of calcium sulfate and calcite (Prisciandaro et al., 2003; 2005; Westin and Rasmuson, 2003). Oxalic acid, citric acid and EDTA were used to remove metal ions such as Fe^{2+} , Ni^{2+} , Cd^{2+} , from contaminated water and soils (Ambikadevi and Lalithambika, 2000; Tandy et al., 2004; Konya and Nagy 1998; Bassi et al., 2000). Ikhsan et al. (2004) reported that aspartic acid could markedly lower the

adsorption of Cu^{2+} and Co^{2+} on kaolinite through the formation of metal-aspartate complexes.

In addition to removing multivalent metal cations from mineral surfaces, organic acids could modify mineral surface properties. Popov et al. (2004) reported that chelating agents including citric acid, EDTA and succinic acid notably increased the zeta potential value of the natural clay particles at different pH. They speculated that the adsorption of the chelating anions and the dissolution of the amorphous hydroxyl/oxide film from the surface of the clay particles were responsible. They also believed that non-phosphorlated chelating agents such as EDTA and citric acid had weaker adsorption capacity on the clay particles than the phosphorlated ones such as 1-hydroxypropane-1,1-bisphosphonic acid (HEDPA). On the other hand, Lackovic et al. (2003) studied the adsorption of citric acid on goethite, kaolinite, and illite using potentiometric titration and attenuated total reflectance Fourier-transform infrared spectroscopy (ATR-FTIR). They observed that citric acid was significantly adsorbed on goethite through surface complexes formation, compared to kaolinite and illite. The adsorption density of citric acid decreased with increasing pH. Their findings were similar to the adsorption of oxalic acid and citric acid on $0.09 \mu\text{m}$ spherical hematite ($\alpha\text{-Fe}_2\text{O}_3$) particles reported by Zhang et al. (1985), and the adsorption of EDTA on goethite (FeOOH) reported by Nowack and Sigg (1996). Ward and Brady (1998) found that oxalic acid had higher affinity to kaolinite than to quartz at pH 6–9. They considered that the presence of alumina sites on kaolinite was accountable.

2.4 Colloidal Particle Interactions

2.4.1 *Classical DLVO Theory*

Liberation of bitumen from associated mineral solids in aqueous solution is a complex process which involves multiple phases (solid/bitumen/water) interaction determined by the relevant colloidal forces. The fundamental colloidal forces, as described by classical DLVO theory (Derjaguin and Landau, 1941; Verwey and Overbeek, 1948), are the

attractive van der Waals forces and the repulsive electrostatic force. The combination of these two interactions, to a large extent, controls the dispersion (liberation) or coagulation of colloidal particles in an aqueous system.

Van der Waals forces consist of *Keesom* interactions (permanent dipole-permanent dipole interactions), *Debye* interactions (permanent dipole-induced dipole interactions) and *London* or *dispersion* interactions (induced dipole-induced dipole interactions) (Hiemenz and Rajagopalan, 1997). They are primarily governed by the nature of macroscopic bodies and the separating media. The free energy of interaction due to van der Waals forces between two spheres (with radius R_1 and R_2 that are much greater than separation distance H) has the form (Israelachvili, 1992),

$$V_V = -\frac{AR_1R_2}{6H(R_1 + R_2)} \quad (2-1)$$

in which the Hamaker constant A can be calculated by Dzyaloshinskii-Lifshitz-Pitaevskii (DLP) theory (Dzyaloshinskii et al., 1961) based on dielectric “constant”, or surface tension measurement (Hiemenz and Rajagopalan, 1997). Rabinovich and Churaev (1979) derived van der Waals interaction energy by considering retardation effect of electromagnetic dipoles:

$$V_V = -\frac{A_{132}R_1R_2}{6H(R_1 + R_2)} \left[1 - \frac{1 + 2bl}{1 + bc/H} \right] \quad (2-2)$$

where $b = 3.1 \times 10^{-17}$ sec/rad, $l = 3.3 \times 10^{15}$ rad/sec, c is the speed of light in vacuum. For the interaction of two different phases 1 and 2 in a medium of 3, the combined Hamaker constant A_{132} can be calculated through the combination law:

$$A_{132} = \left(\sqrt{A_{11}} - \sqrt{A_{33}} \right) \left(\sqrt{A_{22}} - \sqrt{A_{33}} \right) \quad (2-3)$$

Electrostatic double layer force. A surface can carry different charges originating from various mechanisms such as ionization or dissociation of surface functional groups (–OH, –COOH, etc.), specific adsorption from solution, and dissolution of surface lattice ions. The charged surface is balanced by an equal but opposite charged regions of counterions, some of which are bound, usually transiently, to the surface within the so-called Stern plane, while others form an atmosphere of ions in rapid thermal motions close to the surface, known as a diffused electrical double layer (Israelachvili, 1992; Hiemenz and Rajagopalan, 1997).

As the two like charged surfaces approach, they repel each other through electrostatic interaction arising from electrical double layer overlap. The electrostatic interaction energy of two spherical surfaces with radii of R_1 , R_2 in aqueous solution is given by Hogg et al. (1966).

$$V_E = \frac{\epsilon R_1 R_2 (\psi_1^2 + \psi_2^2)}{4(R_1 + R_2)} \left[\frac{2\psi_1 \psi_2}{\psi_1^2 + \psi_2^2} \ln \left(\frac{1 + e^{-\kappa H}}{1 - e^{-\kappa H}} \right) + \ln(1 - e^{-2\kappa H}) \right] \quad (2-4)$$

in which ψ_1 and ψ_2 are the surface potentials, H is the separation distance between surfaces, ϵ is the permittivity of the medium, κ is the inversed Debye length,

$$\kappa^{-1} = \left(\frac{\epsilon k T}{e^2 \sum_i z_i^2 n_{i,\infty}} \right)^{1/2} \quad (2-5)$$

where k is the Boltzmann constant, T is the absolute temperature in Kelvin, z_i is the valence of ion i , $n_{i,\infty}$ is the concentration of ion i in the bulk solution. It is apparent that at a given temperature, the Debye length is only determined by the type and concentration of electrolytes. Multivalent electrolytes have much greater effect to compress the electrical double layer than the monovalent ones of the same concentration. For instance, at 25°C, the Debye length of a surface in 10^{-3} mol/L 1:1 electrolyte is 9.2 nm, compared to 5.6 nm in the presence of 2:1 electrolytes of the same concentration.

Since it is difficult to obtain the surface potential Ψ_1 or Ψ_2 experimentally, zeta potential ζ , the potential at the shear (slipping) plane is often used to approximate the surface potential. Multivalent metal cations significantly affect the zeta potentials of oxides (minerals) by electric screening effect and adsorption (Kaya and Yukselen, 2005). The adsorption of ions on the electrical double layer can substantially modify the zeta potential. If the adsorption only happens in the outer Stern plane, e.g., adsorption of indifferent counter ions, the zeta potential only varies in magnitude. In contrast, if adsorption occurs in the inner Stern plane, e.g., through specific adsorption, ionic exchange, solvation effect, etc., the zeta potential can change in both the magnitude and the sign. Therefore, zeta potential measurement can provide insightful information with respect to the adsorption of ions on the surfaces of interest (Hunter and James, 1992; Fuerstenau and Pradip, 2005).

Classical DLVO theory has been widely used to describe and predict the interaction between two colloidal surfaces approaching each other due to its simplicity. However, it fails to predict many interactions of real systems due to two reasons. Firstly, many assumptions made to derive the DLVO theory, such as dielectric continuum, smooth and homogenous surfaces, etc. break down in real systems. Secondly, non-DLVO forces are present and contribute to the interaction between colloidal particles along with electrostatic double-layer force and van der Waals forces.

2.4.2 *Extended DLVO Theory: Incorporating non-DLVO interactions*

Several new forces have been invoked to explain a variety of short-ranged phenomena. These forces include attractive hydrophobic force between hydrophobic particles (Israelachvili and Pashley, 1984), repulsive hydration force between hydrophilic surfaces (Pashley, 1981; 1982; Israelachvili and Pashley 1983; Ducker et al., 1991), and repulsive steric forces and attractive bridge force for polymer bearing surfaces (Klein, 1980; Israelachvili and Pashley, 1984).

Hydrophobic force, an attractive interaction between two approaching hydrophobic surfaces submerged in aqueous solutions, has been extensively studied (e.g., Derjaguin and Kusakov, 1939; Israelachvili and Pashley, 1984; Ducker et al., 1994; Rabinovich and Yoon, 1994). This attractive interaction not only occurs between hydrophobic surfaces (with surfactant or polymer coating), but also arises between hydrophilic particle and hydrophobic surface (Claesson et al., 1987; Tsao et al., 1993; Ducker et al., 1994).

Many mechanisms have been proposed concerning the origin of the hydrophobic force. These include the entropy increase due to rearrangement of water molecules around a non-polar molecule (Frank and Evans, 1945; Derjaguin and Churaev, 1974); capillary force due to the cavitation in the vicinity of hydrophobic surfaces (Yushchenko et al., 1983); and nano-bubbles from hydrophobic surfaces (Ducker et al., 1994). Regardless of the different mechanisms, many researchers found that the magnitude of the measured hydrophobic interaction was about ten times greater than van der Waals forces for a given system (Israelachvili and Pashley, 1984; Israelachvili and McGuiggan, 1988; Rabinovich and Yoon, 1994). This suggests that the hydrophobic force is too significant to be neglected when evaluating the interaction between hydrophobic particles such as bitumen droplets.

In spite of the extensive studies conducted, no theoretical framework has been developed to describe and interpret all experimental observations. A double-exponential function of the form developed by Pashley et al. (1985) is used by many investigators to describe the hydrophobic forces:

$$\frac{F}{R} = C_1 \exp\left(-\frac{H}{D_1}\right) + C_2 \exp\left(-\frac{H}{D_2}\right) \quad (2-6)$$

in which F is the attractive hydrophobic force, R is the curvature of the surface, H is the closest distance separating the two interacting surfaces, D_1 and D_2 are the decay lengths, and C_1 and C_2 are parameters characterizing the magnitudes of the short- and long-range hydrophobic forces, respectively. The term "short-range" refers to the attractive

hydrophobic forces observed at $H < 10$ nm with decay length of 1–2 nm rather than the true interatomic short-range forces (Pashley et al., 1985).

The hydrophobic forces can also be described by a power law (Rabinovich and Derjaguin, 1988)

$$\frac{F}{R} = -\frac{K}{6H^2} \quad (2-7)$$

where K is the only fitting parameter. This equation is in the form of the van der Waals forces equation. However, K is generally much larger than the Hamaker constant (Rabinovich and Yoon, 1994). An expression has been derived by Yoon and Mao (1996) to calculate the total interaction energy (V_{HB}) between the bubble and particle contributed by hydrophobic interaction:

$$V_{HB} = -\frac{K_{132}R_1R_2}{6(R_1 + R_2)H} \quad (2-8)$$

where R_1 and R_2 are the radii of bubble and particle, respectively; K_{132} is the hydrophobic constant (fitting parameter) which varies substantially due to the differences in surface properties and separating media.

Hydration force is the solvation force in aqueous solution, caused by the structure of water between the surfaces. Pashley and Israelachvili (Pashley, 1981; 1982; Israelachvili and Pashley, 1983) showed that the hydration repulsion between two mica surfaces across a monovalent electrolyte was intimately related to the hydration number of the cation, i.e., the average number of water molecules in the first shell. Pashley and Israelachvili (1984) found that the concentrated (>1 M) divalent cations (Ca^{2+} , Mg^{2+}) prevented two mica surfaces from coagulation due to the strong, short-range (0.2–2.0 nm) repulsive force. They concluded that the repulsion was originated from the residual hydration of the adsorbed divalent cations. Marcelja (1997) found that most counterions

adsorbed on the mica surfaces at separations larger than 2 nm. When the surfaces were brought closer together at about 1.4 nm, the denser surface layers of favorably packed hydrated counterions come into contact, resulting in strong repulsion by the hydration force. Israelachvili and Wennerström (1997) believed that the monotonically repulsive hydration forces were not due to the structured water layers propagating away from a surface, but to the osmotic effect of hydrated ions electrostatically trapped between two approaching surfaces.

On the other hand, Chapel (1994) drew opposite conclusions after studying the hydration force between fused silica surfaces, in the monovalent electrolyte containing Cs^+ , K^+ , Na^+ and Li^+ using a surface force apparatus (SFA). He observed that the hydration force decreased with the size of the hydrated ions, and that the more hydrated the ions, the weaker the hydration force. He considered that the hydroxyl groups present on the silica surface were responsible for the water structure that gave rise to the observed forces. The water structure with hydrogen bonding network was destroyed by the cations with a resultant decrease in hydration force. Chapel's findings confirm the "structure breaking" (Frank and Evans, 1945; Frank and Wen, 1957) effect of some ions on the hydrated surfaces.

Steric and bridging forces. Steric force is a repulsive interaction between two solid surfaces bearing a high surface coverage of adsorbed flexible polymers in aqueous solution, and bridging force is an attractive force between two solid surfaces due to the adsorption of flexible polymer from aqueous solutions (Bigg, 1995). Rutland and Senden (1993) showed that a short range steric barrier occurred between the surfaces of colloidal silica with adsorbed nonionic surfactants. Using an AFM, Biggs (1995) recorded the repulsive force between a 10 μm radius spherical zirconia and a flat polished zirconia ceramic plate with high coverage of polyacrylic acid on both surfaces. The repulsive force increased exponentially with decreasing separation of the surfaces from around 180 nm to 20 nm. In contrast, attractive bridging force was present when the substrates had low coverage of the polymer.

Both classical and extended DLVO theories have been applied to understand the interaction of bitumen with minerals. Dai and Chung (1995), Drelich and Miller (1992) showed that classic DLVO theory could satisfactorily describe the interactions between spherical silica and bitumen plate in aqueous solution. On the other hand, Liu et al. (2005) believed that some non-DLVO forces, such as the repulsive hydration force for hydrophilic surfaces, attractive hydrophobic force between hydrophobic particles, repulsive steric forces and attractive bridge forces for polymer-bearing surfaces should be incorporated into classical DLVO theory to better fit the experimental data. Due to the differences of the systems investigated, neither classical nor extended DLVO theory can predict and interpret all interactions of different systems. The appropriate theory has to be determined in terms of the properties of colloidal particles (hydrophobicity, hydrophilicity) involved and the physicochemical conditions (the presence of surfactant, polymer, etc.).

Nevertheless, it remains difficult to incorporate non-DLVO interactions without clearly quantifying to what extent these non-DLVO forces (hydration force, hydrophobic force, etc.) contribute to the total interaction energies between different surfaces. Despite the fact that the hydrophobic force may exist between bitumen droplet and minerals, kaolinite in particular, hydrophobic interaction is not incorporated in classical DLVO calculation due to the uncertainty of the hydrophobic constant in the expression (2-8).

2.4.3 *Adsorption of Multivalent Metal Cations on Minerals*

The colloidal forces, particularly electrical double layer force, between particles can be significantly influenced by adsorption of multivalent metal cations as a result of modification of surface electrokinetic property. Therefore, a brief literature review is conducted with respect to adsorption of metal cations on minerals.

Cations and anions are hydrated in different ways in aqueous solutions (Webb, 1926; Latimer et al., 1939). The difference in the free energies of ions in aqueous solution and in vacuum is defined as hydration energy. The hydration energy is proportional to the

valence and inversely correlated to the effective ionic radii, i.e., the smaller the ions and the higher the charge valence, the higher the hydration energy. Many models have been developed to evaluate the hydration free energy due to its significant role in the interactions between ions and surfaces in aqueous solutions. For instance, the hydration energy of a metal cation significantly affects its adsorption on a negatively charged surface (Malati, 1987), since energy is required to remove the hydration sheath of metal ions for adsorption to occur.

The adsorption of multivalent metal cations onto minerals has been extensively investigated, and the findings are widely used in many industries including mineral processing. The adsorption of metal cations remarkably alters colloidal stabilities by modifying surface characteristics such as electrokinetic properties (Hunter and James, 1992). Many theories have been proposed to interpret the experimental observations on metal ion adsorption. These include ionic exchange (Huang and Stumm, 1973), surface induced hydrolysis (Davis et al., 1978), surface complexation (James and Healy, 1972a; 1972b; 1972c; Jang and Fuerstenau, 1986) and surface precipitation (Farley et al., 1985). For adsorption of metal ions on oxides, the surface complexation hypothesis is widely accepted (Crawford et al., 1993a, 1993b). A thermodynamic model proposed by James and Healy (1972c) is used to quantify the free energy change of adsorption. In this model, the free energy change for an ion to migrate from an infinite distance in the bulk to a surface, i.e., the free energy change of adsorption ($\Delta G_{ads, i}$) is determined by three terms: an attractive coulombic term ($\Delta G_{coul, i}$), a repulsive secondary solvation energy term ($\Delta G_{solv, i}$), and an adjustable or “chemical” free energy term ($\Delta G_{chem, i}$), as in the form of (2-9).

$$\Delta G_{ads, i} = \Delta G_{coul, i} + \Delta G_{solv, i} + \Delta G_{chem, i} \quad (2-9)$$

The repulsive secondary solvation term stands for the change in energy required to remove the hydration sheath of hydrated ions for adsorption to occur, which is virtually a reverse process of hydration. In calculating the secondary solvation energy, hydrated radii of metal cations are equivalent to the sum of the metal crystal radii and the diameter

of one water molecule. James and Healy (1972c) treated the first-order metal-hydroxyl complexes the same as their hydrated metal cations with respect to the ionic radii, which was not well founded. Therefore, the effective radii of the first-order metal-hydroxyl species have to be established in order to correctly calculate their solvation energies of adsorption. Unfortunately, these are not available in the literature.

It has been observed that the adsorption of multivalent metal cations on metal oxides and clays occurs and reaches a maximum within a very narrow pH range correlated to the hydrolysis and precipitation of the metal cations. These narrow pH ranges make it difficult to differentiate the true adsorption from the surface precipitation/co-precipitation (Sposito, 1986; Kinniburgh and Jackson, 1981), despite the general observation of adsorption prior to the initiation of the bulk precipitation from solution (Tewari et al., 1972; James and Healy, 1972a). Therefore, characterization of the adsorbed metal ionic species is crucial to understand the mechanism of adsorption of metal cations on the hydrous oxides and clay minerals. X-ray photoelectron spectroscopy (XPS) and Fourier-transform infrared spectroscopy (FTIR) have been applied to characterize the surface complexes and/or surface precipitates on minerals (Freeman and Rowell, 1981; Van Riemsdijk and Lyklema, 1980; Goldberg and Sposito, 1985). X-ray diffraction (XRD), Raman Spectroscopy, magnetic resonance spectroscopy (nuclear and electron) and electron spin resonance (ESR) spectroscopy are also reportedly used to detect surface precipitation without dehydrating the sample (Freeman and Rowell, 1981; Goldberg and Sposito, 1985; McBride, 1982). Dillard and Koppelman (1982) analyzed the chemical nature of adsorbed cobalt on the surface of kaolinite at different pH with XPS. They established that with increasing pH, kaolinite-cobalt bonding was similar to that of cobalt hydroxides.

Among the techniques used to characterize the adsorbed ionic species, XPS and ATR-FTIR are considered effective. Since XPS has a high sensitivity in analyzing the valence states and quantifying the adsorbed species, while ATR-FTIR has the advantage that no treatment is required for the samples to be analyzed.

2.4.4 *Ionic Equilibrium: Speciation Diagrams*

In solutions containing multiple components, the components react simultaneously with one another and reach an equilibrium state eventually. The equilibrium concentration of the species is controlled by formation constants under a given condition. Therefore, the distribution of species can be calculated provided that the equilibrium constants are known (Butler and Cogley, 1998). The speciation diagrams are useful in identifying the dominant species in solutions involved in reactions.

Speciation diagrams have been widely used in the studies of adsorption of ionic species on minerals (e.g., Mpofu et al., 2003; Ikhsan et al., 2004; Sverjenski, 2006; Sverjensky and Fukushi, 2006). However, the speciation diagrams should be used with caution due to two reasons. First, the equilibrium constants may be obtained at a certain condition that is different from the experimental conditions used in another study. Second, the reactions in a study may not reach equilibrium under the test conditions.

3 EFFECT OF MULTIVALENT METAL CATIONS ON BITUMEN-MINERAL COAGULATION¹

3.1 Introduction

Poor bitumen liberation from minerals such as quartz, kaolinite and illite arises from its strong interactions (coagulation) with these minerals. As discussed in the literature review, the presence of multivalent metal cations enhances these interactions. However, the mechanisms by which the multivalent metal ions such as Ca^{2+} , Mg^{2+} , Fe^{2+} and Fe^{3+} affect the coagulation between bitumen and minerals remain poorly understood. Thus there is a need to systematically investigate the bitumen-mineral coagulation at different pH in the suspensions containing various multivalent metal cations.

This chapter summarizes the results of testwork on the mutual coagulation between an organic phase (oil or bitumen) and inorganic minerals (quartz, kaolinite, illite and montmorillonite). Hexadecane, with and without doping with sodium oleate, a solvent-diluted-bitumen, high purity quartz, kaolinite, illite and montmorillonite clays are used. The coagulation between the hexadecane (or bitumen) and the mineral particle is studied in the presence and absence of 10^{-3} mol/L of a multivalent metal cation such as Ca^{2+} , Mg^{2+} and Fe^{3+} .

3.2 Experimental

3.2.1 *Materials and Chemicals*

High purity fine quartz sample (<20 μm and >99% SiO_2) was purchased from Boud Minerals and Polymers, UK, and used as received. Kaolinite, illite and montmorillonite samples were purchased from Ward's Natural Scientific Establishment, Ontario. The kaolinite sample was used directly in the tests. Chemical analysis and X-ray diffraction

¹ Portions of this chapter have been published in Journal of Colloid and Interface Science, Vol. 310, 489-497 (2007) by Mingli Cao, Weibing Gan and Qi Liu.

indicated that the sample contained about 86% kaolinite and 6% muscovite. Illite sample was crushed, ground and screened to collect the $-45\ \mu\text{m}$ fraction that was used in the experiments. The illite sample was estimated to contain about 50% illite with the rest being mainly quartz and muscovite. The montmorillonite sample originated from Wyoming and was mainly Na-montmorillonite. It was used in the experiments after soaking in distilled water for more than 12 hours. Quartz, kaolinite and illite were also mixed in some tests at a mass ratio of 80:14:6 and used as the mineral solids to simulate the oil sands.

A $-63+25\ \mu\text{m}$ quartz sample, separated from the $-63\ \mu\text{m}$ quartz (99.4% SiO_2 , purchased from Boud Minerals and Polymers, UK) using a 500-mesh ($25\ \mu\text{m}$) sieve, was used for the visualization experiment.

Hexadecane, model oil or solvent-diluted-bitumen was used as the hydrocarbon phase in coagulation experiments. Hexadecane (density = $0.77\ \text{g/cm}^3$) was used without further treatment. The model oil was obtained by dissolving 10^{-3} mol of sodium oleate in 1 liter hexadecane with the aid of a circular shaker and an ultrasonic bath. The solvent-diluted-bitumen was prepared by dissolving the bitumen froth (Coker feed provided by Syncrude Canada Ltd.) with heptane and toluene at a mass ratio of 1:3:1 (bitumen:heptane:toluene). The solvent-diluted bitumen was allowed to settle for 24 hours to remove solid impurities by decantation before use.

The chemical reagents used in this study were purchased from several suppliers, as listed in Table 3-1.

Table 3-1 Chemical reagents used in the experiments.

Chemical	Supplier	Grade	Use
Aluminum chloride (AlCl_3)	Fisher Scientific	98.5%	Additive electrolyte
Calcium chloride ($\text{CaCl}_2 \cdot 2\text{H}_2\text{O}$)	BDH Inc.	74–78%	Additive electrolyte
Ferric chloride Solution (FeCl_3)	Fisher Scientific	40% W/V	Additive electrolyte
Ferrous chloride ($\text{FeCl}_2 \cdot 4\text{H}_2\text{O}$)	Fluka Chemika	Minimum 99.0%	Additive electrolyte
Hexadecane ($\text{CH}_3(\text{CH}_2)_{14}\text{CH}_3$)	Fisher Scientific	Mol % 99.3%	Simulating bitumen oil phase
Lead nitrate ($\text{Pb}(\text{NO}_3)_2$)	Fisher Scientific	99.6%	Additive electrolyte
Magnesium chloride solution ($\text{MgCl}_2 \cdot 6\text{H}_2\text{O}$)	LabChem Inc.	51%	Additive electrolyte
Manganous Sulfate ($\text{MnSO}_4 \cdot \text{H}_2\text{O}$)	Fisher Scientific	98.2%	Additive electrolyte
Sodium hydroxide (NaOH)	Fisher Scientific	99.0%	pH regulator
Sodium oleate	Riedel-dehaën	Minimum 82%	Additive carboxylate in oil phase

3.2.2 *Experimental Methods*

Coagulation experiments. Coagulation experiments were conducted at room temperature following the procedures of Zhou et al. (1999) with some modifications: two grams of the fine mineral powder (quartz, kaolinite, illite or their mixtures) were dispersed in 200 mL distilled water in a baffled plexiglas agitation cell (Figure 3-1). The suspension was agitated with a mechanical stirrer at 620 rpm for 8 minutes during which the suspension pH was adjusted to a desired value. Metal salts were added at the controlled pH at this stage as well if required. This was followed by the addition of 25 mL oil (hexadecane, model oil or solvent-diluted bitumen) and another 8 minutes of agitation. The mixture of mineral solids and oil was then transferred to the separating column (Figure 3-1). The oil droplets generated during mixing were allowed to rise for 3 minutes (10 minutes for solvent-diluted bitumen). During this period, it was usually observed that an oil-in-water emulsion zone was formed on the top part of the slurry. The suspended mineral solids below the emulsion phase were drained through the bottom of

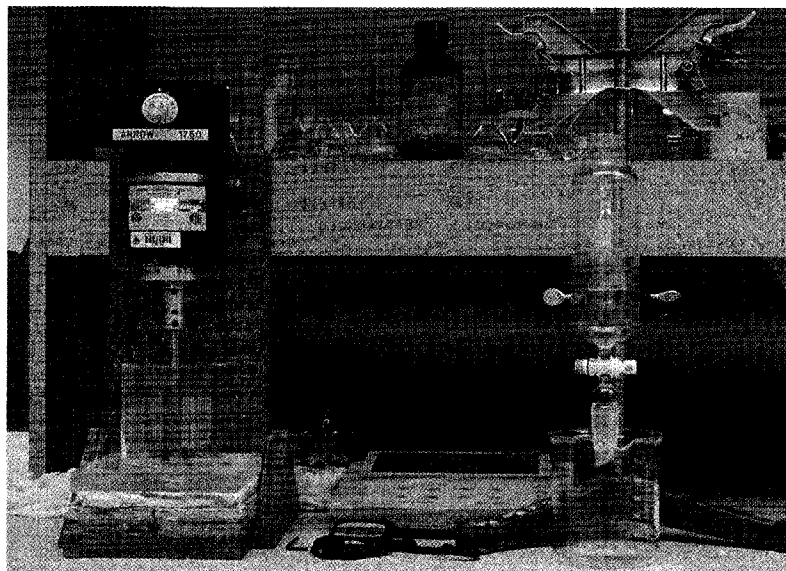


Figure 3-1 Experimental setup for bitumen (oil)-minerals coagulation.



Figure 3-2 Experimental setup for visualization of bitumen (oil)-mineral adhesion.

the separating column. Both the drained aqueous sample and the emulsion sample (i.e. oil/mineral aggregates left in the separation column) were filtered and ashed at 725°C for 6 hours (a standard procedure used by Syncrude Research Centre for ash analysis) to calculate the weight distribution of the mineral solids reporting to the oil phase. Blank tests were also conducted. The weight percentage of the mineral solids reporting to the oil phase was taken as the “Degree of Coagulation” between the mineral solids and oil.

In the above coagulation experiments, the mineral particles could be entrapped in the bitumen (oil)-in-water emulsions, or they could genuinely coagulate with the bitumen (oil) droplets. To distinguish between these two possible mechanisms, direct observations on the coagulation between the bitumen (oil) droplets and mineral particles were also made. This was achieved by using a Cole-Parmer Model EMZ13TR stereomicroscope that was fitted with a Nikon D50 SLR digital camera and a Motic-Cam 350 video capture device (Figure 3-2). In these tests, a bitumen (oil) droplet was formed at the tip of a syringe which was submerged in an aqueous solution. Then slurries containing mineral particles were circulated and video clips and microphotographs were taken to show if the mineral particles attached to the bitumen (oil) droplets.

3.3 Coagulation between Hexadecane and Mineral Solids

3.3.1 Quartz

Without any other additives, quartz did not coagulate with hexadecane in the entire pH range tested (from about 3 to 11). However, in the presence of 10^{-4} mol/L Ca^{2+} (added as CaCl_2 , see Table 3-1), quartz started to coagulate with hexadecane when the solution pH was above about 10.2. Further increase in pH caused a sharp increase in the degree of coagulation, reaching ~60% at pH 11 (Figure 3-3). The pH value, 10.2, is called “critical pH” for this case. Similar phenomena were observed when 10^{-3} mol/L Ca^{2+} was added. The ten-fold increase in Ca^{2+} concentration lowered the critical pH of coagulation slightly, to about 9.6.

The critical pH observed at these two CaCl_2 concentrations corresponds to the appearance of the first-order calcium hydroxyl species (CaOH^+) in the solution (Fuerstenau and Palmer, 1976; Fuerstenau and Han, 2002).

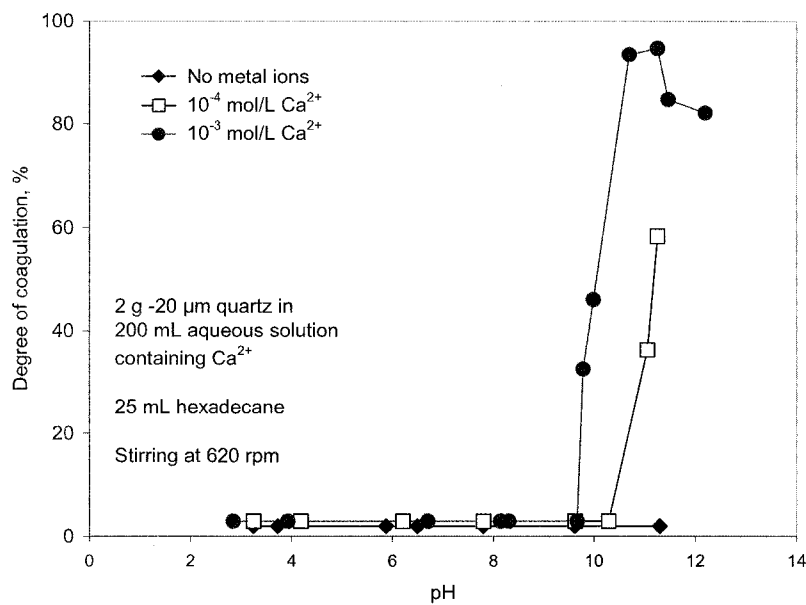


Figure 3-3 Coagulation of hexadecane with quartz at different pH with and without Ca^{2+} .

Figure 3-4 shows the microphotographs of a hexadecane droplet submerged in an aqueous solution at pH ~ 11 . When the slurry of $-63+25$ μm quartz particles was circulated, nearly all the quartz particles went past the oil droplet without forming contact (Figure 3-4a). However, when the solution contained 10^{-3} mol/L Ca^{2+} and was adjusted to pH ~ 11 , a large number of quartz particles were attached to the oil droplets (Figure 3-4b). This shows that the quartz particles are coagulated with the hexadecane droplets at this pH and the particles in the oil phase in the coagulation experiment are not due to “entrapment” by the oil-in-water emulsions.

Several other multivalent metal cations were tested and the results are presented in Figure 3-5. As can be seen, the critical pH for hexadecane-quartz coagulation varied with the type of metal ions, and it was again consistent with the appearance of the first-order metal

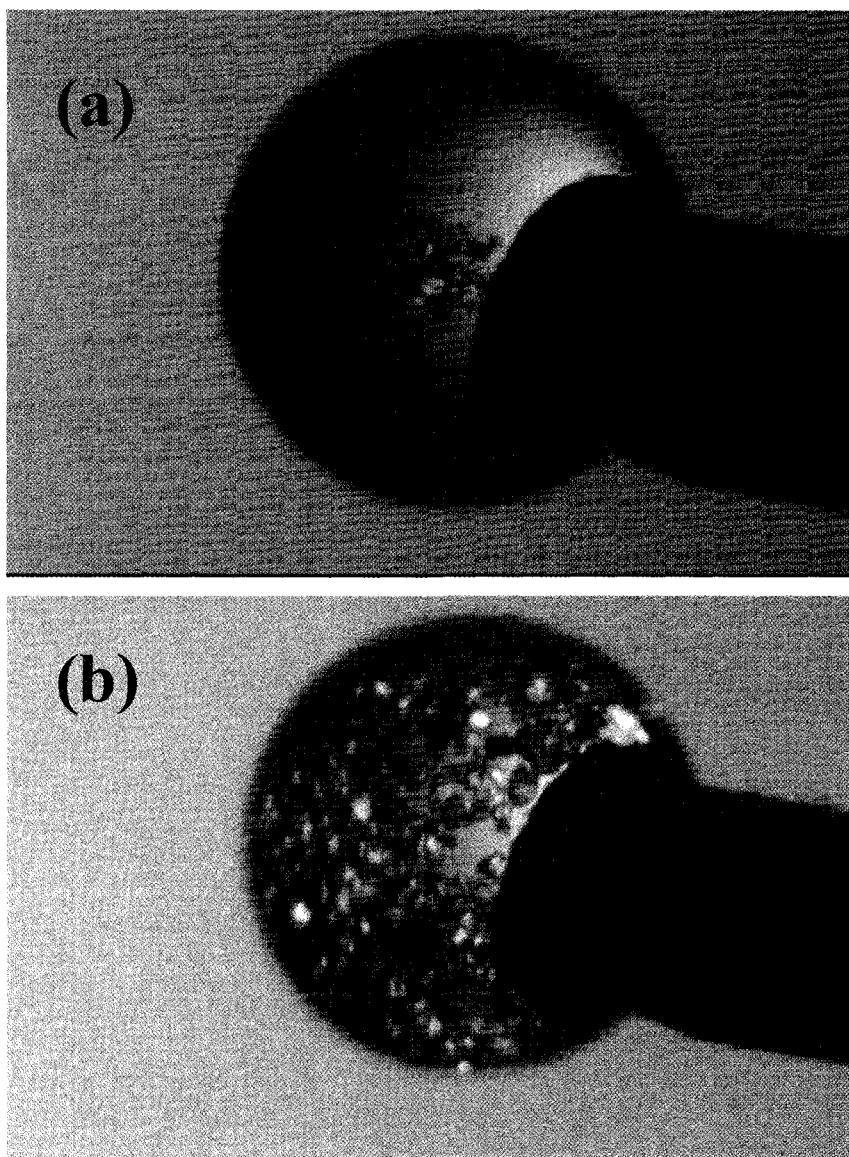


Figure 3-4 Microphotographs of hexadecane droplets and $-63+25 \mu\text{m}$ quartz at pH ~ 11 (a) in the absence and (b) in the presence of $10^{-3} \text{ mol/L Ca}^{2+}$.

hydroxyl species or metal hydroxide precipitate for that particular metal cation. Thus, the critical pH values for 10^{-3} mol/L of Pb^{2+} , Fe^{2+} , Fe^{3+} , Al^{3+} , Mg^{2+} and Mn^{2+} were 5, 5, 4.5, 7, 10 and 8, respectively.

It is known that these multivalent metal cations do not adsorb on quartz surfaces but their first-order hydroxyl species do (Fuerstenau and Palmer, 1976), therefore it seems that the adsorbed metal hydroxyl species contributed to the coagulation of quartz with hexadecane.

Another interesting observation from both Figure 3-3 and Figure 3-5 is that in the presence of the metal cations, the degree of coagulation increased rapidly above the critical pH, reaching a maximum between 70–95%, then dropped sharply at higher pH values. This was observed with all metal cations except Pb^{2+} . It was possible that coagulation maximum was correlated to surface precipitated metal hydroxides. Above the precipitation pH, adsorption of hydroxyl anions could make the hydroxides become negatively charged. Electrostatic repulsion could prevent the quartz and hexadecane from coagulating. As a result, the degree of coagulation would decrease.

3.3.2 *Kaolinite*

Figure 3-6 shows the degree of coagulation between hexadecane and kaolinite as a function of pH with and without Ca^{2+} . It can be seen that the coagulation behavior of kaolinite with hexadecane was very different from quartz. Between pH 3.5 and 5.5, a maximum degree of coagulation of about 85% was observed in the absence of Ca^{2+} between kaolinite and hexadecane, whereas no coagulation was observed in the absence of Ca^{2+} for quartz (Figure 3-3).

In the presence of 10^{-3} mol/L Ca^{2+} , the degree of coagulation between kaolinite and hexadecane remained basically unchanged at about 40–50% in the pH range of 3–11, and was thus lower than in the absence of Ca^{2+} between pH 3 and 9. The addition of Ca^{2+} ions

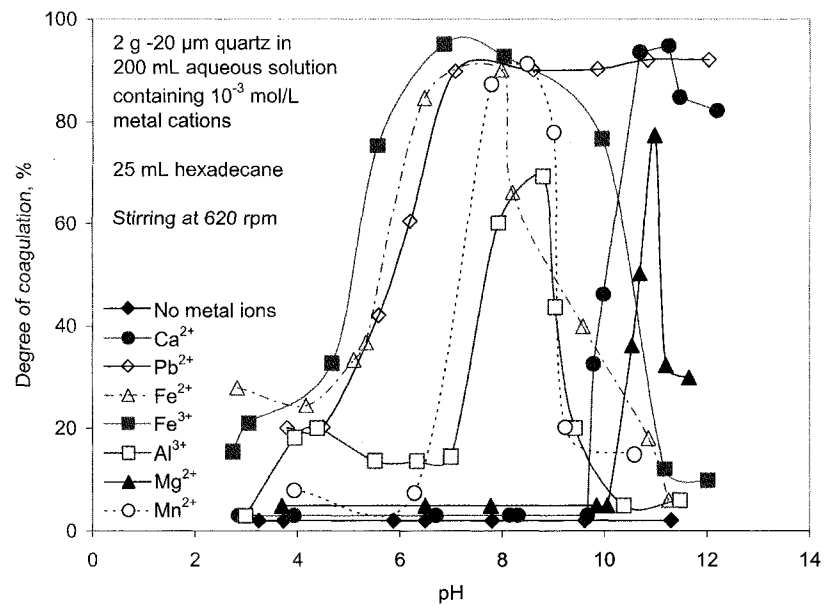


Figure 3-5 Coagulation of hexadecane with quartz at different pH with and without 10^{-3} mol/L metal cations.

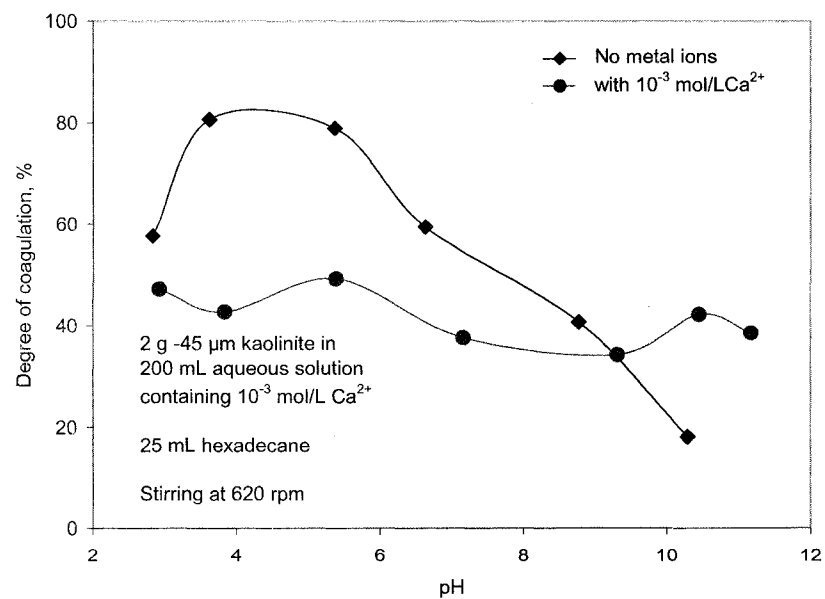


Figure 3-6 Coagulation of hexadecane with kaolinite at different pH with and without 10^{-3} mol/L Ca^{2+} .

10^{-3} mol/L Ca^{2+} . therefore caused a decrease in the degree of coagulation between hexadecane and kaolinite in the pH range of 3 to 9.

3.3.3 Illite

Figure 3-7 shows the degree of coagulation of hexadecane with illite at different pH with and without Ca^{2+} addition. The degree of coagulation, as shown, was almost unchanged at about 30–40% irrespective of Ca^{2+} ions. It was possible that there may have been enough metal ions dissolved from illite so that the addition of 10^{-3} mol/L Ca^{2+} had very little effect on the degree of coagulation. This explanation may also apply to the observation for kaolinite as showed in Fig. 3-6.

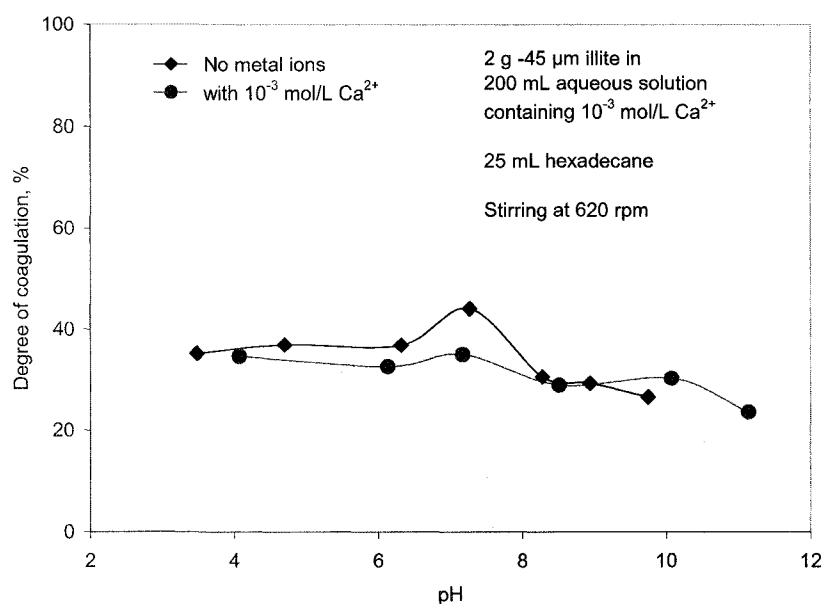


Figure 3-7 Coagulation of hexadecane with illite at different pH with and without 10^{-3} mol/L Ca^{2+} .

3.4 Coagulation between Model Oil and Mineral Solids

Bitumen in the Alberta oil sands is known to contain surfactants that can be leached off in the hot water extraction process. These surfactants contribute to surface charges of bitumen mainly through carboxylic and phenolic groups. Carboxylic surfactants have

been identified the most common ones found in bitumen extraction process (Schramm et al., 1984). To better simulate the behavior of bitumen, sodium oleate was dissolved in hexadecane at the concentration of 10^{-3} mole of sodium oleate per liter of hexadecane and the mixture was used as the model oil phase.

3.4.1 Effect of Agitation Speed

Figure 3-8 shows the effect of agitation speed on the coagulation of the model oil and quartz in the presence of 10^{-3} mol/L Ca^{2+} at pH 10.5–10.7. As can be seen, the degree of coagulation increased with increasing agitation speed. The weight percent of quartz reporting to oil phase (i.e., degree of coagulation) increased to 100% when agitation speed was above 420 rpm. An agitation speed of 620 rpm was used in all coagulation tests. Its effect on experimental errors could thus be reduced.

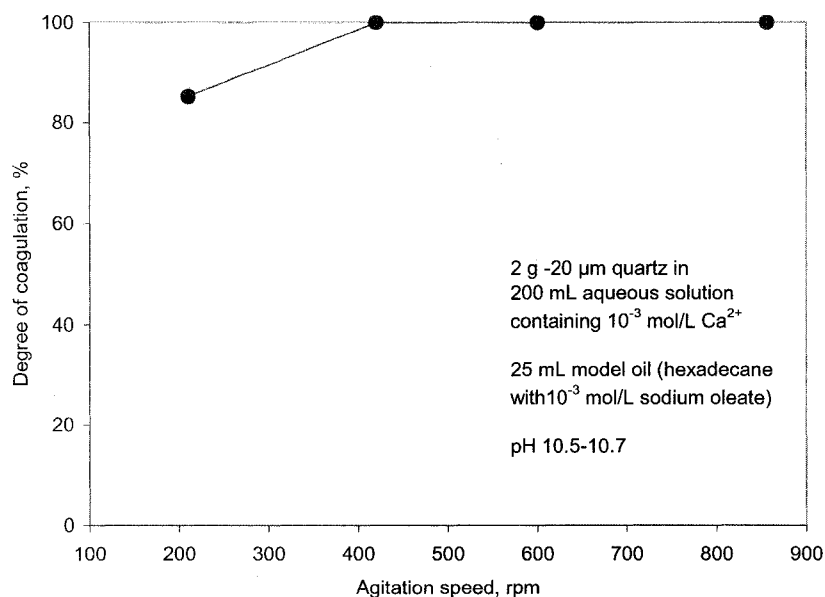


Figure 3-8 Effect of agitation speed on the coagulation of model oil with quartz.

3.4.2 Quartz

Figure 3-9 shows the degree of coagulation of quartz with the model oil in solutions containing 10^{-3} mol/L of Ca^{2+} , Mg^{2+} or Fe^{3+} as a function of pH. As can be seen, in the absence of the metal ions, quartz only slightly coagulated with oil at acidic pH 2–5. The degree of coagulation reached a maximum of 36% at pH 4, and then decreased with pH and leveled off above pH 6 at 12%. With 10^{-3} mol/L Ca^{2+} , the degree of coagulation increased remarkably from below 20% at pH 7 to 100% at pH 9. Similarly, in the presence of 10^{-3} mol/L Mg^{2+} , the degree of coagulation of quartz with oil increased from 13% at pH 9 to 98% at pH 10. In the case of Fe^{3+} , coagulation between quartz and oil gradually increased from about 40% at pH 2.3 to over 90% at pH 7.4, then decreased with increasing pH.

Therefore, the Ca^{2+} , Mg^{2+} and Fe^{3+} ions present in aqueous solution caused extensive coagulation of quartz with the model oil droplets, even at pH 8, the pH at which the oil sands companies currently use to extract the bitumen from the oil sands of Alberta, Canada. These results reveal that the detrimental effect of multivalent metal ions on bitumen recovery from oil sands was at least partly due to the poor liberation between the oil phase and the mineral particles.

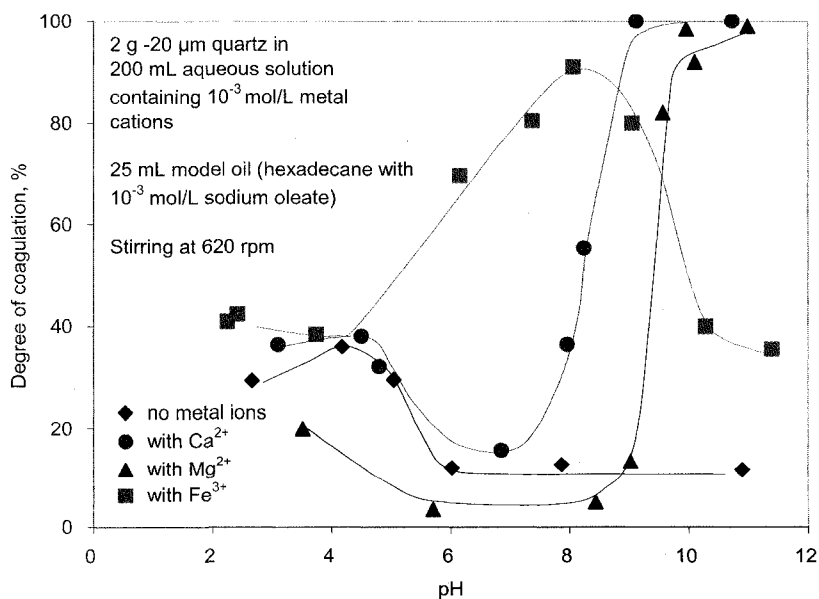


Figure 3-9 Coagulation of model oil with quartz at different pH with and without 10^{-3} mol/L metal ions.

3.4.3 Kaolinite

Figure 3-10 shows the coagulation of the model oil with kaolinite at different pH with and without addition of 10^{-3} mol/L of Ca^{2+} , Mg^{2+} and Fe^{3+} . As can be seen, the model oil strongly coagulated with kaolinite at about pH 4, followed by a consistent drop with increasing pH. At pH 10, about 50% kaolinite remained coagulation with oil. Strong coagulation was observed between the model oil and kaolinite in the presence of 10^{-3} mol/L Ca^{2+} in the entire pH range tested (3 to 10.5), with a degree of coagulation in excess of 90%. Mg^{2+} had less effect on promoting the coagulation than Ca^{2+} . Kaolinite particles strongly coagulated with model oil in the presence of Fe^{3+} below pH 8, evidenced by a degree of coagulation above 85%. These observations indicated that the presence of multivalent metal ions significantly enhanced the mutual coagulation of kaolinite with model oil.

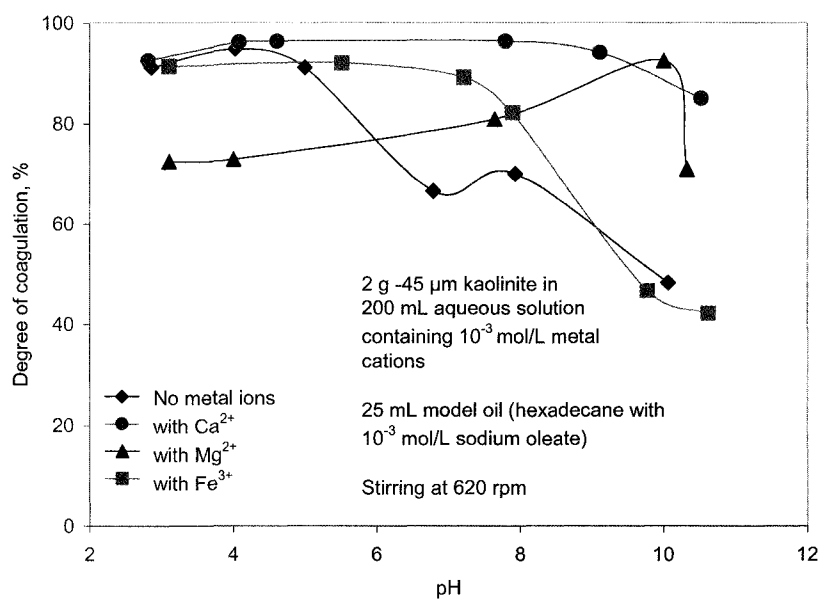


Figure 3-10 Coagulation of model oil with kaolinite at different pH with and without 10^{-3} mol/L metal ions.

On the other hand, the presence of sodium oleate in the model oil apparently increased the coagulation of model oil with kaolinite. In fact, comparison with Figure 3-6 shows

that without sodium oleate the coagulation was much lower even when Ca^{2+} ions were present.

3.4.4 Illite

As can be seen in Figure 3-11, the degree of coagulation between model oil and illite at different pH did not follow a clear trend in the absence and presence of 10^{-3} mol/L metal cations tested. Strong coagulation was observed at pH 5 with or without Ca^{2+} . Comparison with Figure 3-7 indicates that this was caused by the presence of sodium oleate. In addition, in the alkaline pH range, the coagulation was stronger with 10^{-3} mol/L Ca^{2+} than without. Mg^{2+} did not significantly increase the mutual coagulation until above pH 9, likely due to the hydrolysis and precipitation of Mg^{2+} . In the presence of Fe^{3+} , the degree of coagulation of kaolinite with the model oil was 90% at pH 8, followed by a subsequent drop at higher pH. Figure 3-11 shows that illite had higher affinity to oil in the presence of multivalent cations, particularly at alkaline pH.

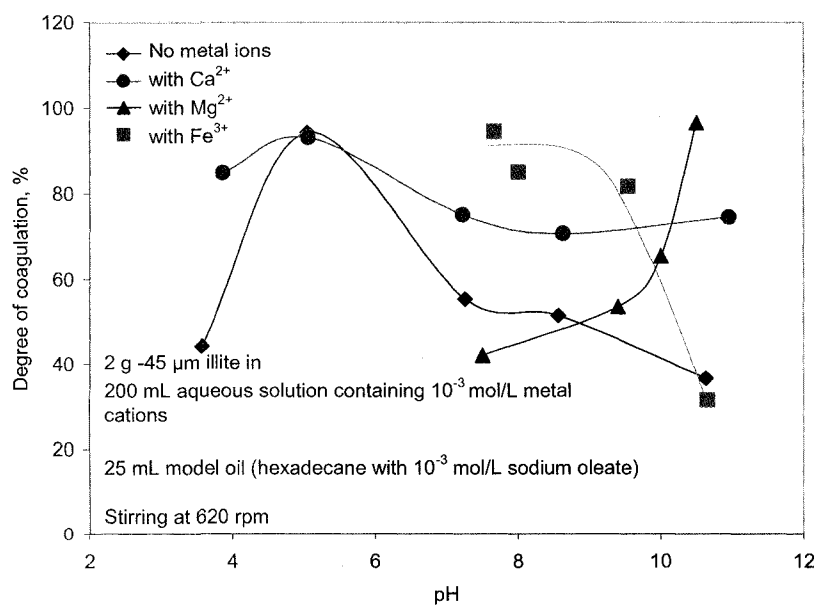


Figure 3-11 Coagulation of model oil with illite at different pH with and without 10^{-3} mol/L metal ions.

3.4.5 Mineral Mixtures

Figure 3-12 shows the degree of coagulation between model oil and the mineral mixtures of quartz:kaolinite:illite (80:14:6) at different pH with and without Ca^{2+} addition. As can be seen, strong coagulation (with degrees of coagulation of 70–80%) was observed at about pH 4 with or without Ca^{2+} . Between pH 4 and 8, coagulation decreased with increasing pH and reached the lowest point of about 20% at pH 7–8. Above pH 8, the degree of coagulation stayed constant at about 20% when no Ca^{2+} ions were added. However, in the presence of 10^{-3} mol/L Ca^{2+} , the coagulation increased rapidly with pH, reaching 100% at about pH 11. Therefore, to achieve the liberation of the model oil phase from the mixed mineral solids, the optimal pH value should be around 7–8. This is consistent with the current practice. It also seems to indicate that the simulated systems are appropriate for liberation studies between bitumen and inorganic mineral matters.

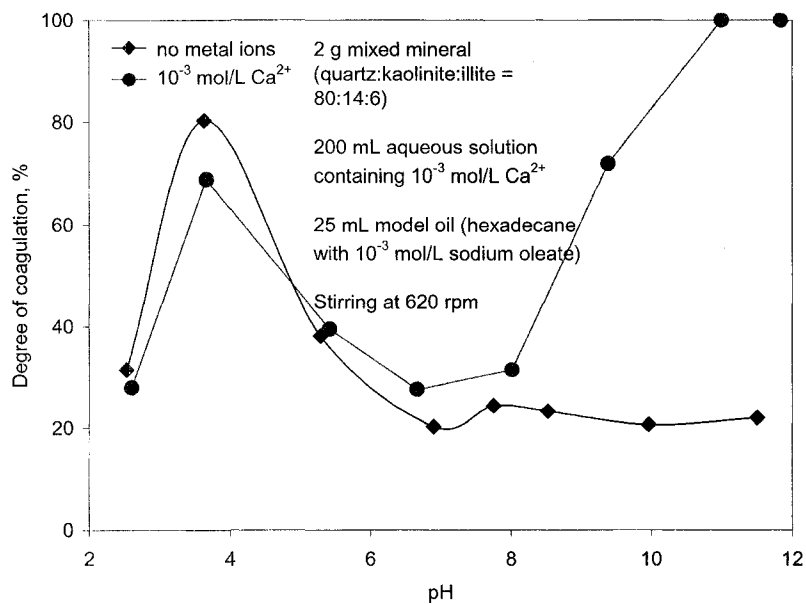


Figure 3-12 Coagulation of model oil with mineral mixtures (quartz:kaolinite:illite = 80:14:6) at different pH with and without 10^{-3} mol/L Ca^{2+} addition.

3.4.6 Effect of Montmorillonite

Figure 3-13 shows the effect of added montmorillonite on the coagulation of the model oil with mixtures of quartz:kaolinite:illite (80:14:6) at pH 7–8. As can be seen, montmorillonite did not have any effect if Ca^{2+} was not present, even at the highest weight percent added (9 wt%). However, in the presence of 10^{-3} mol/L Ca^{2+} , the coagulation increased rapidly with the addition of montmorillonite, reaching a maximum of about 65% when 2.44 wt% montmorillonite was added. Interestingly, further increase in the montmorillonite addition reduced the degree of coagulation. Therefore, when a small amount of montmorillonite was present together with Ca^{2+} ions, the liberation of oil phase from mineral solids would be difficult. Kasongo et al. (2000) reported that the co-presence of Ca^{2+} and montmorillonite affected bitumen flotation. Our results suggest that this is mainly caused by a reduction in the degree of liberation between bitumen and the mineral matter when both montmorillonite and Ca^{2+} are present.

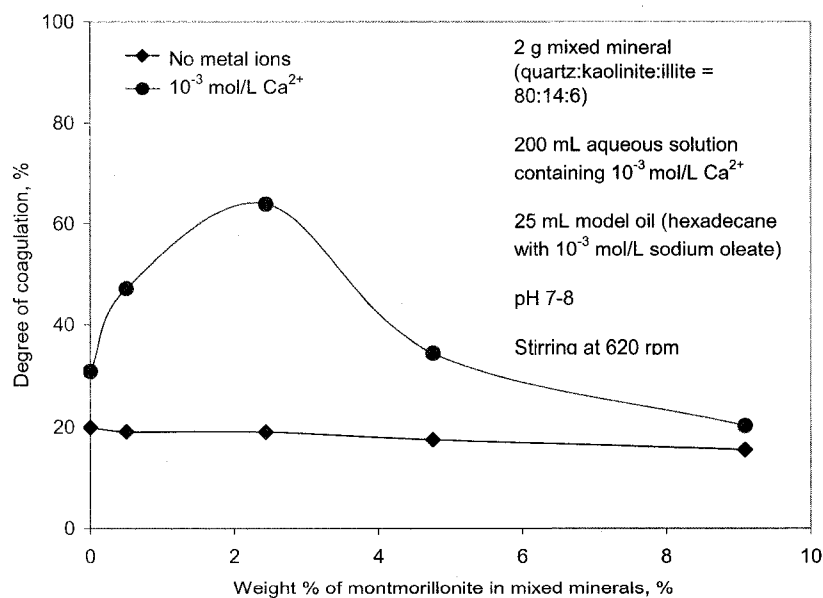


Figure 3-13 Effect of added montmorillonite on the coagulation of model oil with mineral mixtures (quartz:kaolinite:illite = 80:14:6), pH 7–8.

3.5 Coagulation between Solvent-Diluted-Bitumen and Mineral Solids

The findings of coagulation of minerals with the model oil, as described in the previous sections, indicate that the presence of multivalent metal ions Ca^{2+} , Mg^{2+} and Fe^{3+} indeed has a negative impact on oil-mineral liberation due to the resultant stronger coagulation. To confirm the effect of these metal cations on bitumen-mineral interaction, solvent-diluted-bitumen was used as the oil phase in the coagulation experiments. The results are presented in Figures 3-14 to 3-17.

3.5.1 Quartz

As can be seen from Figure 3-14, the coagulation of solvent-diluted-bitumen with quartz significantly increased with increasing concentration of multivalent metal cations in aqueous solution. In the absence of the metal cations, bitumen did not coagulate with quartz at the tested pH's. The degree of coagulation increased abruptly when the concentration of Ca^{2+} was increased to 5×10^{-4} mol/L at pH 10.1, and reached 93% at 1.5×10^{-3} mol/L of Ca^{2+} . In contrast, for Fe^{3+} , coagulation increased gradually from 10.9% to 92.2% as Fe^{3+} concentration increased from 10^{-6} to 10^{-4} mol/L at pH 7.8, and leveled off at higher concentrations. These results indicate that the presence of multivalent metal ions indeed induced strong bitumen-quartz interaction. Removal of these ions or lowering of the concentrations of these ions would potentially benefit bitumen liberation from quartz.

Figure 3-15 presents the coagulation of quartz with bitumen in the absence and presence of 10^{-3} mol/L of Ca^{2+} , Mg^{2+} and Fe^{3+} at different pH. As can be seen, in the absence of any metal ions, over 90% quartz was coagulated with bitumen at an acidic pH of 3. The degree of coagulation decreased above pH 3 and subsequently stabilized at 16% above pH 6. In the presence of Ca^{2+} and Mg^{2+} , quartz extensively coagulated with bitumen within two pH regions: below pH 4 and above pH 10, corresponding to the iso-electric point of quartz (pH 3) and the onset of hydrolysis of Ca^{2+} and Mg^{2+} (pH > 10). In the case of Fe^{3+} , the degree of coagulation remained high at about 95% before a significant drop at

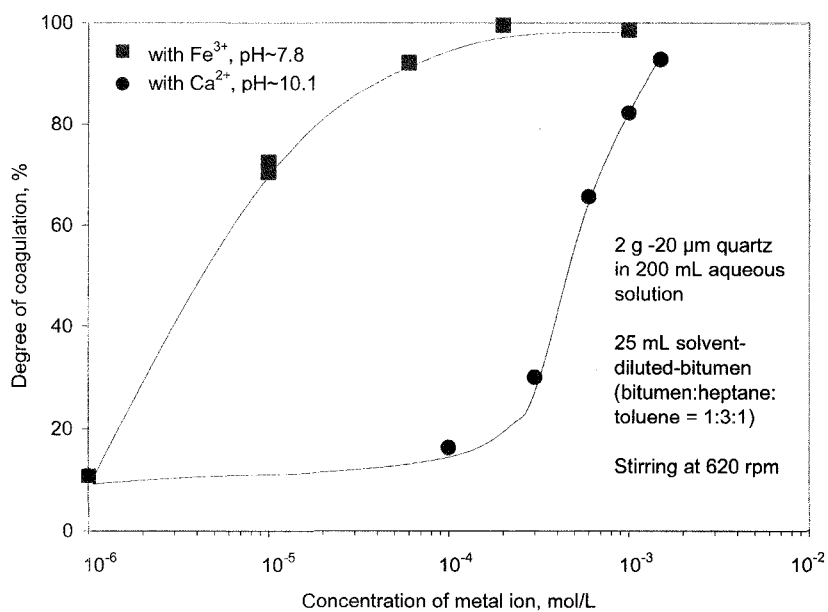


Figure 3-14 Coagulation between bitumen and quartz at different concentrations of Ca^{2+} and Fe^{3+} .

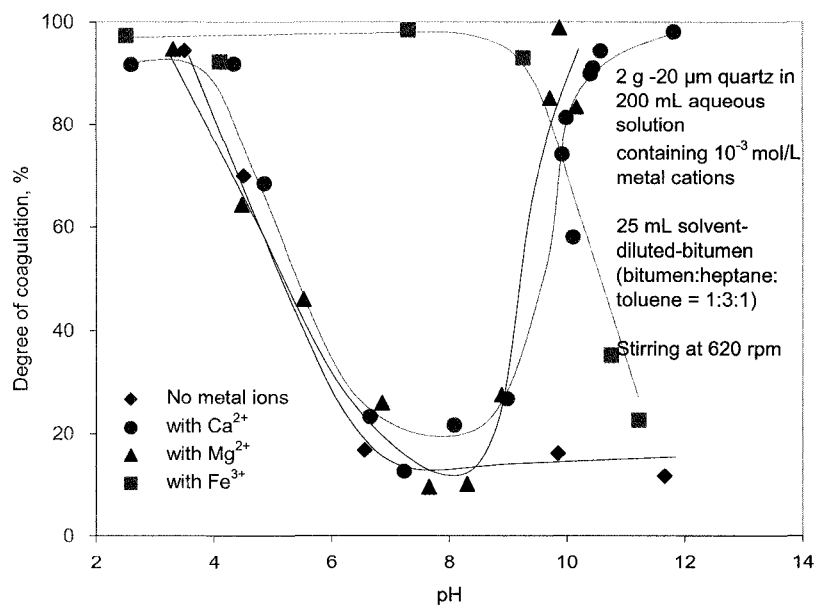


Figure 3-15 Coagulation of bitumen with quartz at different pH with and without 10^{-3} mol/L metal ions.

above pH 10. These indicate that the presence of multivalent metal ions enhances the mutual coagulation at a certain pH region.

3.5.2 Kaolinite

The dependence of coagulation of bitumen with kaolinite on pH in the presence of 10^{-3} mol/L of Ca^{2+} , Mg^{2+} and Fe^{3+} is shown in Figure 3-16. Kaolinite extensively coagulated with bitumen (with a degree of coagulation of over 80%) at acidic pH (pH < 6) without any metal ion addition. The degree of coagulation dropped continuously above pH 6, reaching 68% at pH 9.3 and 14% at pH 10.8. This result was in agreement with the observation on kaolinite-model oil coagulation. In the coagulation tests below pH 7.6, the aqueous phase was clear after 10 minutes of standing, due to the strong kaolinite-bitumen coagulation which removed the kaolinite from the aqueous solution. At higher pH, the turbidity of the aqueous phase increased with pH, indicating that more kaolinite was dispersed in the aqueous solution and implying better liberation of kaolinite particles from bitumen droplets. This correlated to the observations of decreasing bitumen-kaolinite coagulation.

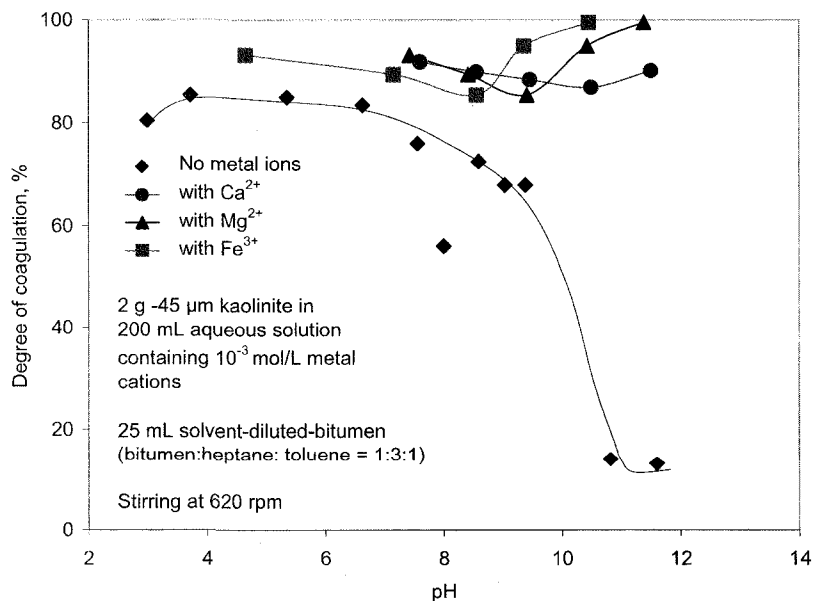


Figure 3-16 Coagulation of bitumen with kaolinite at different pH with and without 10^{-3} mol/L metal ions.

The coagulation behavior of kaolinite with bitumen in the absence of metal cations, shown in Figure 3-16, is to a large extent controlled by the surface properties of kaolinite. Kaolinite has a platelet structure with two different cleavage surfaces: the basal face and the edge. The basal face carries a slight negative charge as a result of the isomorphous substitution of Si^{4+} by Al^{3+} and the charge usually does not change with solution pH. The edge, on the other hand, is occupied by aluminol ($-\text{AlOH}$) and silanol ($-\text{SiOH}$) groups, and can take various charges at different pH due to the protonation and deprotonation of these surface hydroxyl groups. The iso-electric point of the edge is believed to be between pH 6–9 (Schofield and Samson, 1954; Williams and Williams, 1978). Therefore, in a slightly acidic solution, the edge is positively charged through protonation of surface hydroxyl groups, and can interact either with negatively charged basal surfaces to form “edge-to-face” bridging (Schofield and Samson, 1954), or with negatively charged bitumen droplets through electrostatic attraction. With increasing pH, the surface hydroxyl groups successively undergo deprotonation leading to a decrease of the positive charge and eventually reversal of the positive charge to negative on the edge surface. Accordingly, kaolinite has a lower tendency to coagulate with bitumen droplets at above pH 6 due to the decrease of electrostatic attraction. At pH 10, where the edge surfaces carry negative charges, kaolinite is unlikely attracted to the like-charged bitumen due to the electrostatic repulsion. This is in accordance with the continuous reduction of coagulation between bitumen and kaolinite above pH 6.

As can be seen from Figure 3-16, in the presence of metal cations, the mutual coagulation between bitumen and kaolinite was generally higher than without at all pH values tested. Strong mutual coagulation was observed above pH 10 where little kaolinite coagulated with bitumen in the absence of the metal cations.

3.5.3 *Illite*

Figure 3-17 shows the illite-bitumen coagulation at different pH in the absence and the presence of the metal ions. In the absence of metal ions, the degree of coagulation reached a peak at pH 8, and dropped at higher pH. In the presence of metal ions, a

stronger mutual coagulation was observed from pH 4–11, for all three types of metal ions added. When 10^{-3} mol/L Ca^{2+} or Mg^{2+} was added, a marked increase in the degree of coagulation was observed above pH 10. Mg^{2+} showed a stronger effect in promoting the coagulation than Ca^{2+} at all pH values investigated. In the presence of Fe^{3+} , illite-bitumen coagulation increased significantly from about 20% at pH 4 to about 80% at pH 8, followed by a drop above pH 10. These results, combined with those of bitumen-quartz coagulation, and kaolinite-bitumen coagulation presented in previous sections, indicated that the hydrolyzed or precipitated metal ions substantially enhanced the mutual coagulation between bitumen and the silicate minerals (quartz, kaolinite and illite).

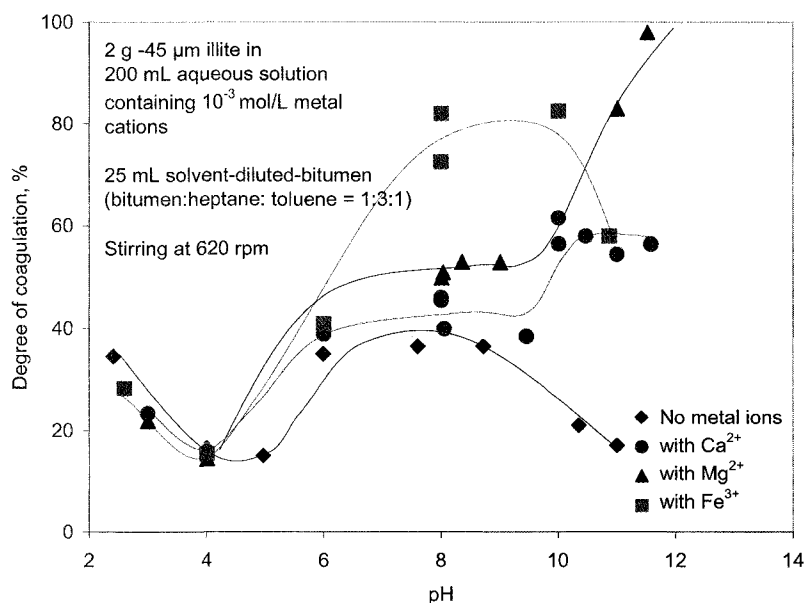


Figure 3-17 Coagulation of bitumen with illite at different pH with and without 10^{-3} mol/L metal ions.

3.6 Summary

Particles of a high purity quartz did not coagulate with hexadecane droplets in the entire pH range tested (from 3 to 11). However, when multivalent metal cations were present, the quartz particles started to coagulate with hexadecane droplets at pH values where the

metal cations formed first-order metal hydroxyl species, such as PbOH^+ , MgOH^+ , CaOH^+ , etc. The degree of coagulation typically went through a maximum with increasing pH.

When the hexadecane was doped with sodium oleate (i.e., model oil), moderate degrees of coagulation (~35%) were observed between the doped hexadecane and the quartz particles at an acidic pH (pH 3–5), and very low coagulation (~10%) was observed at alkaline pH (>8). The presence of Ca^{2+} did not affect the coagulation at acidic pH but significantly increased the coagulation above pH 8, causing it to reach 100% at pH 9.

When the mineral particles contain lattice metal atoms (such as kaolinite and illite), the coagulation between the mineral particles and hexadecane droplets was not clear cut and showed varying behaviors. The presence of multivalent metal cations such as Ca^{2+} in the solution did not usually increase the coagulation.

However, when the hexadecane was doped with sodium oleate, its coagulation with the kaolinite and illite was generally much higher. The presence of Ca^{2+} , Mg^{2+} and Fe^{3+} in the solution significantly increased the coagulation, particularly at pH range of 8–10.

Montmorillonite did not have any effect on the coagulation between hexadecane and mixed mineral (quartz:kaolinite:illite = 80:14:6) at pH 7–8 in the absence of Ca^{2+} ions, even when the hexadecane was doped with sodium oleate. The degree of coagulation remained at about 20% under these conditions. However, in the presence of 10^{-3} M Ca^{2+} the coagulation increased rapidly with the weight percent of montmorillonite added. Maximum coagulation of about 65% was observed at 2.44 wt% montmorillonite addition. Further increase in montmorillonite addition reduced the degree of coagulation, so that at 9 wt% montmorillonite addition, the degree of coagulation dropped to the level as if Ca^{2+} ions were absent.

Ca^{2+} and Mg^{2+} promoted the mutual coagulation between solvent-diluted-bitumen and quartz at above pH 10 and 9, respectively. In the presence of Fe^{3+} , the coagulation

dropped to 20% at pH 11 from about 95% at pH 8. Kaolinite strongly coagulated with bitumen at acidic pH, and the degree of coagulation decreased with increasing pH. However, when 10^{-3} mol/L Ca^{2+} , Mg^{2+} or Fe^{3+} was present, strong bitumen-kaolinite coagulation was observed at pH 6–12. The presence of 10^{-3} mol/L of tested metal cations generally enhanced illite-bitumen coagulation, particularly at pH 6–9 for Fe^{3+} and at above pH 10 for Ca^{2+} and Mg^{2+} .

Generally, the presence of Ca^{2+} , Mg^{2+} and Fe^{3+} promoted the mutual coagulation of silicate minerals (quartz, kaolinite and illite) with oil (bitumen), particularly in the pH range where the metal ions are hydrolyzed to form the first-order metal hydroxyl species or metal hydroxide precipitates. The mechanisms by which the metal cations affect the mutual coagulation between bitumen and the silicate minerals are discussed in Chapters 6 and 7.

4 EFFECT OF COMPLEXING AGENTS ON BITUMEN-MINERAL COAGULATION IN THE PRESENCE OF METAL IONS²

4.1 Introduction

In order to counter the detrimental effect of multivalent metal cations that promote the mutual coagulation between bitumen (oil) and the minerals, three polycarboxylic complexing agents, citric acid, oxalic acid and EDTA are used. Coagulation experiments are carried out to evaluate the effect of the complexing agents on oil (bitumen)-mineral interaction.

The experimental conditions (metal ion concentration and pH) corresponding to strong oil-quartz coagulation are used as a reference to examine the effectiveness of the complexing agents. Therefore, all solutions contained 10^{-3} mol/L of a multivalent metal cation. Solution pH is controlled within 9.8–10.2 for Ca^{2+} and Mg^{2+} , and 7.7–8.3 for Fe^{2+} and Fe^{3+} . The degree of coagulation between mineral and oil (bitumen) is plotted as a function of the concentration of the complexing agents and the experimental procedures and results are presented in the following sections.

4.2 Experimental

4.2.1 *Materials and Chemicals*

The minerals (quartz, kaolinite and illite), model oil and solvent-diluted bitumen used in the coagulation experiments were the same as those used in Chapter 3 and described in section 3.2.1.

The chemical reagents used in this study were purchased from several suppliers, as listed in Table 4-1.

² Portions of this chapter have been published in *Canadian Metallurgical Quarterly*, Vol. 46, n 3, 207-214 (2007) by Weibing Gan, Mingli Cao, Brendan Crozier and Qi Liu.

Table 4-1 Chemical reagents used in the experiments.

Chemical	Supplier	Grade	Use
Calcium chloride (CaCl ₂)	Fisher Scientific	>99%	Additive electrolyte
Citric acid (C ₆ H ₈ O ₇)	Fisher Scientific	100.1%	Complexing agent
Ethylenediaminetetraacetate (EDTA)	Fisher Scientific	≥99.0%	Complexing agent
Ferric chloride Solutions (FeCl ₃)	Fisher Scientific	40% W/V	Additive electrolyte
Ferrous chloride (FeCl ₂ ·4H ₂ O)	Fluka Chemika	Minimum 99.0%	Additive electrolyte
Hexadecane (CH ₃ (CH ₂) ₁₄ CH ₃)	Fisher Scientific	Mol % 99.3%	Simulating bitumen oil phase
Hydrochloric acid (HCl, solution)	Fisher Scientific	36.5–38%	pH regulator
Magnesium nitrate hexahydrate (Mg(NO ₃) ₂ ·6H ₂ O)	Agros Organics	>99%	Additive electrolyte
Oxalic acid (C ₂ H ₂ O ₄ ·H ₂ O)	Fisher Scientific	100.3%	Complexing agent
Sodium hydroxide (NaOH)	Fisher Scientific	99.0%	pH regulator
Sodium oleate	Riedel-dehaën	Minimum 82%	Additive carboxylate in oil phase

4.2.2 *Experimental Methods*

Experimental methods and procedures were the same as described in detail in section 3.2.2, except that a complexing agent was added after metal cations in the conditioning stage.

4.3 Coagulation between Model Oil and Minerals

4.3.1 *Quartz*

The effects of the complexing agents on the coagulation of model oil with quartz in the presence of Ca²⁺ ions are shown in Figure 4-1. As can be seen, all three complexing

agents could significantly decrease the coagulation of the model oil with quartz particles with increasing concentration. EDTA and citric acid were more effective than oxalic acid. The degree of coagulation was reduced from 100% to about 8% at the concentration of 2.5×10^{-3} mol/L of citric acid or EDTA. In contrast, a higher concentration of oxalic acid (5×10^{-3} mol/L) could only lower the degree of coagulation to about 30%.

Visualization of adhesion between quartz particles and a single oil droplet was carried out for illustration purpose. The experiments were conducted by following the procedures described previously in Section 3.2.2. The solutions contained 10^{-3} mol/L Ca^{2+} ions and pH was maintained at pH 10.1 throughout the test. As can be seen from Figure 4-2a, quartz particles adhered to the oil droplet in the absence of citric acid. When 2×10^{-3} mol/L citric acid was added, the quartz particles were virtually completely removed from the oil droplet surface (Figure 4-2b). This visual observation was in good agreement with the results presented in Figure 4-1.

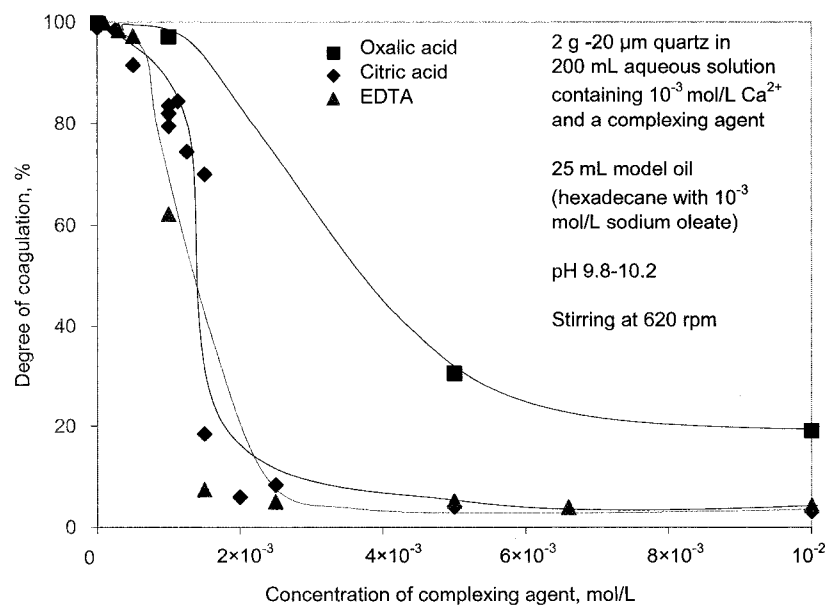


Figure 4-1 Coagulation of model oil with quartz at different concentrations of complexing agents in solutions containing 10^{-3} mol/L Ca^{2+} , pH 9.8–10.2.

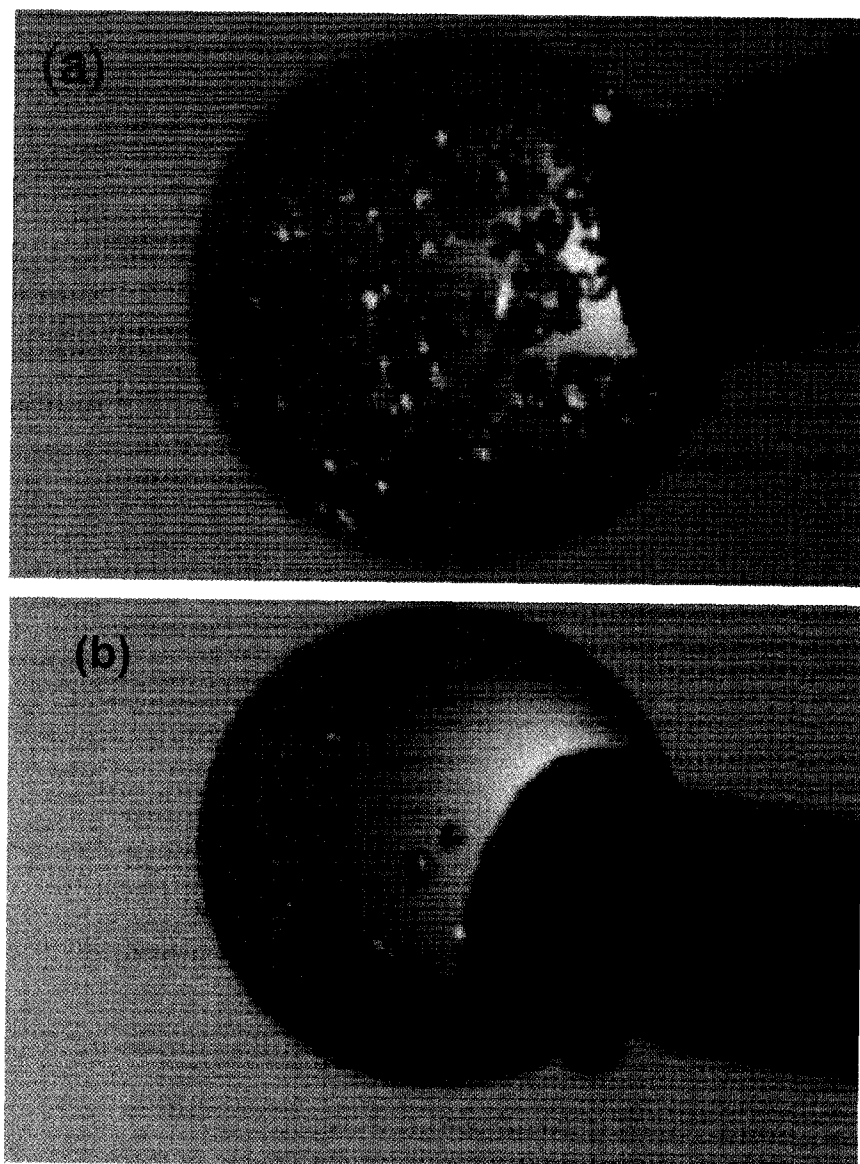


Figure 4-2 Microphotographs of model oil droplets with $-63+25 \mu\text{m}$ quartz with 10^{-3} mol/L Ca^{2+} at pH ~ 10 (a) in the absence and (b) in the presence of 2×10^{-3} mol/L citric acid.

Figure 4-3 shows oil-quartz coagulation in the presence of 10^{-3} mol/L Mg^{2+} as a function of the concentration of the three complexing agents. Both EDTA and citric acid were effective in preventing quartz from coagulating with the model oil. As the concentration of EDTA increased from 10^{-4} to 10^{-3} mol/L, the degree of coagulation was reduced from 96% to 10%. Similarly, the degree of coagulation was decreased from 98% without citric acid to 18.5% when 2×10^{-3} mol/L citric acid was added. In contrast, the addition of oxalic acid did not significantly reduce the coagulation between quartz and the model oil, at least not at the concentrations below 2×10^{-3} mol/L.

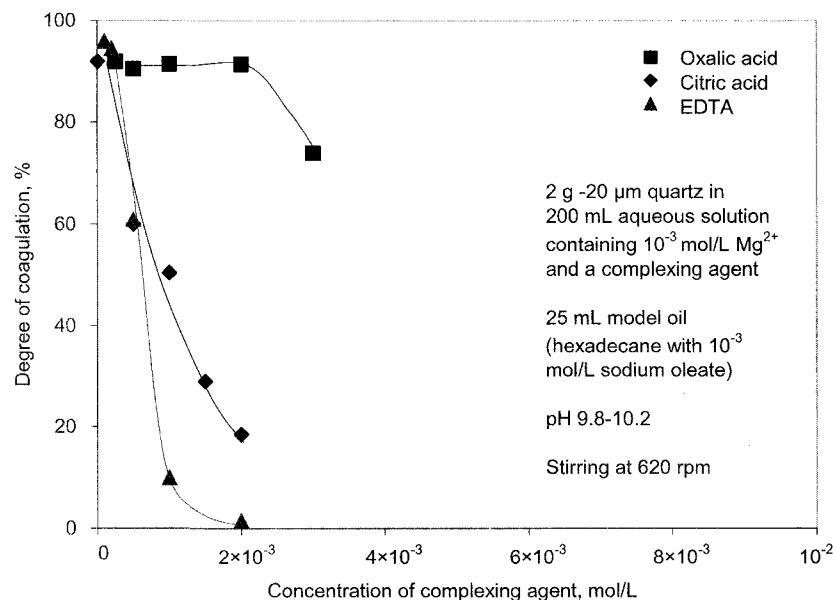


Figure 4-3 Coagulation of model oil with quartz at different concentrations of complexing agents in solutions containing 10^{-3} mol/L Mg^{2+} , pH 9.8–10.2.

Figure 4-4 shows the degree of coagulation of the oil with quartz in solutions containing 10^{-3} mol/L Fe^{2+} at different concentrations of citric acid, EDTA and oxalic acid. As can be seen, citric acid and oxalic acid substantially reduced the coagulation between oil and quartz. At a concentration of as low as 10^{-4} mol/L citric acid, the degree of coagulation dropped from 87% to 14%, and leveled off at about 5% when the citric acid concentration was over 10^{-3} mol/L. Oxalic acid showed a similar trend except that it was not as good as

citric acid. On the other hand, EDTA showed very little effect within the concentration range tested (up to 3×10^{-2} mol/L) on the oil-quartz coagulation in the presence of Fe^{2+} .

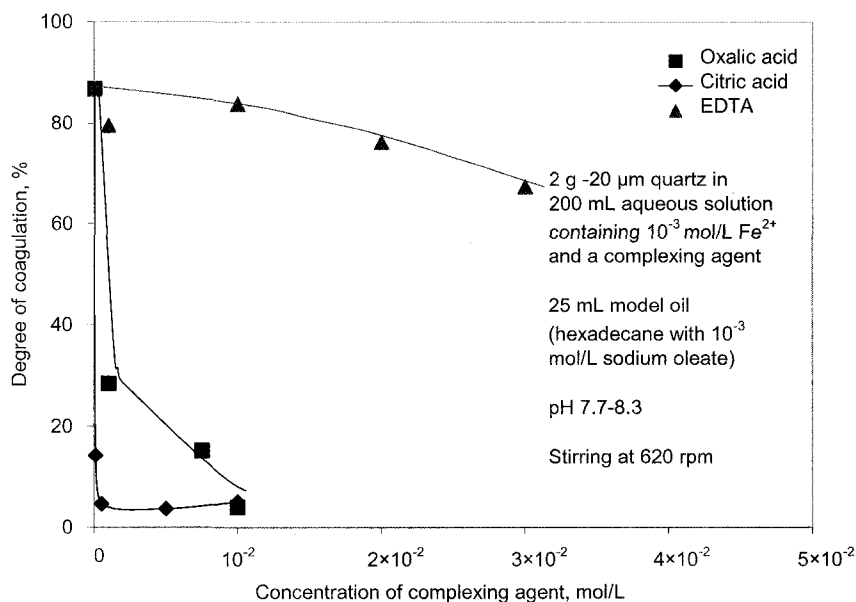


Figure 4-4 Coagulation of model oil with quartz at different concentrations of complexing agents in solutions containing 10^{-3} mol/L Fe^{2+} , pH 7.7–8.3.

Figure 4-5 illustrates the dependence of the degree of coagulation of the model oil with quartz on the concentration of the complexing agents in the presence of 10^{-3} mol/L Fe^{3+} . Similar to the case of Fe^{2+} , the degree of coagulation dropped to about 10% from 85% with the addition of 10^{-3} mol/L citric acid. Oxalic acid demonstrated moderate depressing effect on coagulation, i.e., when 2.5×10^{-3} mol/L oxalic acid was added, the degree of coagulation decreased from 85% to 31%. Oxalic acid and citric acid performed similarly at the concentration of 10^{-2} mol/L by lowering the degree of coagulation to 6.4%. In contrast, EDTA only showed a weak depressing effect, reducing the coagulation to 47% at the concentration of 3×10^{-2} mol/L.

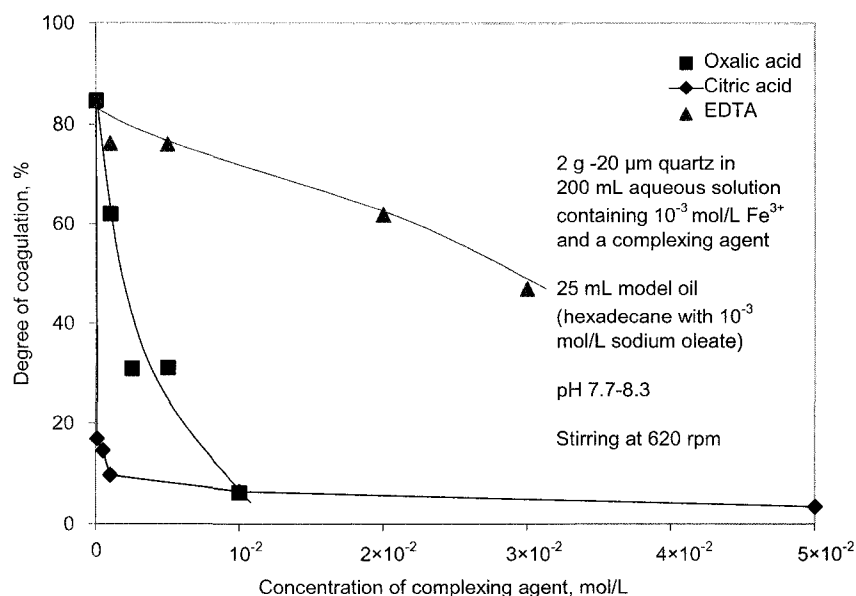


Figure 4-5 Coagulation of model oil with quartz at different concentrations of complexing agents in solutions containing 10^{-3} mol/L Fe^{3+} , pH 7.7–8.3.

The results reported in Figure 4-1 to Figure 4-5 indicated that citric acid was the most effective in inhibiting the mutual coagulation between the model oil and quartz for all the multivalent metal cations tested in this study. Oxalic acid and EDTA, in contrast, showed mixed effects for different metal ions. Oxalic acid could inhibit oil-quartz coagulation in solutions containing Ca^{2+} , $\text{Fe}^{2+}/\text{Fe}^{3+}$, but had little effect for Mg^{2+} . EDTA performed well in decreasing the mutual coagulation of oil and quartz induced by Ca^{2+} and Mg^{2+} , but had little effect for $\text{Fe}^{2+}/\text{Fe}^{3+}$.

Due to its exceptional effect in inhibiting the coagulation of model oil with quartz, citric acid was chosen to study its applicability on oil-clays systems. Thus, the effect of citric acid was examined in the coagulation experiments of model oil with clay minerals (kaolinite, illite) in the presence of Ca^{2+} , Mg^{2+} and Fe^{3+} .

4.3.2 Kaolinite

The coagulation between model oil and kaolinite at different concentrations of citric acid

was measured and the results are plotted in Figure 4-6. It can be seen that the mutual coagulation decreased with increasing dosage of citric acid. The effect was the most pronounced in the presence of Fe^{3+} . The degree of coagulation decreased from ~80% to ~5% with the addition of 2.5×10^{-4} mol/L citric acid. In the presence of 10^{-3} mol/L citric acid, the degree of coagulation decreased from ~90% to ~30 and ~50% in the presence of 10^{-3} mol/L of Ca^{2+} and Mg^{2+} , respectively.

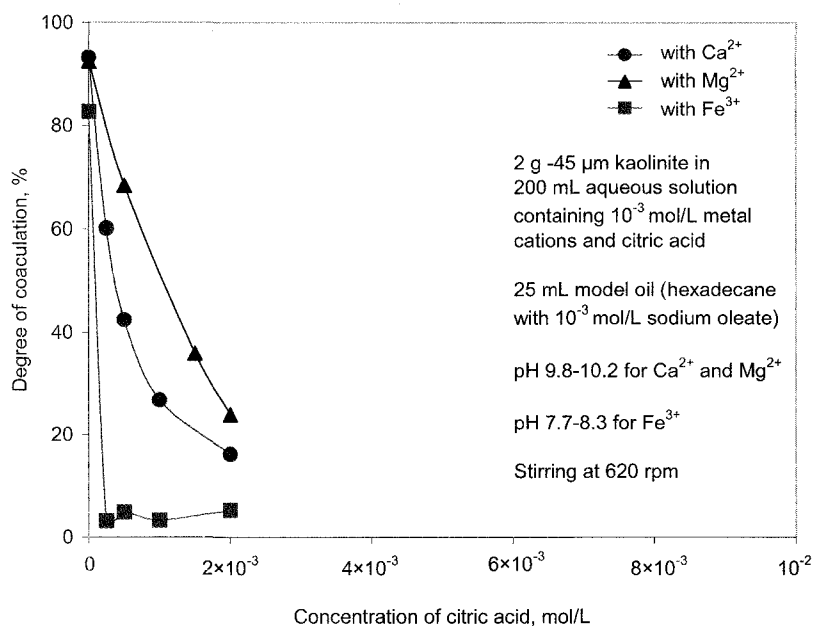


Figure 4-6 Coagulation of model oil with kaolinite at different concentrations of citric acid in the presence of 10^{-3} mol/L metal ions.

4.3.3 Illite

Figure 4-7 shows that citric acid reduced the coagulation between the model oil and illite in the presence of all three metal cations tested. The degree of coagulation in the presence of Ca^{2+} , Mg^{2+} and Fe^{3+} followed one another closely, and decreased from ~80% to ~45% in the presence of 10^{-3} mol/L citric acid.

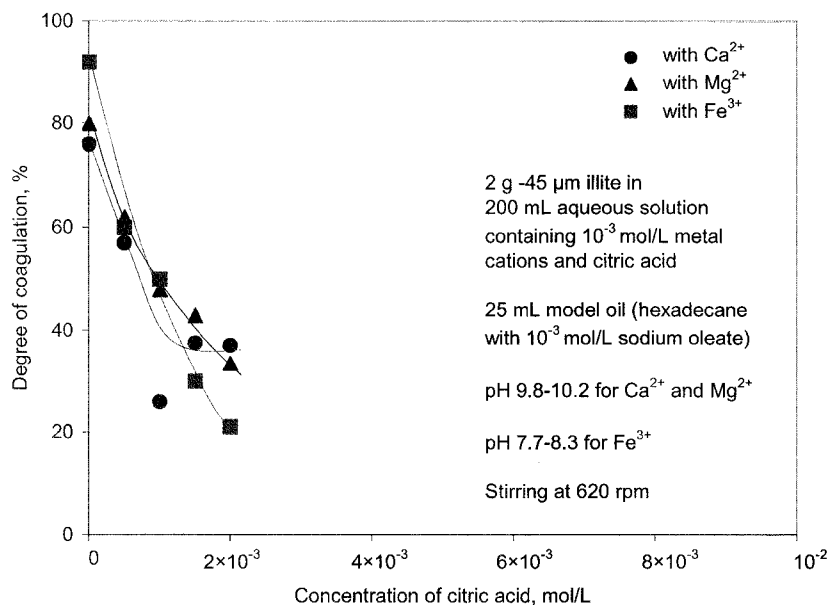


Figure 4-7 Coagulation of model oil with illite at different concentrations of citric acid in the presence of 10^{-3} mol/L metal ions.

4.4 Coagulation between Solvent-Diluted-Bitumen and Minerals

4.4.1 Quartz

Figure 4-8 shows the change in the degree of coagulation between quartz and bitumen in the presence of 10^{-3} mol/L Ca^{2+} as a function of the concentrations of different complexing agents. In the absence of a complexing agent, up to 85% of the quartz coagulated with bitumen, indicating strong bitumen-quartz interaction in aqueous solution containing 10^{-3} mol/L Ca^{2+} . In the presence of complexing agents and with increasing concentration, all complexing agents significantly reduced coagulation between quartz and bitumen. Therefore, they could all potentially eliminate the detrimental effect of Ca^{2+} in bitumen liberation from minerals. Citric acid and EDTA were equally effective by lowering the degree of coagulation from 85% down to 10% at the concentration of 10^{-3} mol/L.

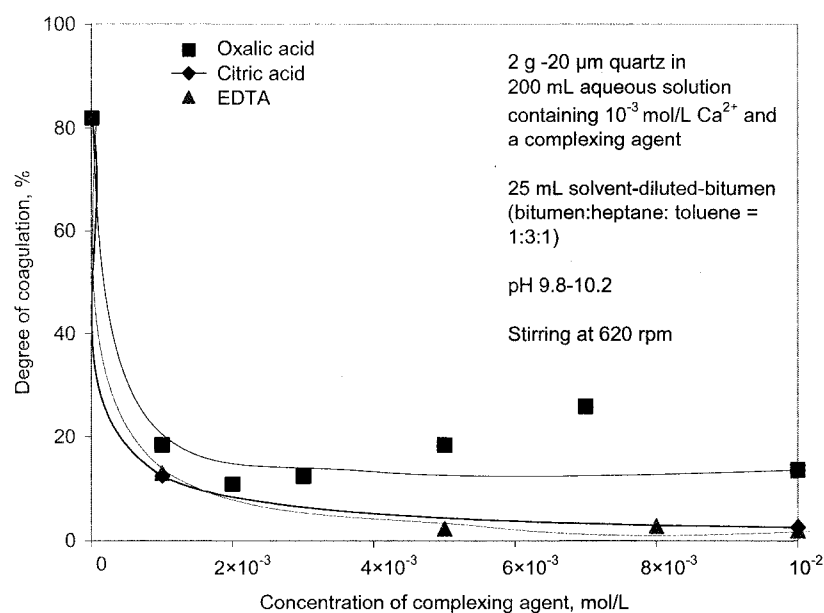


Figure 4-8 Coagulation of bitumen with quartz at different concentrations of complexing agent in the presence of 10^{-3} mol/L Ca^{2+} , pH 9.8–10.2.

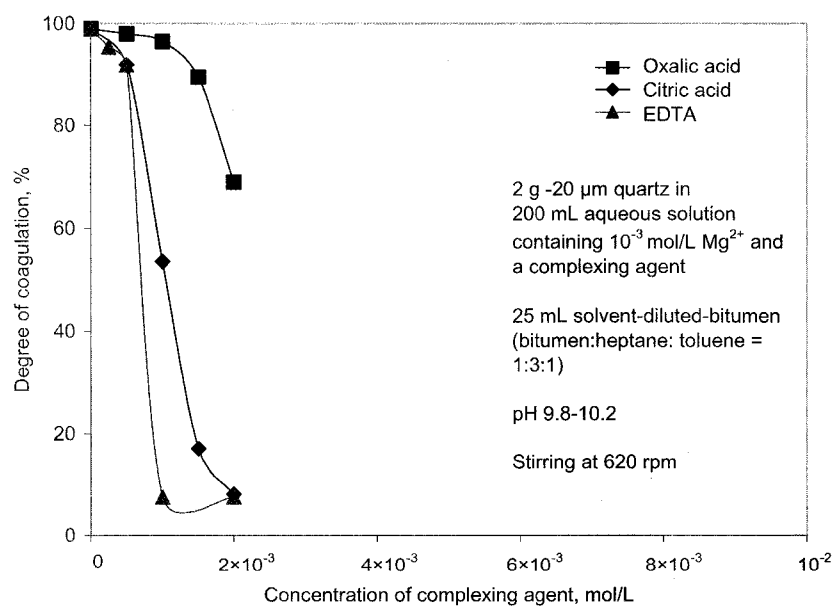


Figure 4-9 Coagulation of bitumen with quartz at different concentrations of complexing agent in the presence of 10^{-3} mol/L Mg^{2+} , pH 9.8–10.2.

Figure 4-9 shows bitumen-quartz coagulation in the presence of 10^{-3} mol/L Mg^{2+} as a function of the concentration of the three complexing agents. Both EDTA and citric acid were effective in preventing quartz from coagulating with the oil. At the concentration of 10^{-3} mol/L EDTA or 2×10^{-3} mol/L citric acid, the degree of coagulation was reduced to about 10% from 100% when no complexing agents were present. On the other hand, the addition of oxalic acid did not significantly reduce the coagulation between quartz and bitumen at the concentrations below 2×10^{-3} mol/L.

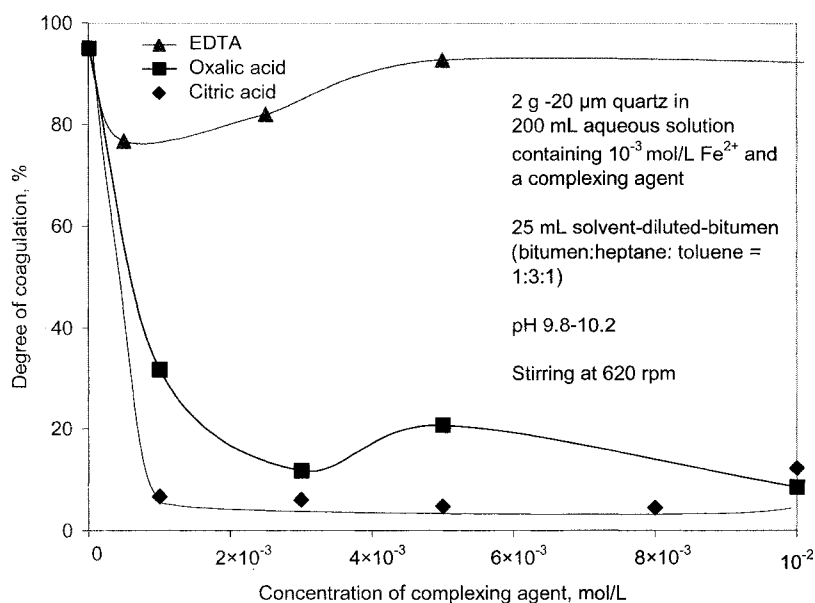


Figure 4-10 Coagulation of bitumen with quartz at different concentrations of complexing agent in the presence of 10^{-3} mol/L Fe^{2+} , pH 7.7–8.3.

As shown in Figure 4-10, when no complexing agents were added, almost 100% of the quartz was coagulated with bitumen in solutions containing 10^{-3} mol/L Fe^{2+} at pH 7.7–8.3. The addition of citric acid and oxalic acid dramatically reduced bitumen-quartz interaction as evidenced by the sharp decline in the degree of coagulation. As 10^{-3} mol/L of citric acid was added, the degree of coagulation was reduced from 95% to ~5%. Oxalic acid showed similar behavior: the degree of coagulation dropped sharply from 95% to ~30% initially and then leveled off at higher concentration, reaching ~10% at an oxalic

concentration of 3×10^{-3} mol/L. In contrast, EDTA showed very little depressive effect on the bitumen-quartz coagulation in the presence of Fe^{2+} .

Figure 4-11 illustrates the effect of citric acid, oxalic acid and EDTA on bitumen-quartz coagulation containing 10^{-3} mol/L Fe^{3+} . Similar to the case of Fe^{2+} , the degree of coagulation between bitumen and quartz was markedly reduced with increasing concentrations of citric acid and oxalic acid. The addition of citric acid caused the degree of coagulation to drop from 95% to below 5% at a low concentration of 10^{-3} mol/L. In contrast, the degree of coagulation was gradually reduced as the concentration of oxalic acid was increased, reaching 5% at a concentration of 10^{-2} mol/L. EDTA, which was ineffective when ferrous ions were present, also showed some effect by bringing the degree of coagulation down to 60% with 4×10^{-3} mol/L EDTA addition.

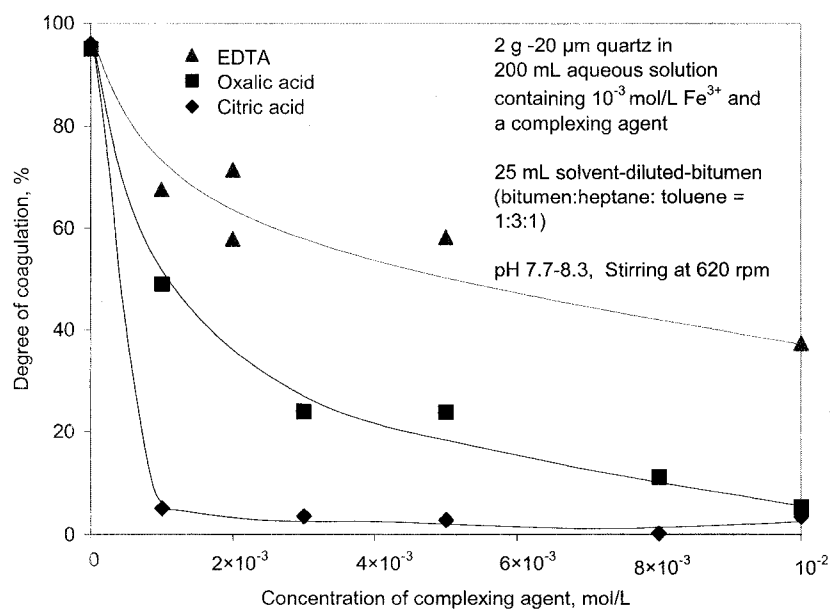


Figure 4-11 Coagulation of bitumen with quartz at different concentrations of complexing agent in the presence of 10^{-3} mol/L Fe^{3+} , pH 7.7–8.3.

The results on the visualization of bitumen-quartz interactions are shown in Figure 4-12. Figure 4-12a shows that quartz exhibited a high propensity to coagulate with bitumen in the presence of 10^{-3} mol/L Ca^{2+} at pH ~ 10 . Almost complete coverage of the bitumen

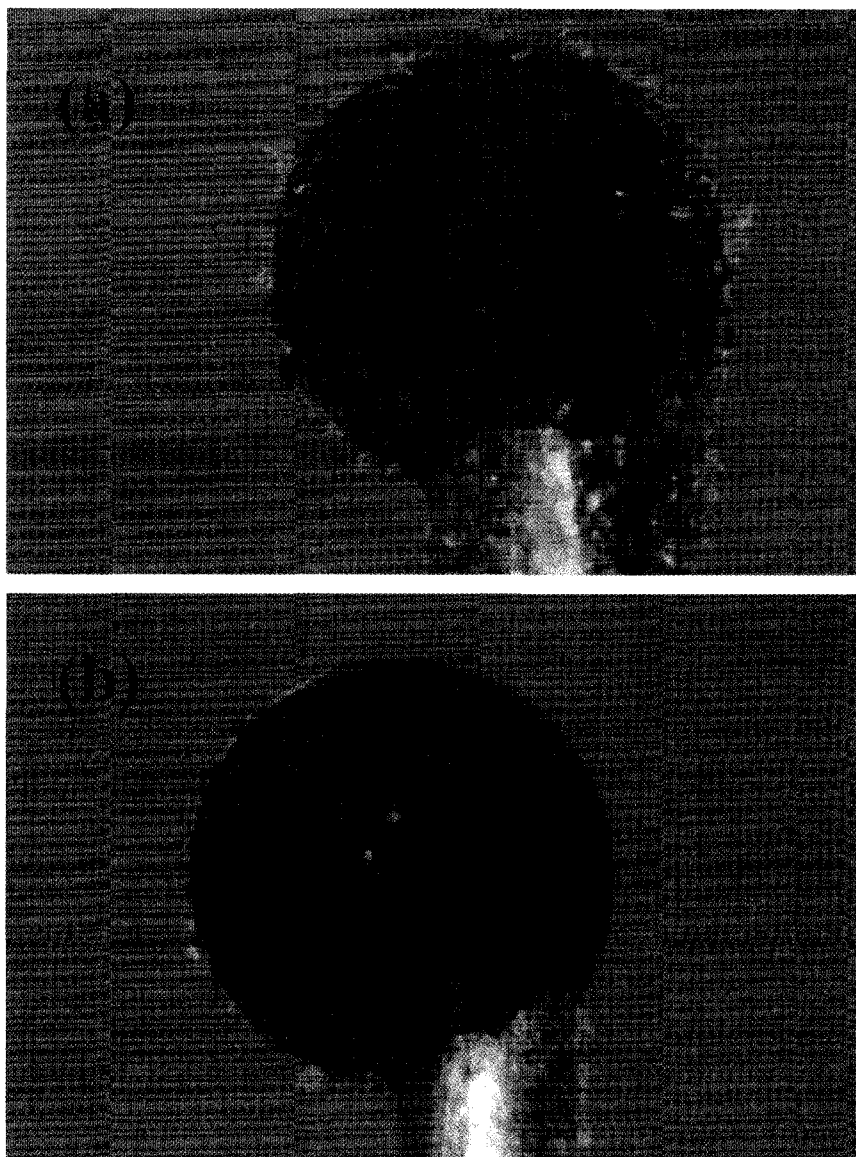


Figure 4-12 Microphotographs of bitumen droplets and $-63+25 \mu\text{m}$ quartz at pH ~ 10 with the addition of $10^{-3} \text{ mol/L Ca}^{2+}$ in (a) absence and (b) presence of 10^{-3} mol/L citric acid.

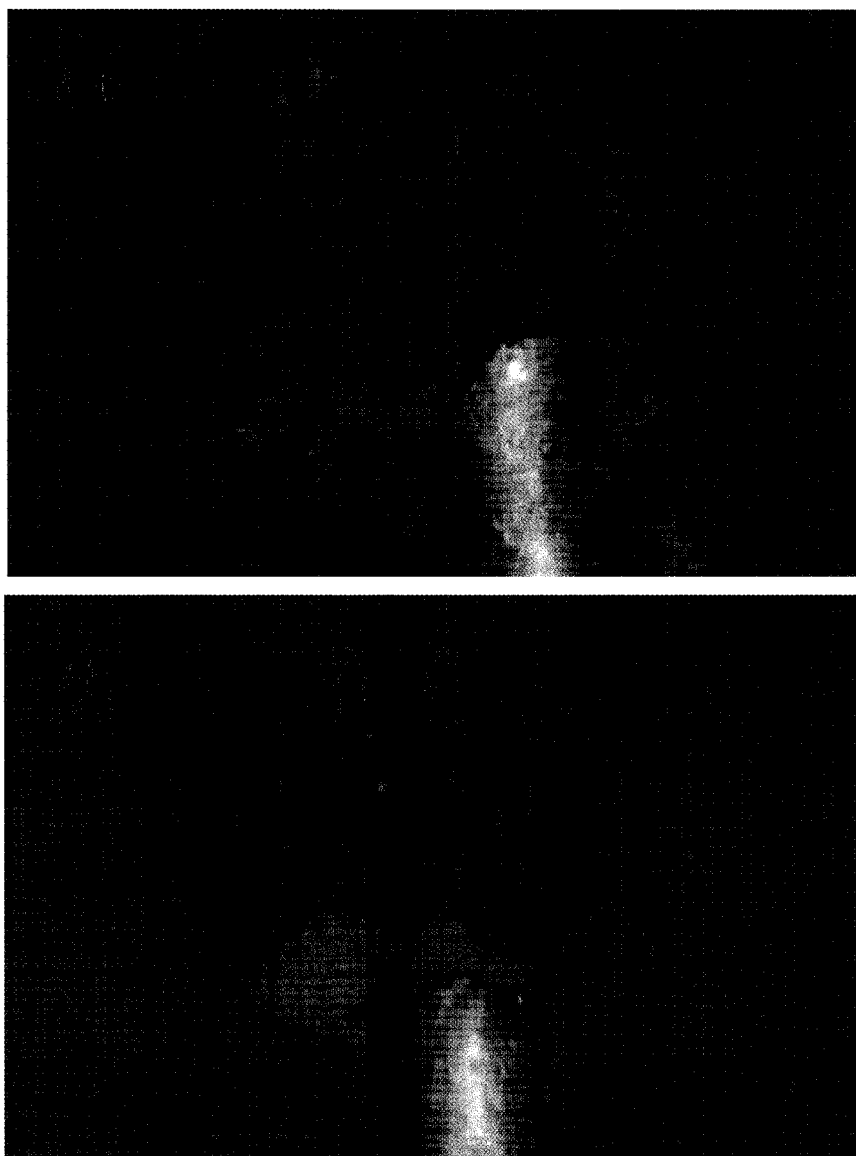


Figure 4-13 Microphotographs of zirconium droplets and $-63+25\ \mu\text{m}$ quartz at pH ~ 7.8 with the addition of $10^{-3}\ \text{mol/L}\ \text{Fe}^{3+}$ in (a) absence and (b) presence of $10^{-3}\ \text{mol/L}$ citric acid.

droplet by quartz particles was observed. This correlated well with coagulation experiment (as shown in Figure 4-8) in which ~85% of quartz was coagulated with bitumen when no complexing agent was added. However, in the presence of 10^{-3} mol/L citric acid, the bitumen droplet was smooth and few quartz particles were attached to it (Figure 4-12b). Similar phenomena were observed when Ca^{2+} was replaced by Fe^{3+} (Figure 4-13).

This direct observation confirmed the results of the coagulation tests which indicated that citric acid could effectively prevent bitumen from coagulating with quartz in aqueous solution containing multivalent metal cations.

In summary, the results of both the coagulation experiments and the visualization of bitumen-quartz adhesion in aqueous solution containing Ca^{2+} , Mg^{2+} , Fe^{2+} and Fe^{3+} showed that citric acid and oxalic acid were effective in preventing the mutual coagulation between bitumen and quartz, and thus could potentially enhance bitumen liberation from minerals. Oxalic acid was, however, the least effective in eliminating the effect of Mg^{2+} . While EDTA was effective in eliminating the effect of Ca^{2+} and Mg^{2+} , it was much less effective on $\text{Fe}^{2+}/\text{Fe}^{3+}$.

4.4.2 *Kaolinite*

Figure 4-14 shows that citric acid can effectively reduce bitumen-kaolinite coagulation in the presence of the three metal cations. The degree of coagulation decreased from about 90% to 33% for Ca^{2+} , 39.5% for Mg^{2+} and 43.5% for Fe^{3+} , as 2.5×10^{-4} mol/L citric acid was added. It indicated that citric acid was effective in breaking bitumen-kaolinite aggregates. However, the increase of citric acid dosage did not further reduce the degree of coagulation. Mechanical entrainment of fine kaolinite particles to bitumen-in-water emulsion was likely the explanation for this observation.

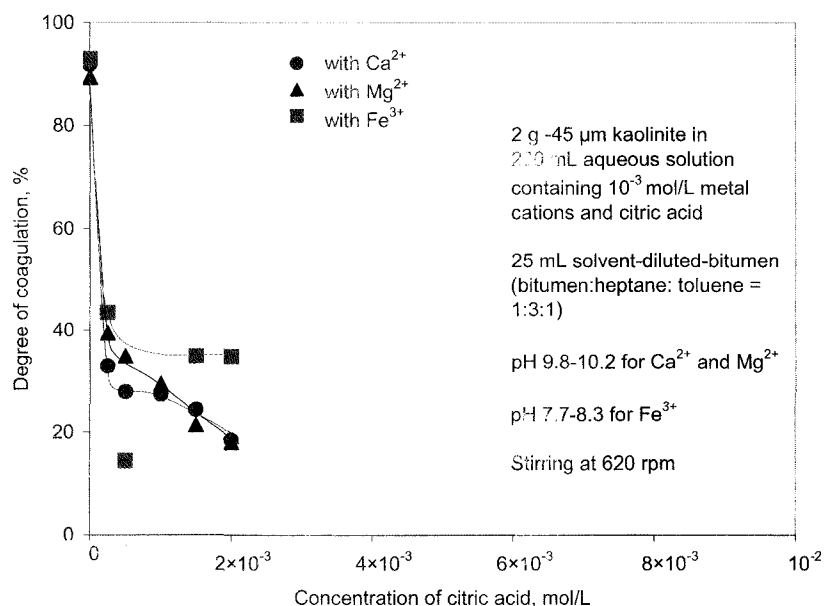


Figure 4-14 Coagulation of bitumen with kaolinite at different concentrations of citric acid in the presence of 10^{-3} mol/L metal ions.

4.4.3 Illite

Similar to the observation of kaolinite-bitumen coagulation, citric acid was effective in reducing the degree of coagulation between illite and bitumen, as shown in Figure 4-15. At the concentration of 10^{-3} mol/L citric acid, about 35% of illite was coagulated with bitumen in the presence of either Ca^{2+} or Mg^{2+} , compared with 60% and 80% in the absence of citric acid. It seems that citric acid was more effective in depressing the effect of Fe^{3+} (at pH 8): the degree of coagulation was reduced from 80% in the absence of citric acid to 20% after adding 10^{-3} mol/L citric acid.

Again, like kaolinite, some fine illite particles might be mechanically entrained in bitumen phase, which prevented the degree of coagulation from further decline as the concentration of citric acid increased up to 2×10^{-3} mol/L.

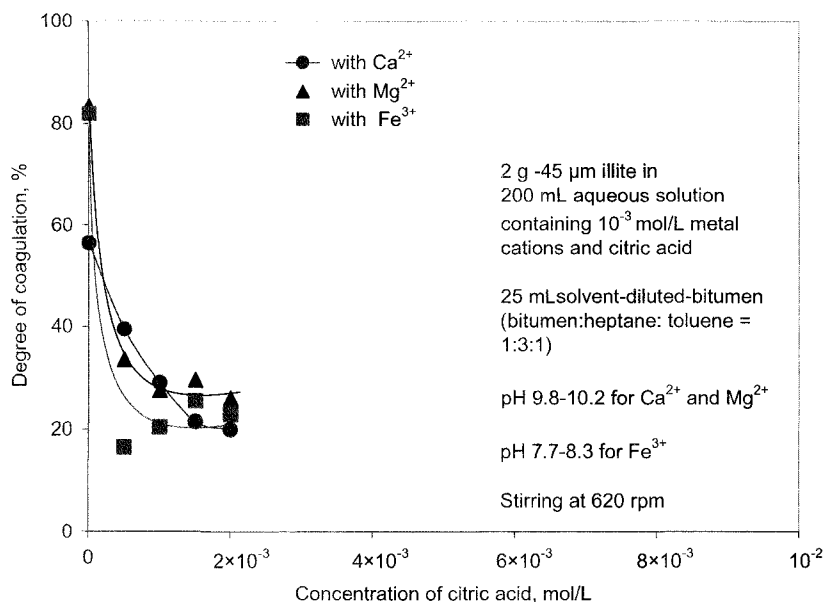


Figure 4-15 Coagulation of bitumen with illite at different concentrations of citric acid in the presence of 10^{-3} mol/L metal ions.

4.5 Summary

The organic complexing agents used in this study, in general, significantly reduced the mutual coagulation between bitumen (or model oil) and the minerals (quartz, kaolinite and illite) in aqueous solutions containing Ca^{2+} , Mg^{2+} , Fe^{2+} and Fe^{3+} ions.

Citric acid shows the best performance in decreasing the mutual coagulation for all the minerals and multivalent metal cations tested. Liberation of bitumen (oil) from quartz is easier to achieve than from other minerals containing lattice metal ions, i.e., kaolinite and illite. For instance, after adding 10^{-3} mol/L of citric acid, the degree of coagulation between bitumen and quartz was lowered to less than 10%, compared to 30–40% for kaolinite and illite after adding the same amount of citric acid.

Oxalic acid significantly reduced the mutual coagulation between bitumen (or model oil) and quartz from over 95% to below 40% at the concentration of 10^{-3} mol/L in the

presence of Fe^{2+} and Fe^{3+} . However, a higher concentration, above 2×10^{-3} mol/L, was generally required to reduce the coagulation in solutions containing Ca^{2+} and Mg^{2+} .

EDTA had a significant effect towards Ca^{2+} and Mg^{2+} , causing the degree of coagulation of bitumen (or model oil) with quartz to drop from ~95% to ~5% after adding 2×10^{-3} mol/L of EDTA in the presence of 10^{-3} mol/L of the Ca^{2+} and Mg^{2+} ions. However, EDTA had little effect in the cases of Fe^{2+} and Fe^{3+} .

5 BITUMEN LIBERATION AND SEPARATION FROM OIL SANDS FROTH TREATMENT TAILINGS

5.1 Introduction

Coagulation test results presented in the previous chapter indicated that the organic complexing agents can effectively reduce or eliminate the mutual coagulation between bitumen and the silicate minerals, implying a better liberation of bitumen. Froth flotation tests are therefore conducted to see if the beneficial role of the complexing agents in preventing the mutual coagulation between bitumen and the minerals can be realized in recovering the residual bitumen from the froth treatment tailings.

Paramagnetic minerals such as leucoxene and iron oxide in the froth treatment tailings may be floated along with bitumen to the froth products (these minerals are known to float with bitumen in the bitumen extraction circuit). In order to prevent their flotation, an external magnetic field was applied to keep the mineral particles in the flotation cell which was placed between the magnetic poles.

To achieve better bitumen liberation and separation, ultrasonic treatment is also used in the present work together with the organic complexing agents in the separation of residual bitumen from the oil sands froth treatment tailings.

5.2 Experimental

5.2.1 Materials and Chemicals

The naphthenic froth treatment tailings samples were provided by Syncrude Canada Ltd. The tailings samples were received in four 20-liter pails and contained 1–5% bitumen, 10–30% clay/solids and the balance was process water. Clarified supernatant was decanted from the pails and saved as “process water” that was used in the experiments.

The remaining tailings were combined, homogenized by a mechanical stirrer, and sampled by a peristaltic pump to aliquots of 50 mL wet samples for bitumen recovery testwork.

Citric acid ($C_6H_8O_7 = 100.3\%$) and oxalic acid ($C_2H_2O_4 \cdot H_2O = 100.1\%$) were purchased from Fisher Scientific and were used as organic complexing agents. Polyacrylamide (PAM, MW = 5–6 million) was obtained from Across Organics and was used as a flocculant. Toluene ($C_6H_5CH_3 \geq 99.5\%$, Fisher Scientific) was used to determine bitumen contents in the test samples.

5.2.2 *Experimental Techniques*

Froth Flotation. The froth flotation tests were conducted in a 200 mL suspension flotation cell to float the residual bitumen from the froth treatment tailings diluted either with distilled water or process water. In each test, 50 mL wet tailings were mixed with 150 mL of water in the flotation cell for 8 minutes by a mechanical stirrer at a desired speed. During the agitation, pulp pH was adjusted and desired chemicals were added. Flotation was conducted for 20 minutes at room temperature (10 minutes for elevated temperature at $40^\circ C$). Both the froth product and the flotation tailings were dried at $85^\circ C$, washed with toluene to remove the bitumen and filtered until the wash solvent became colorless. The filter cakes were air dried and weighed from which the contents of bitumen and mineral matter in the flotation products, and thus their recoveries, were calculated. The difference between the recoveries of bitumen and mineral solids into the froth product was defined as the “Separation Efficiency”.

The separation efficiency was used as an indicator to measure the degree of bitumen liberation from the tailings. The underlining assumption was that the residual bitumen was floatable while the mineral matter was not, and that the only reasons that the mineral matter entered the froth product were 1) that it was not liberated from the residual bitumen and/or 2) it was mechanically entrained. It was envisaged that the degree of liberation may be improved by using the tested complexing agents, whereas the

mechanical entrainment may be reduced by using suitable polymeric depressants with high molecular weights (Liu et al., 2006b).

For each series of flotation tests using a complexing agent, a “blank” test was conducted in which no complexing agent was added. Any improvement in separation efficiency after adding a complexing agent was considered to be the result of better liberation of bitumen from the mineral solids.

Froth Flotation with External Magnetic Field. Flotation tests inside an external magnetic field were carried out using the setup illustrated in Figure 5-1. In these tests, the 200 mL flotation cell was placed in between the two magnetic poles of a wet high intensity magnetic separator (WHIMS, Sepor Inc.). Steel balls with a diameter of 6.5 mm were used. The experimental procedures were the same as described previously.

Froth Flotation with Ultrasonic Treatment. In these tests, 50 mL froth treatment tailings samples were diluted by 150 mL process water in a 600 mL beaker. The suspension was agitated by a mechanical stirrer at a speed of 300 rpm while submerged in a HT150 (VWR CanLab) ultrasonic water bath (50Hz, 160W) for a designated time. Pulp pH was controlled at ~8.3 and citric acid was added as required. After the treatment, the sample was transferred to the suspension flotation cell and floated for 20 minutes at 1900 rpm.

Bitumen Content Determination. A dry sample was dispersed in a beaker containing 100 mL toluene. The mixture was agitated to dissolve the bitumen, then left stand for 30 minutes to allow the coarse solids to settle. The supernatant was centrifuged at 2000 rpm for 20 minutes to recover the fine solids which were combined with the coarse solids. The combined solids were washed again with 100 mL toluene followed the above procedures. The washing was repeated several times until the spent toluene became colorless. The collected solids were filtered and air-dried for 24 hours to a constant weight. The difference between the weights of the sample before and after toluene washing was taken as the mass of bitumen.

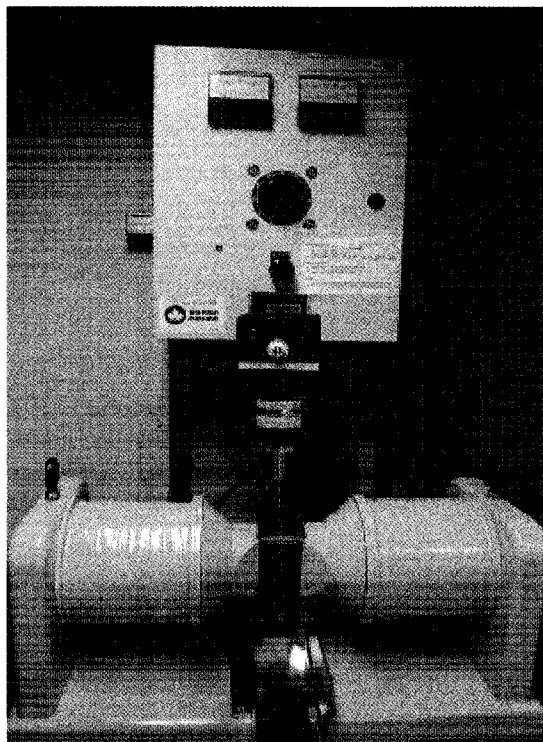


Figure 5-1 Experimental setup for flotation in an external magnetic field.

5.3 Effect of Complexing Agents

In the first series of flotation tests, 50 mL of tailings sample slurry was diluted with 150 mL distilled water and then floated with and without the addition of the complexing agents. The difference between the recoveries of bitumen and mineral solids into the froth product was defined as the “Separation Efficiency”. The results, including separation efficiency (E_s), recoveries of bitumen (R_b) and solid (R_s), into the bitumen froth, are presented in Table 5-1. The separation efficiency E_s was also plotted vs. the concentration of complexing agent in Figure 5-2. As can be seen, the separation efficiency increased by about 24 percentage points from 34% (with no citric acid) to 58% (with the addition of 2×10^{-3} mol/L citric acid). Both increased bitumen recovery and decreased solid recovery contributed to the improvement of separation efficiency, which implied that citric acid indeed benefited bitumen-solid liberation.

When oxalic acid was used, the separation efficiency increased from around 34% (with no oxalic acid) to 45% (with 10^{-3} mol/L oxalic acid), but then fell to around 34% when oxalic acid concentration was increased to 6×10^{-3} mol/L. It was possible that oxalic acid improve bitumen-mineral liberation with appropriate addition, thus significantly increase separation efficiency contributed by bitumen recovery. Overdosed oxalic acid likely made both air bubble and liberated bitumen droplet highly negatively charged, thus reduced bitumen recovery due to deteriorated bitumen aeration.

Table 5-1 Separation efficiency of bitumen at various concentrations of complexing agents (see Figure 5-2).

Citric acid				Oxalic acid			
C, mol/L	R _b , %	R _s , %	E _s =R _b -R _s , %	C, mol/L	R _b , %	R _s , %	E _s =R _b -R _s , %
0	63.0	29.3	33.6	0	63.0	29.3	33.6
1×10^{-3}	69.5	24.4	45.1	1×10^{-3}	88.3	27.1	44.9
2×10^{-3}	78.9	20.0	58.3	3×10^{-3}	68.5	26.9	41.6
3×10^{-3}	82.9	29.1	53.8	6×10^{-3}	70.8	37.3	33.5

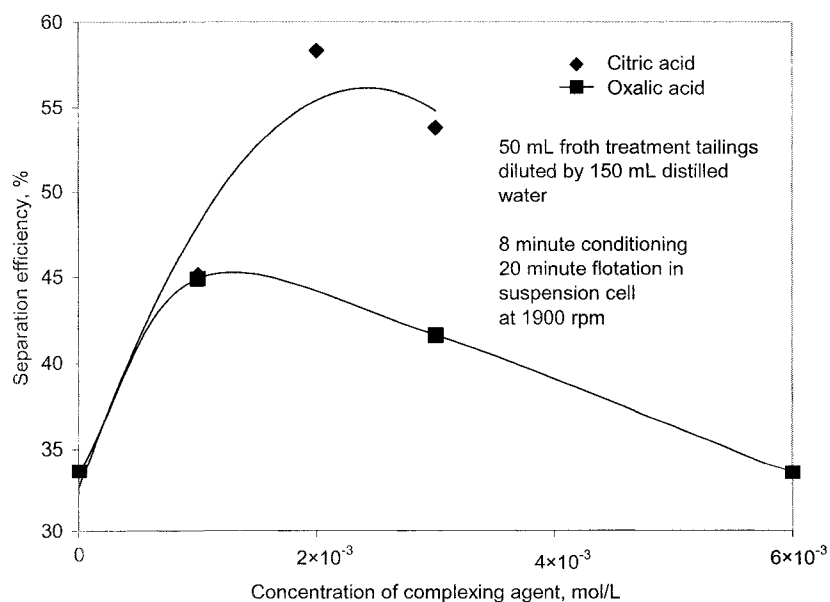


Figure 5-2 Separation efficiency of bitumen from oil sands froth treatment tailings at different concentration of complexing agent, pH ~8.3.

The results indicated that oxalic acid was not as effective as citric acid in increasing the separation efficiency. This was consistent with the coagulation tests which showed that oxalic acid was not as effective as citric acid in eliminating the detrimental effect of multivalent metal cations (Figure 4-8 to Figure 4-15). Clearly, the ability of the organic acids to prevent bitumen/mineral coagulation in the presence of metal cations was correlated to their ability to increase flotation separation efficiency.

5.4 Effect of Sequential Additions of Citric Acid and Polyacrylamide

It is well known that fine and ultrafine particles will be mechanically entrained into the flotation froth product even if they are hydrophilic (Johnson et al., 1974; Trahar, 1981; Warren, 1984). Therefore, the mineral slimes and clays in the oil sands froth treatment tailings may have been carried to the bitumen froth even if they are liberated from the residual bitumen. According to the recent proposal to exploit the dual functions of polymeric reagents as both a flocculant and flotation depressant (Liu et al., 2006b), the froth treatment tailings sample was conditioned with citric acid first, followed by treatment with a polymer prior to flotation. The rationale was that the citric acid would liberate the minerals from the residual bitumen, and the polymer would then flocculate the slimes/clays so that they would not entrain in the froth product.

Polyacrylamide (PAM) as a flocculant has been widely used to facilitate mechanical entrainment of fine particles in froth flotation. Figure 5-3 shows the preliminary results with the use of polyacrylamide (PAM) as the polymer. In these tests, the froth treatment tailings sample was diluted with process water, and 1.5×10^{-3} mol/L citric acid was added prior to PAM and the flotation tests were conducted at a pulp temperature of 40°C. Clearly, separation efficiency was further improved upon the addition of PAM. Another set of data was collected by lowering the agitation speed from 1900 rpm to 1100 rpm to examine if it improved separation efficiency by avoiding breakage of the flocs at the lower agitation speed. It seems that lower speed performed better only at higher concentrations of PAM.

5.5 Combined Effect of Citric Acid and an External Magnetic Field

Figure 5-4 shows that the separation efficiency increased from 35% to 45% as the concentration of citric acid increased from zero to 10^{-3} mol/L with 0.25 Tesla external magnetic field. Similar observation was made at 0.5 and 0.62 Tesla external magnetic field intensity, except for a smaller in magnitude. This indicated that the presence of citric acid was beneficial to bitumen liberation from froth treatment tailings.

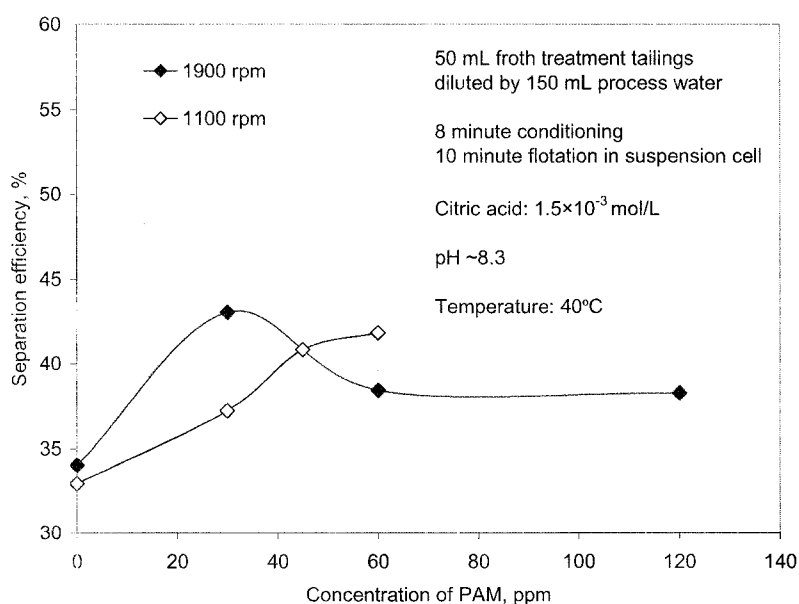


Figure 5-3 Separation efficiency of bitumen from oil sands froth treatment tailings at different concentration of polyacrylamide (PAM) at a pulp temperature of 40°C, pH ~8.3.

However, the separation efficiency progressively decreased as the intensity of external magnetic field increased from 0.25 to 0.7 Tesla. This was mainly due to the decrease in the recovery of the residual bitumen. It was possible that the heavy minerals collected at the magnetic media (steel balls) plugged the channels through which aerated bitumen was supposed to pass to get into the froth layer, resulting in the decrease in bitumen recovery. It was also possible that the bitumen droplets “engulfed” the heavy mineral particles and

thus were retained by the magnetic media together with the minerals. Work along this line was not continued but this is a direction that may be pursued further.

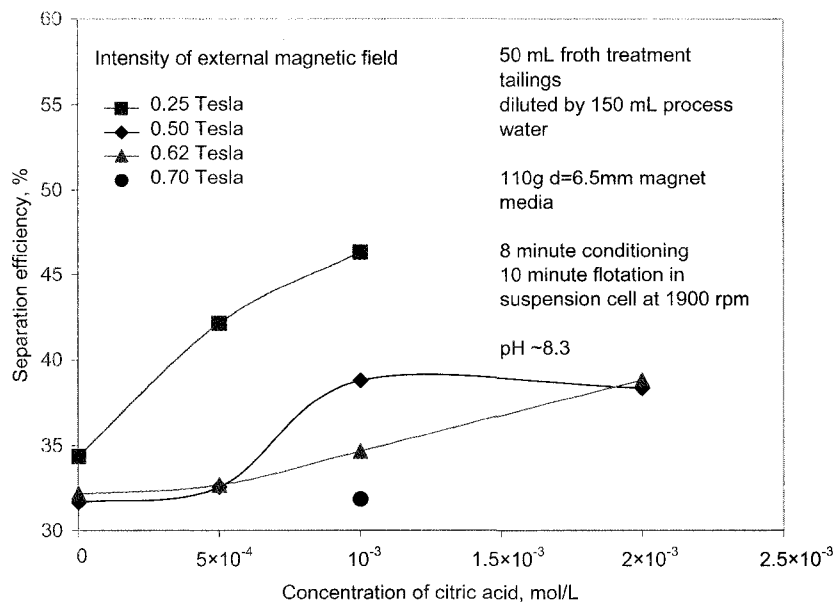


Figure 5-4 Separation efficiency of bitumen from oil sands froth treatment tailings at different intensities of external magnetic field, pH ~8.3.

5.6 Combined Effect of Citric Acid and Ultrasonic Treatment

Ultrasonic treatment is believed to be helpful in bitumen liberation by the cavitation process. The cavitation generated by ultrasonic waves provides additional breakage of the bitumen/solid attachment and results in the detachment of the bitumen from the associated mineral particles.

A number of studies have shown that ultrasonic treatment can promote hydrocarbon extraction from soils (clays) (Hart, 1977; Blanco et al., 1992; Riera et al., 2004). Hart (1977) applied ultrasonic energy with bitumen soluble solvent and successfully extracted bitumen from oil sands at ambient temperature, achieving 78% bitumen extraction in 60 seconds. He believed that ultrasonic energy could break the bonding between hydrocarbons and sand grains. Sadeghi et al. (1990) extracted bitumen from Alberta oil

sands by using sodium silicate and ultrasonic treatment at 45°C and ambient atmosphere for 6 hours. He concluded that the efficient bitumen extraction was due to a combination of ultrasonic treatment and the surfactants that were released from the oil sands. In ultrasonic-assisted oil extraction, organic solvents were normally used, and the time and frequency of sonication were identified as major factors affecting the oil extraction (Sadeghi et al., 1990; Hart, 1977; Romdhane and Gourdon, 2002).

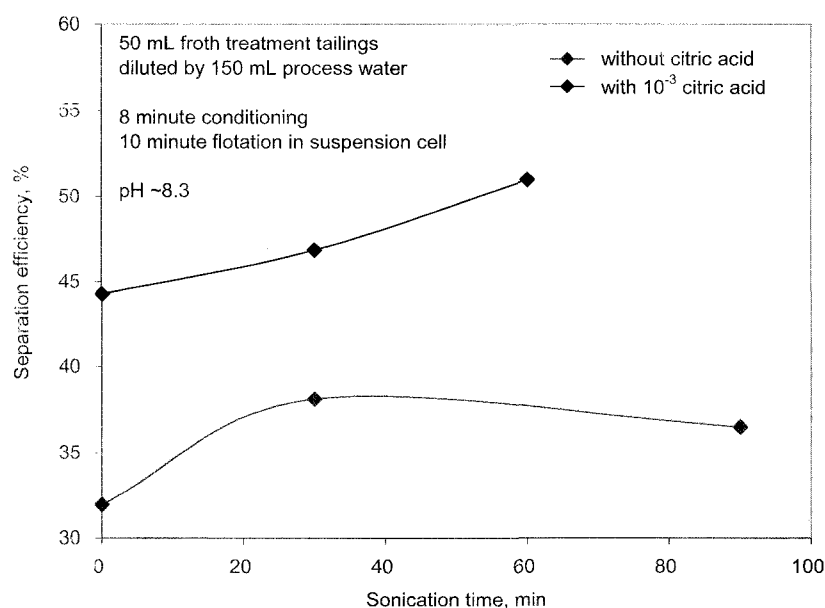


Figure 5-5 Separation efficiency of bitumen from oil sands froth treatment tailings at different sonication pretreatment with or without citric acid addition, pH ~8.3.

Bitumen separation efficiency from froth treatment tailings (diluted by process water) at different sonication time was plotted in Figure 5-5. It shows that separation efficiency was significantly improved with increasing sonication time, with or without the presence of citric acid, although the addition of citric acid resulted in higher separation efficiency. The results indicated that ultrasonic energy had a positive effect on bitumen liberation and flotation from froth treatment tailings. With 30 minutes of ultrasonic treatment, the separation efficiency increased by 3 percentage points from 44% to 47% in the presence of 10^{-3} mol/L citric acid, and from 32% to 38% when no citric acid was added. Thus the

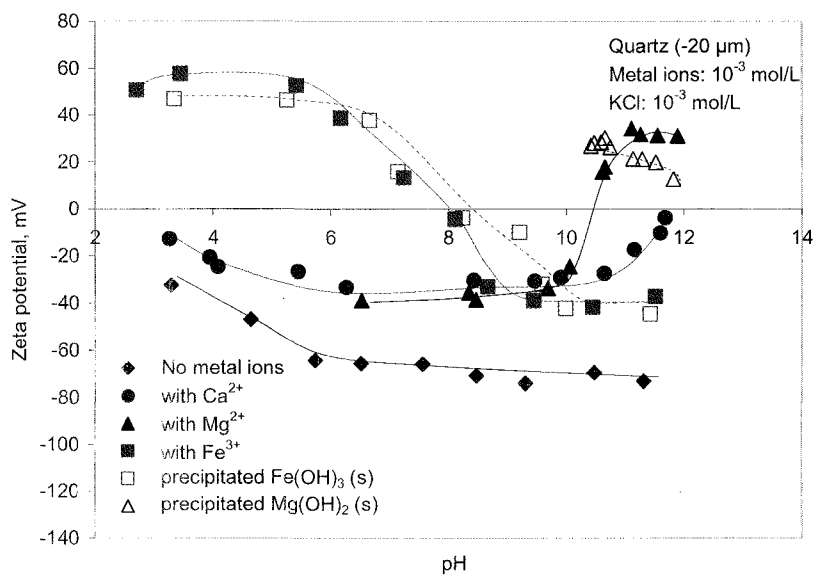


Figure 6-1 Zeta potential of quartz at different pH in the absence and presence of 10^{-3} mol/L metal ions.

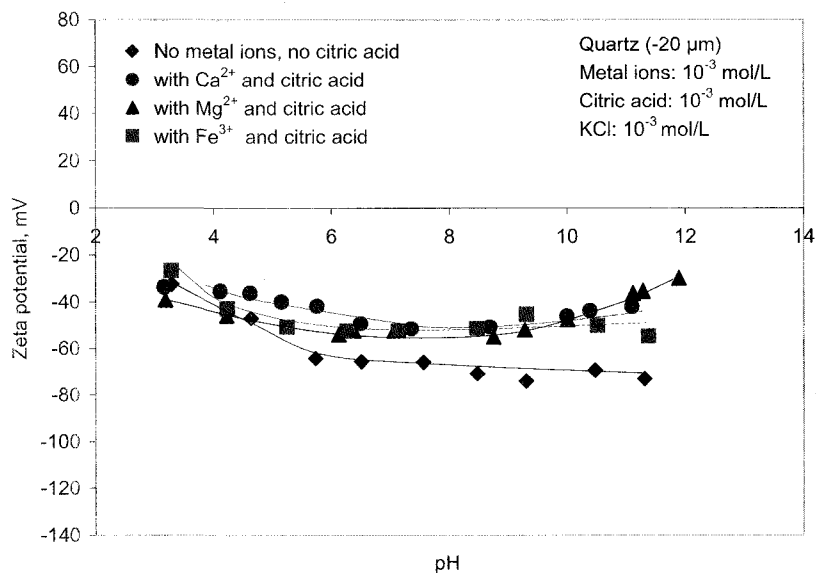


Figure 6-2 Zeta potential of quartz at different pH in the presence of 10^{-3} mol/L metal ions and 10^{-3} mol/L citric acid.

combined use of citric acid and sonication energy could improve bitumen liberation and separation from froth treatment tailings.

5.7 Summary

As a result of reduced mutual coagulation between bitumen and mineral particles, citric acid was found to improve the separation efficiency of bitumen from the froth treatment tailings by 24 percentage points with the addition of 2×10^{-3} mol/L. Separation efficiency was further improved up to 10 percentage point by the combined addition of 1.5×10^{-3} mol/L citric acid and 30 ppm polyacrylamide. This was considered to be due to the improved bitumen liberation from the mineral matter as a result of citric acid addition and also due to the flocculation of the fine minerals such as clays by polyacrylamide which reduced their mechanical entrainment.

Combined treatment by citric acid and sonication was also beneficial to the bitumen liberation from the tailings, as indicated by the increase in separation efficiency. It was likely due to the synergistic effects of ultrasonic energy and citric acid, in that the cavitation process could “rip” bitumen off mineral surface, while citric acid prevented the liberated bitumen from coagulating with the minerals.

The limited number of flotation tests conducted in the presence of an external magnetic field did not improve the efficiency of bitumen separation from the froth treatment tailings. More studies are needed to elucidate the effect of magnetic field on bitumen liberation and separation.

6 MECHANISMS OF ACTION OF THE METAL IONS – ELECTROKINETIC STUDIES³

6.1 Introduction

Coagulation or dispersion of colloidal particles in aqueous solutions is governed by the total interaction energy among the colloidal particles involved. A theory independently developed by Derjaguin and Landau, and Verwey and Overbeek in the 1950s, to describe the total potential energy of interaction is the well known classical DLVO theory. This theory incorporates the electrical double-layer force and the van der Waals forces. The universal attractive van der Waals forces are only a function of separation distance of two colloidal particles for a given system, as the nature and geometry of the substances and dispersing medium are fixed. In contrast, electrical double layer force is strongly dependent on the solution conditions including pH, ionic strength, and specific adsorption of ions or molecules on the particle/solvent interface, etc.

In order to understand the effects of multivalent metal ions and organic complexing agents on the coagulation (liberation) of bitumen with minerals, as observed and reported in preceding chapters, zeta potentials of mineral particles and bitumen droplets are measured, and the measured potentials are used to calculate the interaction potentials between bitumen droplet and the mineral particles using classical DLVO theory. The results are presented in this chapter.

6.2 Experimental

6.2.1 *Materials*

Minerals used in the experiments were the same as in coagulation tests described in Chapter 3 and Chapter 4, except that $-5 \mu\text{m}$ illite, separated from the $-45 \mu\text{m}$ illite

³ Portions of this and the next chapter have been compiled into two papers and submitted to Journal of Colloid and Interface Science & International Journal of Mineral Processing in January & February 2008.

samples, was used. Solvent-diluted-bitumen was prepared using the procedures described in the experimental section 4.2. Chemical reagents used are tabulated in Table 4-1.

Stock suspensions of minerals (quartz, kaolinite and illite) were prepared by dispersing two grams of mineral particles in one liter of distilled water containing 10^{-3} mol/L KCl as supporting electrolyte, and equilibrated for 24 hours at room temperature.

Oil-in-water emulsion was prepared by homogenizing 2 mL of hexadecane with 200 mL 10^{-3} mol/L KCl for 15 minutes by a Model 500 sonic dismembrator (Fisher Scientific). The average droplet size of the oil-in-water emulsion (measured by Brookhaven 90Plus/BI-MAS) was stabilized at 252 ± 10 nm within the initial 4 hours after the emulsion was prepared.

To prepare bitumen stock emulsion, the solvent-diluted-bitumen was centrifuged at 10,000 G (RC-6, Mandel Scientific) to remove the fine solid impurities. Then, 2 mL of the centrifuged solvent-diluted-bitumen was dispersed in 200 mL 10^{-3} mol/L KCl solution, heated to 85°C to evaporate the organic solvents prior to bitumen emulsification, which was performed by the Model 500 sonic dismembrator for 15 minutes. The emulsion thus prepared was assumed to be free of solids and solvent and thus truly reflected the surface nature of bitumen. The effective diameter of the bitumen droplets (measured by the Brookhaven 90Plus/BI-MAS) only increased from 450 nm to 463 nm within the initial 2 hours after the emulsion was prepared. Thus the bitumen-in-water emulsion was considered stable during the period when the zeta potential measurements were performed.

6.2.2 *Experimental Methods*

The zeta potentials of mineral particles and oil droplets were measured at different pH with or without the presence of 10^{-3} mol/L metal cations and 10^{-3} mol/L citric acid. Citric acid was chosen because of its exceptional effect on eliminating the mutual coagulation over oxalic acid and EDTA.

The zeta potentials of mineral particles and oil-in water or bitumen-in-water emulsions were measured by a ZetaPALS zeta potential analyzer (Brookhaven) at 22°C. Five milliliter of stock suspension of minerals or bitumen (oil) emulsion was transferred to a 600 mL glass beaker containing 250 mL of 10^{-3} M KCl solution. The suspension was conditioned with metal cations and/or organic acid for 10 minutes at a controlled pH value. About 1.6 mL of the conditioned suspension was transferred to a sample cuvette for zeta potential measurement. Each measurement was repeated 10 times with 10 cycles for each run. The standard deviation for the 10 runs was within ± 5 mV.

6.3 Zeta Potentials of Minerals

6.3.1 Quartz

Figure 6-1 shows zeta potentials of quartz in solutions containing Ca^{2+} , Mg^{2+} and Fe^{3+} at different pH. As can be seen, the addition of Ca^{2+} and Mg^{2+} rendered quartz particles less negatively charged, which is in agreement with literature (e.g., Kaya and Yukselen, 2005). At above pH 7, the zeta potential of quartz in the presence of Ca^{2+} did not change with pH until pH 10 where it moved towards positive direction, and approached zero at pH 12.

The zeta potential curve of quartz in solutions containing Mg^{2+} closely traced that in the Ca^{2+} solutions from about pH 6.5 to 9.5. The curve rapidly increased at pH 9.5, reached a zeta potential of zero at pH 10.5, and moved into positive region at pH above 10.5. In fact, quartz in the quartz- Mg^{2+} solution had similar zeta potentials as those of magnesium hydroxide precipitates from pH 11 to 12.

In the presence of Fe^{3+} , the zeta potentials of quartz closely followed that of precipitated $\text{Fe}(\text{OH})_3$. Quartz surface was positively charged from pH 3 to 8, and then became negatively charged above pH 8. Since each zeta potential value was the average of 10 runs and no significant variations were observed for the 10 runs, it is likely that most of the quartz surface was masked by precipitated ferric hydroxides (The same was

reported by Krishnan and Iwasaki, 1986) for magnesium hydroxides.

Figure 6-2 shows that the addition of citric acid made quartz negatively charged in the entire pH range tested in the presence of Ca^{2+} , Mg^{2+} or Fe^{3+} ions. From pH 8 to 10, at which quartz and the bitumen (or model oil) was extensively coagulated (Figure 3-9 and Figure 3-15), the magnitude of the zeta potentials was less than 30 mV for all tested cations. However, after adding citric acid, the zeta potentials of quartz were stabilized at about -45 mV, slightly less negative than quartz alone.

6.3.2 *Kaolinite*

As can be seen from Figure 6-3, in the absence of metal cations, kaolinite carried negative charges in the entire pH range tested from pH 3 to 12. The zeta potential increased in the negative direction with increasing pH from pH 4–8 and stabilized at -51 mV above pH 8.

In the presence of Ca^{2+} , the kaolinite became much less negatively charged at pH 6–12. The zeta potential of kaolinite increased from -27 mV at pH 8 to -16 mV at pH 10.5. The zeta potential curve of kaolinite in the presence of Mg^{2+} closely followed that in Ca^{2+} solutions from pH 6 to 10 before an abrupt rise followed by a sign reversal at pH 10.5. The zeta potential of kaolinite from pH 10.6 to 11.5 was similar to that of magnesium hydroxide precipitates. The precipitated $\text{Mg}(\text{OH})_2$ particles have been reported to specifically adsorb on kaolinite particle surfaces (Kaya and Yukselen, 2005). In the case of Fe^{3+} , the zeta potentials of kaolinite resembled that of precipitated $\text{Fe}(\text{OH})_3$. Kaolinite surface was positively charged from pH 3 to pH 8, and became negatively charged above pH 8. Similar to the scenario with Mg^{2+} , kaolinite's surface charge likely resulted from surface precipitation of ferric hydroxide.

Admittedly, the zeta potential of kaolinite was an overall average of the contributions of both the edges and the basal surfaces. Since the edges account for only about 12–34% of the total surface (Ferris and Jepson, 1975; Zhou and Gunter, 1992; Brady et al., 1996),

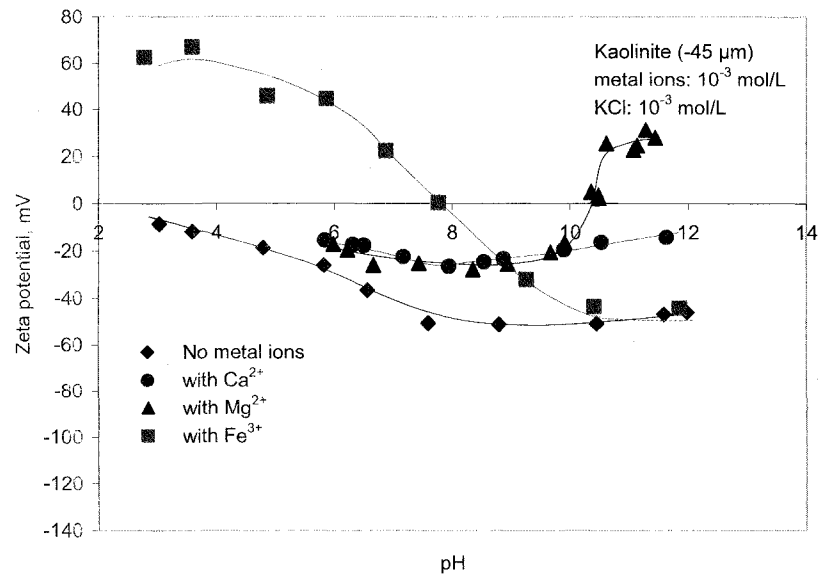


Figure 6-3 Zeta potential of kaolinite at different pH in the presence of 10^{-3} mol/L metal ions.

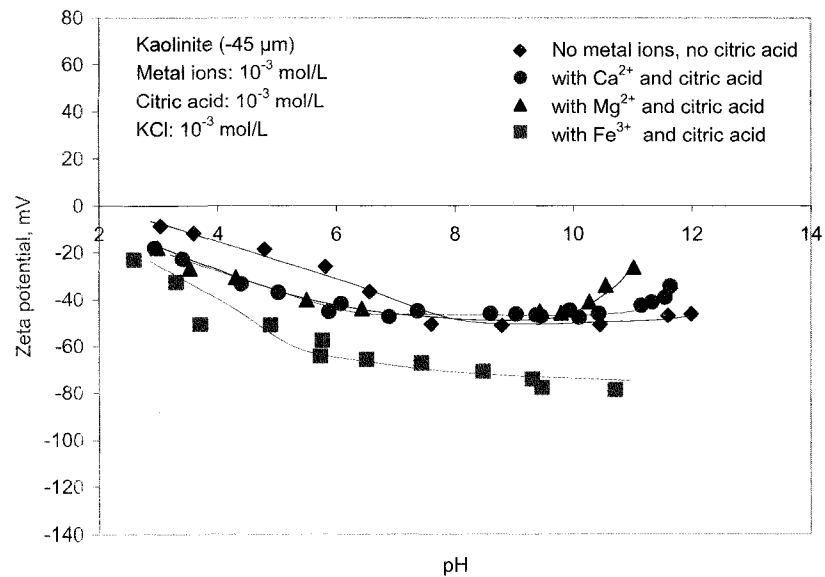


Figure 6-4 Zeta potential of kaolinite at different pH in the presence of 10^{-3} mol/L metal ions and 10^{-3} mol/L citric acid.

the measured zeta potential may have underestimated the effect of edge surfaces of kaolinite on bitumen-kaolinite interaction, particularly at the pH value below the isoelectric point of kaolinite edges.

As can be seen from Figure 6-4, the presence of citric acid made kaolinite more negatively charged in the entire pH range tested. Particularly, for solutions containing ferric ions, the zeta potential of kaolinite became more negative than that in the absence of any metal cation. It may be due to the adsorption of un-complexed (“free”) citrate anions.

6.3.3 *Illite*

Similar to kaolinite, illite was negatively charged above pH 6 when no metal ions were present. As shown in Figure 6-5, in the presence of calcium and magnesium ions, the zeta potential of illite increased significantly at pH 7–9. Above pH 9, the zeta potential of illite became less negative with increasing pH, eventually became positive at pH 10.5, in the presence of Mg^{2+} . No significant change was observed for Ca^{2+} in this pH range. In the presence of Fe^{3+} , the zeta potential of illite was virtually the same as that of ferric hydroxides precipitates (Figure 6-1).

Figure 6-6 illustrates that illite carried negative charges from pH 6–11.5 in the presence of citric acid for all the metal ions used. The zeta potential of illite was slightly less negative in the presence of Ca^{2+} and Mg^{2+} ions than in their absence. However, in the presence of Fe^{3+} , the illite was more negatively charged than the original illite. At pH 8, almost all Fe^{3+} was present as ferric hydroxide precipitate. Therefore, these observations may be attributed to the adsorption of un-complexed citrate anions onto illite surface.

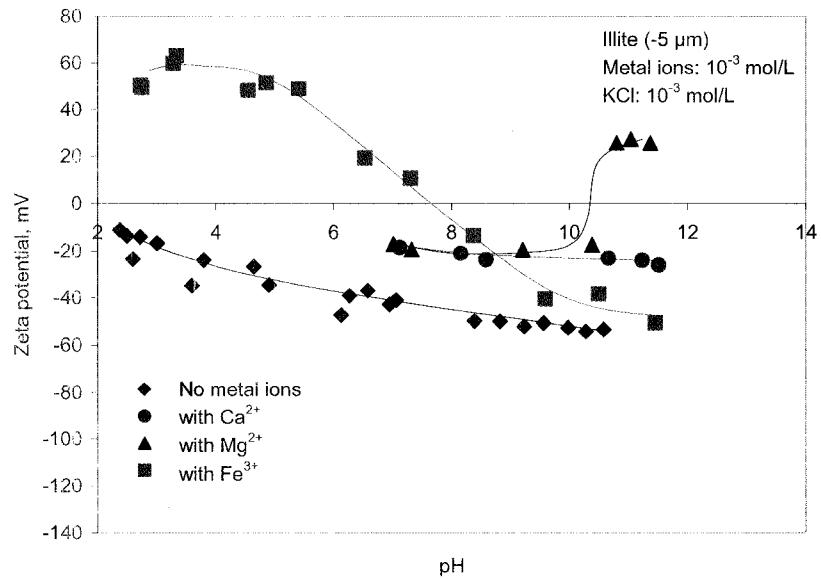


Figure 6-5 Zeta potential of illite at different pH in the presence of 10⁻³ mol/L metal ions.

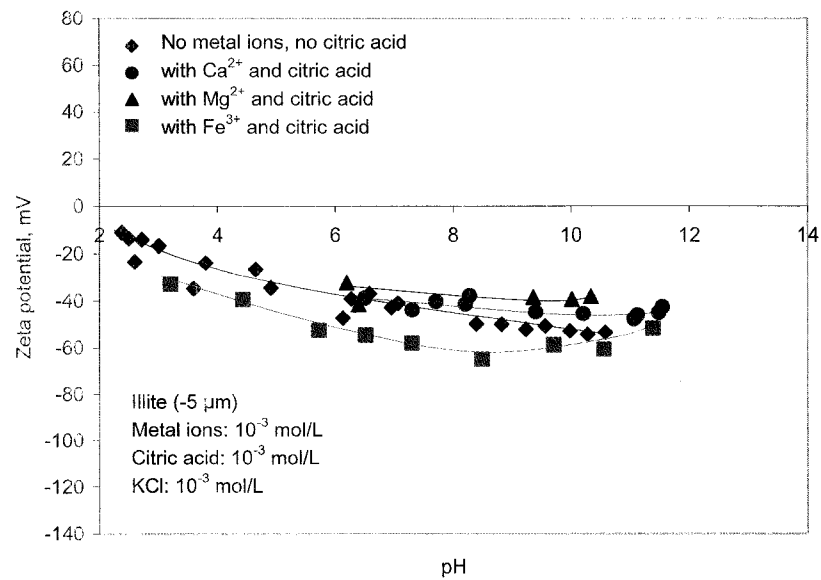


Figure 6-6 Zeta potential of illite at different pH in the presence of 10⁻³ mol/L metal ions and 10⁻³ mol/L citric acid.

6.4 Zeta Potentials of Model Oil and Bitumen

6.4.1 Model Oil

Figure 6-7 shows that the metal ions had a significant effect on the surface charge of oil droplets. In the presence of Ca^{2+} , the zeta potential of an oil droplet changed from -119 mV to -54 mV at pH 9.7. The zeta potential curve in the presence of Mg^{2+} initially overlapped with that of Ca^{2+} from pH 6 to 9.7, then rose with increasing pH, followed by a sign reversal at pH 10.6. When Fe^{3+} was added, the oil droplet exhibited very similar zeta potential profiles as that of precipitated $\text{Fe}(\text{OH})_3$ as shown in Figure 6-1.

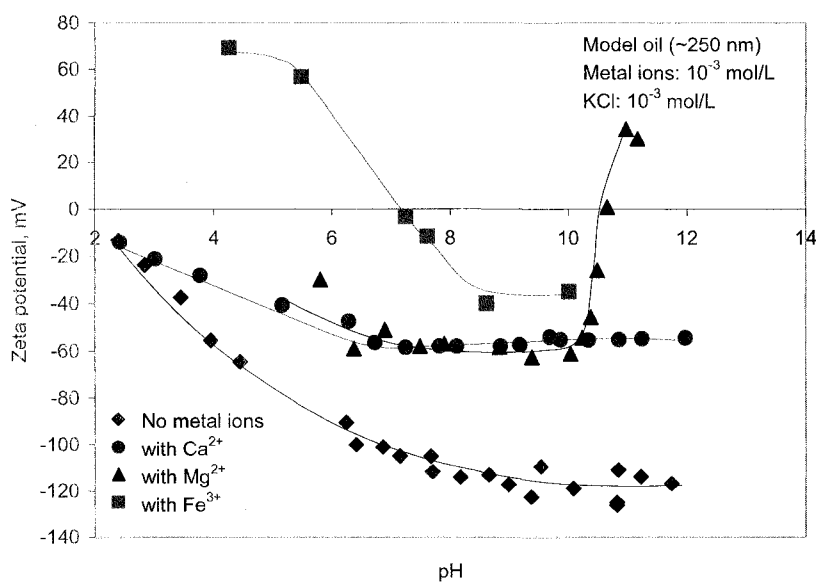


Figure 6-7 Zeta potential of model oil droplet at different pH in the presence and absence of 10^{-3} mol/L metal ions.

As reported earlier, the sodium oleate present in the oil phase did not seem to affect oil-quartz coagulation below pH 9 in solutions containing Ca^{2+} and Mg^{2+} . The zeta potential measurement results did not seem to show any effect of the interaction between the sodium oleate (contained in the oil phase) and the metal cations, either, although it was known that these multivalent cations were able to react with sodium oleate to form

insoluble metal carboxylate salts (Fuerstenau and Palmer, 1976). The zeta potential of the oil droplets in the presence of Ca^{2+} or Mg^{2+} was less negative in the pH range before metal hydroxyl species were formed. But this could be purely due to electrical double layer compression.

Another interesting feature of the zeta potential of the oil droplets is that, unlike that of quartz, it did not show an upward trend at strongly alkaline pH in the presence of Ca^{2+} ions.

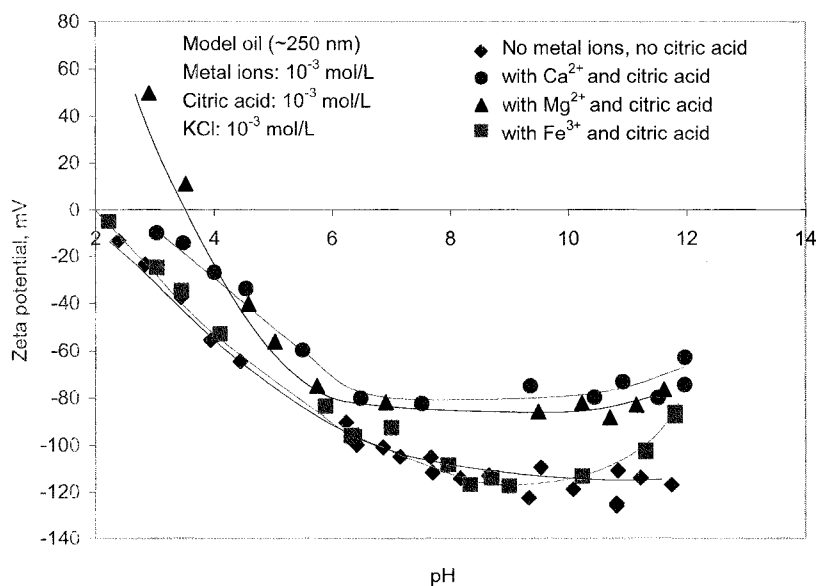


Figure 6-8 Zeta potential of model oil droplet at different pH in the presence of 10^{-3} mol/L metal ions and 10^{-3} mol/L citric acid.

Figure 6-8 shows that the zeta potentials of model oil droplets were negative above pH 4 in the presence of citric acid, irrespective of the type of metal cations. Profiles of the zeta potentials of oil droplets in the presence of Ca^{2+} and Mg^{2+} are similar. Both leveled off at -80 mV above pH 7. The droplets were more negatively charged in the entire pH range when Fe^{3+} was present.

6.4.2 Bitumen

As shown in Figure 6-9, bitumen droplets had an iso-electric point at 3.8. Above pH 3.8, the zeta potential of bitumen droplets significantly increased in the negative direction until about pH 7.5 when it leveled off. The bitumen droplets were highly negatively charged with zeta potentials in the -120 mV range in alkaline solution in the absence of multivalent metal cations. In the presence of 10^{-3} mol/L Ca^{2+} , the bitumen droplets became much less negatively charged, and the change started from pH 4. Since it was unlikely that first-order calcium hydroxyl complexes had formed at such a low pH, the bitumen surfaces seem to be able to interact with the Ca^{2+} cations as well as calcium hydroxyl complexes and calcium hydroxide precipitates. Overall, the zeta potential of bitumen droplets increased by about 80 mV from -120 mV to about -40 mV in the alkaline pH region.

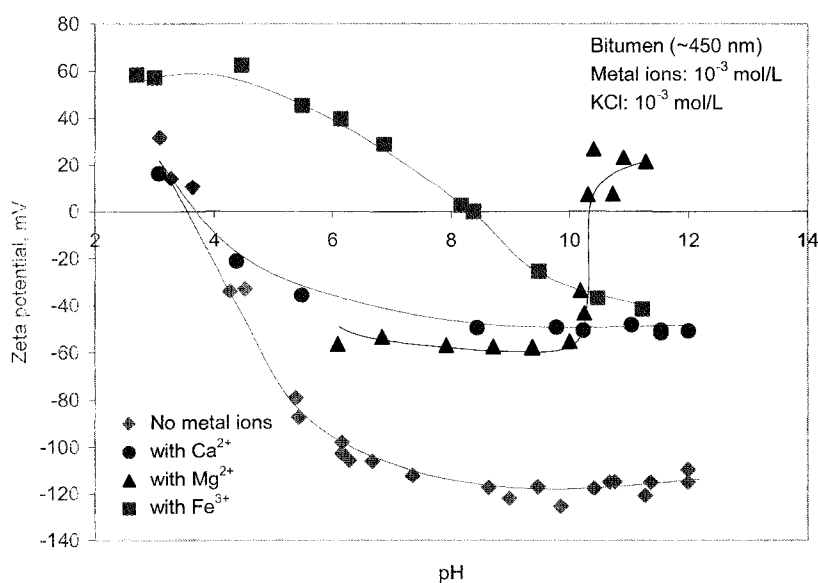


Figure 6-9 Zeta potential of bitumen droplet at different pH in the presence and absence of 10^{-3} mol/L metal ions.

In the presence of Mg^{2+} , the zeta potential of bitumen was stabilized at -55 mV between pH 6 and 10, before abruptly increasing and reversing the sign from pH 10 to 10.5 at which $Mg(OH)_2$ precipitate was formed.

In the presence of 10^{-3} mol/L Fe^{3+} , the iso-electric point of the bitumen shifted to pH 8.2, coinciding with that of ferric hydroxide precipitates. This indicated that the bitumen droplet surface, similar to minerals, was covered by the precipitates of $Fe(OH)_3$.

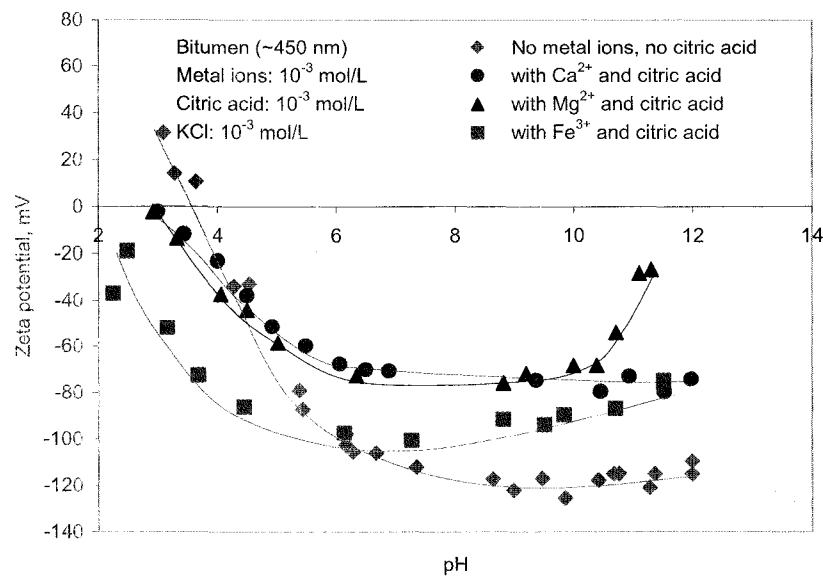


Figure 6-10 Zeta potential of bitumen droplet at different pH in the presence of 10^{-3} mol/L metal ions and 10^{-3} mol/L citric acid.

Figure 6-10 shows that the addition of citric acid increased bitumen surface charge in the negative direction. The effect of citric acid on the zeta potential of bitumen droplets was similar to that of quartz (Fig.6-1). As shown in Figure 6-10, when citric acid was added to the bitumen-in-water emulsions containing Ca^{2+} and Mg^{2+} , the bitumen droplet became more negatively charged, with the zeta potential curve shifting toward the value obtained without the metal ions. Therefore, a better dispersion of bitumen and mineral particles was expected due to the increased electrostatic repulsion. For bitumen droplets in

solutions containing Fe^{3+} , after adding citric acid, surface charge reversal did not occur. Overall, from pH 8 to 10, the bitumen droplet was highly negatively charged after adding citric acid, and the zeta potential of the bitumen droplets was -70 mV in the co-presence of citric acid together with Ca^{2+} or Mg^{2+} , and -90 mV in the co-presence of citric acid and Fe^{3+} .

From the results of zeta potential measurements for minerals and bitumen (oil) droplets, some general observations can be made:

Effect of metal cations:

Ca^{2+} : After adding Ca^{2+} , the zeta potentials of mineral particles and bitumen droplets became less negative. Above pH 10, the zeta potentials of quartz and kaolinite moved to more positive direction, while no significant changes were observed for illite and bitumen droplets.

Mg^{2+} : After adding Mg^{2+} , the mineral particles and bitumen droplets were less negatively charged, which was similar to Ca^{2+} . However, above pH 9.5, the surface charges of bitumen and all minerals moved to more positive direction and became positively charged at about pH 10.5, at which $\text{Mg}(\text{OH})_2$ was precipitated.

Fe^{3+} : After adding the Fe^{3+} ions, the zeta potentials of all minerals and bitumen or oil droplets were positive from pH 3 to 8, and become negative above pH 8. Further increase in pH made the minerals and bitumen or oil droplets more negatively charged. No significant differences were observed in the magnitude of the zeta potentials for all minerals and bitumen or oil droplets.

Effect of citric acid:

Ca^{2+} and Mg^{2+} : In the co-presence of citric acid and Ca^{2+} or Mg^{2+} , all minerals and bitumen droplets were negatively charged, and the charges were even lower (i.e., more

negative) than the original sample in the absence of any metal ions and citric acid.

Fe^{3+} : In the co-presence of citric acid and Fe^{3+} , the zeta potentials of all minerals (except for quartz) and bitumen generally became more negatively charged than the original sample in the absence of metal ions and citric acid.

6.5 Interaction Energy between Bitumen and Minerals

The results of zeta potential measurements indicate that the presence of multivalent metal ions decreased the magnitude of the negative surface charges of both the minerals and bitumen (or model oil) droplets. Consequently it is expected that the electrostatic repulsion between mineral and bitumen would be lower. On the other hand, the zeta potentials of minerals and bitumen droplets are restored or became more negative than the original sample after subsequent citric acid addition following the metal cations. Better bitumen-mineral liberation is expected due to possible significant increase in the electrostatic repulsion.

Therefore, the increase (or decrease) in coagulation observed between bitumen and minerals may be the consequence of reduced (or enhanced) energy barriers due to the absence (or presence) of citric acid. Total potential energy of interaction between bitumen and minerals (quartz, kaolinite and illite) was calculated using classical DLVO theory which incorporated the electrical double layer forces and van der Waals forces. Details of the calculation are shown in Appendix I. The related assumptions were:

- All mineral particles and bitumen droplets were treated as spheres with smooth, homogeneous surface. The radii of mineral particles (quartz, kaolinite and illite) and bitumen droplets were taken as 5 μm .
- The surfaces of minerals and bitumen droplets had a constant potential and constant charge density during the interaction.

The total potential energies of interaction between bitumen droplets and three different minerals in aqueous solutions containing Ca^{2+} , Mg^{2+} and Fe^{3+} were calculated with and

without the presence of citric acid at a given pH. pH 10 was used for the systems containing Ca^{2+} or Mg^{2+} , while pH 8 for Fe^{3+} .

6.5.1 Quartz-Bitumen Interaction Energies

Figure 6-11 shows the total interaction energy of bitumen droplets with quartz particles in solutions containing 10^{-3} mol/L of Ca^{2+} , Mg^{2+} or Fe^{3+} in the absence and presence of 10^{-3} mol/L citric acid, respectively, calculated using classical DLVO theory. As can be seen, in the presence of Ca^{2+} and Mg^{2+} at pH 10, the energy barrier was less than 140 kT (5.8×10^{-19} J) in the absence of citric acid. There was no energy barrier in the presence of Fe^{3+} at pH 8. This suggests that the presence of Fe^{3+} cause strong bitumen-quartz coagulation at those conditions. The addition of citric acid significantly increased the energy barriers. Without or with citric acid, the energy barrier increased from 140 kT to about 750 kT (3.1×10^{-18} J) for Ca^{2+} and Mg^{2+} , and from about zero to 840 kT (3.5×10^{-18} J) for Fe^{3+} .

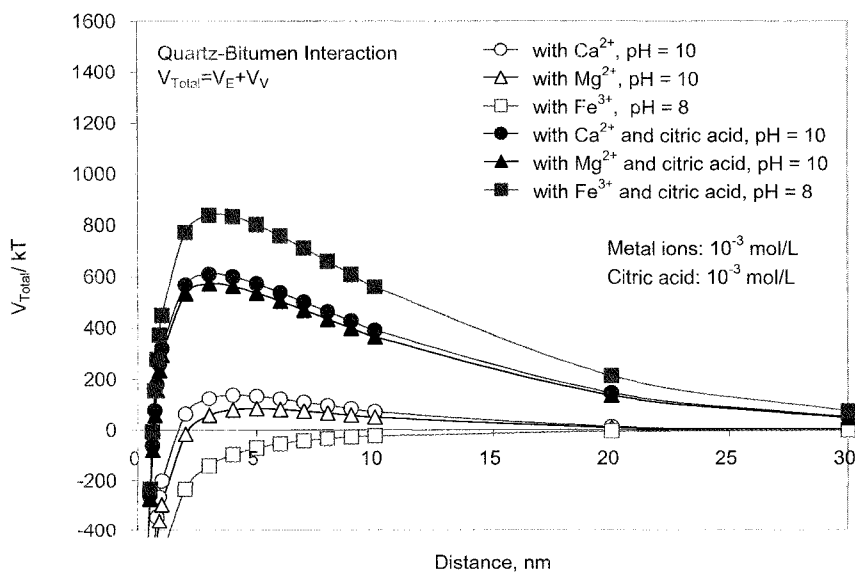


Figure 6-11 Total interaction energy of bitumen with quartz in aqueous solution containing 10^{-3} mol/L metal ions with and without the presence of 10^{-3} mol/L citric acid.

Interestingly, the energy barrier of Ca^{2+} was always slightly higher than that of Mg^{2+} , with or without citric acid at pH 10. This implies that the bitumen and quartz are easier to coagulate in the presence of Mg^{2+} , but harder to liberate by addition of citric acid, compared to the case of Ca^{2+} . In the presence of Fe^{3+} , bitumen spontaneously associated with quartz, but could be dispersed by citric acid. This is consistent with the energy barrier calculations.

The results generally correlated well to the coagulation tests, which showed that the addition of citric acid eliminated bitumen-quartz coagulation, particularly when the slurry contained Fe^{3+} . In contrast, in the absence of citric acid, the presence of the slight energy barriers for Ca^{2+} and Mg^{2+} suggested that bitumen-quartz coagulation could not have occurred, but strong coagulation was observed in the coagulation tests (Figure 3-15). This discrepancy can be attributed to the effect of energy dissipation of agitation used in coagulation tests. It is reasonable to speculate that these small energy barriers are overcome by the energy dissipation of the mixing stirrer. On the other hand, in the presence of citric acid, the energy dissipation effect is not adequate to overcome the energy barriers, thus bitumen and quartz particles remain dispersed.

6.5.2 *Kaolinite-Bitumen Interaction Energies*

Figure 6-12 presents the calculation results of total interaction energy of bitumen with kaolinite in the presence of Ca^{2+} , Mg^{2+} or Fe^{3+} with and without citric acid. As can be seen, the energy barriers in the presence of 10^{-3} mol/L citric acid were much higher than those in its absence. This is in agreement with the experimental observation that the addition of citric acid significantly decreased the mutual coagulation between kaolinite and bitumen.

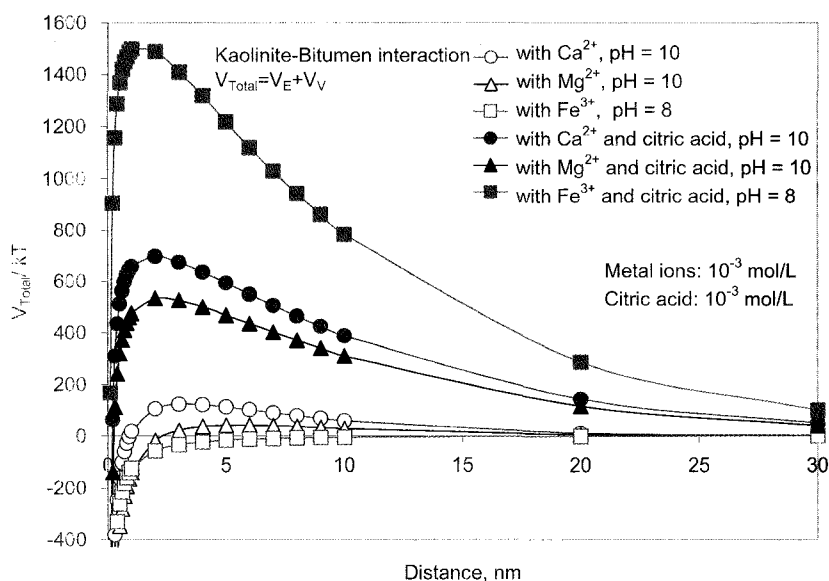


Figure 6-12 Total interaction energy of bitumen with kaolinite in aqueous solution containing 10^{-3} mol/L metal ions with and without the presence of 10^{-3} mol/L citric acid.

6.5.3 Illite-Bitumen Interaction Energies

As shown in Figure 6-13, the total interaction energies between illite particles and bitumen droplets were similar to those between bitumen and quartz or kaolinite. In the presence of Ca^{2+} and Mg^{2+} at pH 10, the energy barrier was less than 80 kT in the absence of citric acid, while no energy barrier exists in the presence of Fe^{3+} at pH 8. This correlates to the strong bitumen-illite coagulations observed in the previous tests. The presence of citric acid results in 6-10 times' increase in the energy barriers for Ca^{2+} and Mg^{2+} , suggesting better liberation between bitumen droplets and illite particles.

From the above calculations it is concluded that classical DLVO theory was valuable to illustrate the distinguished effects of multivalent metal cations and citric acid on the coagulations of bitumen with mineral particles. As well, the DLVO calculations confirm that electrostatic interaction is a determinant for the bitumen-mineral coagulations.

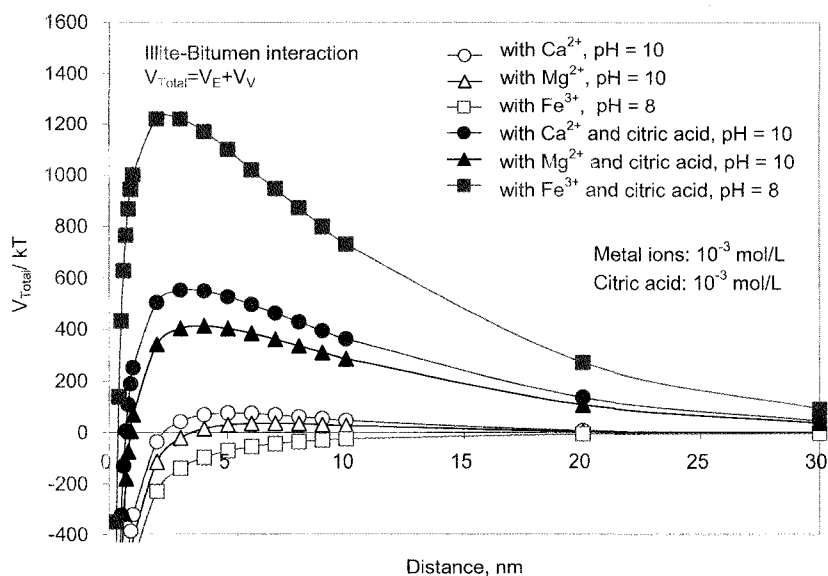


Figure 6-13 Total interaction energy of bitumen with illite in aqueous solution containing 10^{-3} mol/L metal ions with and without the presence of 10^{-3} mol/L citric acid.

6.6 Summary

Multivalent metal cations Ca^{2+} , Mg^{2+} and Fe^{3+} affect zeta potentials of minerals and bitumen droplets in three different ways. (a) Before the metal cations were hydrolyzed, the magnitude of the negative zeta potentials was reduced due to the compression of the electrical double layer. (b) When the metal cations were hydrolyzed, the magnitude of the negative zeta potentials of minerals and bitumen were reduced further. (c) As the metal hydroxides were formed, the zeta potentials of the minerals and bitumen droplets were essentially the same as those of the metal hydroxide precipitates.

In the presence of 10^{-3} mol/L citric acid, the zeta potentials of both bitumen (oil) and mineral particles were negative irrespective of the type of metal ions. In solutions containing 10^{-3} mol/L Ca^{2+} or Mg^{2+} , the zeta potentials of the minerals and oil droplets were slightly less negative after the addition of 10^{-3} mol/L citric acid than the original samples. In solutions with 10^{-3} mol/L Fe^{3+} , the zeta potentials of bitumen (oil) and

minerals (except for quartz) were more negative than those without any addition of multivalent metal cations or citric acid.

Classical DLVO theory could be used to illustrate the effect of metal cations and citric acid on energy barriers of bitumen-mineral interactions. The calculation results indicated the energy barriers were slightly positive or became negative in the presence of the 10^{-3} mol/L metal cations and absence of citric acid, corresponding to the strong coagulations observed in Chapter 3. Addition of 10^{-3} mol/L citric acid significantly increased the energy barriers of bitumen-mineral interactions correlating well to considerable decreases in coagulation, as indicated in Chapter 4.

7 MECHANISMS OF ACTION OF THE METAL IONS – ADSORPTION STUDIES

7.1 Introduction

The zeta potentials of bitumen droplets and mineral particles can be modified by the adsorption of metal ionic species on their surfaces. To understand the mechanisms of interaction between multivalent metal cations and mineral/water or oil/water interfaces, adsorption experiments and speciation calculations are conducted to identify how metal cations (Ca^{2+} , Mg^{2+} and Fe^{3+}) and citric acid affect the surface properties of minerals and bitumen droplets.

7.2 Experimental

7.2.1 *Materials*

Quartz samples ($-20 \mu\text{m}$, $-63+25 \mu\text{m}$), kaolinite ($-45 \mu\text{m}$), illite ($-45 \mu\text{m}$), solvent-diluted-bitumen and chemical reagents used in the experiments in this chapter were described in section 4.2.1.

The specific surface areas for mineral samples were calculated by the software of MasterSizer 2000 (Malvern) from particle size distribution with the assumption of spherical particles. The specific surface area of the $-20 \mu\text{m}$, $-63+25 \mu\text{m}$ quartz, kaolinite and illite was 1.13, 0.12, 1.22 and 1.15 m^2/g , respectively.

To prepare bitumen-in-water emulsion for adsorption tests, the solvent-diluted-bitumen was centrifuged at 10,000 G (RC-6, Mandel Scientific) to remove the fine solid impurities. Then, 20 mL of the centrifuged solvent-diluted-bitumen was dispersed in 800 mL distilled water and emulsified by a Model 500 ultrasonic dismembrator (Fisher Scientific) for 30 minutes. The effective diameter of the bitumen droplets (measured by Brookhaven 90Plus/BI-MAS) stabilized at about 400 nm for one week.

7.2.2 *Experimental Methods*

Adsorption of metal cations on minerals and bitumen droplets. All adsorption tests were carried out in a SI-600 shaking incubator (Jeio Tech) set at 200 rpm and $25\pm 0.5^\circ\text{C}$. Five grams of mineral ($-20\ \mu\text{m}$ quartz, $-45\ \mu\text{m}$ kaolinite, or $-45\ \mu\text{m}$ illite) were dispersed in a 250 mL conical flask containing 100 mL distilled water (for bitumen, 100 mL bitumen-in-water emulsion was used as prepared with no further dilution). The suspension was conditioned for 10 minutes after adjusting to a desired pH, followed by adding a metal cations, re-adjusting pH and agitating for 30 minutes, (if required, subsequently adding citric acid at a controlled pH, stirring for another 30 minute), recording the final pH. A small sample of the final suspension was filtered with a 220-nm pore size membrane to obtain a filtrate. The filtrate was analyzed by a SpectrAA-220FS (Varian) atomic absorption spectrometer to determine the residual metal ion concentration from which the adsorption density of the metal ion was calculated.

In the tests using $-63+25\ \mu\text{m}$ quartz sample, once the reaction was finished, the quartz sample was wet screened using a $25\ \mu\text{m}$ aperture sieve to remove possible precipitates, and rinsed by distilled water of the same pH in the adsorption. The rinsed quartz was oven dried at 80°C to a constant weight, and treated by 50 mL 0.5 mol/L HCl solution with agitation in the incubator for 30 minutes at 200 rpm to dissolve any adsorbed metal species. The metal content dissolved in the HCl solution was analyzed by the SpectrAA-220FS (Varian) atomic absorption spectrometer, and used to determine the metal ion concentration from which the adsorption density of the metal ions was calculated.

Quantification of surface elements by X-ray photoelectron spectroscopy (XPS). The XPS measurements were performed on an AXIS 165 X-ray photoelectron spectrometer (Kratos Analytical) at Alberta Centre for Surface Engineering and Science (ACSES), University of Alberta. The base pressure in the analytical chamber was below 4×10^{-8} Pa. Monochromated Al $K\alpha$ source ($h\nu = 1486.6\ \text{eV}$) was used at a power of 210W. The analysis spot was $700\times 400\ \mu\text{m}$. The resolution of the instrument, as indicated by the measured FWHM (Full Width at Half Maximum), is 0.55 eV for Ag 3d, and 0.7 eV for

Au 4f. Survey scans spanned from binding energy of 0 to 1100 eV. They were collected with an analyzer pass energy (PE) of 160 eV and a step of 0.3 eV. Charge neutralization was applied to compensate the sample charging.

Characterization of quartz samples treated with metal cations by static attenuated total reflectance Fourier-transform infrared spectroscopy (ATR-FTIR). A Nicolet 8700 FTIR spectrometer (Thermo Scientific), equipped with a smart collector of ATR (attenuated total reflectance) accessory with a trough-style 45° ZnSe crystal, was used to collect all ATR-FTIR spectra. Data collection and spectral calculations were performed using the Spectrum software (OMNIC). A spectrum was acquired at 2 cm⁻¹ resolution and resulted from an average of 265 scans between 700 and 4000 cm⁻¹.

To prepare FTIR samples, 2 grams of -20 µm quartz were allowed to react with Ca²⁺, Fe³⁺ and citric acid of a given concentration, following the procedures of adsorption density measurements. At the end of the reaction, a wet quartz paste was obtained by removing the supernatant by centrifugation. The quartz paste was divided into two portions. One portion was tested without any further treatment as “unwashed” sample. The other portion was washed twice by distilled water with the same pH and centrifuged to obtain the “washed” sample. The wet pastes of the quartz samples were applied directly to the ZnSe crystal.

7.3 Adsorption of Ca²⁺, Mg²⁺ and Fe³⁺ on Minerals and Bitumen

The adsorption density of Ca²⁺, Mg²⁺ and Fe³⁺ on minerals (quartz, kaolinite and illite) and bitumen at different pH was measured at an initial concentration of 10⁻³ mol/L metal cations. The results are presented in Figure 7-1 to 7-6.

7.3.1 *On Quartz*

The depletion method was widely used to determine adsorption density of metal ions and other reagents on mineral surface. With this method, adsorption density was taken as the

difference between initial and equilibrium concentrations of the metal ions in the suspension. However, this method could not be applied to study the adsorption of Mg^{2+} and Fe^{3+} in certain pH ranges in which these cations formed precipitates. Using depletion method would result in an overestimate of adsorbed metal cations by reporting bulk precipitated metal ions as adsorption. To eliminate this source of error, the $-63+25 \mu\text{m}$ quartz particles were used in the adsorption tests. Once the reaction was finished, the particle suspension was wet screened with a $25 \mu\text{m}$ aperture sieve and rinsed with water of the same pH as the tested suspension. For comparison, batch depletion method was used to measure the adsorption of Ca^{2+} (pH 5.0–11.5) and Mg^{2+} (pH 7.8–10.2) on $-20 \mu\text{m}$ quartz samples without the wet screening, since no precipitates would form within these pH ranges for the specific metal ions (see Section 7.5).

The adsorption densities of Ca^{2+} , Mg^{2+} and Fe^{3+} on quartz are shown in Figure 7-1 as a function of pH. As can be seen, the adsorption data were scattered for the $-63+25 \mu\text{m}$ quartz sample. Very low adsorption of calcium on quartz ($-63+25\mu\text{m}$), in the order of $4 \times 10^{-6} \text{ mol/m}^2$, was observed at pH below 10 from a solution containing $10^{-3} \text{ mol/L Ca}^{2+}$. Adsorption densities of about 10^{-5} mol/m^2 were observed between pH 10.5 and 12. On the other hand, adsorption density measurement on the $-20 \mu\text{m}$ quartz sample was more consistent. Very low adsorption of the Ca^{2+} ions was observed from pH 6 to 10 on the $-20 \mu\text{m}$ quartz, which was the same as with $-63+25 \mu\text{m}$ quartz sample. However, a rapid increase in the adsorption density of Ca^{2+} was observed at a very narrow pH range from pH 10 to 11.5, and the adsorption density reached over $1.6 \times 10^{-5} \text{ mol/m}^2$ at pH 11.5. This observation was in agreement with the result reported by Clark and Cooke (1968). Within this pH range, no calcium hydroxide precipitates were formed as confirmed by turbidity measurement (see also Section 7.5).

Similarly, very low Mg^{2+} adsorption on quartz ($-63+25 \mu\text{m}$) was observed below pH 10.4, and the adsorption increased abruptly above pH 10.4, with an adsorption density of $6.6 \times 10^{-5} \text{ mol/m}^2$ at pH 11.1. It was possible that the abrupt increase in Mg^{2+} adsorption was due to the formation of magnesium hydroxide ($\text{Mg}(\text{OH})_2$) precipitates on quartz surface above pH 10.4. Prior to the formation of $\text{Mg}(\text{OH})_2$, MgOH^+ was formed which

might have adsorbed on quartz as well. It was suspected that the adsorbed MgOH^+ was washed off in wet-screening and thus not detected. In order to confirm this, the $-20\ \mu\text{m}$ quartz sample was used in the adsorption measurements without the wet screening, with careful control of pH to ensure that no $\text{Mg}(\text{OH})_2$ would form. The results show that the adsorption of Mg^{2+} on quartz increased from $1.7 \times 10^{-6}\ \text{mol/m}^2$ at pH 9.5 to $4.8 \times 10^{-6}\ \text{mol/m}^2$ at pH 10, slightly higher at each pH point than the adsorption densities obtained with sieving-rinsing method for the $-63+25\ \mu\text{m}$ quartz samples. This observation, along with the adsorption results of Ca^{2+} on quartz, indicates that the first-order hydrolysis metal species of Ca^{2+} and Mg^{2+} were probably adsorbed on quartz through relatively weak physical adsorption, since wet-sieving resulted in lower detected adsorption densities for both metal ions.

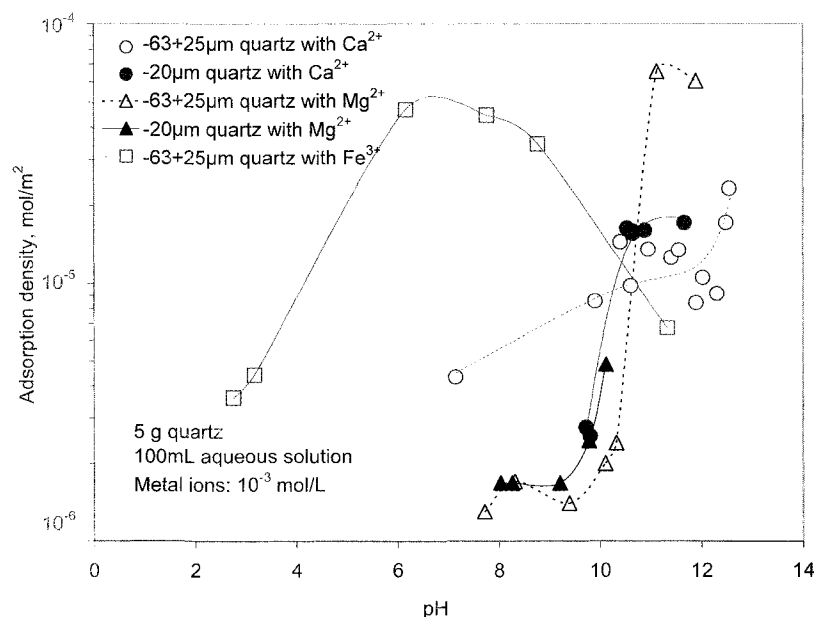


Figure 7-1 Adsorption density of metal ions on quartz with initial concentration of $10^{-3}\ \text{mol/L}$ at different pH.

The adsorption of Fe^{3+} on quartz showed a different pattern. Instead of a rapid increase in adsorption density in a very narrow pH range (as for Ca^{2+} and Mg^{2+}), the adsorption density increased gradually from pH 3, where $\text{Fe}(\text{OH})_3$ precipitate was formed, reached a

maximum at about pH 7.5 and then decreased at higher pH. This result was related to the surface charge of $\text{Fe}(\text{OH})_3$ in aqueous solution, for the adsorption maximum correlated to the iso-electric point (pH 8) of ferric hydroxide (Figure 6-1).

The calculated adsorption density for $\text{Fe}(\text{OH})_3$ monolayer coverage, using structural parameters of $\text{Fe}(\text{OH})_3$ by van der Giessen (1966), was $1.72 \times 10^{-5} \text{ mol/m}^2$, comparable to our result (by extrapolation) at about pH 5, but smaller than that at pH 8 ($4.7 \times 10^{-5} \text{ mol/m}^2$). These results suggested that at the start of $\text{Fe}(\text{OH})_3$ precipitation, monolayer adsorption of positively charged ferric hydroxide precipitates on quartz was formed. Once the monolayer precipitates were formed, they would prevent the accumulation of further precipitates, possibly due to electrostatic repulsion.

Multilayer adsorption of $\text{Fe}(\text{OH})_3$ was most likely at the vicinity of its iso-electric point (pH 8). Since the precipitates became less positively charged at this pH region, the electrical double layer repulsion decreased accordingly. The bulk precipitated $\text{Fe}(\text{OH})_3$ could build up on those previously precipitated on quartz surface, due to the dominated van der Waals attractions. When the pH was increased beyond the iso-electric point, the ferric hydroxide precipitates became negatively charged, so that the electrostatic repulsion progressively drove the physically adsorbed ferric hydroxide on top of the first layer away from the quartz surface. This desorption process could be facilitated by the mechanical shearing forces, causing a reduction in the adsorption density of $\text{Fe}(\text{OH})_3$.

To understand how complexing agents such as citric acid affected the adsorbed metal ions on quartz surface, the adsorption density of Ca^{2+} on quartz at different concentrations of citric acid was measured at pH 10, at an initial concentration of $10^{-3} \text{ mol/L Ca}^{2+}$. Figure 7-2 shows that the adsorption density of Ca^{2+} on quartz continuously decreased from $6.3 \times 10^{-6} \text{ mol/m}^2$ to $5.1 \times 10^{-7} \text{ mol/m}^2$ as the concentration of citric acid increased from 10^{-4} to $2 \times 10^{-3} \text{ mol/L}$. These results demonstrated that the adsorbed Ca^{2+} could be removed by citric acid, most likely through complexation, leading to the restoration of negatively charged surfaces of quartz which is beneficial to quartz-oil liberation due to the increase of electrostatic repulsions.

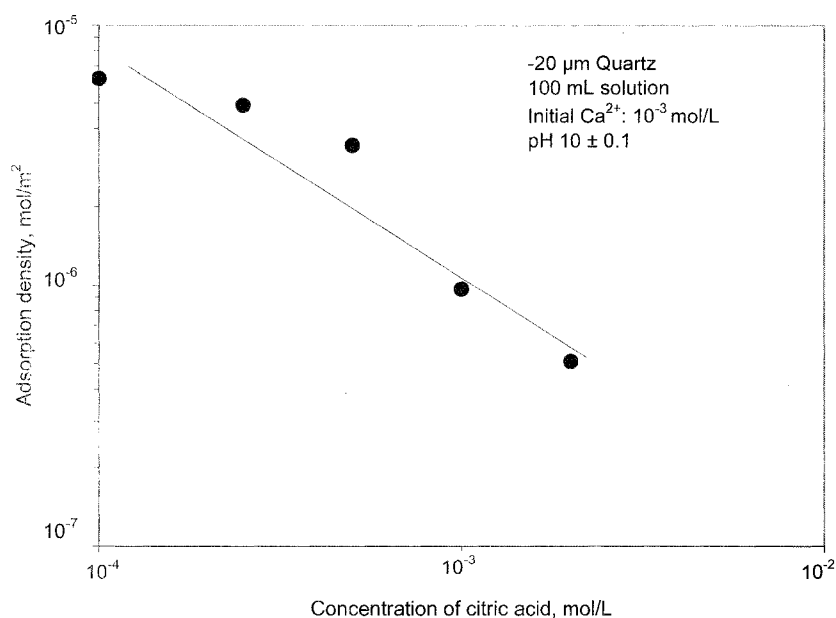


Figure 7-2 Adsorption density of Ca^{2+} on quartz at different concentration of citric acid, pH ~10.

7.3.2 On Kaolinite

Figure 7-3 shows the adsorption of Ca^{2+} and Mg^{2+} on kaolinite as a function of pH, at an initial concentration of 10^{-3} mol/L of the metal ions. As can be seen, the adsorption of both Ca^{2+} and Mg^{2+} was low and only increased slightly from pH 3.2 to 4.8, then leveled off at about 5.0×10^{-6} mol/m² between pH 5 and 7. However, there was a rapid increase in the adsorption densities of both Ca^{2+} and Mg^{2+} when pH was increased above pH 8, reaching about 1.5×10^{-5} mol/m² at pH 11–12.

The adsorption of Ca^{2+} and Mg^{2+} on kaolinite below pH 8 was probably through either cation exchange or surface induced hydrolysis, since it occurred in the pH range in which Ca^{2+} and Mg^{2+} were not hydrolyzed (Section 7.5). The marked increase in Ca^{2+} and Mg^{2+} adsorption above pH 9 was most likely due to the adsorption of the first-order metal hydroxyl species such as CaOH^+ and MgOH^+ .

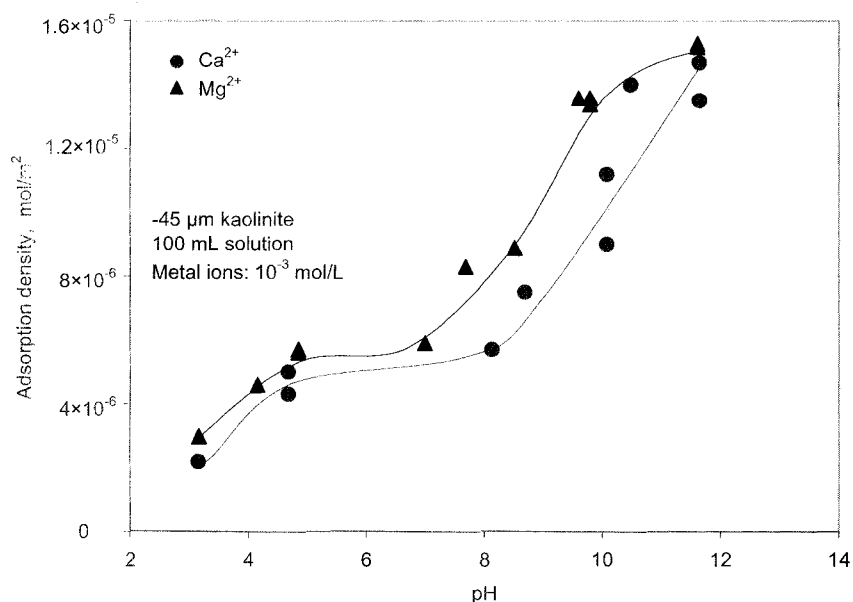


Figure 7-3 Adsorption density of Ca^{2+} and Mg^{2+} on kaolinite with initial concentration of 10^{-3} mol/L at different pH.

Figure 7-4 shows the adsorption density of Ca^{2+} and Mg^{2+} on kaolinite at different concentrations of citric acid, with an initial concentration of 10^{-3} mol/L Ca^{2+} or Mg^{2+} at pH 10. As can be seen, the citrate anions did not significantly remove the adsorbed Ca^{2+} and Mg^{2+} from the kaolinite surface within the tested time period (30 minutes). Since the coagulation tests were conducted within a time period shorter than 30 minutes, it can be seen that the citrate anions did not lower kaolinite-bitumen coagulation by removing adsorbed metallic species from kaolinite surface. It probably adsorbed on the kaolinite surface as metal-citrate complexes.

7.3.3 On Illite

As can be seen in Figure 7-5, the adsorption of Ca^{2+} and Mg^{2+} on illite, at an initial concentration of 10^{-3} mol/L of the metal ions, was notably increased with pH. The adsorption densities at pH 10 were much higher than those at pH 8. The uptake of Ca^{2+} and Mg^{2+} was likely related to ionic exchange and hydrolysis reaction of these metal ions.

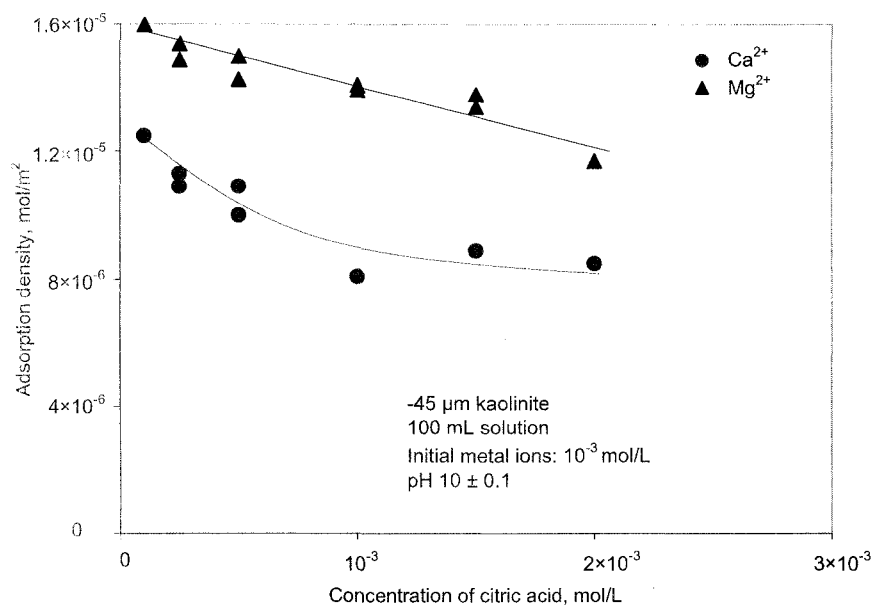


Figure 7-4 Adsorption of Ca^{2+} and Mg^{2+} on kaolinite at different concentrations of citric acid. pH ~ 10 .

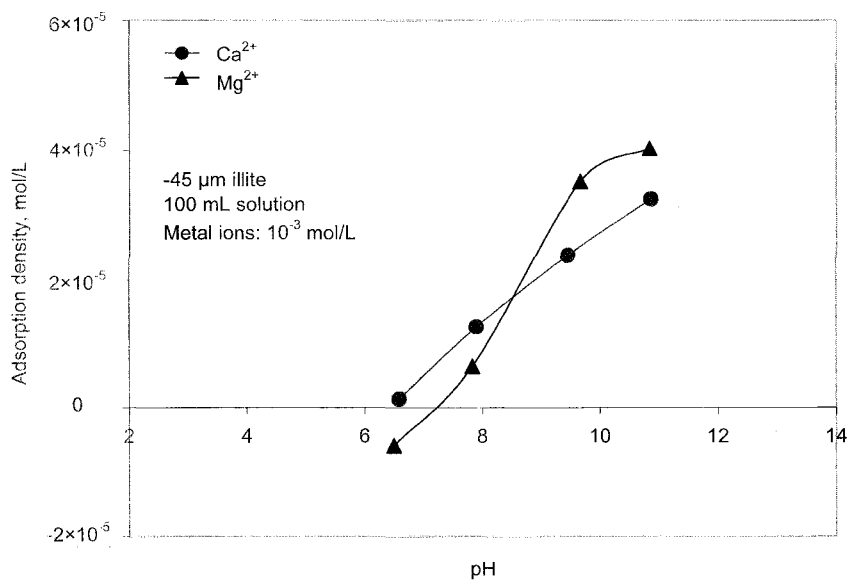


Figure 7-5 Adsorption density of Ca^{2+} and Mg^{2+} on illite with initial concentration of 10^{-3} mol/L at different pH.

In Figure 7-5, a negative adsorption density of Mg^{2+} at pH 6.5 was likely due to the dissolution of amorphous substituted Mg^{2+} from illite particle. On the other hand, experimental error cannot be excluded. But this error did not change the overall trends of adsorption density of Mg^{2+} .

7.3.4 On Bitumen

Accurately measuring adsorption density of metal ions at the bitumen/water interface was almost impossible due to the many difficulties and uncertainties involved. Bitumen droplets were deformable and very small in size. Separating bitumen droplets from the solution was a challenge. Moreover, the droplet coalescence during adsorption and separation would result in a decrease of total adsorption surface area.

However, evaluating adsorption of metal ions on bitumen was important to this research. For this purpose, some assumptions were made to calculate the total surface areas. (1) the bitumen concentration in the emulsion was assumed to be 2% (vol%) (this was 0.5% lower than the stock emulsion to account for some droplets creaming to the surface during storage); (2) total surface areas of bitumen droplets remained constant throughout the test; (3) the average effective diameter of bitumen droplets was 500 nm as measured. With these assumptions, the surface area of bitumen was determined to be about 0.12 m^2/mL of bitumen emulsion.

Figure 7-6 shows that the adsorption density of Ca^{2+} on bitumen was 2×10^{-7} mol/m^2 below pH 10, and increased to 4×10^{-7} mol/m^2 at pH 12. The increase was considered insignificant. For Mg^{2+} , adsorption density was below 10^{-7} mol/m^2 at below pH 10, then increased by about 7 times to 7×10^{-7} mol/m^2 at pH 11.5. Since $Mg(OH)_2$ precipitates formed at pH 10.5, as indicated in Figure 6-1, this increase of adsorption density was most likely due to the depletion of Mg^{2+} by precipitation, rather than genuine adsorption on bitumen droplet.

Therefore, the results shown in Figure 7-6 suggested that the adsorption of metal cations, such as Ca^{2+} and Mg^{2+} , on bitumen was insignificant, even when they were hydrolyzed. This explains why the zeta potential of bitumen droplet did not change at the pH where Ca^{2+} was hydrolyzed (Figure 6-9).

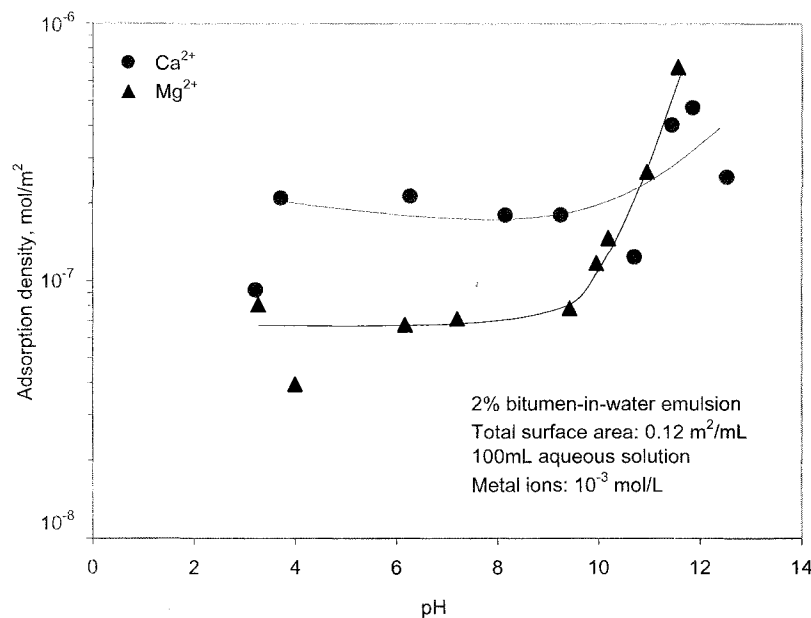


Figure 7-6 Adsorption of Ca^{2+} and Mg^{2+} on bitumen with initial concentration of 10^{-3} mol/L at different pH.

7.3.5 Quantification of the Adsorbed Metal Ions by XPS

For these experiments, glass slides and quartz particles ($-63+25 \mu\text{m}$) were used as adsorbing substrates. The substrates were exposed to solutions containing 10^{-3} mol/L Ca^{2+} , Mg^{2+} or Fe^{3+} for 30 minutes at a controlled pH. Afterwards, the glass slide was dried with blowing air to remove residual solution and visible precipitates. Quartz particles were wet-screened to remove precipitated metal hydroxides, washed with distilled water of the same pH and air dried. The quantification results of metal cations by XPS are summarized in Table 7-1 (raw data and other details are included in Appendix II). All peaks in all experiments were calibrated with the 284.8 eV peak (Wagner, 1990). Reference binding energies used for peak identification were: Ca^{2+} : 347.8 eV (Wren et al., 1979); $\text{Ca}(\text{OH})_2$: 346.7 eV (Sugama et al., 1989); Mg^{2+} : 50.5 eV (Kinno and Onaka,

1980); Mg(OH)₂: 49.5 eV (Haycock and Kasrai, 1978); Fe³⁺: 711.3 eV (Carver et al., 1972); Fe₂O₃: 710.7 eV (Mathieu and Landolt, 1986).

The quantitative XPS survey results for Ca²⁺, Mg²⁺ and Fe³⁺ on the glass substrates and -63+25 μm quartz shown in Table 7-1 were in good agreement with those of the adsorption density presented in Figure 7-1. The adsorption of the multivalent metal ions on glass surface was low at pH where metal ions were present as free ions in the solutions. In contrast, substantial increase in the amount of metal ions on the glass slides, as shown in the last two columns in Table 7-1, was observed at the pH where metal ions were hydrolyzed and/or precipitated.

Table 7-1 Quantification of metal cations adsorbed on glass slide and -63+25 μm quartz by XPS.

Peak	Test No.	pH	Binding Energy (eV)	FWHM (eV)	Atomic conc. (%)	Metal/Si	
Ca 2p	1	On glass	6.0	347.45	2.76	2.01	0.074
	2	On glass	11.7	347.45	2.56	4.70	0.200
	3	On glass (rinsed)	11.7	347.45	2.87	1.51	0.055
	4	On quartz *	12.58	346.30	2.59	4.24	0.169
	5	On quartz (rinsed)*	12.58	346.65	2.36	0.59	0.020
Mg 2p	6	On glass	6.0	50.65	2.12	1.30	0.049
	7	On glass	10.9	49.25	2.72	16.76	1.864
	8	On glass (rinsed)	10.9	49.60	2.57	11.43	0.658
	9	On quartz	10.75	49.50	2.65	1.57	0.067
	10	On quartz (rinsed)	10.75	48.80	2.69	1.42	0.049
Fe 2p	11	On glass	2.5	711.45	3.7	1.14	0.043
	12	On glass	9.1	710.75	5.81	4.54	0.189
	13	On quartz	9.27	710.65	4.53	2.57	0.090
	14	On quartz (rinsed)	9.27	710.30	4.46	1.59	0.088

* The concentration of Ca²⁺ used in these tests was 0.1 mol/L.

The high content of Mg²⁺ and Fe³⁺ detected at the higher pH might be partly due to sampling on “free” (un-adsorbed) hydroxide precipitates on the glass slides. To double

check, Samples 2 (Ca^{2+} , pH 11.7) and 6 (Mg^{2+} , pH 10.9) were rinsed with distilled water with the corresponding pH and re-analyzed. It can be seen that the surface concentrations of Ca^{2+} and Mg^{2+} were decreased as a result of rinsing. The Ca/Si ratio of Sample 2 decreased from 0.200 to 0.055, comparable to 0.074 for Sample 1 at a lower pH of 6.0. However, Mg^{2+} adsorbed on the glass slide at the higher pH (10.9) remained much higher than that at a lower pH of 6.0 (Sample 6), as indicated by the Mg/Si ratios of 0.658 (pH 10.7, after rinsing) and 0.048 (pH 6.0). The results on the rinsed -63+25 μm quartz were similar to the glass slides.

No binding energy shift was observed for Ca2p at the low and high pH (6.0 versus 11.7). This implied that the mode of adsorption of Ca^{2+} and CaOH^+ did not differ from each other. The substantial decrease in surface concentration of Ca^{2+} after rinsing indicated that the bonding between CaOH^+ and the glass surface was not strong. It was probably largely a physical adsorption, such as through electrostatic forces.

There was, however, a marked shift in electron binding energies for adsorbed Ca^{2+} , Mg^{2+} and Fe^{3+} as pH was increased to the point such that the correspondent metal hydroxides were formed, as shown in Table 7-1. For instance, the binding energy for Mg2p shifted from 50.65 eV at pH 6 to 49.25 eV at pH 10.9. Since the step resolution of the X-ray photoelectron spectrometer was 0.3 eV, this shift (1.4 eV) was significant, which signified that there was a change in the chemical environment for Mg^{2+} adsorption with a change of pH from 6 to 10.9. The binding energy for Mg2p of Mg^{2+} and $\text{Mg}(\text{OH})_2$ was 50.5 eV (Kinno and Onaka, 1980) and 49.5 eV (Haycock and Kasrai, 1978) respectively. Compared the measured with reference binding energy, we were convinced that $\text{Mg}(\text{OH})_2$ was formed on the surface of glass substrate. which closely correspond to the measured . Similarly, the binding energy for Fe2p shifted from 711.45 eV at pH 2.5 to 710.75 eV at pH 9.1. With a 0.7 eV shift, it indicated that the bonding mechanism of Fe^{3+} with the surface was different from that of $\text{Fe}(\text{OH})_3$. The binding energy for electron Fe2p of FeCl_3 and Fe_2O_3 ($\text{Fe}(\text{OH})_3$ was readily oxidized and dehydrated in XPS analysis chamber) was 711.3 eV and 710.4 eV. Thus, metal hydroxides were precipitated on and strongly bond with quartz particle surfaces.

Since rinsing with distilled water of the same pH did not significantly remove the adsorbed metal ions, it was reasonable to conclude that both the ferric hydroxide and the magnesium hydroxide chemically adsorbed on quartz. These results were confirmed by the adsorption of metal ions on quartz particles as can be seen in Figure 7-1. These results may explain why zeta potentials of quartz were similar to those of the corresponding metal hydroxides precipitates, as indicated in Figure 6-1.

In order to characterize the adsorption of metal cations on bitumen surface, glass slides with bitumen coatings were used. The slides were immersed in solutions containing 10^{-3} mol/L metal cations for 30 minutes, then blow-dried with air and analyzed by XPS. The results are presented in Table 7-2 and raw data are presented in Appendix II. As can be seen, no metal ions were detected. This might be due to the fact that the adsorption was too low to be detected.

Table 7-2 Quantification of adsorbed metal cations on bitumen by XPS.

Peak	Sample No.	pH	Binding Energy (eV)	Atom conc., (%)	Metal/C
Ca 2p	1	6.0	NA	Not detected	NA
	2	11.7	NA	Not detected	NA
Mg 2p	3	6.0	NA	Not detected	NA
	4	10.9	49.25	2.01	0.022
Fe 2p	5	2.5	NA	Not detected	NA
	6	9.1	NA	Not detected	NA

7.3.6 Characterization of the Adsorbed Metal Ions by ATR-FTIR

To further study the nature of adsorption of metal ions on quartz surface, ATR-FTIR was applied. This technique can provide valuable information as to how metal ions interact with quartz surface. In these tests, the $-20\ \mu\text{m}$ quartz was equilibrated with Ca^{2+} or Fe^{3+} at different pH, in the absence or presence of citric acid. For comparison, a blank sample,

–20 μm quartz paste without metal ion treatment was tested. The results are presented in Figure 7-7 to 7-9.

Figure 7-7 shows the ATR-FTIR spectra of quartz treated by 0.1 mol/L Ca^{2+} at pH 10.5 and pH 12. It can be seen that the quartz sample has an absorption band at 1054.87 cm^{-1} , which was assigned to the Si-O-Si stretching on quartz. Dean (1999) pointed out that the Si-O-Si stretching band falls in $1100\text{--}1000\text{ cm}^{-1}$. The absorption band for -Si-OH at $820\text{--}870\text{ cm}^{-1}$ (OH stretching) was not observed, likely not resolvable from the strong Si-O-Si absorption band nearby. However, any change of bonding environment of Si-O-Si was revealed by the variations in peak shifting and intensity.

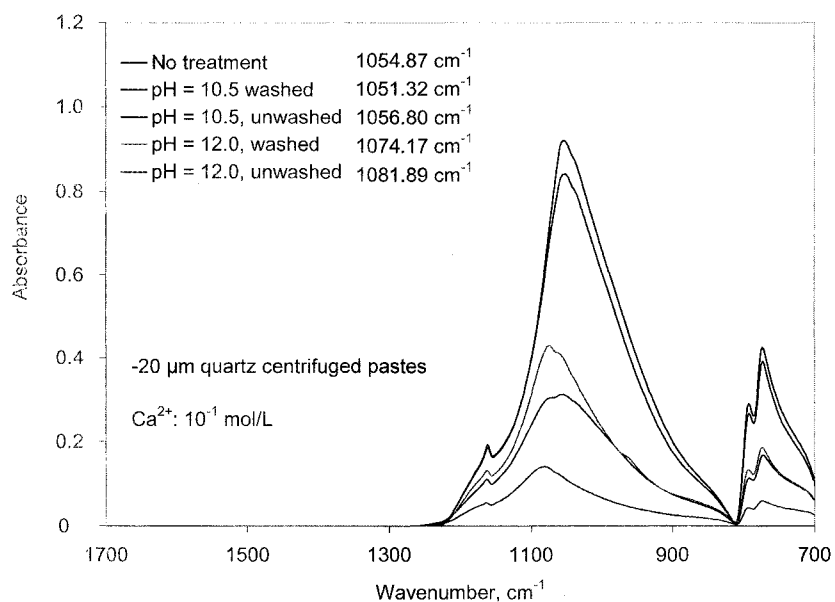


Figure 7-7 ATR-FTIR spectra of –20 μm quartz with and without treatment by 0.1 mol/L Ca^{2+} solution.

For quartz treated by Ca^{2+} solution at pH 10.5, the position of the Si-O-Si absorption band did not change, but the intensity of the band was lowered. Washing the treated quartz restored the intensity. On the other hand, for quartz treated at pH 12, at which Ca(OH)_2 was precipitated (It was observed that Ca(OH)_2 began to precipitate at pH 11.9), the absorption band shifted to higher frequency by 26 cm^{-1} from 1054.87 cm^{-1} to

1081.89 cm^{-1} . Washing the treated quartz slightly moved the band to 1074.17 cm^{-1} . These results indicated that the first-order hydroxyl species CaOH^+ did not specifically interact with quartz surface silanol groups, but $\text{Ca}(\text{OH})_2$ precipitates did.

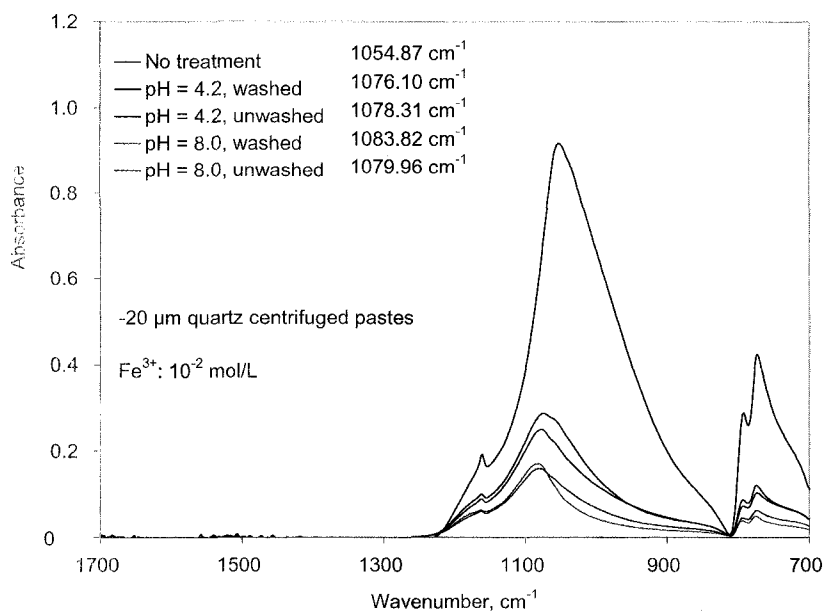


Figure 7-8 ATR-FTIR spectra of $-20 \mu\text{m}$ quartz with and without treatment by $0.01 \text{ mol/L Fe}^{3+}$ solution.

In the case of Fe^{3+} , as shown in Figure 7-8, at pH 4.2 and 8, where $\text{Fe}(\text{OH})_3$ were precipitated, the absorption band of silanol shifted more than 20 cm^{-1} to higher frequency, signifying a substantial change of Si-O-Si bonding environment. No significant difference was observed between the absorbance bands for washed and unwashed samples, indicating that the adsorption of $\text{Fe}(\text{OH})_3$ on quartz surface was irreversible.

The results shown in Figure 7-7 and Figure 7-8 were in agreement with the adsorption density measurement and XPS analysis: metal hydroxyls such as CaOH^+ did not chemically interact with silanol groups on quartz, but their hydroxide precipitates (e.g., $\text{Fe}(\text{OH})_3$) did. The metal hydroxyl species were likely adsorbed on quartz surface through physical interaction such as electrostatic effect.

Figure 7-9 shows the effect of citric acid on modifying the quartz surfaces treated by Ca^{2+} and Fe^{3+} . It can be seen that the ≡Si-O-Si≡ peak shifted from 1082 to 1051 cm^{-1} in the presence of citric acid and Fe^{3+} , while from 1074 to 1057 cm^{-1} for Ca^{2+} . The resulted peak frequency was very close to that of the untreated quartz at 1055 cm^{-1} , as was the peak intensity. These results demonstrated that the presence of citric acid was able to restore quartz surfaces which adsorbed precipitated metal hydroxides.

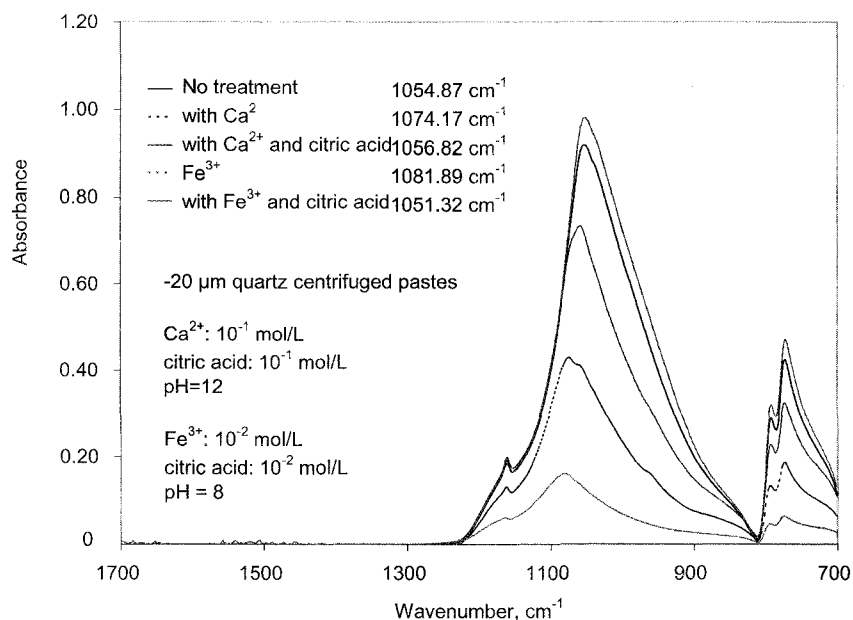


Figure 7-9 ATR-FTIR spectra of $-20\ \mu\text{m}$ quartz with and without treatment by citric acid in the presence of Ca^{2+} and Fe^{3+} .

The changes in peak intensity as showed in Figs. 7-7 to 7-9 implied adsorption or desorption of metal ionic species on the quartz surfaces. As adsorbed metal ions increased, the ≡Si-O-Si≡ peaks had lower intensity, since less ≡Si-O-Si≡ was detected. On the other hand, when adsorbed metal species was removed, more ≡Si-O-Si≡ was exposed on the surface and detected, thus the peaks show higher intensity.

7.4 Thermodynamics of the Adsorption of Metal Ionic Species

As solution pH increases, multivalent metal cations undergo hydrolysis reactions to form metal hydroxyl complexes. The pH regions in which the metal cations form such

complexes differ from one another. It is interesting to observe that the metal cations did not adsorb on minerals and thus did not have a significant effect on the coagulation between quartz and bitumen, whereas the metal hydroxyl complexes did.

Multivalent metal cations are hydrated in aqueous solutions with coordinated water molecule sheaths. These hydrated sheaths must at least be partially removed for adsorption of these metal cations on the surface of minerals to occur. The energy required to remove the hydration sheath is called the secondary solvation energy. The higher the secondary solvation energy, the more difficult the metal cations adsorb on a negatively charged minerals surface. Therefore, the evaluation of the secondary solvation energy is useful to predict the adsorption of different metal ionic species on different negatively charged surfaces such as quartz and bitumen.

7.4.1 *James and Healy's Thermodynamic Model*

One of the well accepted thermodynamic models to evaluate the free energy change for adsorption was proposed by James and Healy in 1972. In this model, three terms, an attractive coulombic term $\Delta G_{coul,i}$, a repulsive secondary solvation energy term $\Delta G_{solv,i}$, and an adjustable or "chemical" free energy term $\Delta G_{chem,i}$, contribute to the overall free energy of adsorption, $\Delta G_{ads,i}$, with the assumption that the metal cations are adsorbed near the inner Helmholtz plane with rearrangement of hydration sheath of the adsorbed ions.

$$\Delta G_{ads,i} = \Delta G_{coul,i} + \Delta G_{solv,i} + \Delta G_{chem,i} \quad (7-1)$$

The first term is attractive and is determined by

$$\Delta G_{coul,i} = z_i F \Delta \psi_{x_i} \quad (7-2)$$

$$\Delta\psi_{x_i} = \frac{2RT}{z_i F} \ln \left(\frac{(e^{z_i F \psi_0 / 2RT} + 1) + (e^{z_i F \psi_0 / 2RT} - 1)e^{-\kappa x_i}}{(e^{z_i F \psi_0 / 2RT} + 1) - (e^{z_i F \psi_0 / 2RT} - 1)e^{-\kappa x_i}} \right) \quad (7-3)$$

where F is Faraday constant, z_i is the valence of ionic species i , ψ_0 is the surface charge of the sorbent, κ is inverse Debye length and a function of solution ionic strength.

The repulsive secondary solvation term $\Delta G_{solv,i}$ represents the change in energy required to remove the hydration sheath of hydrated ions for adsorption of occur, and has the following expression:

$$\Delta G_{solv,i} = \frac{z_i^2 e^2 N}{16\pi\epsilon_0} \left(\frac{1}{x_i} - \frac{r_i}{2x_i} \right) \left(\frac{1}{\epsilon_{int}} - \frac{1}{\epsilon_{bulk}} \right) + \frac{z_i^2 e^2 N}{32\pi\epsilon_0 x_i} \left(\frac{1}{\epsilon_{solid}} - \frac{1}{\epsilon_{int}} \right) \quad (7-4)$$

In equation 7-4, ϵ_0 the permittivity of vacuum, e is elementary electron charge, N is Avogadro constant, ϵ_{bulk} and ϵ_{solid} are the dielectric constants of bulk solvent and sorbent solid, respectively. ϵ_{int} is the dielectric constant of the surface water and is a function of the electric field strength ($d\psi/dx$). x_i is the radius of hydrated ionic species i , determined by the radii of water molecule and adsorbing ion.

Clearly, the attractive coulombic term $\Delta G_{coul,i}$ is a function of ionic strength and pH for a given system, while the repulsive secondary solvation energy $\Delta G_{solv,i}$ is principally decided by ionic radius and charge of the adsorbing ion. However, the “chemical” free energy term $\Delta G_{chem,i}$, an adjustable term which is difficult to quantify by either calculation or by experimental measurement, is always used as a “fitting” parameter in all studies (James and Healy, 1972c). In this study, we only consider the first two terms in our calculation.

7.4.2 Ionic Radii of Metal Hydroxyl Species

To correctly assess the secondary solvation energy, ionic radii of ionic species have to be determined. Due to the unavailability of ionic radii for many metal hydroxyl species such as CaOH^+ , some researchers (James and Healy, 1972c; Agashe and Regalbuto, 1997) simply used the radii of the metal ions (e.g., Ca^{2+}) as an approximation. This obviously caused errors in calculation.

To obtain the ionic radii of metal hydroxyl species, molecular dynamics simulation was performed by Dr. P. Choi's group in the Department of Chemical and Materials Engineering at the University of Alberta. The simulation assumes that molecules and ions are isolated in vacuum and only one molecule or ion was considered in the calculation. The initial structure of the ion was optimized by energy minimization using DMol3, a density functional theory (DFT) quantum mechanical code, and the total charge of the ion was specified. In their simulation, initial structures of the ions were constructed in the vacuum with the assignment of their corresponding charges. After that, potential energy of these initial structures was optimized by using DMol3 algorithm built in Materials Studio software purchased from Accelrys (Accelrys, 2004). The solvent radius was set to be 0.14 nm, which is the value for water molecules.

From this simulation, solvent (i.e., water) accessible surface area and volume of the ion were calculated. Since the radii of the metal cation or metal hydroxyl ion calculated from solvent accessible surface area or volume did not exclude solvent (water) molecule effect, the radii used in this study were calculated from van der Waals surface areas and volumes assuming the metal hydroxyl ions have a spherical geometry, called van der Waals radii. The simulation and calculation results are presented in Table 7-3. The simulation results were consistent with van der Waals radii of metal cations found in literature, particularly for calcium and magnesium. On the other hand, the ionic radii calculated from both surface areas and volumes are very comparable. In the following calculation, the ionic radii calculated from van der Waals surface areas were used.

7.4.3 *Free Energy Change of Adsorption*

Table 7-3 Van der Waals radii of metal ionic species obtained by molecular dynamics simulation.

	Solvent accessible		Solvent accessible radii		Van der Waals radii		Literature
	Surface	Volume	r_s (Å)	r_v (Å)	$r_s-1.4$ (Å)	$r_v-1.4$ (Å)	
	area(Å ²)	(Å ³)					
CaOH ⁺	174.95	210.65	3.73	3.69	2.33	2.29	NA
MgOH ⁺	114.20	116.98	3.01	3.03	1.61	1.63	NA
FeOH ⁺	135.60	144.60	3.28	3.26	1.88	1.86	NA
FeOH ²⁺	136.93	147.01	3.30	3.27	1.90	1.87	NA
PbOH ⁺	114.2	117.03	3.02	3.03	1.62	1.63	NA
AlOH ²⁺	114.72	117.67	3.02	3.04	1.62	1.64	NA
MnOH ⁺	122.49	132.42	3.12	3.16	1.72	1.76	NA
Fe(OH) ₂ ⁺	182.45	210.71	3.81	3.69	2.41	2.29	NA
Al(OH) ₂ ⁺	179.60	206.99	3.78	3.67	2.38	2.27	NA
Ca ²⁺	142.10	157.82	3.36	3.35	1.96	1.95	2.00 ^a
Mg ²⁺	122.49	132.42	3.12	3.16	1.72	1.76	1.73 ^a
Fe ²⁺	88.33	78.63	2.65	2.66	1.25	1.26	2.00 ^a
Pb ²⁺	146.40	171.24	3.41	3.44	2.01	2.04	2.02 ^a
Mn ²⁺	95.80	85.99	2.76	2.74	1.36	1.34	1.50 ^b
Fe ³⁺	88.33	78.68	2.65	2.66	1.25	1.26	1.40 ^b
Al ³⁺	100.07	97.93	2.82	2.86	1.42	1.46	1.38 ^b
	Van der Waals		Van der Waals radii				
	Surface	Volume	$r_{s,w}$ (Å)	$r_{v,w}$ (Å)			
	area(Å ²)	(Å ³)					
Ca ²⁺	48.14	30.41	1.96	1.94	2.00 ^a		
Mg ²⁺	36.99	21.91	1.72	1.74	1.73 ^a		
Fe ²⁺	19.60	7.78	1.25	1.23	2.00 ^a		
Pb ²⁺	50.69	35.43	2.01	2.04	2.02 ^a		
Mn ²⁺	22.96	10.00	1.35	1.34	1.50 ^b		
Fe ³⁺	19.36	7.78	1.24	1.23	1.40 ^b		
Al ³⁺	25.10	11.40	1.41	1.40	1.38 ^b		

a. Source: Bondi, A., J. Phys. Chem. 68 (3), 441 (1964).

b. Source: Latimer, W. M., J. Chem. Phys. 23 (1), 90 (1955).

Table 7-4 Calculated free energy of adsorption for metal ionic species on minerals and bitumen at 25°C.

Ionic species	Minerals ΔG_{ads} (kJ/mol)			Bitumen	pH
	Quartz	Kaolinite	Illite	ΔG_{ads} (kJ/mol)	
CaOH ⁺	-4.30	-5.31	-6.15	3.09	10
FeOH ⁺	-3.98	-4.61	-5.86	4.54	8
MnOH ⁺	-3.87	-4.53	-5.82	4.95	8
MgOH ⁺	-3.89	-5.06	-6.04	4.71	10
PbOH ⁺	-3.80	-4.47	-5.79	5.23	8
Al(OH) ₂ ⁺	1.12	3.95	1.34	12.08	4
Fe(OH) ₂ ⁺	1.09	3.91	1.31	12.00	4
FeOH ²⁺	25.54	24.88	19.49	61.39	4
AlOH ²⁺	27.33	26.58	20.93	65.42	4
Pb ²⁺	19.18	15.19	11.41	51.01	8
Ca ²⁺	19.36	14.87	11.37	51.11	10
Mg ²⁺	20.76	16.02	12.34	54.20	10
Mn ²⁺	23.30	18.68	14.32	60.10	8
Fe ²⁺	24.14	19.40	14.91	61.94	8
Al ³⁺	73.18	65.83	55.08	157.85	4
Fe ³⁺	76.46	68.69	57.54	164.59	4

Table 7-4 shows the calculated free energy change of adsorption (details are shown in Appendix III). It can be seen that the multivalent metal cations Pb²⁺, Ca²⁺, Mg²⁺, Fe²⁺, Fe³⁺ and Al³⁺, and the first-order hydroxyl complexes FeOH²⁺ and AlOH²⁺ had large

positive adsorption free energy change ΔG_{ads} , therefore, they could not adsorb on either quartz or bitumen spontaneously. On the other hand, the adsorption energy for the monovalent metal hydroxyl complexes such as CaOH⁺, MgOH⁺ on quartz was negative, indicating that the adsorption on quartz was possible. Similar results were obtained for kaolinite and illite, indicating that formation of metal hydroxyl products indeed makes their adsorption on minerals thermodynamically favorable. However, the adsorption energies of these monovalent ionic complexes on bitumen were positive; thus in theory their adsorption on the bitumen surface would not be possible.

7.5 Speciation of Ca^{2+} , Mg^{2+} and Fe^{3+} in Aqueous Solutions

7.5.1 Without Any Complexing Agent

Figure 7-10 shows the speciation diagrams for 10^{-3} mol/L Ca^{2+} , Mg^{2+} , and Fe^{3+} in aqueous solutions without complexing agents, while Figure 7-11 to Figure 7-19 show the speciation diagrams of these ions in the presence of 10^{-3} mol/L of oxalic acid, citric acid and EDTA, respectively. The diagrams were constructed using data from the literature as summarized in Appendix IV.

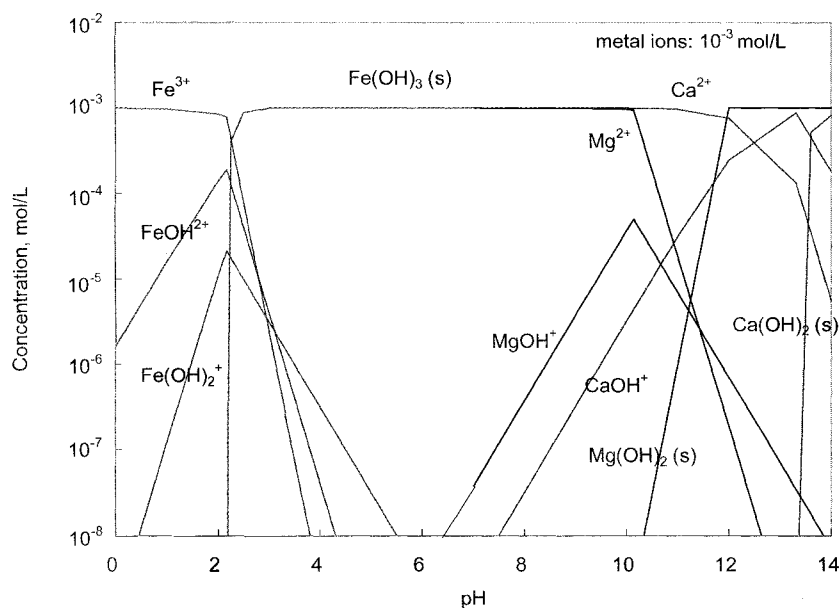


Figure 7-10 Speciation diagram of 10^{-3} mol/L of Ca^{2+} , Mg^{2+} and Fe^{3+} in aqueous solution. Constructed using data from Furia (1972), Butler and Cogley (1998), Weistin and Rasmuson (2005) and Dean (1999).

As can be seen from Figure 7-10, Ca^{2+} , Mg^{2+} and Fe^{3+} started to form first-order metal hydroxyl species above pH 10.5, 9 and 1.5, respectively, at an initial concentration of 10^{-3} mol/L. The concentration of the first-order hydroxyl products CaOH^+ , MgOH^+ and FeOH^{2+} increased significantly above these pH's. For instance, the concentration of

CaOH^+ increased from less than 10^{-5} mol/L at pH 10.5 to over 8.7×10^{-4} mol/L at pH 13, accompanied by a drop in Ca^{2+} ion concentration. The rapid increase in CaOH^+ concentration coincided with the adsorption of Ca^{2+} on quartz (Figure 7-1). Compared to CaOH^+ , the hydroxylized species of Mg^{2+} and Fe^{3+} , MgOH^+ and FeOH^{2+} , had lower peak concentrations, at 5×10^{-5} mol/L (MgOH^+) and 1.9×10^{-4} mol/L (FeOH^{2+}), before forming corresponding hydroxide precipitates. When compared with the coagulation test results, it can be seen that these precipitates also played important roles in the interaction between bitumen (oil) and minerals.

7.5.2 Oxalic Acid

It can be seen from Figure 7-11 that calcium oxalate is precipitated out above pH 1.8 and its concentration is constant at 7×10^{-4} mol/L from pH 3–12. At pH 10, the concentration of CaOH^+ is 8.5×10^{-8} mol/L, two orders of magnitude smaller than that without oxalic acid (3.2×10^{-6} mol/L). The concentration of Ca^{2+} decreases from 10^{-3} to 3×10^{-4} mol/L in the presence of oxalic acid at pH 10. Therefore, theoretically Ca^{2+} and CaOH^+ are essentially removed due to the formation of calcium oxalate complex.

Figure 7-12 shows that the concentration of Mg^{2+} ions is reduced slightly between pH 2 and 10 by oxalic acid. Further decrease in the concentration of Mg^{2+} above pH 10 is due to the formation of magnesium hydroxide precipitates. The concentration of MgOH^+ is slightly reduced from 3.8×10^{-6} to 3.0×10^{-6} mol/L at pH 9. Thus, oxalic acid is not as effective in removing Mg^{2+} as Ca^{2+} .

For ferric ions, the presence of oxalic acid causes the onset pH for $\text{Fe}(\text{OH})_3$ precipitation to shift from pH 2.2 to pH 3.4 (Figure 7-13). At pH 8, virtually all ferric ions are precipitated as hydroxides.

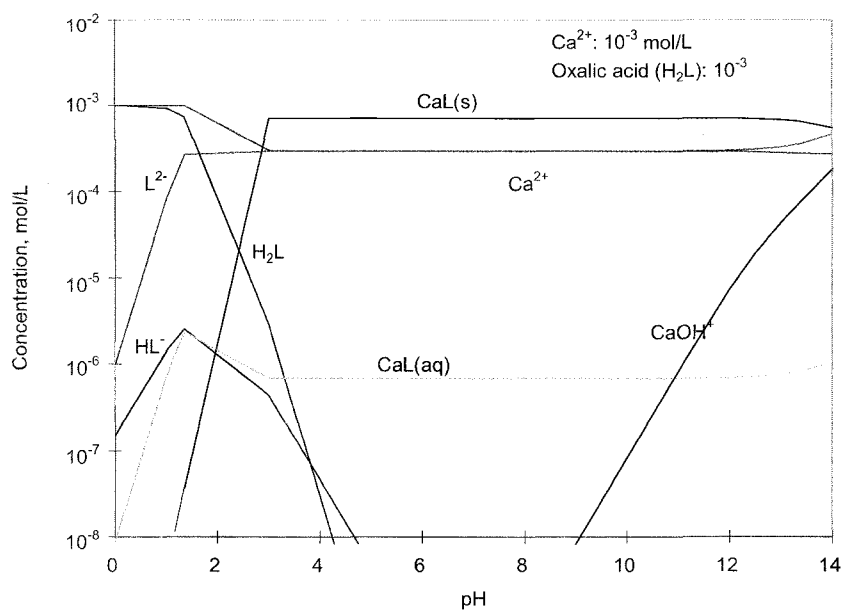


Figure 7-11 Speciation diagram of 10^{-3} mol/L of Ca^{2+} in aqueous solution containing 10^{-3} mol/L oxalic acid. Constructed using data from Furia (1972), Butler and Cogley (1998), Weistin and Rasmuson (2005) and Dean (1999).

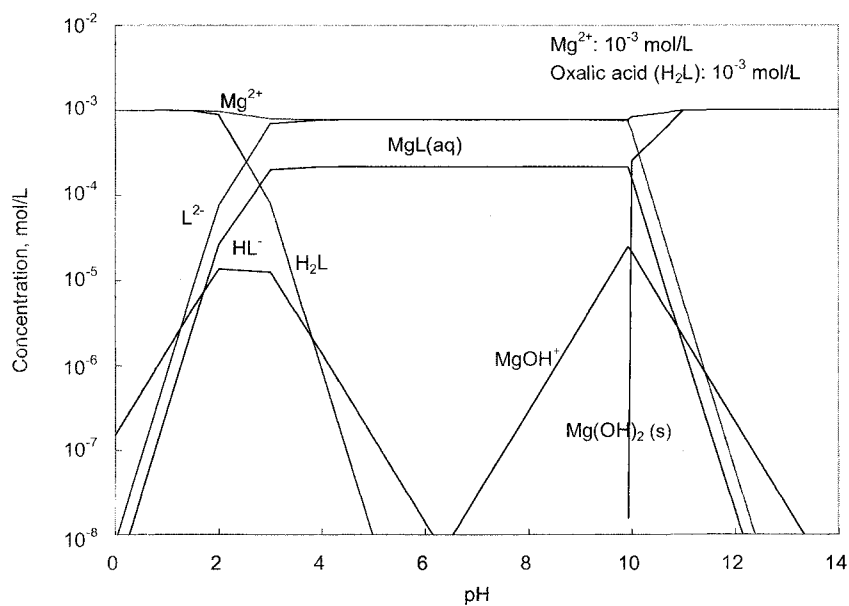


Figure 7-12 Speciation diagram of 10^{-3} mol/L of Mg^{2+} in aqueous solution containing 10^{-3} mol/L oxalic acid. Constructed using data from Furia (1972), Butler and Cogley (1998), Weistin and Rasmuson (2005) and Dean (1999).

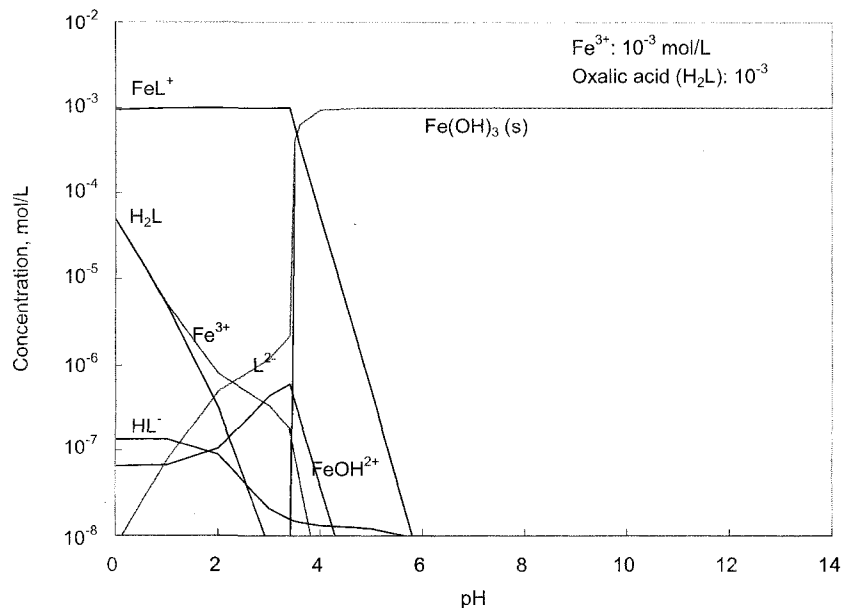


Figure 7-13 Speciation diagram of 10^{-3} mol/L of Fe^{3+} in aqueous solution containing 10^{-3} mol/L oxalic acid. Constructed using data from Furia (1972), Butler and Cogley (1998), Weistin and Rasmuson (2005) and Dean (1999).

7.5.3 Citric Acid

Figure 7-14 to Figure 7-16 show the speciation diagrams in the co-presence of 10^{-3} mol/L of metal cations and 10^{-3} mol/L citric acid. It can be seen from Figure 7-14 that Ca^{2+} is complexed by the citrate anions cit^{3-} above pH 4. The concentration of Ca-cit^- increases from $3.4 \times 10^{-5} \text{ mol/L}$ at pH 4 to a plateau of $8.7 \times 10^{-4} \text{ mol/L}$ at pH 7. The concentration of free Ca^{2+} ions decreases from the initial 10^{-3} mol/L to $1.3 \times 10^{-4} \text{ mol/L}$ between pH 7 and 11. The concentration of CaOH^+ is $4.1 \times 10^{-7} \text{ mol/L}$ at pH 10, which is significantly reduced from in the absence of the citric acid ($3.2 \times 10^{-6} \text{ mol/L}$). Therefore, Ca^{2+} and CaOH^+ are virtually eliminated by the citric acid between pH 7 and 11.

Similarly, Figure 7-15 shows that about 50% of the Mg^{2+} ions are removed by complexation with citric acid between pH 7 and 10. At pH 10, Mg(OH)_2 begins to precipitate, having a concentration of $4.3 \times 10^{-8} \text{ mol/L}$. At this point, magnesium is predominantly present in the form of the Mg^{2+} ions (49.1%) and Mg-cit^- (48.9%). The

concentration of MgOH^+ is 2×10^{-5} mol/L, lower than 3.7×10^{-5} mol/L without citric acid. On the other hand, 5.1×10^{-4} mol/L of uncomplexed citrate anions are present in solution at the same pH (pH 10).

Figure 7-16 illustrates that the onset pH for ferric hydroxide precipitation shifts from 2.2 (without citric acid, Figure 7-10) to 7.3 (in the presence of citric acid). Below about pH 7.7, virtually 100% of the ferric ions are complexed by the citric acid. At pH 8, about 92% of the Fe^{3+} ions are precipitated as ferric hydroxides, while 7.7% as Fe-citrate complex.

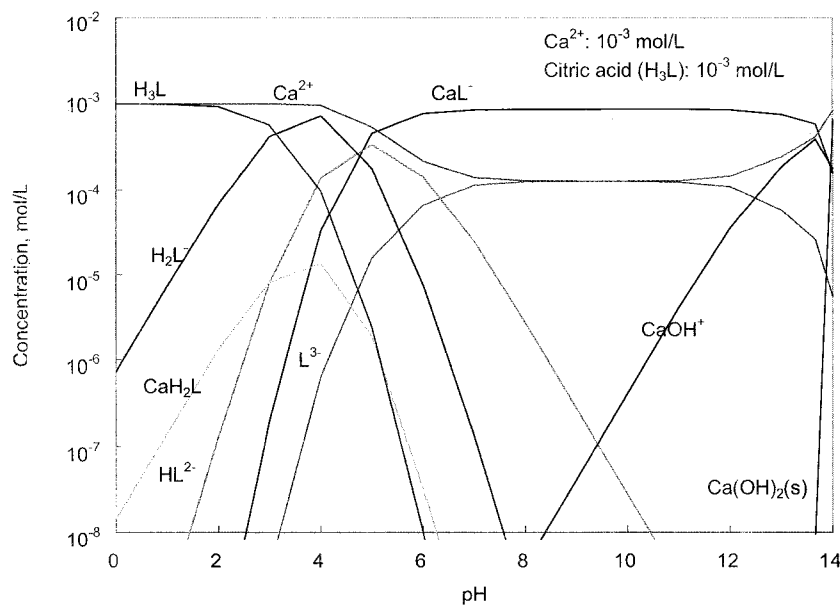


Figure 7-14 Speciation diagram of 10^{-3} mol/L of Ca^{2+} in aqueous solution containing 10^{-3} mol/L citric acid. Constructed using data from Furia (1972), Butler and Cogley (1998), Weistin and Rasmuson (2005) and Dean (1999).

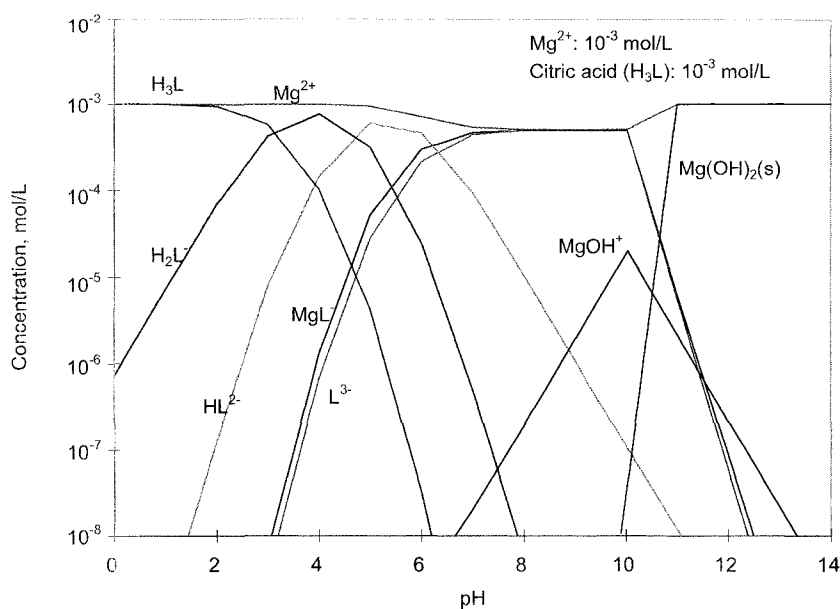


Figure 7-15 Speciation diagram of 10^{-3} mol/L of Mg^{2+} in aqueous solution containing 10^{-3} mol/L citric acid. Constructed using data from Furia (1972), Butler and Cogley (1998), Weistin and Rasmuson (2005) and Dean (1999).

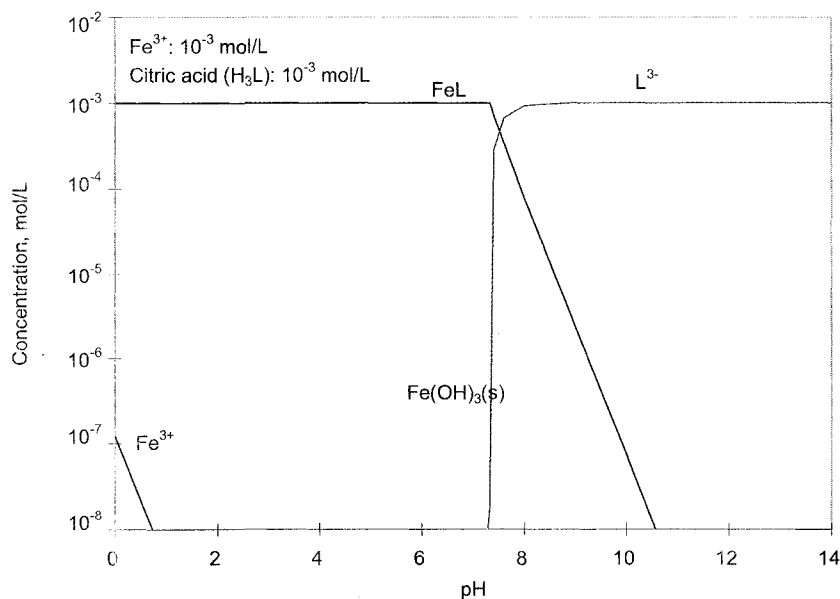


Figure 7-16 Speciation diagram of 10^{-3} mol/L of Fe^{3+} in aqueous solution containing 10^{-3} mol/L citric acid. Constructed using data from Furia (1972), Butler and Cogley (1998), Weistin and Rasmuson (2005) and Dean (1999).

7.5.4 EDTA

Speciation diagrams of 10^{-3} mol/L Ca^{2+} , Mg^{2+} and Fe^{3+} in the presence of 10^{-3} mol/L EDTA are plotted in Figure 7-17 to 7-19. Figure 7-17 shows that Ca^{2+} ions are complexed by edta^{4-} with increasing pH and are rapidly removed from the solutions. At pH 10, there are only 2.4×10^{-7} mol/L Ca^{2+} present. The concentrations of other calcium ionic species such as CaOH^+ and CaHedta^- are in the order of 10^{-10} mol/L. Hence, EDTA removes Ca^{2+} and CaOH^+ from solution, which explains its effect on eliminating the mutual coagulation between minerals and bitumen induced by the Ca^{2+} ions.

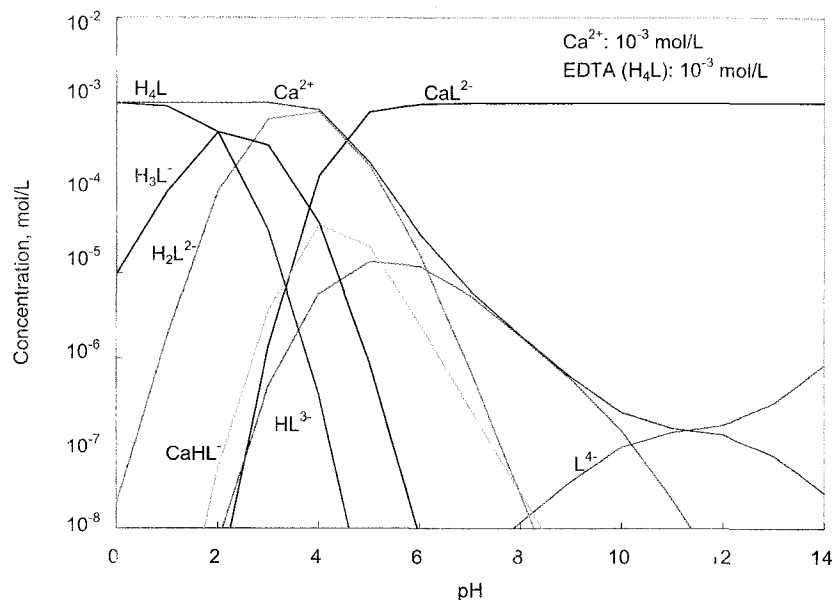


Figure 7-17 Speciation diagram of 10^{-3} mol/L of Ca^{2+} in aqueous solution containing 10^{-3} mol/L EDTA. Constructed using data from Furia (1972), Butler and Cogley (1998), Weistin and Rasmuson (2005) and Dean (1999).

For Mg^{2+} , the Mg-edta^{2-} complex dominates the solution at pH 8–12 with concentration at 9.9×10^{-4} mol/L, as can be seen in Figure 7-18. No $\text{Mg}(\text{OH})_2$ precipitates are formed until pH 11.4. At pH 10, the concentrations of Mg^{2+} , MgOH^+ and MgHedta^- are 1.9×10^{-6} , 7.1×10^{-8} and 1.9×10^{-9} mol/L respectively, which are all very low.

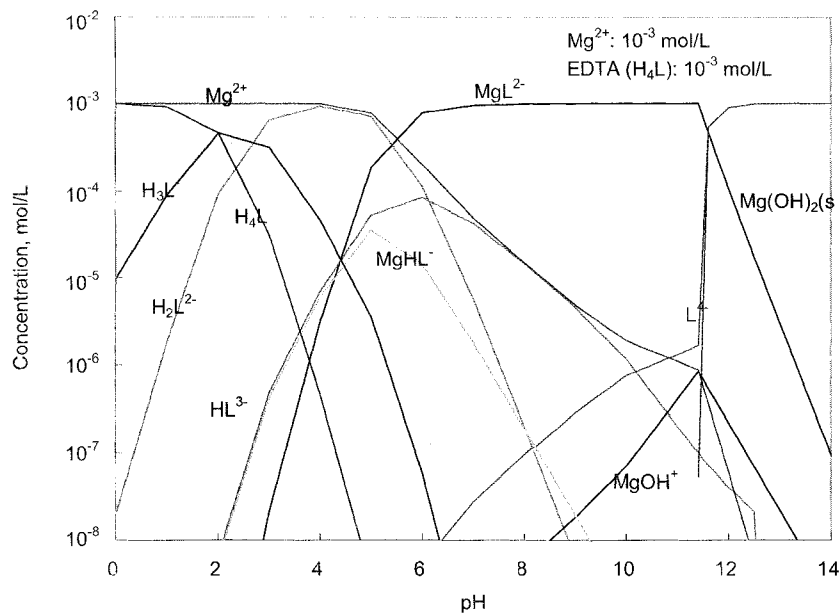


Figure 7-18 Speciation diagram of 10^{-3} mol/L of Mg^{2+} in aqueous solution containing 10^{-3} mol/L EDTA. Constructed using data from Furia (1972), Butler and Cogley (1998), Weistin and Rasmuson (2005) and Dean (1999).

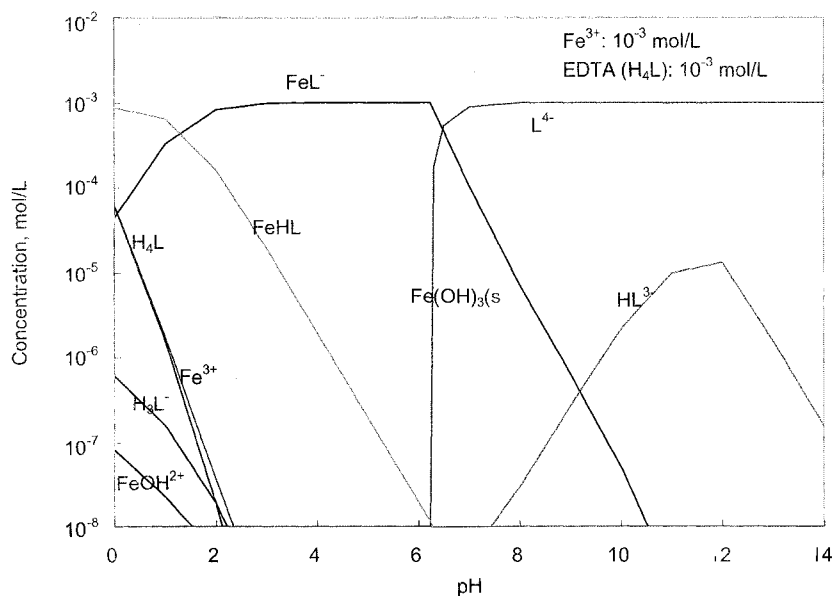


Figure 7-19 Speciation diagram of 10^{-3} mol/L of Fe^{3+} in aqueous solution containing 10^{-3} mol/L EDTA. Constructed using data from Furia (1972), Butler and Cogley (1998), Weistin and Rasmuson (2005) and Dean (1999).

Figure 7-19 shows that the speciation of Fe^{3+} is different from Ca^{2+} and Mg^{2+} . Due to the higher stability constant of ferric-EDTA complexes, almost all ferric ions are complexed in the form of Fe-edta^- and FeHedta below pH 8, and edta^{4-} ions are released from ferric-EDTA complexes with increasing pH through the formation of ferric hydroxide precipitates. This suggests that EDTA may not be as effective in depressing the effect of Fe^{3+} on mineral-bitumen coagulation as on Ca^{2+} and Mg^{2+} at pH larger than 6.

7.6 Mechanisms of Bitumen (Oil)-Mineral Interaction

The coagulation between bitumen (oil) and mineral particles in the absence of multivalent metal ions (Ca^{2+} , Mg^{2+} and Fe^{3+}) can be explained by electrostatic forces. For instance, at pH 2–4, both quartz and bitumen (oil) droplets were only slightly negatively charged since the pH is close to the iso-electric points. The resultant electrostatic repulsion between the oil droplets and mineral particles is low, and the attractive van der Waals forces can lead to coagulation. Kaolinite-bitumen coagulation at low pH regions (pH < 7), as has been discussed previously in 3.5.2, is probably due to the interaction of the positively charged edge surface with negatively charged bitumen or oil droplets. The coagulation is reduced with increasing pH due to an increase in the negative surface potentials and thus an increase in electrostatic repulsion.

7.6.1 *Effect of Ca^{2+} , Mg^{2+} and Fe^{3+}*

When the metal cations were not hydrolyzed, they adsorb much less on mineral surface or bitumen droplet surface, and they affected bitumen-mineral interaction through electrical double layer compression. Ca^{2+} and Mg^{2+} did not cause quartz-bitumen (oil) coagulation at the dosage of 10^{-3} mol/L, as they did for kaolinite (or illite)-bitumen (oil) coagulation. This may have been caused by differences in particle size, presence of lattice metal ions, etc. Difference in the surface hydrophobicity of quartz and the clay minerals may also be responsible.

When the multivalent metal cations were hydrolyzed, metal hydroxyl species such as CaOH^+ and MgOH^+ adsorbed on mineral surfaces. The adsorption was thermodynamically favorable as indicated by James and Healy's model. On the other hand, there was a critical concentration of the metal hydroxyl species to result in a measurable effect on mineral-oil(bitumen) coagulation. Speciation diagrams show that the concentrations of CaOH^+ and MgOH^+ was 3.2×10^{-6} and 3.8×10^{-6} mol/L at pH 9.0 and pH 10.0, respectively, corresponding to the peak of mutual coagulation of bitumen(oil) with quartz in the presence of these metal ions.

James and Healy (1972a; 1972b; 1972c) considered that the first-order hydrolysis product of metal ions was specifically adsorbed on quartz based on its ability to reverse the sign of quartz surface charge. On the other hand, Fuerstenau (1970) indicated that "the specific adsorption was attributed to the hydrated metal ions rather than hydroxyl complexes". Our adsorption/desorption, XPS and FTIR results disagreed with both. Metal cations hardly adsorb on the mineral or bitumen surfaces while the first-order metal hydroxyl complexes such as CaOH^+ and MgOH^+ adsorbed on quartz through non-specific physisorption such as electrostatic attraction.

In the adsorption tests using $-63+25 \mu\text{m}$ quartz, it was observed that at the pH where CaOH^+ was the dominant ionic species in solution, the measured adsorption density of Ca^{2+} was low and scattered. This was probably due to two reasons. Firstly, CaOH^+ was physically adsorbed on quartz through electrostatic attraction between CaOH^+ and the deprotonated surface silanol (Si-O-) groups, and could be removed by rinsing water. This was consistent with XPS results as shown in Table 7-1. Secondly, the scattering of the results may be caused by the low total surface areas (0.6 m^2) of the quartz samples used in each adsorption experiment for the $-63+25 \mu\text{m}$ quartz sample.

Combined with the adsorption results of Mg^{2+} on quartz, it could be generalized that the adsorption of the first-order hydrolysis product of multivalent metal cations such as CaOH^+ and MgOH^+ on quartz was through electrostatic attraction.

When the metal cations are precipitated as hydroxides, the adsorption on mineral surface seemed to be through chemical bonding. This was confirmed by XPS analysis of the adsorption of magnesium and ferric ions on glass slides, and ATR-FTIR measurement results on quartz surfaces. Zeta potential measurements of mineral and bitumen (oil) showed that the mineral particles and bitumen droplets exhibited the same zeta potentials as the metal hydroxide precipitates.

7.6.2 *Effect of Complexing Agents*

As suggested by the speciation diagrams, the complexing agents reduced coagulation between bitumen (oil) and minerals through two possible mechanisms, 1) removal of the free metal cations through metal-organic ligand complexation, and 2) adsorption of negatively charged uncomplexed organic ligands on precipitated metal hydroxides or/and mineral and bitumen surfaces.

(1) Removal of the free metal cations through metal- organic ligand complexation.

Adding complexing agents into suspensions containing multivalent metal cations resulted in the formation of metal-organic ligand complexes. This was the case for oxalic acid, citric acid and EDTA which sequestered Ca^{2+} and Mg^{2+} at pH 10. In this case, it was required that the formation constants of the complexes to be higher than those of the metal hydroxide precipitates or metal hydroxyl complexes.

The complexing agents with higher stability constants to the metal cations have higher capacity to eliminate metal ions from aqueous solutions. Stability constants of the metal cations (e.g., Ca^{2+} , Mg^{2+} and Fe^{3+}) with oxalic acid, citric acid and EDTA are compiled in Table 7-5 based on data collected from literature (Butler and Cogley, 1998; Dean, 1999; Furia, 1972; Westin and Rasmuson 2005). It can be seen that the stability constants decrease in the order of EDTA > citric acid > oxalic acid for all metal-organic ligand complexes relevant to this study. Therefore, the effectiveness of the organic chemicals in eliminating the free metal cations from solution would follow the same order, which was

indeed confirmed by the coagulation results in Figure 4-1 to Figure 4-5 and Figure 4-8 to Figure 4-119.

Table 7-5 Stability constant ($\log K_1$) of metal-organic complexes (see Appendix IV)

Ligands Cations	Oxalate	Citrate		EDTA	
	L^{2-}	HL^{2-}	L^{3-}	HL^{3-}	L^{4-}
Mg^{2+}	2.55	3.29	2.80	13.13	8.64
Ca^{2+}	3.00	4.68	4.73	14.07	11.00
Fe^{3+}	9.40	12.50	25.00	26.40	24.23

With the depletion of Ca^{2+} and Mg^{2+} ions from solution, the first-order metal hydrolysis products $CaOH^+$ or $MgOH^+$ would decompose to maintain the equilibrium of the $Ca^{2+}/CaOH^+$ and $Mg^{2+}/MgOH^+$ pairs, resulting in a reduction in the concentrations of $CaOH^+$ or $MgOH^+$. It is possible that the organic ligands could also react with the first-order metal hydroxyl species directly. The consequence of these reactions was the restoration of the mineral/water and oil(bitumen)/water interfacial properties, at least partially, to the state where the metal cations were absent, in which case the bitumen (oil) and minerals did not coagulate. This argument was supported by the zeta potential measurements shown in Chapter 6, which showed that the zeta potentials of the minerals were restored by citric acid.

- (2) Adsorption of negatively charged organic ligands on precipitated metal hydroxides or/and mineral and bitumen surfaces.

When the stability constants of the metal-organic complexes are lower than those of the metal hydroxides, metal hydroxide precipitates can form at high pH. In this case, the effect of the organic complexing agents is shown by its adsorption on the precipitates or on the mineral and bitumen interfaces. For instance, citric acid is very effective in breaking bitumen-mineral coagulation in solutions containing ferric ions at pH 8. At this pH, over 90% of the Fe^{3+} were precipitated as ferric hydroxides. As this pH was close to the iso-electric point of the $Fe(OH)_3$, the $Fe(OH)_3$ precipitates were expected to promote

mineral-bitumen interaction, which was confirmed in the coagulation tests. However, after adding citric acid, the mutual coagulation was significantly reduced. It was possible that the uncomplexed citrate anions adsorbed on the $\text{Fe}(\text{OH})_3$ precipitates which coated the mineral surfaces. Zeta potential measurements showed that mineral particles indeed carried more negative charges after the addition of citric acid. In fact, Zhang et al. (1985) reported the adsorption of oxalic acid and citric acid on $0.09 \mu\text{m}$ spherical hematite ($\alpha\text{-Fe}_2\text{O}_3$) particles, indicating that adsorption of uncomplexed citric and oxalic anions on Fe-bearing oxides/hydroxides was possible.

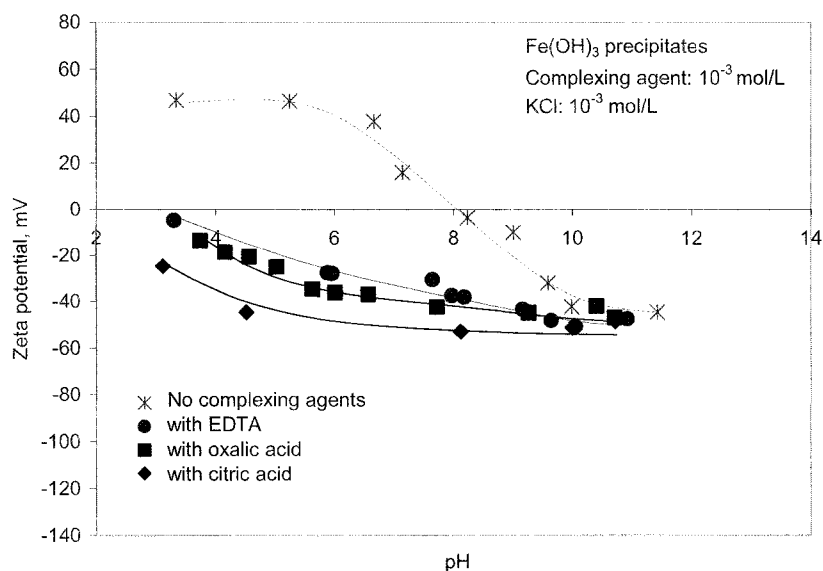


Figure 7-20 Zeta potential of $\text{Fe}(\text{OH})_3$ precipitates at different pH with and without the addition of organic complexing agents.

On the other hand, EDTA is not effective in inhibiting bitumen-quartz coagulation in solutions containing Fe^{3+} . edta^{4-} possibly did not substantially adsorb on ferric hydroxides. In fact, Nowack and Sigg (1996) found that the adsorption of EDTA on goethite (FeOOH) was significantly decreased with increasing pH, from $4.6 \times 10^{-7} \text{ mol/L}$ at pH 6 to $1 \times 10^{-7} \text{ mol/m}^2$ at pH 8. We measured the zeta potentials of freshly precipitated $\text{Fe}(\text{OH})_3$ as a function of pH in the presence of 10^{-3} mol/L of EDTA, citric acid or oxalic acid (Figure 7-20). As can be seen, at pH 8, at which coagulation tests were performed,

all complexing agents were able to reverse the positive zeta potential of $\text{Fe}(\text{OH})_3$ to negative. However, while citric acid demonstrated the strongest ability to increase the zeta potential in the negative direction, EDTA was the least effective.

7.7 Summary

Strong coagulation between mineral particles and bitumen (oil) droplets in solutions containing multivalent metal ions, Ca^{2+} , Mg^{2+} and Fe^{3+} was caused by the adsorption of metal hydroxyl complexes and precipitated metal hydroxides on the minerals, through electrostatic attraction for the metal hydroxyl species or chemical bonding for the metal hydroxide precipitates. The adsorption of the metal hydroxyl species and/or metal hydroxides led to a significant drop in the magnitude of the negative zeta potentials of both the minerals and bitumen droplets, which lowered the electrostatic repulsion and triggered mutual coagulation.

The organic complexing agents were able to break the bitumen (oil)-mineral mutual coagulation through two possible mechanisms. These are 1) removal of the first-order metal hydroxyl species from the solution through complexation of the metal cations, and 2) adsorption of the un-complexed organic ligands on the metal hydroxide precipitates. Both mechanisms caused an increase in the zeta potentials of the mineral particles and bitumen (oil) droplets to the negative direction, leading to an increase in electrostatic repulsion, and a decrease in the mutual coagulation.

8 CONCLUSIONS AND RECOMMENDATIONS

8.1 General Findings

8.1.1 *Effect of Multivalent Metal Cations on Bitumen(oil)-Mineral Coagulation*

The presence of multivalent metal cations in aqueous solutions was found to significantly increase the mutual coagulation between bitumen or oil droplets and mineral particles. Such enhancement was strongly dependent on pH.

(1) In the pH ranges where the multivalent metal cations are not hydrolyzed

The tested multivalent metal ions Ca^{2+} , Mg^{2+} and Fe^{3+} did not adsorb on the surfaces of mineral particles or bitumen/oil droplets in the pH ranges in which they were not hydrolyzed (pH < 9 for Mg^{2+} , pH < 10 for Ca^{2+} and pH < 1.5 for Fe^{3+}). They decreased the magnitude of the negative zeta potentials of bitumen and oil droplets as well as mineral particles through the compression of the electrical double layers. However, at the tested concentrations of the metal ions (i.e., 10^{-3} mol/L), the reduction in the magnitude of the negative zeta potentials was not sufficient to trigger mutual coagulation between quartz and bitumen or oil droplets. On the other hand, the metal cations did promote the mutual coagulation between bitumen or oil droplets and the tested clay minerals (kaolinite, illite).

(2) In the pH ranges where the metal cations form first-order hydroxyl species

The first-order metal hydroxyl species, CaOH^+ and MgOH^+ , were adsorbed on the surfaces of quartz and kaolinite. Their adsorption substantially enhanced the mutual coagulation between bitumen or oil droplets and mineral particles. The magnitude of the negative zeta potentials of both the minerals and bitumen or oil droplets were significantly reduced, which was the main reason for the enhanced mutual coagulation.

Calculation using the James and Healy model, coupled with the molecular dynamics calculation of the ionic radii of the first-order metal hydroxyl species, indicated that the adsorption of the first-order metal hydroxyl species was thermodynamically more favorable compared with the metal cations. Adsorption density measurements, X-ray photoelectron spectroscopic and attenuated total reflectance Fourier-transform infrared spectroscopic analyses indicated that the first-order metal hydroxyl species adsorbed on the mineral surface. However, the adsorption seemed to stem from relatively weak physisorption, and the adsorbed metal ions could be washed off with rinse water of the same pH as used in the adsorption.

(3) In the pH range where the metal cations form metal hydroxide precipitates

The formation of metal hydroxide precipitates ($\text{Fe}(\text{OH})_3$ and $\text{Mg}(\text{OH})_2$) also contributed to the strong coagulation between bitumen or oil droplets and mineral particles. Zeta potential measurements showed charge reversal of both the mineral particles and bitumen or oil droplets in the presence of the metal hydroxides. X-ray photoelectron spectroscopic analyses showed that there were significant chemical shifts of the binding energies of the Fe2p and Mg2p electrons, suggesting that the ferric hydroxides and magnesium hydroxides adsorbed through chemisorption. The adsorbed metal hydroxides could not be completely washed off by rinse water.

8.1.2 *Effect of Complexing Agents on Bitumen(oil)-Mineral Coagulation*

The three complexing agents used in this study, citric acid, oxalic acid and ethylenediaminetetraacetic acid (EDTA), in general, significantly reduced or virtually eliminated the mutual coagulation between bitumen or oil droplets and mineral particles induced by the Ca^{2+} , Mg^{2+} and Fe^{3+} ions. This is mainly due to:

(1) Removal of the metal cations from solution through complexation

The tested organic acids can form metal-organic ligand complexes. Citric acid, oxalic acid and EDTA sequestered Ca^{2+} and Mg^{2+} at pH 10 through the formation of the metal-organic ligand complexes. The complexing agents with higher stability constants to the metal cations have higher capacity to eliminate metal ions from aqueous solutions. Thus the effectiveness of the tested organic agents followed the order EDTA > citric acid > oxalic acid. Once the metal ions were removed from solution, the adsorption of the hydroxylated metal species (metal hydroxyls and/or metal hydroxides) was considerably lowered, causing the restoration of the negative zeta potentials of the mineral particles and bitumen or oil droplets, with the consequent reduction in mutual coagulation.

(2) Adsorption of un-complexed organic ligands on metal hydroxide precipitates

When the metal-organic ligand complex of a metal ion (e.g., Fe^{3+}) has lower formation constant than its metal hydroxide, metal hydroxide precipitate forms at certain pH in preference of the metal-organic ligand complex. In this case, the metal hydroxide may have adsorbed on the mineral or bitumen or oil droplets first, followed by the adsorption of the un-complexed organic ligands. Such adsorption also resulted in the high negative surface charge on the surfaces of both the mineral particles and bitumen or oil droplets, leading to a reduction in the mutual coagulation between the bitumen or oil droplets and mineral particles. The effect of citric acid on eliminating the coagulation-promoting function of the ferric ions at pH 8 seems to be the result of this mechanism.

8.1.3 *Effect of Citric Acid on Bitumen Liberation*

Of the three organic complexing agents tested, citric acid was found the most effective in improving bitumen-mineral liberation in solutions containing multivalent metal cations at pH 8–10. In small scale flotation experiment, the addition of 2×10^{-3} mol/L citric acid improved bitumen separation efficiency by 24 percentage points from Syncrude froth treatment tailings.

Combined addition of 1.5×10^{-3} mol/L citric acid and 30 mg/L polyacrylamide could further increase the bitumen separation efficiency. This was probably due to the improved liberation of bitumen from minerals caused by citric acid, and the reduced mechanical entrainment of the liberated clays by polyacrylamide. The use of a polymer flocculant such as polyacrylamide is expected to improve the tailings settling and dewatering behavior as well.

8.2 Claims of Original Research

- Systematic studies on the mutual coagulation between an organic phase such as bitumen or oil droplets and an inorganic phase such as mineral particles in aqueous solutions with and without the presence of multivalent metal cations Ca^{2+} , Mg^{2+} and Fe^{3+} ; Identification of metal hydroxyl species and metal hydroxide precipitates as the major ionic species that were responsible for the enhanced mutual coagulation.
- Studies on the effect of organic complexing agents citric acid, oxalic acid and ethylenediaminetetraacetic acid on reducing the mutual coagulation of bitumen or oil droplets with mineral particles (quartz, kaolinite and illite)
- Calculation of the ionic radii of first-order metal hydroxyl species (CaOH^+ , MgOH^+ , etc.) using molecular dynamics simulation (with help from Dr. C. Li and Dr. P. Choi).
- Identification of the different adsorption mechanisms for metal hydroxyl species (physisorption) and metal hydroxide precipitates (chemisorption).
- Construction of complete speciation diagrams of Ca^{2+} , Mg^{2+} and Fe^{3+} in the presence of oxalic acid, citric acid and ethylenediaminetetraacetic acid.
- Flotation tests combining the addition of citric acid with ultrasonic treatment, and with external magnetic fields to recover residual bitumen from oil sands froth treatment tailings.
- Sign reversal of the zeta potentials of bitumen and oil droplets in the presence of Mg^{2+} at pH 10.4, but no sign reversal in the presence of Ca^{2+} .

8.3 Recommendations for Further Research

There are at least three types of interactions in the water-based oil sands extraction system that are of interest. These are the bitumen-mineral, bitumen-bitumen, and bitumen-bubble interactions. While the bitumen-mineral interactions affect bitumen liberation from the oil sands minerals, the coalescence of bitumen droplets and the adhesion of bitumen droplets to air bubbles will influence the kinetics of the flotation recovery of the bitumen. It will be interesting, and necessary, to study the effect of the metal cations and metal ionic complexes on all three interactions. The bitumen-mineral interaction has been studied in this work to some degree. Further studies on the following subjects would form a complete picture of the roles played by multivalent metal cations in the oil sands extraction system:

- 1) Effect of multivalent metal cations on the coalescence of oil and bitumen droplets by investigating oil-in-water emulsion stability as a function of pH at different concentrations of the metal ions.
- 2) More detailed study on the adsorption of metal ionic complexes and metal hydroxide precipitates on oil and bitumen.
- 3) The nature of the charges at the oil (non-polar hydrocarbon)/water interfaces, and the effects of the multivalent metal cations and organic acids on these surface charges.
- 4) The effect of metal cations and metal ionic complexes on the gas bubble surface properties such as surface charge, surface viscosity, etc., and how the changes in these properties affect the bitumen-bubble attachment.
- 5) Characterization of the metal ionic species adsorbed on minerals, bitumen and gas bubbles.

REFERENCES

1. Accelrys, Materials Studio, User Manual, Accelrys Inc., 2004
2. Agashe, K. B. and Regalbuto, J. R., *J. Colloid Interface Sci.* 185, 174 (1997).
3. Ambikadevi, V. R. and Lalithambika, M., *Appl. Clay Sci.* 16 (3-4), 133 (2000).
4. Bantignies, J. L., Moulin, C. C. D., and Dexpert, H., *J. Petrol. Sci. Eng.* 20 (3-4), 233 (1998).
5. Bassi, R., Prasher, S. O., and Simpson, B. K., *Environ. Progr.* 19 (4), 275 (2000).
6. Basu, S., Nandakumar, K., and Masliyah, J. H., *Can. J. Chem. Eng.* 75 (2), 476 (1997).
7. Basu, S., Nandakumar, K., and Masliyah, J. H., *Colloids Surf. A: Physicochem. Eng. Asp.* 136 (1-2), 71 (1998).
8. Basu, S., Nandakumar, K., and Masliyah, J. H., *J. Colloid Interface Sci.* 205 (1), 201 (1998).
9. Basu, S., Nandakumar, K., Lawrence, S., and Masliyah, J., *Fuel* 83 (1), 17 (2004).
10. Bayliss, P. and A. A. Levinson, *Bull. Petrol. Geol.* 24, 211(1976).
11. Beattie, J. K. and Djerdjev, A. M., *Angew. Chem. Int. Ed.* 43 (27), 3568 (2004).
12. Beattie, J. K., Djerdjev, A. M., Franks, G. V., and Warr, G. G., *J. Phys. Chem. B* 109 (33), 15675 (2005).
13. Beetge, J. H., et al., Canadian Patent, 2,535,702 (2005).
14. Bensebaa, F., Majid, A., and Deslandes, Y., *Spectrochim. Acta Part A-Mol. Biomol. Spectrosc.* 57 (13), 2695 (2001).
15. Berka, M. and Rice, J. A., *Langmuir* 20 (15), 6152 (2004).
16. Bichard, J. A. and Edward, P., US Patent, 3,330,757 (1967).
17. Biggs, S., *Langmuir* 11 (1), 156 (1995).
18. Blanco, C. G., Prado, J. G., Guillen, M. D., and Borrego, A. G., *Org. Geochem.* 18 (3), 313 (1992).
19. Bondi, A., *J. Phys. Chem.* 68 (3), 441 (1964).
20. Brady, P. V., Cygan, R. T., and Nagy, K. L., *J. Colloid Interface Sci.* 183 (2), 356 (1996).

21. Butler, J. N. and Cogley, D. R., *Ionic Equilibrium: Solubility and pH Calculations*, John Wiley and Sons, Inc. New York, 1998, p. 295.
22. Canada Energy Board, "Canada's Oil Sands: Opportunities and Challenges to 2015: an Update", Canada Energy Board report, 2006.
23. Carty, W. M., *Am. Ceramic Soc. Bull.* 78 (8), 72 (1999).
24. Carver, J. C., Schweitzer, G. K., Carlson, T. A., *J. Chem. Phys.* 57, 973 (1972).
25. Chapel, J. P., *Langmuir* 10 (11), 4237 (1994).
26. Cheng, Y. H., Mikhail, M. W., Salama, A. I. A., and Burns, B., *J. Can. Petrol. Technol.* 38 (9), 20 (1999).
27. Claesson, P. M., Herder, P. C., Blom, C. E., and Ninham, B. W., *J. Colloid Interface Sci.* 118 (1), 68 (1987).
28. Clark, K. A. and Pasternack, D. S., *Ind. Eng. Chem.* 24, 1410 (1932).
29. Clark, S.W. and Cooke, S. R. B., *Trans. AIME.* 241, 334 (1968).
30. Coleman, R. D., Sparks, B. D., Majid, A., and Toll, F. N., *Fuel* 74 (8), 1156 (1995).
31. Crawford, R. J., Harding, I. H., and Mainwaring, D. E., *Langmuir* 9 (11), 3050 (1993a).
32. Crawford, R. J., Harding, I. H., and Mainwaring, D. E., *Langmuir* 9 (11), 3057 (1993b).
33. Cymerman, G. J. and Kwong, T., in: *Proceedings of the 1st UBC-McGill Bi-annual International Symposium* (J. S. Laskowski and G. W. Poling, Eds.), Vancouver, BC, Canada, August, 20-24, 1995, p319.
34. Czarnecki, J., Radoev, B., Schramm, L. L., and Slavchev, R., *Advan. Colloid Interface Sci.* 114, 53 (2005).
35. Dai, Q. and Chung, K. H., *Fuel* 74 (12), 1858 (1995).
36. Dai, Q. and Chung, K. H., *Fuel* 75 (2), 220 (1996).
37. Darcovich, K. et al., *Energy & Fuels* 3 (3), 386 (1989).
38. Davis, J. A., James, R. O., and Leckie, J. O., *J. Colloid Interface Sci.* 63 (3), 480 (1978).
39. Dean, J. A., *Lange's Handbook of Chemistry*, 15th Ed., McGraw-Hill, Inc. 1999, p.83.
40. Derjagui, B. V. and Churaev, N. V., *J. Colloid Interface Sci.* 49 (2), 249 (1974).

41. Derjaguin, B. V. and Landau, L., *Acta Physicochim. URSS* 14, 633 (1941).
42. Derjaguin, B. V. and Kusakov, M. M., *Acta Physicochim. URSS* 10, 25 (1939).
43. Dillard, J. G. and Koppelman, M. H., *J. Colloid Interface Sci.* 87 (1), 46 (1982).
44. Ding, X. L., Repka, C., Xu, Z. H., and Masliyah, J., *Can. J. Chem. Eng.* 84 (6), 643 (2006).
45. Drelich, J. and Miller, J. D., *Colloids Surf.* 69 (1), 35 (1992).
46. Ducker, W. A., Senden, T. J., and Pashley, R. M., *Nature* 353 (6341), 239 (1991).
47. Ducker, W. A., Xu, Z. G., and Israelachvili, J. N., *Langmuir* 10 (9), 3279 (1994).
48. Dzyaloshinskii, I. E., Lifshitz, E. M., and Pitaevskii, L. P., *Advan. Phys.* 10 (38), 165 (1961).
49. Farley, K. J., Dzombak, D. A., and Morel, F. M. M., *J. Colloid Interface Sci.* 106 (1), 226 (1985).
50. Farnand, J. R., Meadus, F. W., and Sparks, B. D., *Fuel Proc. Technol.* 10 (2), 131 (1985).
51. Ferris, A. P. and Jepson, W. B., *J. Colloid Interface Sci.* 51 (2), 245 (1975).
52. Fong, N., et al., *Fuel* 83 (14-15), 1865 (2004).
53. Frank, H. S. and Evans, M. W., *J. Chem. Phys.* 13 (11), 507 (1945).
54. Frank, H. S. and Wen, W. Y., *Disc. Farad. Soc.* (24), 133 (1957).
55. Franks, G. V., Djerdjev, A. M., and Beattie, J. K., *Langmuir* 21 (19), 8670 (2005).
56. Freeman, J. S. and Rowell, D. L., *J. Soil Sci.* 32 (1), 75 (1981).
57. Fuerstenau, D. W. and Pradip, *Advan. Colloid Interface Sci.* 114, 9 (2005).
58. Fuerstenau, D. W. and Raghavan, S., In: *Flotation – A. M. Gaudin Memorial Volume* (M. C. Fuerstenau, Ed.), SME/AIME, 1976, Vol. 1, p.21.
59. Fuerstenau, M. C. and Han, K. N., *J. Colloid Interface Sci.* 256 (1), 175 (2002).
60. Fuerstenau, M. C. and Palmer, B. R., In: *Flotation – A. M. Gaudin Memorial Volume* (M. C. Fuerstenau, Ed.), SME/AIME, 1976, Vol. 1, p.148.
61. Fuerstenau, M. C., *Soc. Mining Eng. AIME Trans.* 247 (1), 11(1970).
62. Furia, T. E., *CRC Handbook of Food Additives*, 2nd Ed. 1972, Vol. 1, p.275.
63. Goldberg, S. and Sposito, G., *Comm. Soil Sci. Plant Anal.* 16 (8), 801 (1985).
64. Grim, R. E., *Clay Mineralogy*, 2nd Ed. McGraw-Hill, New York, 1968, p.596.
65. Hall, E. S. and Tollefson, E. L., *Canadian Patent* 1164383 (1984).

66. Hall, E. S. and Tollefson, E. L., In: *The Future of Heavy Crude Oils and Tar Sands* (proceedings of First International Conference), Edmonton, AB, Canada, June 4-12, 1979, p751.
67. Hall, E. S. and Tollefson, E. L., *AOSTRA J. Res.* 4(1), 7 (1987).
68. Hall, E. S. and Tollefson, E. L., *Energy Proc. Can.* 9-10, 39 (1980).
69. Hamshar, J. A., Gregoli, A. A., Rimmer, D. P., and Yildirim, E., in: *proceedings of Oil Sands – Our Petroleum Future Conference*, Edmonton, AB, Canada, April 4-7, 1993.
70. Hanna, H. S. and Somasundaran, P., In: *Flotation – A. M. Gaudin Memorial Volume* (M. C. Fuerstenau, Ed.), SME/AIME, 1976, Vol. 1, p.197.
71. Hart, L. I., Jr. and Schmidit-Collerus, J. J., US Patent 4,054,506 (1977).
72. Haycock, D. E., Kasrai, M., Nicholls, C. J., Urch, D. S., *J. Chem. Soc. Dalton Trans.* 1791 (1978).
73. Hiemenz, P. C. and Rajagopalan, R., *Principles of Colloid and Surface Chemistry*, 3rd Ed., Marcel Dekker Inc, New York, 1997, p.528.
74. Hindle, W. S, Oxenford, R. J., and Shook, C. A., “Hydrotransport Developments at Syncrude Canada Ltd.”, National Conference Publication - Institution of Engineers, Australia 1(92), 191 (1992).
75. Hogg, R., Healy, T. W., and Fuerstenau, D. W., *Trans. Farad. Soc.* 62 (522P), 1638 (1966).
76. Hough, D. B. and White, L. R., *Advan. Colloid Interface Sci.* 14 (1), 3 (1980).
77. Houlihan, R., in: *The Future of Heavy Crude Oils and Tar Sands* (proceedings of Second International Conference), Caracas, Venezuela, February 7-17, 1982, p.1076.
78. Hu, Y., Liu, X., and Xu, Z., *Miner. Eng.* 16, 219 (2003)
79. Huang, C. P. and Stumm, W., *J. Colloid Interface Sci.* 43 (2), 409 (1973).
80. Hunter, R. J. and James, M., *Clays Clay Miner.* 40 (6), 644 (1992).
81. Ignasiak, T. M. et al., *Fuel* 62 (3), 353 (1983).
82. Ikhsan, J., Wells, J. D., Johnson, B. B., and Angove, M. J., *J. Colloid Interface Sci.* 273 (1), 6 (2004).
83. Israelachvili, J. N. and McGuiggan, P. M., *Science* 241 (4867), 795 (1988).

84. Israelachvili, J. N. and Pashley, R. M., *J. Colloid Interface Sci.* 98 (2), 500 (1984).
85. Israelachvili, J. N. and Pashley, R. M., *Nature* 306 (5940), 249 (1983).
86. Israelachvili, J. N. and Pashley, R., *Nature* 300 (5890), 341 (1982).
87. Israelachvili, J. N. and Wennerström, H., *Nature* 385(6618), 690 (1997).
88. Israelachvili, J. N., *Intermolecular and Surface Forces*, 2nd Ed., Academic Press, London, 1992.
89. Jada, A., Akbour, R. A., and Douch, J., *Chemosphere* 64 (8), 1287 (2006).
90. James, R. O. and Healy, T. W., *J. Colloid Interface Sci.* 40 (1), 42 (1972a).
91. James, R. O. and Healy, T. W., *J. Colloid Interface Sci.* 40 (1), 53 (1972b).
92. James, R. O. and Healy, T. W., *J. Colloid Interface Sci.* 40 (1), 65 (1972c).
93. Jang, H. M. and Fuerstenau, D. W., *Colloids Surf.* 21, 235 (1986).
94. Johnson, N. W., McKee, D. J. and Lynch, A. J., *Trans. AIME* 256, 204 (1974).
95. Kasongo, T., Zhou, Z., Xu, Z. H., and Masliyah, J., *Can. J. Chem. Eng.* 78 (4), 674 (2000).
96. Kaya, A. and Yukselen, Y., *Can. Geotech. J.* 42 (5), 1280 (2005).
97. Kessick, M. A., *J. Can. Petrol. Technol.* 18 (1), 49 (1979).
98. Kinniburgh, D. G. and M. L. Jackson, in: *Adsorption of Inorganics at Solid-Liquid Interfaces* (M. A. Anderson and A. J. Rubin, Eds.), Ann Arbor Sci. Publishers, Inc., Michigan, 1981, p.91.
99. Kinno, S. and Onaka, R., *J. Physical Soc. Japan*, 49(4) (1980).
100. Klein, J., *Nature* 288 (5788), 248 (1980).
101. Kónya, J. and Nagy, N. M., *Colloid Surf. A: Physicochem. Eng. Asp.* 136, 299 (1998).
102. Kotlyar, L. S. et al., *Fuel* 74 (8), 1146 (1995).
103. Kotlyar, L. S. et al., *Petrol. Sci. Technol.* 16 (1-2), 1 (1998).
104. Kotlyar, L. S., Kodama, H., and Ripmeester, J. A., *Appl. Clay Sci.* 5, 1 (1990).
105. Kotlyar, L. S., Kodama, H., Sparks, B. D., and Grattan-Bellew, P. E., *Appl. Clay Sci.* 2, 253 (1987).
106. Kotlyar, L. S., Sparks, B. D., Woods, J. R., and Chung, K. H., *Energy Fuels* 13 (2), 346 (1999).

107. Kotlyer, L. S., Ripmeester, J. A., Sparks, B. D., Montgomery, D. S., *Fuel*, 67, 221 (1988).
108. Krishnan, S. V. and Iwasaki, I., *Environ. Sci. Technol.* 20 (12), 1224 (1986).
109. Kruyer, J., in: *Future of Heavy Crude and Tar Sands, 2nd International Conference (Proceeding of Second International Conference, Caracas Venezuela, February 7-17, 1982, p.1087.*
110. Kumar, A., Sparks, B. D., and Majid, A., *Separ. Sci. Technol.* 21 (3), 315 (1986).
111. Lackovic, K., Johnson, B. B., Angove, M. J., and Wells, J. D., *J. Colloid Interface Sci.* 267 (1), 49 (2003).
112. Latimer, W. M., *J. Chem. Phys.* 23 (1), 90 (1955).
113. Latimer, W. M., Pitzer, K. S., and Slansky, C. M., *J. Chem. Phys.* 7 (2), 108 (1939).
114. Li, H., Zhou, Z. A., Xu, Z., and Masliyah, J. H., *Ind. Eng. Chem. Res.* 44 (13), 4753 (2005).
115. Liu, J. J., Xu, Z. H., and Masliyah, J., *AIChE J.* 50 (8), 1917 (2004).
116. Liu, J. J., Xu, Z. H., and Masliyah, J., *J. Colloid Interface Sci.* 287 (2), 507 (2005).
117. Liu, J. J., Xu, Z. H., and Masliyah, J., *Langmuir* 19 (9), 3911 (2003).
118. Liu, J., Zhou, Z., Xu, Z., and Masliyah, J., *J. Colloid Interface Sci.* 252 (2), 409 (2002).
119. Liu, Q. and Zhang, Y. H., *Miner. Eng.* 13 (13), 1405 (2000).
120. Liu, Q., Cui, Z., and Etsell, T. H., *Fuel* 85 (5-6), 807 (2006a).
121. Liu, Q., Wannas, D., and Peng, Y., *Int. J. Miner. Proc.* 80 (2-4), 244 (2006b).
122. Long, J., Xu, Z. H., and Mashyah, J. H., *Colloids Surf. A: Physicochem. Eng. Asp.* 281 (1-3), 202 (2006).
123. Ma, C. and Eggleton, R. A., *Clays Clay Miner.* 47(2), 174 (1999).
124. Majid, A. and Sparks, B. D., *Fuel* 62 (7), 772 (1983).
125. Majid, A., Sirianni, A. F., and Ripmeester, J. A., *Canadian Patent* 1,200,778 (1983).
126. Majid, A., Sparks, B. D., and Ripmeester, J. A., *Fuel Sci. Technol. Int.* 11(2), 279 (1993).
127. Malati, M. A., *Surf. Coat. Technol.* 30 (3), 317 (1987).
128. Marcelja, S., *Nature* 385 (6618), 689 (1997).
129. Marinova, K. G. et al., *Langmuir* 12 (8), 2045 (1996).

130. Masliyah, J. H., et al., *Can. J. Chem. Eng.* 82 (4), 628 (2004).
131. Mathieu, H.J., Landolt, D., *Corros. Sci.* 26, 547 (1986).
132. McBride, M. B., *Clays Clay Miner.* 24 (2), 88 (1976).
133. McBride, M. B., *Clays Clay Miner.* 30 (3), 200 (1982).
134. Medout-Marere, V., *J. Colloid Interface Sci.* 228 (2), 434 (2000).
135. Mitchell, J. K., *Fundamentals of Soil Behavior*, 2nd Ed., John Wiley and Sons, Inc., New York, 1993, p.32.
136. Moran, K., Yeung, A., and Masliyah, J. H., *Can. J. Chem. Eng.* 78 (4), 625 (2000).
137. Mporfu, P., Addai-Mensah, J., and Ralston, J., *Int. J. Miner. Proc.* 71 (1-4), 247 (2003).
138. Nowack, B. and Sigg, L., *J. Colloid Interface Sci.* 177 (1), 106 (1996).
139. Omotoso, O. E. and Mikula, R. J., *Appl. Clay Sci.* 25 (1-2), 37 (2004).
140. Pashley, R. M. and Israelachvili, J. N., *J. Colloid Interface Sci.* 97 (2), 446 (1984).
141. Pashley, R. M., *Advan. Colloid Interface Sci.* 16 (7), 57 (1982).
142. Pashley, R. M., *J. Colloid Interface Sci.* 80 (1), 153 (1981).
143. Pashley, R. M., McGuiggan, P. M., Ninham, B. W., and Evans, D. F., *Science* 229 (4718), 1088 (1985).
144. Petzold, G., Geissler, U., Smolka, N., and Schwarz, S., *Colloid Polym. Sci.* 282, 670 (2004).
145. Popov, K. et al., *Colloids Surf. A: Physicochem. Eng. Asp.* 244 (1-3), 25 (2004).
146. Prisciandaro, M., Lancia, A., and Musmarra, D., *Ind. Eng. Chem. Res.* 42 (25), 6647 (2003).
147. Prisciandaro, M., Santucci, A., Lancia, A., and Musmarra, D., *Can. J. Chem. Eng.* 83 (3), 586 (2005).
148. Rabinovich, Y. I. and Churaev, N. V., *Colloid J. USSR*, 41, 1146 (1979).
149. Rabinovich, Y. I. and Yoon, R. H., *Langmuir* 10 (6), 1903 (1994).
150. Riera, E. et al., *Ultrasonics Sonochem.* 11 (3-4), 241 (2004).
151. Robinson, D. A., *Vadose Zone J.* 3 (5), 705 (2004)
152. Romdhane, M. and Gourdon, C., *Chem. Eng. J.* 87, 11 (2002).
153. Russel, W. B., Saville, D. A., and Schowalter, W. R., *Colloidal Dispersions*, Cambridge University Press, Cambridge, 1989.

154. Rutland, M. W. and Senden, T. J., *Langmuir* 9, 637 (1993).
155. Saada, A., Siffert, B., and Papirer, E., *J. Colloid Interface Sci.* 174 (1), 185 (1995).
156. Sadeghi, K. M., Sadeghi, M. A., and Yen, T. F., *Energy Fuels* 4, 604 (1990).
157. Sanford, E. C. and Seyer, F. A., *CIM Bull.* 72 (803), 164 (1979).
158. Sanford, E. C., *Can. J. Chem. Eng.* 61 (4), 554 (1983).
159. Schindler, P. W. and Stumm, W., in: *Aquatic Surface Chemistry* (W. Stumm, ed.) Wiley Interscience, New York, 1987, p.83.
160. Schofield, R. K. and Samson, H. R., *Disc. Farad. Soc.* 65, 135 (1954).
161. Schramm, L. L. and Smith, R. G., *Colloids Surf.* 14 (1), 67 (1985).
162. Schramm, L. L., Morrison, C., and Stasiuk, E. N., *Fuel Proc. Technol.* 56 (3), 243 (1998).
163. Schramm, L. L., Smith, R. G., and Stone, J. A., in: *proceedings of Symposium on Characterization and Chemistry of Oil Shales*, St. Louis, Missouri, USA, April 8-13, 1984, p.209.
164. Schramm, L. L., Stasiuk, E. N., and Turner, D., *Fuel Proc. Technol.* 80 (2), 101 (2003).
165. Smith, R. G. and Schramm, L. L., *Fuel Proc. Technol.* 30 (1), 1 (1992).
166. Sowa, J. M., Sheng, P., Zhou, M. Y., Chen T., Serres, A. J., and Sieben, M. C., *Fuel* 74(8), 1176 (1995).
167. Sparks, B. D., Kotlyar, L. S., O'Carroll, J. B., and Chung, K. H., *J. Petrol. Sci. Eng.* 39 (3-4), 417 (2003).
168. Sposito, G., *ACS Symposium Series* 323, 217 (1986).
169. Sposito, G., *The Surface Chemistry of Soils*, Oxford University Press, New York, 1984, p.227.
170. St. Denis, C. E. and Kessick, M. A., *Can. J. Chem. Eng.* 60 (5), 675 (1982).
171. Strausz, O. P., in: *The Oil Sands of Canada-Venezuela* (D. A. Redford and A. G. Winestock, Eds.), *CIM Special Volume* 17, 1977, p.146.
172. Sugama, T., KuKacka, L. E., Carciello, N., Hocker, N. J., *Cement and Concrete Research* 19, 857 (1989).
173. Surry, K. N., "Low Temperature Bitumen Recovery Process", *US Patent* 4,946,597 (1990).

174. Sverjensky, D. A. and Fukushi, K., *Environ. Sci. Technol.* 40 (1), 263 (2006).
175. Sverjensky, D. A., *Geochim. Cosmochim. Acta* 70 (10), 2427 (2006).
176. Takamura, K. and Chow, R. S., *J. Can. Petrol. Technol.* 22 (6), 22 (1983).
177. Takamura, K. and Wallace, D., *J. Can. Petrol. Technol.* 27 (6), 98 (1988).
178. Takamura, K., *AOSTRA J. Res.* 2(1), 1 (1985).
179. Tandy, S. et al., *Environ. Sci. Technol.* 38 (3), 937 (2004).
180. Tewari, P. H., Lee, W., and Campbell, A. B., *Can. J. Chem.* 50 (11), 1642 (1972).
181. Trahar, W. J., *Int. J. Miner. Proc.* 8 (4), 289 (1981).
182. Tsamantakis, C., Masliyah, J., Yeung, A., and Gentsis, T., *J. Colloid Interface Sci.* 288 (1), 129 (2005).
183. Tsao, Y. H., Evans, D. F., and Wennerstrom, H., *Langmuir* 9 (3), 779 (1993).
184. Tu, Y. et al., *Petrol. Sci. Technol.* 24 (3-4), 327 (2006).
185. Van der Giessen, A., *J. Inorg. Nucl. Chem.* 28 (10), 2155 (1966).
186. Van Riemsdijk, W. H. and Lyklema, J., *J. Colloid Interface Sci.* 76 (1), 55 (1980).
187. Verwey, E. J. W. and Overbeek, J. T. G., *Theory of Stability of Lyophobic Colloids*, Elsevier, Amsterdam, 1948.
188. Wagner, C. D., in *Practical Surface Analysis*. 2nd edn, Vol 1, (D. Briggs and M. P. Seah, eds.), Appendix 5. John Wiley and Sons, Chichester, 1990, p. 595-634
189. Wang, N. and Mikula, R. J., *J. Can. Petrol. Technol.* 41 (1), 8 (2002).
190. Ward, D. B. and Brady, P. V., *Clays Clay Miner.* 46 (4), 453 (1998).
191. Warren, L. J., in: *The Principles of Mineral Flotation* (M.H. Jones and J.T. Woodcock, Eds.), Australian IMM, Melbourne, 1984, p.185.
192. Webb, T. J., *J. Am. Chem. Soc.* 48, 2589 (1926).
193. Westin, K. J. and Rasmuson, A. C., *Desalination* 159 (2), 107 (2003).
194. Westin, K. J. and Rasmuson, A. C., *J. Colloid Interface Sci.* 282 (2), 370 (2005).
195. Williams, D. J. A. and Williams, K. P., *J. Colloid Interface Sci.* 65 (1), 79 (1978).
196. Wren, A. G., Phillips, R. W., Tolentino, C. U., *J. Colloid Interface Sci.* 70, 544 (1979).
197. Wu, X. and Czarnecki, J., *Energy Fuels* 19 (4), 1353 (2005).
198. Wu, X., Czarnecki, J., Hamza, N., and Masliyah, J. H., *Langmuir* 15, 5244 (1999).

199. Yan, N. X. and Masliyah, J. H., *Colloids Surf. A: Physicochem. Eng. Asp.* 96 (3), 243 (1995).
200. Yan, N. X. and Masliyah, J. H., *J. Colloid Interface Sci.* 168 (2), 386 (1994).
201. Yoon, R. H. and Mao, L. Q., *J. Colloid Interface Sci.* 181 (2), 613 (1996).
202. Yushchenko, V. S., Yaminsky, V. V., and Shchukin, E. D., *J. Colloid Interface Sci.* 96 (2), 307 (1983).
203. Zhang, Y., Kallay, N., and Matijevic, E., *Langmuir* 1 (2), 201 (1985).
204. Zhou, Z. A., Xu, Z. H., Masliyah, J. H., and Czarnecki, J., *Colloids Surf. A: Physicochem. Eng. Asp.* 148 (3), 199 (1999).
205. Zhou, Z. H. and Gunter, W. D., *Clays Clay Miner.* 40 (3), 365 (1992).

APPENDIX I CALCULATION OF TOTAL INTERACTION ENERGY

Total interaction energies of interaction between bitumen and mineral particles (quartz, kaolinite and illite) are calculated using classical DLVO theory, as follows:

$$V_{\text{Total}} = V_E + V_V \quad (\text{A-1})$$

V_E is calculated by adopting Hogg, Furstenau and Healy's expression (1966)

$$V_E = \frac{\epsilon R_1 R_2 (\psi_1^2 + \psi_2^2)}{4(R_1 + R_2)} \left[\frac{2\psi_1 \psi_2}{\psi_1^2 + \psi_2^2} \ln \left(\frac{1 + e^{-\kappa H}}{1 - e^{-\kappa H}} \right) + \ln(1 - e^{-2\kappa H}) \right] \quad (\text{A-2})$$

Here ψ_1 and ψ_2 are the Stern potential (approximately equal to zeta potential) of the bitumen and mineral particles, $\epsilon = \epsilon_r \epsilon_0$, ϵ_r is the relative dielectric constant of the medium, ϵ_0 is the permittivity of vacuum, κ^{-1} is the Debye length. Assuming particle and bitumen droplets are rigid sphere with radii $R_1 = R_2 = 5 \mu\text{m}$. Debye length $\kappa^{-1} = 5.6 \text{ nm}$, a typical value in the presence of 10^{-3} mol/L 1:2 asymmetric electrolyte (CaCl_2 and MgCl_2) in the absence of citric acid, while $\kappa^{-1} = 9.2 \text{ nm}$ (10^{-3} mol/L 1:1 symmetric electrolyte, KCl) was used in the presence of citric acid. It was assumed that the presence of citric acid completely restored the electrical double layers compressed due to the multivalent metal cations.

The van der Waals interaction energy of two spherical macroscopic bodies of radii R_1 and R_2 , V_V , is given by Rabinovich and Churaev, (1979)

$$V_V = -\frac{A_{132} R_1 R_2}{6H(R_1 + R_2)} \left[1 - \frac{1 + 2bl}{1 + bc/H} \right] \quad (\text{A-3})$$

where $b = 3.1 \times 10^{-17} \text{ sec/rad}$, $l = 3.3 \times 10^{15} \text{ rad/sec}$, c is the speed of light in vacuum. For interaction of two different phases dispersed in a medium, the combined Hamaker constant A_{132} can be calculated through the combination law:

$$A_{132} = \left(\sqrt{A_{11}} - \sqrt{A_{33}} \right) \left(\sqrt{A_{22}} - \sqrt{A_{33}} \right) \quad (\text{A-4})$$

Table A-1 Parameters used for the calculation of total interaction energies between bitumen and minerals with classical DLVO theory

Terminology		Parameters	Reference
Hamaker constant of bitumen	A_{BB}	6.1×10^{-20} J	Czarnecki et al., 2005
Hamaker constant of water	A_{WW}	3.7×10^{-20} J	Hough and White, 1980
Hamaker constant of quartz,	A_{QQ}	8.8×10^{-20} J	Russel et al., 1989
Hamaker constant of kaolinite	A_{KK}	4.7×10^{-20} J	Berka and Rice, 2004
Hamaker constant of illite	A_{II}	8.6×10^{-20} J	Medout-Marere, 2000
Hamaker constant of bitumen/water/quartz	A_{BWQ}	5.7×10^{-21} J	Calculated using (A-4)
Hamaker constant of bitumen/water/kaolinite	A_{BWK}	1.34×10^{-21} J	Calculated using (A-4)
Hamaker constant of bitumen/water/illite	A_{BWI}	5.51×10^{-21} J	Calculated using (A-4)
Radii of bitumen, quartz, kaolinite and illite particles (R_1, R_2)		5 μm	Typical size of the particles studied
Thickness of the electrical double layer κ^{-1} (in the absence of citric acid)		5.6 nm	κ^{-1} value in 10^{-3} mol/L of 1:2 electrolyte
Thickness of the electrical double layer κ^{-1} (in the presence of citric acid)		9.2 nm	κ^{-1} value in 10^{-3} mol/L of 1:1 electrolyte

Table A-2 Total interaction energy (kT) of bitumen with quartz in solution containing 10^{-3} mol/L metal ions with or without the presence of 10^{-3} mol/L citric acid, calculated by classical DLVO theory. For a plot of the calculation results see Figure 6-11.

Distance nm	No citric acid			10^{-3} mol/L citric acid		
	Ca ²⁺ pH = 10	Mg ²⁺ pH=10	Fe ³⁺ pH=8	Ca ²⁺ pH = 10	Mg ²⁺ pH =10	Fe ³⁺ pH=8
0.1	-5.45E+03	-5.58E+03	-5.71E+03	-4.94E+03	-4.92E+03	-1.12E+06
0.2	-2.54E+03	-2.66E+03	-2.82E+03	-2.02E+03	-2.02E+03	-2.15E+03
0.3	-1.56E+03	-1.68E+03	-1.86E+03	-1.04E+03	-1.04E+03	-1.10E+03
0.4	-1.07E+03	-1.18E+03	-1.38E+03	-5.51E+02	-5.60E+02	-5.61E+02
0.5	-7.80E+02	-8.87E+02	-1.09E+03	-2.57E+02	-2.71E+02	-2.31E+02
0.6	-5.85E+02	-6.89E+02	-8.99E+02	-6.18E+01	-7.93E+01	-6.97E+00
0.7	-4.46E+02	-5.48E+02	-7.62E+02	7.66E+01	5.63E+01	1.55E+02
0.8	-3.43E+02	-4.42E+02	-6.60E+02	1.79E+02	1.57E+02	2.77E+02
0.9	-2.63E+02	-3.61E+02	-5.80E+02	2.58E+02	2.34E+02	3.72E+02
1.0	-2.00E+02	-2.95E+02	-5.16E+02	3.20E+02	2.94E+02	4.48E+02
2.0	6.28E+01	-1.69E+01	-2.32E+02	5.68E+02	5.33E+02	7.72E+02
3.0	1.24E+02	5.69E+01	-1.40E+02	6.09E+02	5.72E+02	8.38E+02
4.0	1.38E+02	8.02E+01	-9.53E+01	6.00E+02	5.63E+02	8.35E+02
5.0	1.34E+02	8.48E+01	-6.95E+01	5.73E+02	5.36E+02	8.03E+02
6.0	1.23E+02	8.13E+01	-5.31E+01	5.38E+02	5.03E+02	7.59E+02
7.0	1.10E+02	7.44E+01	-4.18E+01	5.00E+02	4.68E+02	7.10E+02
8.0	9.64E+01	6.62E+01	-3.37E+01	4.62E+02	4.32E+02	6.59E+02
9.0	8.34E+01	5.79E+01	-2.77E+01	4.25E+02	3.97E+02	6.08E+02
10.0	7.15E+01	4.99E+01	-2.31E+01	3.89E+02	3.63E+02	5.59E+02
20.0	1.15E+01	7.65E+00	-5.65E+00	1.45E+02	1.35E+02	2.12E+02
30.0	1.17E+00	5.17E-01	-1.75E+00	4.99E+01	4.64E+01	7.33E+01

Table A-3 Total interaction energy (kT) of bitumen with kaolinite in solution containing 10^{-3} mol/L metal ions with or without the presence of 10^{-3} mol/L citric acid, calculated by classical DLVO theory. For a plot of the calculation results see Figure 6-12.

Distance nm	No citric acid			10^{-3} mol/L citric acid		
	Ca ²⁺ pH = 10	Mg ²⁺ pH = 10	Fe ³⁺ pH=8	Ca ²⁺ pH = 10	Mg ²⁺ pH = 10	Fe ³⁺ pH=8
0.1	-1.38E+03	-1.63E+03	-1.35E+03	-6.57E+02	-8.64E+02	1.67E+02
0.2	-6.42E+02	-8.63E+02	-6.68E+02	6.36E+01	-1.38E+02	9.06E+02
0.3	-3.81E+02	-5.86E+02	-4.42E+02	3.11E+02	1.13E+02	1.16E+03
0.4	-2.45E+02	-4.39E+02	-3.29E+02	4.37E+02	2.43E+02	1.29E+03
0.5	-1.60E+02	-3.46E+02	-2.61E+02	5.14E+02	3.21E+02	1.37E+03
0.6	-1.02E+02	-2.80E+02	-2.15E+02	5.64E+02	3.74E+02	1.42E+03
0.7	-5.97E+01	-2.31E+02	-1.83E+02	6.00E+02	4.12E+02	1.45E+03
0.8	-2.74E+01	-1.93E+02	-1.59E+02	6.26E+02	4.40E+02	1.47E+03
0.9	-2.12E+00	-1.63E+02	-1.40E+02	6.45E+02	4.62E+02	1.49E+03
1.0	1.82E+01	-1.38E+02	-1.24E+02	6.60E+02	4.78E+02	1.50E+03
2.0	1.05E+02	-1.78E+01	-5.65E+01	6.99E+02	5.35E+02	1.49E+03
3.0	1.23E+02	2.15E+01	-3.42E+01	6.76E+02	5.27E+02	1.41E+03
4.0	1.21E+02	3.67E+01	-2.34E+01	6.38E+02	5.02E+02	1.32E+03
5.0	1.12E+02	4.17E+01	-1.71E+01	5.95E+02	4.70E+02	1.22E+03
6.0	1.01E+02	4.18E+01	-1.30E+01	5.50E+02	4.37E+02	1.12E+03
7.0	8.96E+01	3.95E+01	-1.02E+01	5.07E+02	4.04E+02	1.03E+03
8.0	7.83E+01	3.60E+01	-8.25E+00	4.65E+02	3.72E+02	9.44E+02
9.0	6.78E+01	3.21E+01	-6.76E+00	4.26E+02	3.41E+02	8.62E+02
10.0	5.82E+01	2.82E+01	-5.62E+00	3.89E+02	3.11E+02	7.85E+02
20.0	1.05E+01	5.27E+00	-1.35E+00	1.43E+02	1.16E+02	2.88E+02
30.0	1.61E+00	7.25E-01	-4.14E-01	4.91E+01	3.97E+01	9.85E+01

Table A-4 Total interaction energy (kT) of bitumen with illite in solution containing 10^{-3} mol/L metal ions with or without the presence of 10^{-3} mol/L citric acid, calculated by classical DLVO theory. For a plot of the calculation results see Figure 6-13.

Distance nm	No citric acid			10^{-3} mol/L citric acid		
	Ca ²⁺ pH = 10	Mg ²⁺ pH=10	Fe ³⁺ pH=8	Ca ²⁺ pH = 10	Mg ²⁺ pH=10	Fe ³⁺ pH=8
0.1	-5.49E+03	-5.62E+03	-5.53E+03	-1.05E+04	-1.07E+04	-9.77E+03
0.2	-2.65E+03	-2.77E+03	-2.74E+03	-4.84E+03	-5.04E+03	-4.11E+03
0.3	-1.69E+03	-1.80E+03	-1.81E+03	-2.95E+03	-3.15E+03	-2.21E+03
0.4	-1.20E+03	-1.31E+03	-1.34E+03	-2.01E+03	-2.20E+03	-1.26E+03
0.5	-9.10E+02	-1.02E+03	-1.06E+03	-1.44E+03	-1.63E+03	-6.84E+02
0.6	-7.14E+02	-8.17E+02	-8.75E+02	-1.06E+03	-1.25E+03	-3.04E+02
0.7	-5.73E+02	-6.74E+02	-7.43E+02	-7.89E+02	-9.76E+02	-3.34E+01
0.8	-4.68E+02	-5.66E+02	-6.43E+02	-5.87E+02	-7.72E+02	1.68E+02
0.9	-3.85E+02	-4.81E+02	-5.66E+02	-4.31E+02	-6.14E+02	3.23E+02
1.0	-3.20E+02	-4.14E+02	-5.04E+02	-3.07E+02	-4.87E+02	4.45E+02
2.0	-3.48E+01	-1.12E+02	-2.28E+02	2.25E+02	6.16E+01	9.42E+02
3.0	4.40E+01	-2.08E+01	-1.38E+02	3.66E+02	2.17E+02	1.04E+03
4.0	7.06E+01	1.58E+01	-9.43E+01	4.09E+02	2.74E+02	1.03E+03
5.0	7.76E+01	3.10E+01	-6.90E+01	4.15E+02	2.91E+02	9.89E+02
6.0	7.59E+01	3.63E+01	-5.28E+01	4.03E+02	2.91E+02	9.31E+02
7.0	7.02E+01	3.66E+01	-4.16E+01	3.83E+02	2.81E+02	8.67E+02
8.0	6.30E+01	3.45E+01	-3.36E+01	3.58E+02	2.65E+02	8.01E+02
9.0	5.53E+01	3.12E+01	-2.76E+01	3.32E+02	2.48E+02	7.36E+02
10.0	4.79E+01	2.75E+01	-2.30E+01	3.06E+02	2.29E+02	6.74E+02
20.0	7.47E+00	3.88E+00	-5.58E+00	1.08E+02	8.05E+01	2.43E+02
30.0	5.14E-01	-9.29E-02	-1.71E+00	2.81E+01	1.88E+01	7.41E+01

**APPENDIX II QUANTIFICATION OF ADSORBED METAL CATIONS BY XPS
ANALYSIS**

Table A-5 XPS analysis of adsorbed Ca^{2+} , Mg^{2+} and Fe^{3+} on quartz surface.

Peak	Position BE, (eV)	FWHM (eV)	Atomic conc.(%)	Peak	Position BE, (eV)	FWHM (eV)	Atomic conc.(%)
Ca^{2+} : 10^{-1} mol/L pH = 12.58, unrinsed sample				rinsed sample			
Ca 2p	344.9	2.59	4.24	Ca 2p	345.25	2.36	0.59
O1s	530.4	2.88	70.63	O1s	530.75	2.60	69.28
Si 2p	101.3	2.67	25.13	Si 2p	101.3	2.52	30.13
Mg^{2+} : 10^{-3} mol/L, pH = 10.75, unrinsed sample				rinsed sample			
Mg 2p	48.1	2.65	1.57	Mg 2p	47.4	2.69	1.42
O1s	530.4	2.74	75.17	O1s	530.75	2.66	69.89
Si 2p	101.3	2.66	23.26	Si 2p	101.3	2.56	28.69
Fe^{3+} : 10^{-3} mol/L, pH = 9.27, unrinsed sample				rinsed sample			
Fe 2p	709.6	4.53	2.57	Fe 2p	709.25	4.46	1.59
O1s	530.4	2.66	68.78	O1s	530.05	2.85	80.39
Si 2p	101.3	2.60	28.64	Si 2p	100.95	2.63	18.03

Table A-6 XPS analysis of adsorbed Ca^{2+} , Mg^{2+} and Fe^{3+} on glass slide.

Peak	Position BE, (eV)	FWHM (eV)	Atomic conc.(%)	Peak	Position BE, (eV)	FWHM (eV)	Atomic conc.(%)
Ca^{2+} : 10^{-3} mol/L, unrinsed				pH = 6.0			
Ca 2p	346.05	2.76	2.00	Ca 2p	346.05	2.56	3.85
O 1s	531.20	2.78	70.34	O 1s	530.85	2.84	58.70
Cl 2p	198.70	1.37	0.11	C 1s	283.40	2.57	18.02
Si 2p	101.75	2.8	27.08	Si 2p	101.75	2.69	19.29
Mg 2p	48.90	1.55	0.47	Mg 2p	48.25	2.27	0.77
Ca^{2+} : 10^{-3} mol/L, rinsed				pH = 6.0			
				pH = 11.72			
				Ca 2p	346.05	2.87	1.22
				O 1s	531.20	2.78	57.33
				C 1s	283.75	2.76	16.81
				Si 2p	101.40	2.75	22.18
				Mg 2p	49.25	2.64	0.78
				Na 1s	1070.55	2.66	1.68
Mg^{2+} : 10^{-3} mol/L, unrinsed				pH = 6.0			
				pH = 10.89			
Mg 2p	48.90	2.12	1.11	Mg 2p	48.20	2.72	12.06
O 1s	530.85	2.77	61.18	O 1s	530.15	3.08	53.42
Ca 2p	397.85	7.26	1.42	Ca 2p			
C 1s	283.05	2.73	13.37	C 1s	283.75	2.70	28.05
Si 2p	101.75	2.72	22.91	Si 2p	101.40	2.70	6.47
Mg^{2+} : 10^{-3} mol/L, rinsed				pH = 6.0			
				pH = 10.89			
				Mg 2p	48.55	2.57	8.03
				O 1s	530.50	3.00	50.05
				Ca 2p	350.25	3.87	3.06
				C 1s	283.75	2.52	25.94
				Si 2p	101.75	2.64	12.2
				Na 1s	1070.55	2.61	0.72
Fe^{3+}				pH = 2.5			
				pH = 9.14			
Fe 2p	710.40	3.7	0.94	Fe 2p	709.35	5.81	3.66
O 1s	531.20	3.21	59.68	O 1s	530.85	2.93	57.52
Ca 2p	349.90	7.07	1.09	Ca 2p	346.05	3.08	1.05
C 1s	283.75	5.06	16.21	C 1s	283.40	2.59	17.89
Si 2p	102.10	3.23	21.65	Si 2p	101.75	2.74	19.40
Mg 2p	48.20	1.99	0.45	Mg 2p	49.25	3.02	0.49

Table A-7 Element quantification of bitumen film without any treatment by XPS.

Peak	Position, BE (eV)	FWHM (eV)	Atomic Conc.(%)
O 1s	530.85	2.20	2.1
N 1s	397.85	2.04	0.47
C 1s	283.40	92.97	95.29
S 2p	163.00	4.00	1.42
Si 2p	100.70	0.83	0.71

Table A-8 XPS analysis of adsorbed Ca^{2+} , Mg^{2+} and Fe^{3+} on bitumen film.

Peak	Position BE, (eV)	FWHM (eV)	Atomic conc.(%)	Peak	Position BE, (eV)	FWHM (eV)	Atomic conc.(%)
Ca^{2+} : 10^{-3} mol/L, unrinsed				pH = 6.0			
Ca 2p				Ca 2p			
O 1s	530.85	2.88	1.67	O 1s	530.50	2.91	2.00
N 1s	398.55	0.99	0.26	N 1s			
C 1s	283.05	2.44	96.26	C 1s	283.05	2.39	96.09
S 2p	162.65	3.35	1.54	S 2p	162.65	3.30	1.38
Si 2p	100.70	2.43	0.27	Si 2p	100.35	2.29	0.53
Mg^{2+} : 10^{-3} mol/L, unrinsed				pH = 6.0			
Mg 2p				Mg 2p			
O 1s	530.85	2.73	2.49	O 1s	529.80	2.93	7.55
N 1s	397.85	2.93	0.56	N 1s			
C 1s	283.05	2.40	94.80	C 1s	283.40	2.42	89.16
S 2p	162.65	3.26	1.40	S 2p	163.00	3.41	1.28
Si 2p	101.50	3.02	0.75	Mg 2p	47.85	2.60	2.01
Fe^{3+} : 10^{-3} mol/L, unrinsed				pH = 2.5			
Fe 2p				Fe 2p			
O 1s	530.15	3.18	2.20	O 1s	530.50	2.89	2.79
N 1s				N 1s			
C 1s	283.40	2.54	92.97	C 1s	283.05	2.40	95.12
S 2p	162.65	3.65	4.00	S 2p	162.65	3.10	1.49
Si 2p	100.70	2.04	0.83	Si 2p	101.05	2.42	0.60

APPENDIX III ADSORPTION THERMODYNAMICS

Based on James and Healy (1972c), overall free energy change of adsorption $\Delta G_{ads, i}$, consists of three terms, attractive coulombic term, repulsive secondary solvation energy term ΔG_{solv} , and an adjustable or “chemical” free energy term $\Delta G_{chem, i}$ (is not included in this proposal) with assumption that the metal cations are adsorbed near inner Helmholtz plane with rearrangement of hydration sheath of the adsorbed ions.

$$\Delta G_{ads, i} = \Delta G_{coul, i} + \Delta G_{solv, i} \quad (A-5)$$

The repulsive solvation term, as developed by James and Healy, is calculated by,

$$\Delta G_{solv, i} = \frac{z_i^2 e^2 N}{16\pi\epsilon_0} \left(\frac{1}{x_i} - \frac{r_i}{2x_i} \right) \left(\frac{1}{\epsilon_{int}} - \frac{1}{\epsilon_{bulk}} \right) + \frac{z_i^2 e^2 N}{32\pi\epsilon_0 x_i} \left(\frac{1}{\epsilon_{solid}} - \frac{1}{\epsilon_{int}} \right) \quad (A-6)$$

ΔG_{solv} represents the change in energy required to remove the hydration sheath of hydrated ions for adsorption of occur, and has a unit of joule/mol.

In the expression of (A-6), r_i is the radius of ion i , ϵ_{int} is the dielectric constant of the surface water and is a function of the electric field strength ($d\psi/dx$).

$$\epsilon_{int} = \left(\frac{\epsilon_{bulk} - 6}{1 + 1.2 \times 10^{-17} (d\psi/dx_i)^2} \right) + 6 \quad (A-7)$$

The $d\psi/dx$ can be approximated from the Gouy-Chapman model of the double layer by the formula of (A-8):

$$\frac{d\psi}{dx_i} = -2\kappa \frac{RT}{zF} \sinh \left(\frac{zF\Delta\psi_{x_i}}{2RT} \right) \quad (V/m) \quad (A-8)$$

$$\Delta\psi_{x_i} = \frac{2RT}{z_i F} \ln \left(\frac{(e^{z_i F \psi_0 / 2RT} + 1) + (e^{z_i F \psi_0 / 2RT} - 1)e^{-\kappa x_i}}{(e^{z_i F \psi_0 / 2RT} + 1) - (e^{z_i F \psi_0 / 2RT} - 1)e^{-\kappa x_i}} \right) \quad (\text{V}) \quad (\text{A-9})$$

ψ_0 is the surface charge of the sorbent and a function of pH:

$$\psi_0 = 2.3RT / zF(pH_{PZC} - pH) \quad (\text{V}) \quad (\text{A-10})$$

$$\kappa = 0.328 \times 10^{10} I^{1/2} \quad (\text{m}^{-1}) \quad (\text{A-11})$$

$$x_i = r_i + 2r_w \quad (\text{m}) \quad (\text{A-12})$$

The attractive coulombic term is given by $\Delta G_{coul,i} = z_i F \Delta\psi_{x_i}$, where z_i is the sign and valence of the adsorbing ion i , F is Faraday constant, and $\Delta\psi_{x_i}$ is given by (A-9).

Table A-9 Selected parameters used in the calculation of free energy change of adsorption of metal species

	Dielectric constant	pH _{pzc}	Reference
water	78.5 ^a		a. (Dean, 1999)
quartz	4.4 ^b	2.0 ^d	b. (Robinson, 2004)
kaolinite	5.1 ^b	3.4 ^d	c. (Sowa et al., 1995)
illite	5.8 ^b	2.8 ^e	d.(Fuerstenau and Raghavan, 1976)
bitumen	2.25 ^c	3.5 ^f	e. (Hu et al., 2003)
Radius of water molecule $r_w = 1.4 \text{ \AA}$ ^a			f. measured in this study

Table A-10 The change in free energy of adsorption of metal ionic species on minerals and bitumen at different pH at 25°C, kJ/mol

	On Quartz				On Kaolinite			
	ΔG_{solv}	pH = 4.0	pH = 8.0	pH = 10.	ΔG_{solv}	pH = 4.0	pH = 8.0	pH = 10.
CaOH ⁺	7.27	0.51	-4.22	-4.30	6.21	3.93	-4.79	-5.31
FeOH ⁺	7.96	1.06	-3.98	-4.08	6.81	4.51	-4.61	-5.18
MnOH ⁺	8.25	1.29	-3.87	-3.97	7.05	4.74	-4.53	-5.11
MgOH ⁺	8.45	1.46	-3.79	-3.89	7.22	4.91	-4.46	-5.06
PbOH ⁺	8.43	1.44	-3.80	-3.90	7.21	4.90	-4.47	-5.07
Al(OH) ₂ ⁺	7.20	1.12	-2.46	-2.51	6.15	3.95	-3.18	-3.52
Fe(OH) ₂ ⁺	7.15	1.09	-2.47	-2.52	6.11	3.91	-3.18	-3.53
FeOH ²⁺	31.72	25.44	21.56	21.50	27.10	24.88	17.32	16.93
AlOH ²⁺	33.73	27.33	23.26	23.19	28.82	26.58	18.74	18.33
Pb ²⁺	30.99	24.13	19.18	19.09	26.48	24.19	15.19	14.64
Ca ²⁺	31.32	24.44	19.46	19.36	26.76	24.47	15.42	14.87
Mg ²⁺	32.98	26.02	20.86	20.76	28.18	25.88	16.61	16.02
Mn ²⁺	35.83	28.75	23.30	23.19	30.62	28.30	18.68	18.05
Fe ²⁺	36.81	29.69	24.14	24.03	31.45	29.13	19.40	18.74
Al ³⁺	79.67	73.18	68.95	68.88	68.08	65.83	57.78	57.34
Fe ³⁺	83.02	76.46	72.10	72.02	70.95	68.69	60.45	59.99
	On Illite				On Bitumen			
	ΔG_{solv}	pH = 4.0	pH = 8.0	pH = 10.	ΔG_{solv}	pH = 4.0	pH = 8.0	pH = 10.
CaOH ⁺	5.41	1.07	-5.93	-6.15	14.62	12.12	3.56	3.09
FeOH ⁺	5.93	1.52	-5.86	-6.10	16.02	13.50	4.54	4.03
MnOH ⁺	6.14	1.70	-5.82	-6.06	16.59	14.06	4.95	4.42
MgOH ⁺	6.29	1.84	-5.78	-6.04	17.00	14.47	5.25	4.71
PbOH ⁺	6.28	1.83	-5.79	-6.04	16.97	14.43	5.23	4.69
Al(OH) ₂ ⁺	5.35	1.34	-4.20	-4.34	14.48	12.08	5.11	4.80
Fe(OH) ₂ ⁺	5.32	1.31	-4.20	-4.34	14.39	12.00	5.06	4.75
FeOH ²⁺	23.61	19.49	13.56	13.40	63.82	61.39	53.99	53.64
AlOH ²⁺	25.10	20.93	14.75	14.58	67.87	65.42	57.74	57.36
Pb ²⁺	23.07	18.68	11.41	11.18	62.36	59.85	51.01	50.51
Ca ²⁺	23.31	18.91	11.60	11.37	63.02	60.50	51.61	51.11
Mg ²⁺	24.55	20.11	12.59	12.34	66.36	63.83	54.72	54.20
Mn ²⁺	26.67	22.18	14.32	14.05	72.11	69.56	60.10	59.52
Fe ²⁺	27.39	22.89	14.91	14.64	74.07	71.51	61.94	61.35
Al ³⁺	59.30	55.08	48.70	48.52	160.31	157.85	149.96	149.56
Fe ³⁺	61.79	57.54	50.99	50.80	167.06	164.59	156.51	156.10

APPENDIX IV SPECIATION DIAGRAMS

Equilibrium speciation calculation is based on the mass balance of ionic species involved in the system. This concentration distribution of an ionic species is governed by the equilibrium constants of all reactions in the system of interest. We use Ca^{2+} hydrolysis reactions to illustrate the method used for all speciation calculations in this study.

Ca^{2+} ions are hydrolyzed in aqueous solution with the reactions:

1. $\text{Ca}^{2+} + \text{OH}^- \rightleftharpoons \text{CaOH}^+ \quad [\text{CaOH}^+] = \beta_1[\text{Ca}^{2+}][\text{OH}^-]$
2. $\text{Ca}^{2+} + 2\text{OH}^- \rightleftharpoons \text{Ca}(\text{OH})_2(\text{aq}) \quad [\text{Ca}(\text{OH})_2(\text{aq})] = \beta_2[\text{Ca}^{2+}][\text{OH}^-]^2$
3. $\text{Ca}^{2+} + 2\text{OH}^- \rightleftharpoons \text{Ca}(\text{OH})_2(\text{s}) \quad K_{s0} = [\text{Ca}^{2+}][\text{OH}^-]^2$

In the unsaturated or supersaturated solutions, the mass balance of Ca can be expressed as follows:

$$[\text{Ca}]_{\text{total}} = [\text{Ca}^{2+}] + [\text{CaOH}^+] + [\text{Ca}(\text{OH})_2(\text{aq})] \quad (\text{A-13})$$

The fraction factor of Ca^{2+} , CaOH^+ and $\text{Ca}(\text{OH})_2(\text{aq})$ was denoted as partition of α_0 , α_1 , α_2 respectively and calculated by the following equations.

$$\alpha_0 = \frac{[\text{Ca}^{2+}]}{[\text{Ca}^{2+}] + [\text{CaOH}^+] + [\text{Ca}(\text{OH})_2(\text{aq})]} \quad (\text{A-14})$$

denominator

$$\text{Den} = [\text{Ca}^{2+}] + [\text{CaOH}^+] + [\text{Ca}(\text{OH})_2(\text{aq})] = [\text{Ca}^{2+}](1 + \beta_1[\text{OH}^-] + \beta_2[\text{OH}^-]^2) \quad (\text{A-15})$$

$$\alpha_0 = \frac{1}{1 + \beta_1[\text{OH}^-] + \beta_2[\text{OH}^-]^2} \quad (\text{A-16})$$

$$\alpha_1 = \frac{\beta_1[OH^-]}{1 + \beta_1[OH^-] + \beta_2[OH^-]^2} \quad (A-17)$$

$$\alpha_2 = \frac{\beta_2[OH^-]^2}{1 + \beta_1[OH^-] + \beta_2[OH^-]^2} \quad (A-18)$$

At higher pH, the solution becomes saturated with calcium hydroxide and the solubility products are obeyed at equilibrium. $[Ca^{2+}]$ becomes a simple function of pH,

$$[Ca^{2+}]_{sat} = \frac{K_{s0}}{[OH^-]^2}, \text{ from this, the other concentrations can be calculated directly.}$$

β_1 , β_2 and solubility product K_0 can be seen from Table A-11. The concentration of various species of Ca^{2+} as a function of pH in an aqueous solution containing 10^{-3} M Ca^{2+} initially was calculated. Similarly, speciation of Mg^{2+} and Fe^{3+} was performed and presented in Table A-13.

Speciation of Ca^{2+} , Mg^{2+} and Fe^{3+} and complexing agents(oxalic acid, citric acid and EDTA) as a function of pH in an aqueous solution containing 10^{-3} mol/L of metal ions and 10^{-3} M of H_mL was constructed using formation constants summarized in Table A-11 and Table A-12, in terms of the mass balances of metal ions and organic ligand L.

The results are present in Tables A-14 to A-22.

Table A-11 Selected formation constants of metal hydroxyl products and organic acids at 25°C (I = 0.001M).

Reactions	Log K ₁	Reference
Hydrolysis of Ca ²⁺ , Mg ²⁺ , Fe ³⁺		
Ca ²⁺ + OH ⁻ = CaOH ⁺	1.51	Westin and Rasmuson, 2005
Ca ²⁺ + 2OH ⁻ = Ca(OH) ₂ (aq.)	-3.75	Westin and Rasmuson, 2005
Ca ²⁺ + 2OH ⁻ = Ca(OH) ₂ (s)	5.26	Westin and Rasmuson, 2005; Dean, 1999
Mg ²⁺ + OH ⁻ = MgOH ⁺	2.58	Butler and Cogley, 1998
Mg ²⁺ + 2OH ⁻ = Mg(OH) ₂ (aq.)	8.26	Butler and Cogley, 1998
Mg ²⁺ + 2OH ⁻ = Mg(OH) ₂ (s)	11.25	Butler and Cogley, 1998
Fe ³⁺ + OH ⁻ = FeOH ²⁺	11.21	Butler and Cogley, 1998, Dean, 1999
Fe ³⁺ + 2OH ⁻ = Fe(OH) ₂ ⁺	22.1	Butler and Cogley, 1998, Dean, 1999
Fe ³⁺ + 3OH ⁻ = Fe(OH) ₃ (aq.)	28.8	Butler and Cogley, 1998, Dean, 1999
Fe ³⁺ + 3OH ⁻ = Fe(OH) ₃ (s)	38.55	Butler and Cogley, 1998; Dean, 1999
Protonation of oxalic acid, citric acid and EDTA		
H ⁺ + oxal ²⁻ = Hoxal ⁻	1.25	Westin and Rasmuson, 2005
2H ⁺ + oxal ²⁻ = H ₂ oxal	3.81	Westin and Rasmuson, 2005
H ⁺ + cit ³⁻ = Hcit ²⁻ (cit= C ₆ H ₅ O ₇)	6.33	Westin and Rasmuson, 2005
2H ⁺ + cit ³⁻ = H ₂ cit ⁻	11.05	Westin and Rasmuson, 2005
3H ⁺ + cit ³⁻ = H ₃ cit	14.18	Westin and Rasmuson, 2005
H ⁺ + edta ⁴⁻ = Hedta ³⁻	10.19	Westin and Rasmuson, 2005
2H ⁺ + edta ⁴⁻ = H ₂ edta ²⁻	16.32	Westin and Rasmuson, 2005
3H ⁺ + edta ⁴⁻ = H ₃ edta ⁻	19.01	Westin and Rasmuson, 2005
4H ⁺ + edta ⁴⁻ = H ₄ edta	21.01	Westin and Rasmuson, 2005

Table A-12 Selected formation constants of metal-complexes at 25°C (I = 0.001M).

Reactions	Log K ₁	Reference
Metal-oxalic acid complexes		
$\text{Ca}^{2+} + \text{oxal}^{2-} = \text{Ca-oxal (aq)}$	3.00	Furia, 1972
$\text{Mg}^{2+} + \text{oxal}^{2-} = \text{Mg-oxal (aq)}$	2.55	Furia, 1972
$\text{Fe}^{3+} + \text{oxal}^{2-} = \text{Fe-oxal}^+$	9.4	Furia, 1972
$\text{Ca}^{2+} + \text{oxal}^{2-} + \text{H}_2\text{O} = \text{Ca-oxal}\cdot\text{H}_2\text{O (s)}$	8.63	Dean, 1999
$\text{Mg}^{2+} + \text{oxal}^{2-} + 2\text{H}_2\text{O} = \text{Mg-oxal}\cdot 2\text{H}_2\text{O (s)}$	5.32	Dean, 1999
Metal-citric acid complexes		
$\text{Ca}^{2+} + \text{cit}^{3-} = \text{Ca-cit}^-$	4.73	Westin and Rasmuson, 2005
$\text{Ca}^{2+} + \text{cit}^{3-} + \text{H}^+ = \text{Ca-Hcit (aq.)}$	4.68	Dean, 1999
$\text{Mg}^{2+} + \text{cit}^{3-} + \text{H}^+ = \text{Mg-Hcit (aq.)}$	3.29	Westin and Rasmuson, 2005
$\text{Mg}^{2+} + \text{cit}^{3-} = \text{Mg-cit}^- \text{ (aq.)}$	2.80	Furia, 1972
$\text{Fe}^{3+} + \text{cit}^{3-} + \text{H}^+ = \text{Fe-Hcit}^+$	12.50	Westin and Rasmuson, 2005
$\text{Fe}^{3+} + \text{cit}^{3-} = \text{Fe-cit (aq.)}$	25.00	Westin and Rasmuson, 2005
Metal-EDTA complexes		
$\text{Ca}^{2+} + \text{edta}^{4-} + \text{H}^+ = \text{Ca-Hedta}^-$	14.07	Butler and Cogley, 1998
$\text{Ca}^{2+} + \text{edta}^{4-} = \text{Ca-edta}^{2-}$	11.00	Dean, 1999
$\text{Mg}^{2+} + \text{edta}^{4-} + \text{H}^+ = \text{Mg-edta}^-$	13.13	Butler and Cogley, 1998
$\text{Mg}^{2+} + \text{edta}^{4-} = \text{Mg-edta}^{2-}$	8.64	Dean, 1999
$\text{Fe}^{3+} + \text{edta}^{4-} + \text{H}^+ = \text{Fe-Hedta(aq)}$	26.4	Butler and Cogley, 1998
$\text{Fe}^{3+} + \text{edta}^{4-} = \text{Fe-edta}^-$	24.23	Butler and Cogley, 1998

Table A-13 Speciation of 10^{-3} mol/L of Ca^{2+} , Mg^{2+} and Fe^{3+} (see Figure 7-10).

Ca^{2+}					
pH	$\text{Ca(OH)}_2(\text{s})$	Ca^{2+}	CaOH^+	$\text{Ca(OH)}_2(\text{aq})$	
7.00		1.00E-03	3.24E-09	1.78E-17	
8.00		1.00E-03	3.24E-08	1.78E-15	
9.00		1.00E-03	3.23E-07	1.78E-13	
10.00		9.97E-04	3.23E-06	1.77E-11	
11.00		9.69E-04	3.13E-05	1.72E-09	
12.00		7.56E-04	2.44E-04	1.34E-07	
13.31	9.46E-10	1.31E-04	8.69E-04	9.77E-06	
13.60	5.19E-04	3.47E-05	4.47E-04	9.77E-06	
14.00	8.17E-04	5.50E-06	1.78E-04	9.77E-06	
Mg^{2+}					
pH	$\text{Mg(OH)}_2(\text{s})$	Mg^{2+}	MgOH^+	$\text{Mg(OH)}_2(\text{aq})$	
7.00		1.00E-03	3.80E-08	6.92E-12	
8.00		1.00E-03	3.80E-07	6.92E-10	
9.00		9.96E-04	3.79E-06	6.89E-08	
10.00		9.63E-04	3.66E-05	6.66E-06	
10.14	2.59E-09	9.50E-04	5.00E-05	1.26E-05	
12.00	9.99E-04	1.82E-07	6.92E-07	1.26E-05	
13.60	1.00E-03	1.15E-10	1.74E-08	1.26E-05	
14.00	1.00E-03	1.82E-11	6.92E-09	1.26E-05	
15.00	1.00E-03	1.82E-13	6.92E-10	1.26E-05	
Fe^{3+}					
pH	$\text{Fe(OH)}_3(\text{s})$	Fe^{3+}	FeOH^{2+}	Fe(OH)_2^+	$\text{Fe(OH)}_3(\text{aq})$
0.00		9.98E-04	1.62E-06	1.26E-09	6.30E-17
1.00		9.84E-04	1.60E-05	1.24E-07	6.21E-14
2.00		8.43E-04	1.37E-04	1.06E-05	5.32E-11
2.17	3.75E-09	7.86E-04	1.88E-04	2.15E-05	1.58E-10
4.00	1.00E-03	2.51E-09	4.07E-08	3.16E-07	4.25E-07
5.00	1.00E-03	2.51E-12	4.07E-10	3.16E-08	4.92E-06
6.00	1.00E-03	2.51E-15	4.07E-12	3.16E-09	4.77E-05
7.00	1.00E-03	2.51E-18	4.07E-14	3.16E-10	3.29E-04
8.00	1.00E-03	2.51E-21	4.07E-16	3.16E-11	6.26E-04

Table A-14 Speciation of 10^{-3} mol/L Ca^{2+} in 10^{-3} mol/L oxalic acid at 25°C (see Figure 7-11).

pH	L^{2-}	HL^-	H_2L	$\text{CaL}(\text{aq})$
0.00	9.98E-07	1.55E-07	9.99E-04	8.69E-09
1.00	8.38E-05	1.42E-06	9.14E-04	7.29E-07
1.35	2.70E-04	2.53E-06	7.25E-04	2.34E-06
3.00	2.93E-04	4.41E-07	2.85E-06	6.97E-07
5.00	2.95E-04	4.68E-09	3.02E-10	6.93E-07
7.00	2.95E-04	4.68E-11	3.02E-14	6.93E-07
9.00	2.95E-04	4.68E-13	3.02E-18	6.93E-07
10.00	2.95E-04	4.69E-14	3.03E-20	6.93E-07
11.00	2.95E-04	4.76E-15	3.07E-22	6.94E-07
12.00	2.99E-04	5.42E-16	3.50E-24	7.02E-07
13.00	3.25E-04	1.01E-16	6.53E-26	7.64E-07
12.50	3.07E-04	2.15E-16	4.38E-25	7.20E-07
13.35	3.51E-04	6.54E-17	1.88E-26	8.24E-07
14.00	4.57E-04	3.37E-17	2.17E-27	1.07E-06
14.85	9.98E-04	1.85E-17	1.71E-28	2.34E-06

pH	Ca^{2+}	CaOH^+	$\text{Ca}(\text{OH})_2(\text{aq})$	$\text{CaL}(\text{s})$
0.00	1.00E-03	3.23E-16	1.78E-35	
1.00	9.99E-04	2.96E-15	1.63E-33	
1.35	9.98E-04	5.33E-15	6.60E-33	3.80E-08
3.00	2.97E-04	9.09E-15	5.00E-31	7.03E-04
5.00	2.95E-04	8.52E-13	4.68E-27	7.05E-04
7.00	2.95E-04	8.52E-11	4.68E-23	7.05E-04
9.00	2.95E-04	8.52E-09	4.68E-19	7.05E-04
10.00	2.95E-04	8.50E-08	4.67E-17	7.04E-04
11.00	2.94E-04	8.39E-07	4.61E-15	7.04E-04
12.00	2.91E-04	7.45E-06	4.10E-13	7.00E-04
12.50	2.87E-04	1.93E-05	3.36E-12	6.93E-04
13.00	2.82E-04	4.35E-05	2.39E-11	6.74E-04
13.35	2.78E-04	7.25E-05	8.95E-11	6.48E-04
14.00	2.74E-04	1.84E-04	1.01E-09	5.41E-04
14.85	2.70E-04	7.28E-04	2.80E-08	3.35E-08

Table A-15 Speciation of 10^{-3} mol/L Mg^{2+} in 10^{-3} mol/L oxalic acid at 25°C (see Figure 7-12).

pH	L^{2-}	HL^{-}	H_2L	$MgL(aq)$
0.00	8.71E-09	1.55E-07	1.00E-03	3.09E-09
2.00	7.69E-05	1.37E-05	8.83E-04	2.66E-05
4.00	7.81E-04	1.39E-06	8.96E-07	2.17E-04
5.00	7.83E-04	1.39E-07	8.98E-09	2.17E-04
6.00	7.83E-04	1.39E-08	8.99E-11	2.17E-04
7.00	7.83E-04	1.39E-09	8.99E-13	2.17E-04
8.00	7.83E-04	1.39E-10	8.99E-15	2.17E-04
9.00	7.83E-04	1.39E-11	8.99E-17	2.17E-04
9.93	7.87E-04	1.63E-12	1.22E-18	2.13E-04
10.00	8.43E-04	1.40E-12	9.05E-19	1.57E-04
11.00	9.98E-04	1.47E-13	9.47E-21	1.65E-06
12.00	1.00E-03	1.66E-14	1.07E-22	1.87E-08
13.00	1.00E-03	1.76E-15	1.14E-24	1.98E-10
13.75	1.00E-03	3.16E-16	3.63E-26	6.30E-12
14.00	1.00E-03	1.78E-16	1.15E-26	1.99E-12

pH	Mg^{2+}	$MgOH^{+}$	$Mg(OH)_2(aq)$	$Mg(OH)_2(s)$
0.00	1.00E-03	3.80E-15	5.50E-40	
2.00	9.73E-04	3.70E-13	5.35E-36	
4.00	7.83E-04	2.98E-11	4.30E-32	
5.00	7.83E-04	2.98E-10	4.30E-30	
6.00	7.83E-04	2.98E-09	4.30E-28	
7.00	7.83E-04	2.98E-08	4.30E-26	
8.00	7.82E-04	2.97E-07	4.30E-24	
9.00	7.80E-04	2.97E-06	4.29E-22	
9.93	7.62E-04	2.49E-05	3.09E-20	1.58E-08
10.00	5.62E-04	2.14E-05	3.09E-20	2.59E-04
11.00	5.62E-06	2.14E-06	3.09E-20	9.91E-04
12.00	5.62E-08	2.14E-07	3.09E-20	1.00E-03
13.00	5.62E-10	2.14E-08	3.09E-20	1.00E-03
13.75	1.78E-11	3.80E-09	3.09E-20	1.00E-03
14.00	5.62E-12	2.14E-09	3.09E-20	1.00E-03

Table A-16 Speciation of 10^{-3} mol/L Fe^{3+} in 10^{-3} mol/L oxalic acid at 25°C (see Figure 7-13).

pH	L^{2-}	HL^-	H_2L	FeL^+	
0.00	7.65E-09	1.36E-07	4.94E-05	9.50E-04	
2.00	5.00E-07	8.88E-08	3.23E-07	9.99E-04	
3.40	2.24E-06	1.56E-08	2.27E-09	9.98E-04	
5.00	1.00E-03	1.22E-08	4.44E-11	4.87E-07	
6.00	1.00E-03	9.05E-09	3.28E-12	3.60E-09	
7.00	1.00E-03	1.76E-09	6.37E-14	6.99E-12	
8.00	1.00E-03	1.78E-10	6.46E-16	7.08E-15	
9.00	1.00E-03	1.78E-11	6.46E-18	7.08E-18	
10.03	1.00E-03	1.66E-12	5.64E-20	5.78E-21	
11.00	1.00E-03	1.78E-13	6.45E-22	7.08E-24	
12.00	1.00E-03	0.00E+00	0.00E+00	0.00E+00	
13.00	1.00E-03	2.82E-48	1.02E-59	0.00E+00	
13.50	1.00E-03	2.82E-52	1.02E-64	0.00E+00	
14.00	1.00E-03	2.82E-53	1.02E-66	0.00E+00	

pH	Fe^{3+}	FeOH^{2+}	$\text{Fe}(\text{OH})_2^+$	$\text{Fe}(\text{OH})_3(\text{aq})$	$\text{Fe}(\text{OH})_3(\text{s})$
0.00	4.95E-05	6.52E-08	6.23E-11	3.12E-18	
2.00	7.96E-07	1.05E-07	1.00E-08	5.02E-14	
3.40	1.82E-07	5.98E-07	1.42E-06	1.78E-10	5.81E-08
5.00	2.82E-12	3.72E-10	3.55E-08	1.78E-10	9.99E-04
6.00	2.82E-15	3.72E-12	3.55E-09	1.78E-10	1.00E-03
7.00	2.82E-18	3.72E-14	3.55E-10	1.78E-10	1.00E-03
8.00	2.82E-21	3.72E-16	3.55E-11	1.78E-10	1.00E-03
9.00	2.82E-24	3.72E-18	3.55E-12	1.78E-10	1.00E-03
10.03	2.30E-27	3.24E-20	3.32E-13	1.78E-10	1.00E-03
11.00	2.82E-30	3.72E-22	3.55E-14	1.78E-10	1.00E-03
12.00	2.82E-33	3.72E-24	3.55E-15	1.78E-10	1.00E-03
13.00	2.82E-36	3.72E-26	3.55E-16	1.78E-10	1.00E-03
13.50	8.91E-38	3.72E-27	1.12E-16	1.78E-10	1.00E-03
14.00	2.82E-39	3.72E-28	3.55E-17	1.78E-10	1.00E-03

Table A-17 Speciation of 10^{-3} mol/L Ca^{2+} in 10^{-3} mol/L citric acid at 25°C (see Figure 7-14).

pH	L^{3-}	HL^{2-}	H_2L^-	H_3L	CaH_2L^+
0.00	6.60E-18	1.41E-11	7.41E-07	9.99E-04	1.44E-08
2.00	6.15E-12	1.31E-07	6.90E-05	9.31E-04	1.35E-06
3.00	3.76E-09	8.04E-06	4.22E-04	5.70E-04	8.23E-06
4.00	6.49E-07	1.39E-04	7.29E-04	9.83E-05	1.37E-05
5.00	1.60E-05	3.41E-04	1.79E-04	2.42E-06	1.88E-06
6.00	6.69E-05	1.43E-04	7.51E-06	1.01E-08	3.19E-08
7.00	1.15E-04	2.46E-05	1.29E-07	1.74E-11	3.51E-10
8.00	1.26E-04	2.69E-06	1.41E-09	1.91E-14	3.55E-12
9.00	1.27E-04	2.72E-07	1.43E-11	1.93E-17	3.55E-14
10.00	1.28E-04	2.73E-08	1.43E-13	1.93E-20	3.55E-16
11.00	1.29E-04	2.77E-09	1.45E-15	1.96E-23	3.55E-18
12.00	1.45E-04	3.10E-10	1.63E-17	2.20E-26	3.48E-20
13.00	2.44E-04	5.22E-11	2.74E-19	3.70E-29	3.08E-22
13.66	4.15E-04	1.94E-11	2.22E-20	6.56E-31	1.14E-23
14.00	8.42E-04	1.80E-11	9.44E-21	1.27E-31	1.01E-24

pH	Ca^{2+}	CaOH^+	$\text{Ca(OH)}_2(\text{aq})$	$\text{Ca(OH)}_2(\text{s})$	CaL^-	CaHL
0.00	1.00E-03	3.24E-16	1.78E-35		3.55E-16	3.16E-16
2.00	1.00E-03	3.24E-14	1.78E-31		3.30E-10	2.94E-12
3.00	1.00E-03	3.24E-13	1.78E-29		2.02E-07	1.80E-10
4.00	9.66E-04	3.13E-12	1.72E-27		3.37E-05	3.00E-09
5.00	5.39E-04	1.74E-11	9.58E-26		4.61E-04	4.11E-09
6.00	2.18E-04	7.04E-11	3.87E-24		7.82E-04	6.97E-10
7.00	1.40E-04	4.51E-10	2.48E-22		8.60E-04	7.67E-11
8.00	1.29E-04	4.17E-09	2.29E-20		8.71E-04	7.77E-12
9.00	1.28E-04	4.13E-08	2.27E-18		8.72E-04	7.78E-13
10.00	1.27E-04	4.12E-07	2.26E-16		8.72E-04	7.77E-14
11.00	1.25E-04	4.06E-06	2.23E-14		8.71E-04	7.76E-15
12.00	1.10E-04	3.55E-05	1.95E-12		8.55E-04	7.62E-16
13.00	5.76E-05	1.87E-04	1.03E-10		7.56E-04	6.74E-17
13.66	2.63E-05	3.89E-04	9.77E-10	9.45E-09	5.85E-04	1.14E-17
14.00	5.50E-06	1.78E-04	9.77E-10	6.58E-04	1.58E-04	2.21E-18

Table A-18 Speciation of 10^{-3} mol/L Mg^{2+} in 10^{-3} mol/L citric acid at 25°C (see Figure 7-15).

pH	L^{3-}	HL^{2-}	H_2L^-	H_3L
0.00	6.61E-18	1.41E-11	7.42E-07	1.00E-03
2.00	6.15E-12	1.31E-07	6.90E-05	9.31E-04
3.00	3.76E-09	8.05E-06	4.22E-04	5.70E-04
4.00	6.71E-07	1.43E-04	7.53E-04	1.02E-04
5.00	2.81E-05	6.01E-04	3.15E-04	4.25E-06
6.00	2.16E-04	4.63E-04	2.43E-05	3.27E-08
7.00	4.42E-04	9.45E-05	4.96E-07	6.69E-11
8.00	4.97E-04	1.06E-05	5.58E-09	7.53E-14
9.00	5.04E-04	1.08E-06	5.66E-11	7.63E-17
10.03	5.11E-04	1.02E-07	5.00E-13	6.31E-20
11.00	9.94E-04	1.19E-08	6.27E-15	8.46E-23
12.00	1.00E-03	1.63E-09	8.57E-17	2.41E-29
13.00	1.00E-03	5.58E-17	2.93E-26	3.95E-37
13.50	1.00E-03	5.62E-19	2.95E-29	3.98E-41
14.00	1.00E-03	5.62E-18	2.95E-29	3.98E-42

pH	Mg^{2+}	$MgOH^+$	$Mg(OH)_2(aq)$	$Mg(OH)_2(s)$	MgL^-
0.00	1.00E-03	3.80E-15	5.50E-40		1.29E-17
2.00	1.00E-03	3.80E-13	5.50E-36		1.20E-11
3.00	1.00E-03	3.80E-12	5.50E-34		7.34E-09
4.00	9.99E-04	3.80E-11	5.49E-32		1.31E-06
5.00	9.48E-04	3.60E-10	5.21E-30		5.19E-05
6.00	7.03E-04	2.67E-09	3.86E-28		2.97E-04
7.00	5.37E-04	2.04E-08	2.95E-26		4.63E-04
8.00	5.08E-04	1.93E-07	2.79E-24		4.92E-04
9.00	5.03E-04	1.91E-06	2.77E-22		4.95E-04
10.03	4.91E-04	2.00E-05	3.09E-20	4.31E-08	4.89E-04
11.00	5.62E-06	2.14E-06	3.09E-20	9.86E-04	6.13E-06
12.00	5.62E-08	2.14E-07	3.09E-20	1.00E-03	8.37E-08
13.00	5.62E-10	2.14E-08	3.09E-20	1.00E-03	1.05E-09
13.50	5.62E-11	6.76E-09	3.09E-20	1.00E-03	1.08E-10
14.00	5.62E-12	2.14E-09	3.09E-20	1.00E-03	1.09E-11

Table A-19 Speciation of 10^{-3} mol/L Fe^{3+} in 10^{-3} mol/L citric acid at 25°C (see Figure 7-16).

pH	L^{3-}	HL^{2-}	H_2L^-	H_3L	FeHL^+
0.00	8.13E-22	1.74E-15	9.12E-11	1.23E-07	3.16E-16
2.00	8.39E-19	1.79E-14	9.41E-12	1.27E-10	3.16E-18
3.00	3.67E-17	7.84E-14	4.12E-12	5.55E-12	3.16E-19
4.00	3.07E-15	6.56E-13	3.44E-12	4.64E-13	3.16E-20
5.00	1.95E-13	4.16E-12	2.18E-12	2.95E-14	3.16E-21
6.00	6.38E-12	1.36E-11	7.16E-13	9.66E-16	3.16E-22
7.00	1.25E-10	2.67E-11	1.40E-13	1.89E-17	3.16E-23
7.32	1.91E-08	3.26E-11	8.25E-14	5.37E-18	1.53E-23
8.00	9.23E-04	5.82E-11	3.05E-14	4.12E-19	2.43E-25
9.00	9.98E-04	1.71E-10	8.99E-15	1.21E-20	7.14E-28
10.00	1.00E-03	5.37E-10	2.82E-15	3.80E-22	2.24E-30
11.00	1.00E-03	1.63E-09	8.57E-16	1.16E-23	6.80E-33
12.00	1.00E-03	1.88E-09	9.85E-17	1.33E-25	7.82E-36
13.00	1.00E-03	2.14E-10	1.12E-18	1.51E-28	8.91E-40
14.00	1.00E-03	2.14E-11	1.12E-20	1.51E-31	8.91E-44

pH	Fe^{3+}	FeOH^{2+}	$\text{Fe}(\text{OH})_2^+$	$\text{Fe}(\text{OH})_3(\text{aq})$	$\text{Fe}(\text{OH})_3(\text{s})$	FeL
0.00	1.23E-07	1.62E-10	1.55E-13	7.76E-21		1.00E-03
2.00	1.19E-10	1.57E-11	1.50E-12	7.52E-18		1.00E-03
3.00	2.73E-12	3.59E-12	3.43E-12	1.72E-16		1.00E-03
4.00	3.26E-14	4.30E-13	4.10E-12	2.06E-15		1.00E-03
5.00	5.14E-16	6.77E-14	6.47E-12	3.24E-14		1.00E-03
6.00	1.57E-17	2.07E-14	1.97E-11	9.89E-13		1.00E-03
7.00	8.02E-19	1.06E-14	1.01E-10	5.06E-11		1.00E-03
7.32	3.16E-19	8.64E-15	1.71E-10	1.78E-10	1.88E-08	1.00E-03
8.00	2.82E-21	4.84E-15	4.62E-10	1.78E-10	9.23E-04	7.67E-05
9.00	2.82E-24	3.72E-18	3.55E-12	1.78E-10	9.98E-04	2.26E-06
10.00	2.82E-27	3.72E-20	3.55E-13	1.78E-10	1.00E-03	7.08E-08
11.00	2.82E-30	3.72E-22	3.55E-14	1.78E-10	1.00E-03	2.15E-09
12.00	2.82E-33	3.72E-24	3.55E-15	1.78E-10	1.00E-03	2.47E-11
13.00	2.82E-36	3.72E-26	3.55E-16	1.78E-10	1.00E-03	2.82E-14
14.00	2.82E-39	3.72E-28	3.55E-17	1.78E-10	1.00E-03	2.82E-17

Table A-20 Speciation of 10^{-3} mol/L Ca^{2+} in 10^{-3} mol/L EDTA at 25°C (see Figure 7-17).

pH	L^{4-}	HL^{3-}	H_2L^{2-}	H_3L^-	H_4L
0.00	9.68E-25	1.50E-14	2.02E-08	9.90E-06	9.90E-04
2.00	4.43E-17	6.87E-09	9.26E-05	4.54E-04	4.54E-04
3.00	3.09E-14	4.79E-07	6.46E-04	3.17E-04	3.17E-05
4.00	3.74E-12	5.79E-06	7.81E-04	3.83E-05	3.83E-07
5.00	8.81E-11	1.36E-05	1.84E-04	9.01E-07	9.01E-10
6.00	7.72E-10	1.20E-05	1.61E-05	7.90E-09	7.90E-13
7.00	3.56E-09	5.51E-06	7.43E-07	3.64E-11	3.64E-16
8.00	1.19E-08	1.84E-06	2.48E-08	1.22E-13	1.22E-19
9.00	3.68E-08	5.70E-07	7.69E-10	3.77E-16	3.77E-23
10.00	9.39E-08	1.45E-07	1.96E-11	9.60E-19	9.60E-27
11.00	1.41E-07	2.19E-08	2.96E-13	1.45E-21	1.45E-30
12.00	1.71E-07	2.65E-09	3.57E-15	1.34E-27	1.75E-34
13.00	3.08E-07	4.01E-15	5.41E-23	2.65E-34	3.15E-38
13.50	5.01E-07	1.28E-16	1.73E-25	8.48E-38	5.13E-40
14.00	8.64E-07	3.95E-15	5.33E-25	2.61E-38	8.84E-42

pH	Ca^{2+}	CaOH^+	$\text{Ca(OH)}_2(\text{aq})$	CaL^{2-}	CaHL^-	CaH_2L
0.00	1.00E-03	3.24E-16	1.78E-35	4.32E-17	1.14E-13	9.68E-17
2.00	1.00E-03	3.24E-14	1.78E-31	1.98E-09	5.21E-08	4.43E-13
3.00	9.95E-04	3.22E-13	1.77E-29	1.37E-06	3.62E-06	3.08E-12
4.00	8.26E-04	2.67E-12	1.47E-27	1.38E-04	3.63E-05	3.09E-12
5.00	1.99E-04	6.42E-12	3.53E-26	7.81E-04	2.05E-05	1.75E-13
6.00	2.81E-05	9.09E-12	5.00E-25	9.69E-04	2.55E-06	2.17E-15
7.00	6.25E-06	2.02E-11	1.11E-23	9.93E-04	2.61E-07	2.22E-17
8.00	1.88E-06	6.08E-11	3.34E-22	9.98E-04	2.63E-08	2.23E-19
9.00	6.08E-07	1.97E-10	1.08E-20	9.99E-04	2.63E-09	2.24E-21
10.00	2.38E-07	7.72E-10	4.24E-19	1.00E-03	2.63E-10	2.24E-23
11.00	1.58E-07	5.12E-09	2.81E-17	1.00E-03	2.63E-11	2.24E-25
12.00	1.31E-07	4.24E-08	2.33E-15	1.00E-03	2.63E-12	2.24E-27
13.00	7.27E-08	2.35E-07	1.29E-13	1.00E-03	2.63E-13	2.24E-29
13.50	4.46E-08	4.57E-07	7.94E-13	9.99E-04	8.31E-14	2.24E-30
14.00	2.59E-08	8.38E-07	4.61E-12	9.99E-04	2.63E-14	2.24E-31

Table A-21 Speciation of 10^{-3} mol/L Mg^{2+} in 10^{-3} mol/L EDTA at 25°C (see Figure 7-18).

pH	L^{4-}	HL^{3-}	H_2L^{2-}	H_3L^-	H_4L
0.00	9.68E-25	1.50E-14	2.02E-08	9.90E-06	9.90E-04
2.00	4.43E-17	6.87E-09	9.26E-05	4.54E-04	4.54E-04
3.00	3.11E-14	4.81E-07	6.49E-04	3.18E-04	3.18E-05
4.00	4.49E-12	6.95E-06	9.38E-04	4.59E-05	4.59E-07
5.00	3.44E-10	5.33E-05	7.18E-04	3.52E-06	3.52E-09
6.00	5.52E-09	8.55E-05	1.15E-04	5.65E-08	5.65E-12
7.00	2.76E-08	4.28E-05	5.77E-06	2.83E-10	2.83E-15
8.00	9.39E-08	1.45E-05	1.96E-07	9.61E-13	9.61E-19
9.00	2.92E-07	4.53E-06	6.11E-09	2.99E-15	2.99E-22
10.00	7.58E-07	1.17E-06	1.58E-10	7.75E-18	7.75E-26
11.00	1.30E-06	2.01E-07	2.71E-12	1.33E-20	1.33E-29
11.40	1.67E-06	9.86E-08	5.24E-13	5.46E-25	3.98E-31
13.00	9.97E-04	9.32E-15	1.26E-22	6.16E-34	7.56E-37
13.50	9.99E-04	2.88E-16	3.88E-25	1.90E-37	1.33E-38
14.00	1.00E-03	8.41E-15	1.13E-24	5.56E-38	2.35E-40

pH	Mg^{2+}	MgOH^+	$\text{Mg}(\text{OH})_2(\text{aq})$	MgL^{2-}	MgHL^-	$\text{Mg}(\text{OH})_2(\text{s})$
0.00	1.00E-03	3.80E-15	5.50E-40	6.85E-19	1.31E-14	
2.00	1.00E-03	3.80E-13	5.50E-36	3.14E-11	5.98E-09	
3.00	1.00E-03	3.80E-12	5.49E-34	2.20E-08	4.19E-07	
4.00	9.91E-04	3.77E-11	5.45E-32	3.15E-06	6.00E-06	
5.00	7.75E-04	2.95E-10	4.26E-30	1.89E-04	3.60E-05	
6.00	2.01E-04	7.63E-10	1.10E-28	7.84E-04	1.49E-05	
7.00	4.86E-05	1.85E-09	2.67E-27	9.50E-04	1.81E-06	
8.00	1.48E-05	5.64E-09	8.15E-26	9.85E-04	1.88E-07	
9.00	4.81E-06	1.83E-08	2.64E-24	9.95E-04	1.90E-08	
10.00	1.86E-06	7.07E-08	1.02E-22	9.98E-04	1.90E-09	
11.00	1.09E-06	4.13E-07	5.97E-21	9.99E-04	1.90E-10	
11.40	8.72E-07	8.42E-07	3.09E-20	9.98E-04	7.49E-11	5.18E-08
13.00	5.62E-10	2.14E-08	3.09E-20	2.94E-06	5.61E-15	9.97E-04
13.50	5.62E-11	6.76E-09	3.09E-20	5.17E-07	3.12E-16	9.99E-04
14.00	5.62E-12	2.14E-09	3.09E-20	9.13E-08	1.74E-17	1.00E-03

Table A-22 Speciation of 10^{-3} mol/L Fe^{3+} in 10^{-3} mol/L EDTA at 25°C (see Figure 7-19).

pH	L^{4-}	HL^{3-}	H_2L^{2-}	H_3L^-	H_4L	FeHL
0.00	5.87E-26	9.10E-16	1.23E-09	6.01E-07	6.01E-05	8.94E-04
2.00	1.83E-21	2.84E-13	3.83E-09	1.88E-08	1.88E-08	1.66E-04
3.00	9.31E-20	1.44E-12	1.94E-09	9.52E-10	9.52E-11	1.96E-05
4.00	7.09E-18	1.10E-11	1.48E-09	7.26E-11	7.26E-13	1.99E-06
5.00	6.71E-16	1.04E-10	1.40E-09	6.87E-12	6.87E-15	1.99E-07
6.00	5.37E-14	8.32E-10	1.12E-09	5.50E-13	5.50E-17	2.00E-08
6.23	1.86E-08	1.26E-09	1.00E-09	2.88E-13	1.70E-17	1.17E-08
8.00	9.93E-04	3.02E-08	4.08E-10	2.00E-15	2.00E-21	1.38E-12
9.00	9.99E-04	2.72E-07	3.68E-10	1.80E-16	1.80E-23	1.25E-14
10.03	9.98E-04	2.29E-06	2.89E-10	1.32E-17	1.23E-25	8.54E-17
11.00	9.90E-04	9.82E-06	1.33E-10	6.49E-19	6.49E-28	4.49E-19
12.00	9.87E-04	1.31E-05	1.76E-11	1.39E-46	8.63E-31	5.97E-22
13.00	9.98E-04	1.55E-06	3.31E-47	1.62E-58	1.02E-34	7.07E-26
13.50	1.00E-03	4.90E-07	3.31E-52	1.62E-64	1.02E-36	7.08E-28
14.00	1.00E-03	1.55E-07	3.31E-54	1.62E-67	1.02E-38	7.08E-30

pH	Fe^{3+}	FeOH^{2+}	$\text{Fe}(\text{OH})_2^+$	$\text{Fe}(\text{OH})_3(\text{aq})$	FeL^-	$\text{Fe}(\text{OH})_3(\text{s})$
0.00	6.06E-05	7.99E-08	7.63E-11	3.83E-18	4.48E-05	
2.00	3.61E-08	4.76E-09	4.55E-10	2.28E-15	8.34E-04	
3.00	8.37E-10	1.10E-09	1.05E-09	5.28E-14	9.80E-04	
4.00	1.12E-11	1.47E-10	1.41E-09	7.05E-13	9.98E-04	
5.00	1.18E-13	1.56E-11	1.49E-09	7.47E-12	1.00E-03	
6.00	1.48E-15	1.95E-12	1.86E-09	9.33E-11	1.00E-03	
6.23	5.73E-16	1.28E-12	2.09E-09	1.78E-10	1.00E-03	1.86E-08
8.00	2.82E-21	5.37E-14	5.13E-09	1.78E-10	6.92E-06	9.93E-04
9.00	2.82E-24	5.95E-15	5.68E-09	1.78E-10	6.24E-07	9.99E-04
10.03	2.30E-27	3.24E-20	3.32E-13	1.78E-10	4.58E-08	1.00E-03
11.00	2.82E-30	3.72E-22	3.55E-14	1.78E-10	2.25E-09	1.00E-03
12.00	2.82E-33	3.72E-24	3.55E-15	1.78E-10	2.99E-11	1.00E-03
13.00	2.82E-36	3.72E-26	3.55E-16	1.78E-10	3.54E-14	1.00E-03
13.50	8.91E-38	3.72E-27	1.12E-16	1.78E-10	1.12E-15	1.00E-03
14.00	2.82E-39	3.72E-28	3.55E-17	1.78E-10	3.55E-17	1.00E-03